Title
Intrinsic Cardiac Neuronal Control of the Heart in Health and Disease

Author
Rajendran, Pradeep Sundaram

Publication Date
2017

Peer reviewed|Thesis/dissertation

UNIVERSITY OF CALIFORNIA

Los Angeles

Intrinsic Cardiac Neuronal Control of the Heart in Health and Disease

A dissertation submitted in partial satisfaction of the requirements for the degree

Doctor of Philosophy in Molecular, Cellular, & Integrative Physiology

by

Pradeep Sundaram Rajendran

2017

ABSTRACT OF THE DISSERTATION

Intrinsic Cardiac Neuronal Control of the Heart in Health and Disease

by

Pradeep Sundaram Rajendran

Doctor of Philosophy in Molecular, Cellular, & Integrative Physiology

University of California, Los Angeles, 2017

Professor Kalyanam Shivkumar, Chair

Cardiovascular diseases including hypertension, arrhythmias, and heart failure are the leading causes of morbidity and mortality in the world. The autonomic nervous system (ANS) regulates the electrical and mechanical function of the heart, and its dysfunction plays an important role in the pathophysiology of cardiovascular diseases, representing an emerging target for therapeutic intervention. However, fundamental gaps in our knowledge regarding autonomic control of the heart in health and the adverse remodeling that occurs in disease have impeded the development of neuromodulation therapies. The cardiac ANS consists of neurons located from the level of the brain to that of the heart itself. At the organ level, the intrinsic cardiac nervous system (ICNS), a distributed network of ganglia and interconnecting nerves, serves as the final common pathway for the integration of neural inputs to the heart. Despite the importance of the ICNS, the impact of acute and chronic stress on the function of this neural network is not well-characterized. Therefore, we investigated the acute effects of premature ventricular contractions (PVCs) and the chronic remodeling induced by myocardial infarction (MI) on the ICNS by obtaining *in vivo* neuronal recordings from beating hearts. Both PVCs and MI affect a critical population of neurons within the ICNS—local circuit neurons. Given that they receive a

convergence of afferent and efferent inputs and have intra- and interganglionic projections, local circuit neurons integrate information and coordinate regional cardiac function. Further, MI results in the formation of a neural sensory border zone, characterized by diminished afferent signals from the infarct and preserved signals from border and remote regions of the heart. These neural effects may underlie, at least in part, the mechanical dyssynchrony, electrical instability, and reflex activation of the ANS noted with PVCs and after MI. In addition, we demonstrated that the evoked cardiac response to vagus nerve stimulation, a neuromodulation therapy being evaluated for cardiac conditions, represents the dynamic interplay between afferent and efferent vagal fibers and reflex responses of the ANS. In conclusion, a better understanding of autonomic regulation of the heart will lead to the development of rationale neuroscience-based therapies for cardiovascular diseases.

The dissertation of Pradeep Sundaram Rajendran is approved.

Jeffrey L. Ardell

Ronald M. Harper

Yvette F. Taché

Kalyanam Shivkumar, Committee Chair

University of California, Los Angeles

2017

DEDICATION

To the curious.

To my teachers, family, and friends who have provided me with unconditional support and encouragement.

TABLE OF CONTENTS

PREFACE

Chapter 1. A version of this manuscript is published: Rajendran PS*, Chui RW*, Ajijola OA, Vaseghi M, Armour JA, Ardell JL and Shivkumar K. Neural Control of Cardiac Function in Health and Disease. In: V. Dilsizian and J. Narula, eds. *Atlas of Cardiac Innervation.* Switzerland: Springer International Publishing; 2017: 13-35. *Equal contributions.

Chapter 2. A version of this manuscript is published: Yamakawa K, Rajendran PS, Takamiya T, Yagishita D, So EL, Mahajan A, Shivkumar K and Vaseghi M. Vagal nerve stimulation activates vagal afferent fibers that reduce cardiac efferent parasympathetic effects. *Am J Physiol Heart Circ Physiol*. 2015;309:H1579-90.

Chapter 3. A version of this manuscript is published: Ardell JL, Rajendran PS, Nier HA, KenKnight BH and Armour JA. Central-peripheral neural network interactions evoked by vagus nerve stimulation: functional consequences on control of cardiac function. *Am J Physiol Heart Circ Physiol*. 2015;309:H1740-52.

Chapter 4. A version of this manuscript is published: Hamon D*, Rajendran PS*, Chui RW, Ajijola OA, Irie T, Talebi R, Salavatian S, Vaseghi M, Bradfield JS, Armour JA, Ardell JL and Shivkumar K. Premature Ventricular Contraction Coupling Interval Variability Destabilizes Cardiac Neuronal and Electrophysiological Control: Insights From Simultaneous Cardioneural Mapping. *Circ Arrhythm Electrophysiol*. 2017;10. *Equal contributions.

Chapter 5. A version of this manuscript is published: Rajendran PS, Nakamura K, Ajijola OA, Vaseghi M, Armour JA, Ardell JL and Shivkumar K. Myocardial infarction induces structural and functional remodeling of the intrinsic cardiac nervous system. *J Physiol*. 2016;594:321-41.

This work was supported by the National Institutes of Health National Institute of General Medical Sciences Training Grant 2T32GM065823, awarded to the University of California - Los Angeles Molecular, Cellular, & Integrative Physiology Program; American Heart Association Western States Affiliate Predoctoral Fellowship 15PRE22230011; and National Institutes of Health National Heart, Lung, and Blood Institute Ruth L. Kirschstein Predoctoral Individual National Research Service Award F31HL127974.

VITA

EDUCATION

Stanford University, Stanford, CA 2005-2009

Bachelor of Science, Biomechanical Engineering

RESEARCH EXPERIENCE

Argonne National Laboratory, Argonne, IL 2006

In-Q-Tel, Arlington, VA 2007

Stanford Institute for Stem Cell Biology & Regenerative Medicine, Stanford, CA 2008-2011

Cardiac Arrhythmia Center, University of California – Los Angeles (UCLA),

Los Angeles, CA 2011-present

AWARDS, HONORS, & FELLOWSHIPS

Paul Harris Fellow, Rotary International, Evanston, IL 2008

Major Grant, Stanford University, Stanford, CA 2008

Bio-X Grant, Stanford University, Stanford, CA 2008

Third Place, Basic Science Poster Competition, Department of Medicine Research Day,

UCLA, Los Angeles, CA 2014

Basic Cardiovascular Sciences Travel Award, American Heart Association, Chicago, IL 2014

Best in Basic Science, American Heart Association Scientific Sessions, Chicago, IL 2014

Predoctoral Training Program in Molecular, Cellular, & Integrative Physiology,

National Institute of General Medical Sciences, National Institutes of Health 2015

Western States Affiliate Predoctoral Fellowship, American Heart Association 2015

Ruth L. Kirschstein Predoctoral Individual National Research Service Award,

National Heart, Lung, & Blood Institute, National Institutes of Health 2015-2017

First Place, Basic Science Poster Competition, Department of Medicine Research Day, UCLA, Los Angeles, CA 2016

Best Presentation, Molecular, Cellular, & Integrative Physiology Program Retreat, UCLA, Los Angeles, CA 2017

Semi-Finalist, Grad Slam, UCLA, Los Angeles, CA 2017

ORGANIZATIONAL AFFILIATIONS

American Heart Association, American Physiological Society, Heart Rhythm Society, Society for Neuroscience

BOOK CHAPTERS

Rajendran PS and Dalerba P. Theoretical and experimental foundations of the "cancer stem cell" model. In: V.K. Rajasekhar, ed. *Cancer Stem Cells.* Hoboken, NJ: Wiley-Blackwell; 2014: 3-16.

Chui RW*, Rajendran PS*, Buckley U, Shivkumar K and Ardell JL. Vagus Nerve Stimulation: Therapeutic Applications for Cardiac Disease. In: K. Horch and D. Kipke, eds. *Neuroprosthetics: Theory and Practice*. 2 ed. Singapore: World Scientific; 2017: 601-630. *Equal contributions.

CHAPTER 1

Introduction

The human heart beats approximately 100,000 times each day, which amounts to 2.5 billion times over the lifetime of an individual. Each of these beats is sensed and dynamically regulated by the autonomic nervous system (ANS). The ANS modulates all aspects of cardiac function, including chronotropy, dromotropy, inotropy, and lusitropy.[1] Early studies suggested that the heart was reciprocally regulated by the parasympathetic and sympathetic divisions of the ANS under the direct control of the central nervous system.[2-4] However, it is clear from more recent work that autonomic control of the heart is much more complex.[5-7] The cardiac ANS is thought to be composed of a series of interacting feedback loops consisting of intrinsic cardiac ganglia,[8] extracardiac intrathoracic ganglia,[9] the spinal cord,[10] the brainstem, and higher centers (Figure 1).[11, 12] Together, this neuronal network intricately modulates cardiac excitability and contractile function on a beat-to-beat basis. Furthermore, autonomic dysregulation has severe consequences and is central to the evolution of cardiac diseases, including hypertension,[13] arrhythmias,[1, 14] and heart failure,[15] that are major causes of morbidity and mortality. The global burden of hypertension is 972 million people;[16] sudden cardiac death due to ventricular arrhythmias is responsible for 4 to 5 million deaths each year, making it the single leading cause of mortality in the world;[17, 18] and heart failure has a prevalence of more than 23 million people worldwide.[19] Despite its importance, major gaps remain in our understanding of autonomic control of the heart in health and the adverse remodeling that occurs in disease, particularly at the foundation of the neuronal hierarchy—the intrinsic cardiac nervous system (ICNS).

Intrinsic cardiac nervous system: the "little brain" on the heart

At the organ level, autonomic regulation of the heart occurs via the ICNS, a distributed network of ganglia and interconnecting nerves.[8] An ICNS has been identified in fish and several mammalian species, including zebrafish,[20] mice,[21] rats,[22] rabbits,[23] guinea pigs,[24] pigs,[25] canines,[26] and humans.[27] Armour and colleagues showed that the human heart contains over 14,000 neurons.[27] Contrary to prior belief, these neurons are not simply a motor relay station for

autonomic projections to the heart, but instead work in concert with higher centers to modulate cardiac function.[8] Further, the ICNS contains all the basic constituents of a neuronal circuit for cardio-cardiac reflexes, namely afferent neurons, parasympathetic and sympathetic efferent neurons, and local circuit neurons (LCNs; Figure 2).[8] Within the ICNS, LCNs represent the predominant subpopulation, and they function to integrate and process information from afferent neurons regarding the local mechanical environment and chemical milieu and from efferent neurons.[8, 28] The convergence of inputs onto these neurons is supported by immunohistochemical studies showing that these neurons display colocalization for multiple neuronal markers[29, 30] and from *in vitro* and *in vivo* neuronal recordings.[28, 31] LCNs project to not only neurons contained within the same intrinsic cardiac ganglion but also those in different intrinsic cardiac ganglia, extracardiac intrathoracic ganglia, and the central nervous system.[8] The convergence of inputs onto and the high degree of interconnectivity between these neurons is consistent with the idea of local information processing and also allows for dynamic regulation of cardiac output to meet the body's requirements. Hence, the ICNS has been referred to as the "little brain" on the heart.[8]

ICNS neurons are aggregated in epicardial fat pads overlying discrete regions of the heart termed ganglionated plexi (GPs). In the human heart, for example, there are 5 atrial and 5 ventricular GPs.[27] Cardinal *et al.* demonstrated that GPs exert preferential, but not exclusive, influence over specific regions by locally administering nicotine, which activates the ganglionic synapse, to different GPs (Figure 3).[8, 32] For instance, the right atrial GP primarily controls the sinoatrial node;[33] however, ventricular GPs such as the ventral interventricular GP can modulate heart rate.[8, 32] The overlap in regions of GP influence is mediated by LCNs.

Extrinsic inputs to the ICNS

The ICNS receives efferent inputs from both the sympathetic (Figure 4) and parasympathetic division of the ANS (Figure 5). Cardiac sympathetic preganglionic neurons have cell bodies in

the intermediolateral cell column between the first and fourth thoracic segments of the spinal cord.[10] Axons from these neurons travel through ventral rami and synapse on postganglionic neurons in primarily extracardiac intrathoracic ganglia (stellate,[34] middle cervical,[35] and mediastinal ganglia[36]) but also intrinsic cardiac ganglia.[8] Postganglionic neurons then project to the conduction system (i.e., sinoatrial and atrioventricular node),[37] atrial and ventricular myocardial tissue, and coronary arteries.[38] Cardiac afferent neurons that course with sympathetic efferent fibers to the heart have cell bodies in the dorsal root ganglia and are pseudounipolar with central axons that synapse on second order neurons in the dorsal horn of the spinal cord.[39]

Regarding the parasympathetic division, the vagus nerve is the main efferent and afferent pathway between the central nervous system and peripheral organs, including the heart. The cervical vagus is composed of approximately 15% efferent and 85% afferent fibers.[40] Standish and colleagues showed that cardiac parasympathetic preganglionic neurons have cell bodes in the nucleus ambiguus and, to a lesser degree, dorsal motor nucleus of the medulla by injecting pseudorabies virus, a trans-synaptic retrograde neuronal tracer, into rat intrinsic cardiac ganglia.[41] These neurons have axons that travel via the vagus to synapse on postganglionic neurons in the ICNS. Postganglionic neurons then project to the sinoatrial and atrioventricular node[37] and atrial and ventricular myocardial tissue.[42-46] Cardiac afferent neurons that course with the vagus to the heart have cell bodies in the nodose (inferior jugular) ganglia and are pseudounipolar with central axons that synapse on second order neurons in the nucleus tractus solitarii of the medulla.[39, 47] Thus, the vagus serves as a major bidirectional conduit for information between central and peripheral aspects of the cardiac ANS.

Numerous functional studies have investigated the role of the sympathetic and parasympathetic nervous system on cardiac electrical and mechanical indices.[38, 48-52] Cumulatively, these studies have shown that stellate ganglia stimulation enhances heart rate, atrioventricular conduction, and ventricular contractility, while vagus nerve stimulation (VNS)

reduces these indices.[38, 48-51] In terms of ventricular electrophysiology, there are differences in functional innervation between the right and left stellate ganglion. Right stellate ganglion stimulation leads to shortening of activation recovery interval, a surrogate for local action potential duration, of the anterolateral walls, whereas left stellate ganglion stimulation leads to shortening of the posterolateral walls.[51] However, right and left VNS lead to similar and homogenous prolongation of ventricular activation recovery intervals.[52] Interestingly, this finding suggests that vagal efferent inputs are uniformly distributed to the ventricles by the ICNS, and these inputs modulate the activity of not only parasympathetic postganglionic neurons but also LCNs, which mediate intra- and interganglionic communication.

Although sympathetic and parasympathetic nerves follow different paths to the heart and mediate distinct cardiac effects, interactions between these systems occur both centrally[53] and peripherally.[54-57] Centrally, sympathetic-parasympathetic interactions occur in the nucleus tractus solitarii. Neurons in the nucleus tractus solitarii project to the nucleus ambiguus and dorsal motor nucleus to modulate parasympathetic efferent outflow and to the rostral and caudal ventrolateral medulla to modulate sympathetic efferent outflow (Figures 4 and 5).[47, 53, 58, 59] Interactions also occur at the paraventricular nucleus of the hypothalamus, which receives viscerosensory inputs from vagal and spinal afferents and projects to autonomic nuclei in the brainstem and spinal cord.[59] Peripherally, interactions occur pre- and post-synaptically at the neuroeffector junction on the sinoatrial and atrioventricular node[55, 60, 61] and cardiomyocytes.[57, 62] Pre-synaptically, norepinephrine and neuropeptide Y released from sympathetic nerve terminals can suppress the release of acetylcholine from parasympathetic nerve terminals,[63, 64] and conversely, acetylcholine can suppress the release of norepinephrine.[55, 65] Post-synaptic mechanisms involve norepinephrine activating beta receptors and triggering a G protein coupled-receptor signaling cascade to increase cyclic adenosine monophosphate and acetylcholine activating muscarinic receptors to decrease cyclic adenosine monophosphate (Figure 2).[55, 62] Furthermore, while the responses to sympathetic and parasympathetic activation

on the end-effector have been well characterized, the effects on and interactions between these extrinsic inputs at the level of the ICNS remain largely unknown. Chapters 2, 3, and 5 will evaluate the role of stellate and vagal inputs on the neuronal subpopulations of the ICNS and this neuronal network overall.

Afferent inputs to the ICNS and potential for cardio-cardiac reflexes

Afferent neurons provide information regarding the local chemical milieu and mechanical environment of the heart to the ANS on a beat-to-beat basis.[8, 39] The processing of these sensory signals at multiple levels provides a mechanism for fine-tuned regulation of efferent signals to the heart (Figure 2). Cardiac afferents include chemosensitive, mechanosensitive, and nocioceptive neurons, many of which are multimodal.[8, 39]

Premature ventricular contractions (PVCs) are abnormal, extra heart beats that originate from the ventricles. They are often seen in association with structural heart disease where they increase the risk for cardiomyopathy and sudden cardiac death; yet, even in structurally normal hearts, they are ubiquitous.[66, 67] Precise mechanisms underlying the adverse effects of PVCs remain unknown, but are likely multifactorial, including mechanical dyssynchrony,[68, 69] abnormalities in calcium handling and oxygen consumption,[70] and autonomic imbalance.[71, 72] Regarding the ANS, microneurography studies have shown that PVCs increase sympathetic activity,[71, 72] but how this occurs is not well understood. In addition, patients with variability in the PVC coupling interval have a worse prognosis, with increased risk of left ventricular dysfunction[73] and sudden cardiac death.[74, 75] Intriguingly, sensory neurons in the visual, auditory, and olfactory systems are known to display enhanced responses to variable compared to constant stimuli.[76, 77] Thus, an afferent-mediated mechanism provides a potential link between variable coupling PVCs and adverse outcomes. Chapter 4 characterizes the effects of PVCs and coupling interval on the ICNS and cardiac electrical stability.

Cardiac pacing is commonly used in the clinical setting, despite having detrimental effects. Pacing has been reported to cause ventricular dyssnchrony,[78] electrical storm in the presence of an infarct scar,[79] and accelerated progression of heart failure and increased mortality.[80, 81] Similar to PVCs, pacing also alters autonomic tone and causes sympathoexcitation,[82, 83] likely though activation of afferent mechanosensitive neurons. Chapter 5 investigates the effects of pacing on the ICNS in healthy and infarcted hearts.

ICNS in physiological and pathological states

In physiological states, the ICNS is thought to act as a low-pass filter to minimize the potential for imbalances in the diverse, extrinsic inputs to the heart.[84-86] Not surprisingly, studies have shown that targeting atrial GPs of the ICNS, a therapy being evaluated for atrial fibrillation, has no effect on atrial fibrillation reoccurrence[87] but increases the risk for sinus node dysfunction[87] and ventricular arrhythmias.[88-90] The ICNS is also capable of modulating cardiac function even when disconnected from higher centers of the cardiac ANS, such as occurs following heart transplantation.[91, 92] Interestingly, heart transplant patients have a decreased susceptibility to atrial[93] and ventricular fibrillation,[94] suggesting that the ICNS itself has stabilizing features that include an anti-arrhythmic effect. It is also known that delinking the higher centers from the ICNS (e.g., bilateral cervicothoracic sympathetic decentralization) has a profound protective effect against ventricular arrhythmias.[95] Further, Kember *et al.* used mathematical modeling to demonstrate that the cardiac ANS has not evolved to deal with myocardial infarction (MI), due to conflicts between central and peripheral aspects,[96] lending support to the physiological function of the ICNS.

Pathological states such as MI have direct and indirect effects on neurons within the cardiac ANS (Figure 6). A lack of energy substrates and an accumulation of chemicals, such as adenosine and reactive oxygen species, secondary to the ischemia leads to altered activity of cardiac afferent neurons.[97-99] Aberrant and excessive activity of these neurons leads to reflex

sympathoexcitation.[100] While acutely sympathoexcitation helps maintain cardiac output, chronically it leads to maladaptive neuronal remodeling throughout the cardiac ANS.[1] At the level of the myocardium, there is denervation of infarct scar and hyperinnervation of the scar border zone, resulting from the production and release of nerve growth factor and other signaling molecules from injured nerves.[101] In the stellate ganglia, an increase in neuronal size, synaptic density, and neural activity has been reported.[102-105]

There is limited data on the structural and functional remodeling that occurs in the ICNS after MI. Neurons have been observed to contain lamellated inclusions and vacuoles and display degenerative changes in dendrites and axons.[106] In addition to histologic and morphological changes, neurons show augmented excitability, synaptic efficacy, and neurochemical modulation post-MI.[107, 108] However, it is not yet understood how this MI-induced remodeling impacts the ability of this neuronal network to process and integrate the multimodal afferent and efferent inputs it receives. Chapter 5 will characterize the effects of MI on the structure and *in vivo* function of the ICNS.

Neuromodulatory approaches for cardiac disease

Given the adverse remodeling that occurs at multiple levels of the cardiac ANS, neuromodulatory approaches such as VNS have emerged as novel treatments for cardiac disease. However, despite showing promise in animal models,[109] the results from large-scale clinical trials of VNS for heart failure have been mixed.[110-113] This variability is likely due to conceptual and technical limitations, as successful application of VNS requires understanding the effects of fiber composition (afferent *vs.* efferent) and stimulation parameters (current, frequency, and pulse width) on the evoked cardiac response. It is also critical to consider the direct and reflex responses to VNS. Since ANS functions to maintain cardiac stability, artificially perturbing this system in one direction induces a reflex response in the opposite direction.

Chapters 2 and 3 will dissect the effects of fiber type and stimulation parameters on the integrated cardiac response to VNS.

Conclusion

The ICNS is the final common pathway for integration of neural inputs to the heart and is critical for maintaining normal rhythm and sustaining circulation. The overarching focus of this dissertation will be to characterize the structure and function of the ICNS as it adapts to acute and chronic pathology. Understanding the neural signature of the ICNS in healthy and disease states could provide insights into how the nervous system responds to injury of a vital organ. Moreover, neuroscience-based therapies for cardiac disease could emerge from further study of the cardiac ANS, starting at its foundation—the ICNS.

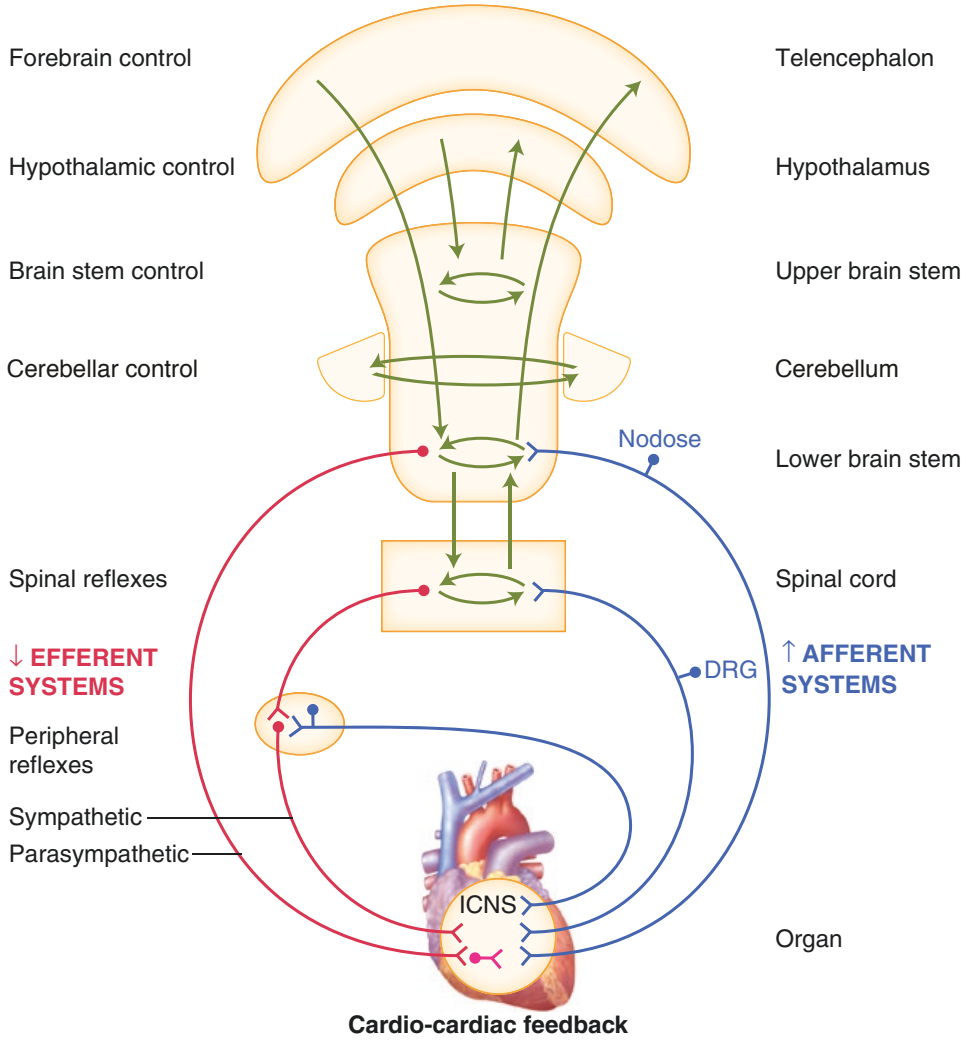

Figure 1. Schematic of cardiac autonomic nervous system. Autonomic control of cardiac function is mediated by a series of interacting feedback loops from the level of the heart to that of the brain. Cardiac afferents (blue lines) provide beat-to-beat information regarding cardiac muscle activity to the autonomic nervous system. The integration and processing of these sensory inputs at multiple levels provides a mechanism for fine-tuned regulation of efferent signals (red lines) to the heart. DRG, dorsal root ganglia.

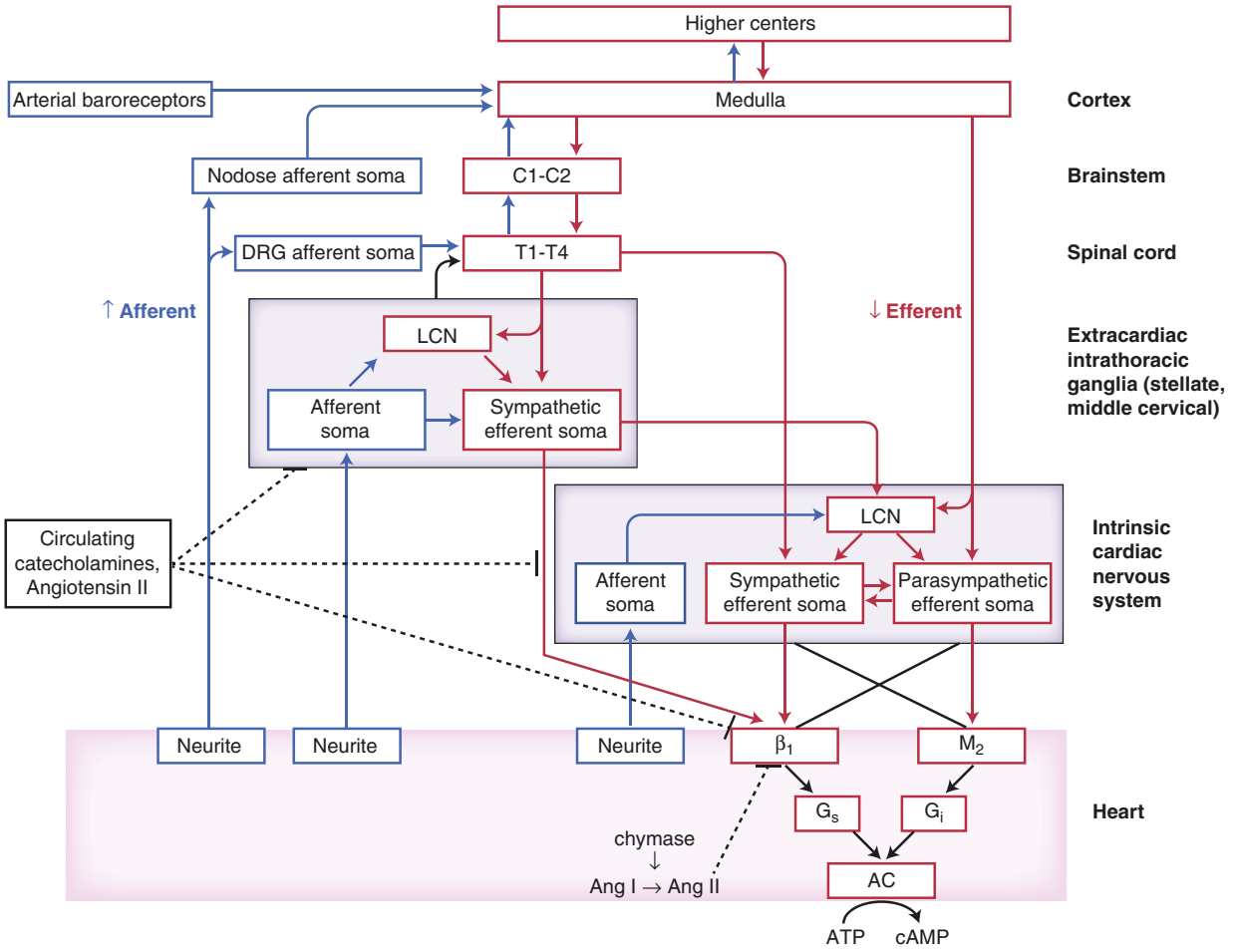

Figure 2. Schematic of functional organization of cardiac autonomic nervous system. AC, adenylate cyclase; Ang, angiotensin; ATP, adenosine triphosphate; C, cervical; cAMP. cyclic adenosine monophosphate; DRG, dorsal root ganglion; G_i, inhibitory G protein-coupled receptor; G_s, stimulatory G protein-coupled receptor; LCN, local circuit neuron; T, thoracic.

NICOTINE INJECTION	RAGP	DAGP	LAGP	IVC-ILAGP	RVGP	VSVGP	CMVGP
Heart rate effects	13 / 13	7 / 8	5 / 10	5 / 9	3 / 3	5 / 7	7 / 9
Tachycardia post-bradycardia	8 / 13	2 / 8	2 / 10	2 / 9	1 / 3	0 / 7	4 / 9
Atrial tachydysrhythmias	**0 / 13**	**2 / 8**	**1 / 10**	**0 / 9**	**0 / 3**	**0 / 7**	**3 / 9**
AV nodal block	7 / 11	3 / 6	2 / 9	1 / 7	1 / 3	0 / 5	6 / 8

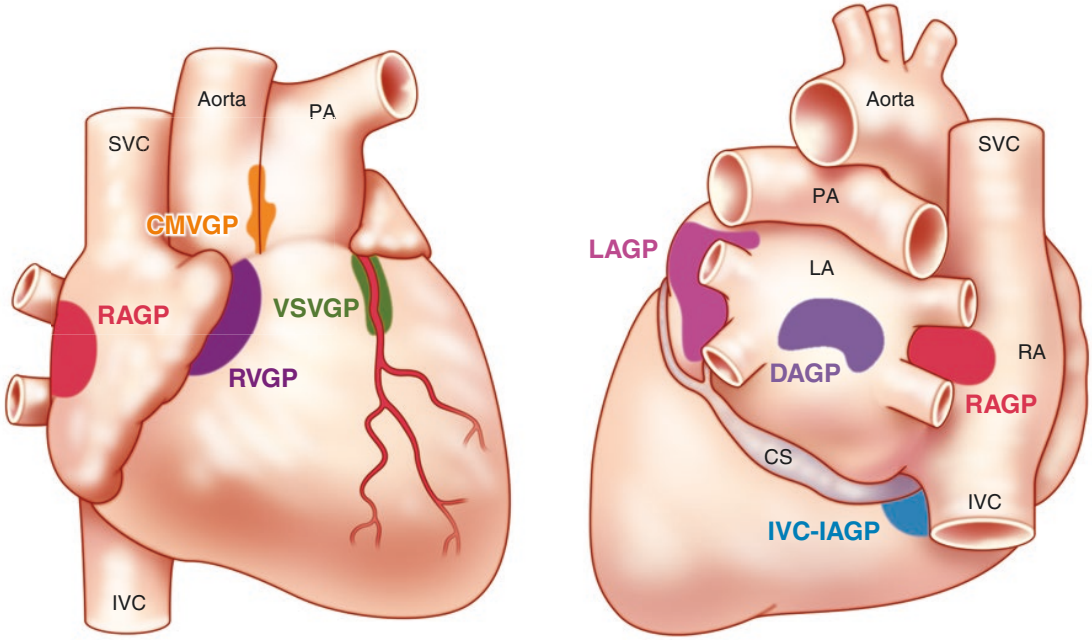

Figure 3. Interconnectivity of ganglionated plexi (GPs) of the intrinsic cardiac nervous system. Nicotine, which activates the ganglionic synapse, was applied to different GPs and evoked changes in cardiac indices was evaluated. AV, atrioventricular; CMVGP, craniomedial ventricular GP; CS, coronary sinus; DAGP, dorsal atrial GP; IVC, inferior vena cava; IVC-ILA, inferior vena cava-inferior left atrial GP; LA, left atrium; LAGP, left atrial GP; PA, pulmonary artery; RA, right atrium; RVGP, right ventricular GP; SVC, superior vena cava.

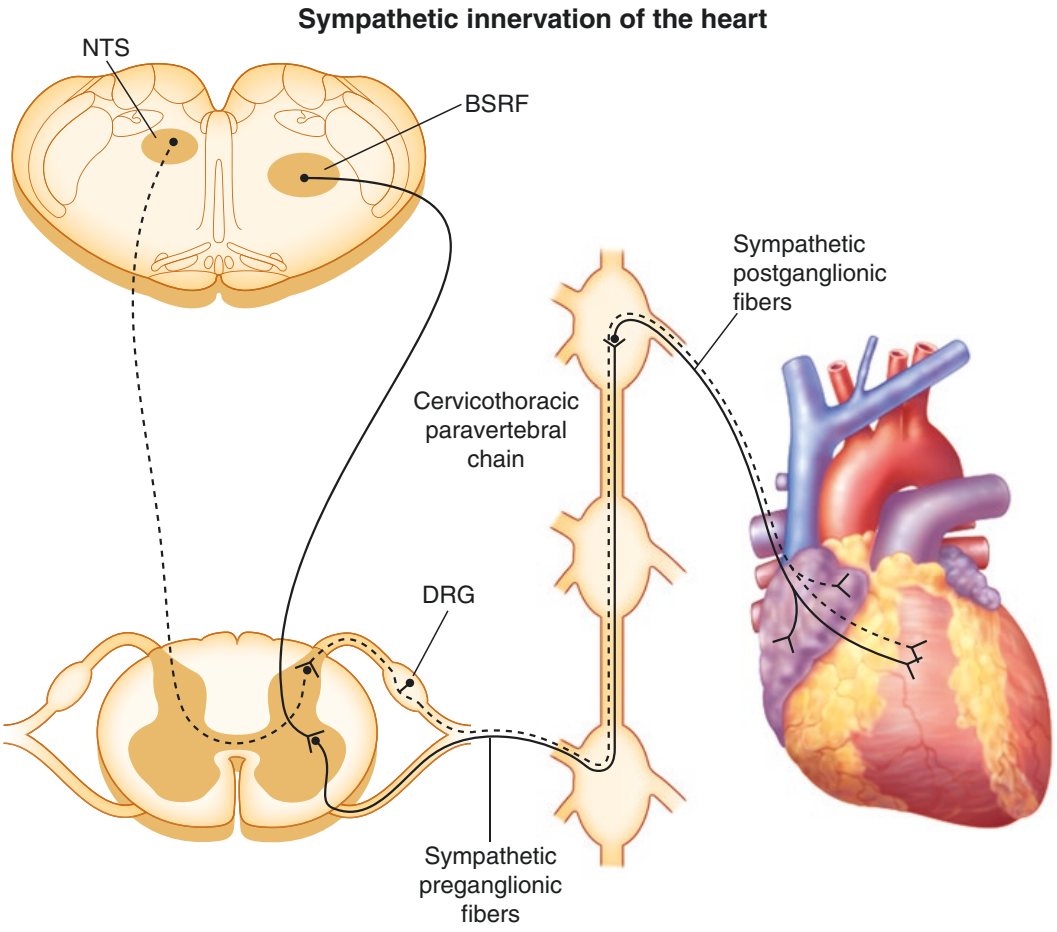

Figure 4. Cardiac sympathetic innervation. Efferent pathways are depicted by solid lines and afferent pathways by dashed lines. BSRF, brain stem reticular formation; DRG, dorsal root ganglia; NTS, nucleus tractus solitarius.

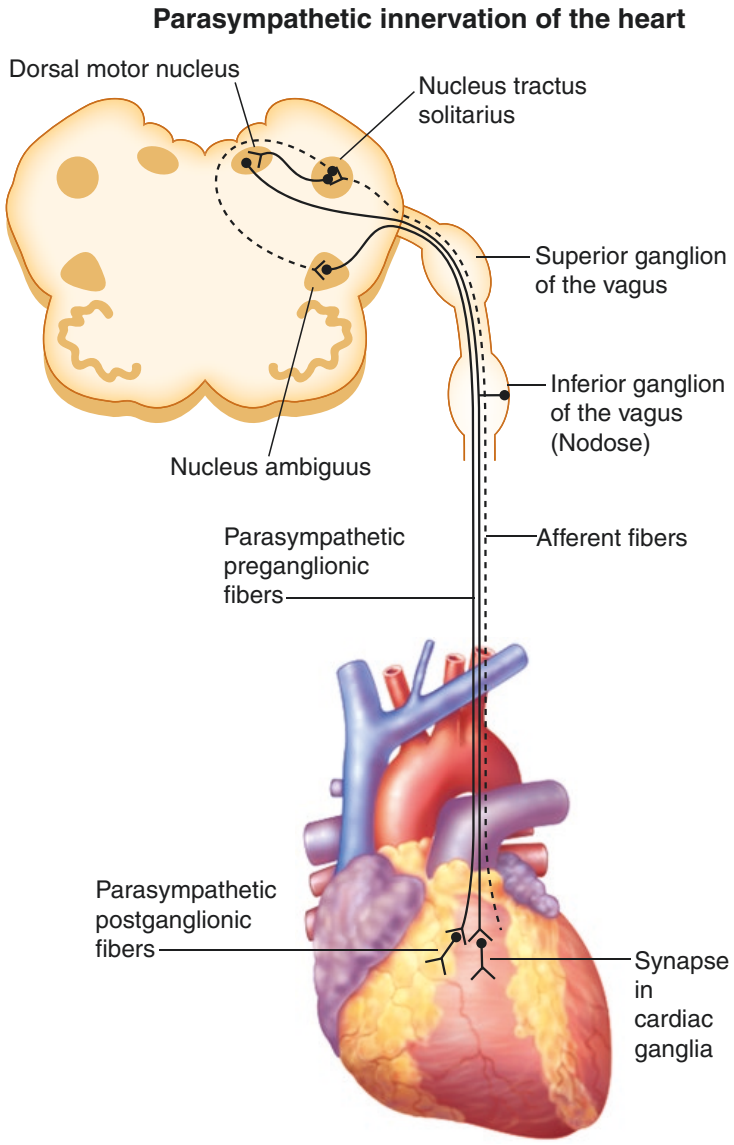

Figure 5. Cardiac parasympathetic innervation. Efferent pathways are depicted by solid lines and afferent pathways by dashed lines.

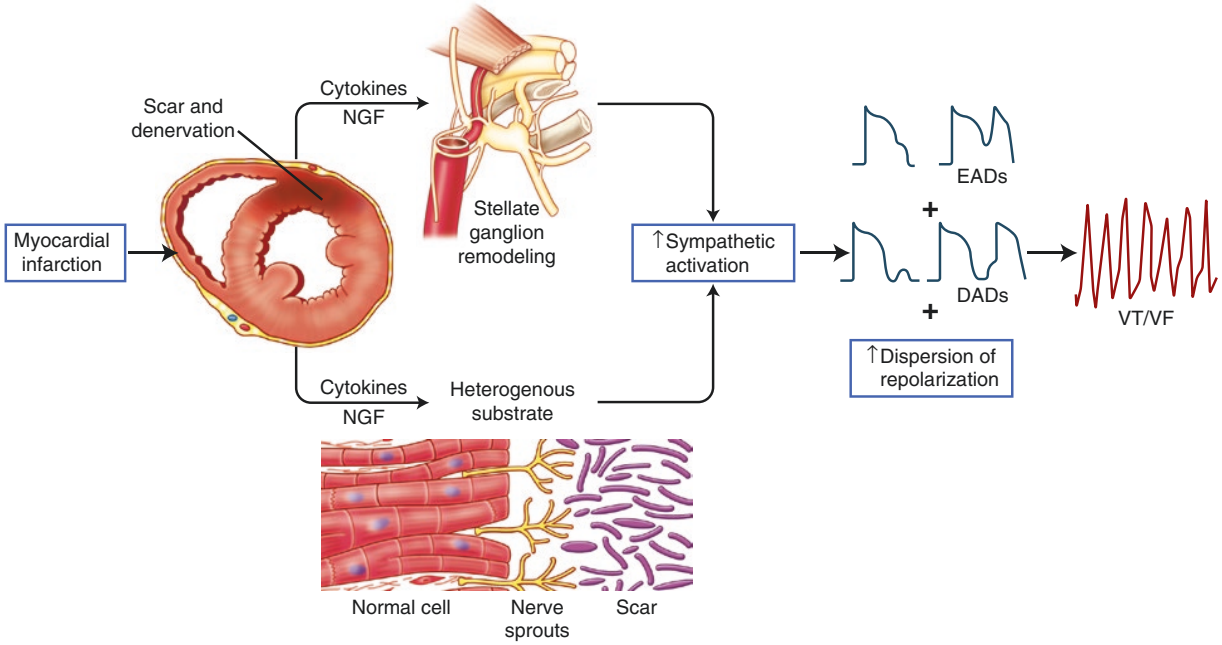

Figure 6. Neural remodeling post-myocardial infarction. DAD, delayed afterdepolarizations; EADs, early afterdepolarizations; NGF, nerve growth factor.

REFERENCES

1. Fukuda K, Kanazawa H, Aizawa Y, Ardell JL and Shivkumar K. Cardiac innervation and sudden cardiac death. *Circ Res*. 2015;116:2005-19.
2. Langley JN. The Autonomic Nervous System Part 1. 1921:80.
3. Kollai M and Koizumi K. Reciprocal and non-reciprocal action of the vagal and sympathetic nerves innervating the heart. *J Auton Nerv Syst*. 1979;1:33-52.
4. Levy MN and Martin PJ. Neural control of the heart. In: R. M. Berne, ed. *The Cardiovascular System* Bethesda, MD: American Physiological Society; 1979(1): 581-620.
5. Armour JA. Cardiac neuronal hierarchy in health and disease. *Am J Physiol Regul Integr Comp Physiol*. 2004;287:R262-71.
6. Shivkumar K, Ajijola OA, Anand I, Armour JA, Chen PS, Esler M, De Ferrari GM, Fishbein MC, Goldberger JJ, Harper RM, Joyner MJ, Khalsa SS, Kumar R, Lane R, Mahajan A, Po S, Schwartz PJ, Somers VK, Valderrabano M, Vaseghi M and Zipes DP. Clinical neurocardiology defining the value of neuroscience-based cardiovascular therapeutics. *J Physiol*. 2016;594:3911-54.
7. Ardell JL, Andresen MC, Armour JA, Billman GE, Chen PS, Foreman RD, Herring N, O'Leary DS, Sabbah HN, Schultz HD, Sunagawa K and Zucker IH. Translational neurocardiology: preclinical models and cardioneural integrative aspects. *J Physiol*. 2016;594:3877-909.
8. Armour JA. Potential clinical relevance of the 'little brain' on the mammalian heart. *Exp Physiol*. 2008;93:165-76.
9. Ardell JL. Intrathoracic Neuronal Regulation of Cardiac Function. In: J. A. Armour and J. L. Ardell, eds. *Basic and Clinical Neurocardiology* New York, NY: Oxford University Press; 2004: 118-152.

10. Foreman RD, DeJongste MJL and Linderoth B. Integrative Control of Cardiac Function by Cervical and Thoracic Spinal Neurons. In: J. A. Armour and J. L. Ardell, eds. *Basic and Clinical Neurocardiology* New York, NY: Oxford University Press; 2004: 153-186.
11. Andresen MC, Kunze DL and Mendelowitz D. Central Nervous System Regulation of the Heart. In: J. A. Armour and J. L. Ardell, eds. *Basic and Clinical Neurocardiology* New York, NY: Oxford University Press; 2004: 187-219.
12. Gray MA, Taggart P, Sutton PM, Groves D, Holdright DR, Bradbury D, Brull D and Critchley HD. A cortical potential reflecting cardiac function. *Proc Natl Acad Sci U S A*. 2007;104:6818-23.
13. Mancia G and Grassi G. The autonomic nervous system and hypertension. *Circ Res*. 2014;114:1804-14.
14. Shen MJ and Zipes DP. Role of the autonomic nervous system in modulating cardiac arrhythmias. *Circ Res*. 2014;114:1004-21.
15. Florea VG and Cohn JN. The autonomic nervous system and heart failure. *Circ Res*. 2014;114:1815-26.
16. Kearney PM, Whelton M, Reynolds K, Muntner P, Whelton PK and He J. Global burden of hypertension: analysis of worldwide data. *Lancet*. 2005;365:217-23.
17. Zipes DP and Wellens HJ. Sudden cardiac death. *Circulation*. 1998;98:2334-51.
18. Chugh SS, Reinier K, Teodorescu C, Evanado A, Kehr E, Al Samara M, Mariani R, Gunson K and Jui J. Epidemiology of sudden cardiac death: clinical and research implications. *Prog Cardiovasc Dis*. 2008;51:213-28.
19. Roger VL. Epidemiology of heart failure. *Circ Res*. 2013;113:646-59.
20. Stoyek MR, Croll RP and Smith FM. Intrinsic and extrinsic innervation of the heart in zebrafish (Danio rerio). *J Comp Neurol*. 2015;523:1683-700.

21. Rysevaite K, Saburkina I, Pauziene N, Noujaim SF, Jalife J and Pauza DH. Morphologic pattern of the intrinsic ganglionated nerve plexus in mouse heart. *Heart Rhythm*. 2011;8:448-54.

22. Horackova M, Slavikova J and Byczko Z. Postnatal development of the rat intrinsic cardiac nervous system: a confocal laser scanning microscopy study in whole-mount atria. *Tissue Cell*. 2000;32:377-88.

23. Saburkina I, Gukauskiene L, Rysevaite K, Brack KE, Pauza AG, Pauziene N and Pauza DH. Morphological pattern of intrinsic nerve plexus distributed on the rabbit heart and interatrial septum. *J Anat*. 2014;224:583-93.

24. Horackova M, Armour JA and Byczko Z. Distribution of intrinsic cardiac neurons in whole-mount guinea pig atria identified by multiple neurochemical coding. A confocal microscope study. *Cell Tissue Res*. 1999;297:409-21.

25. Arora RC, Waldmann M, Hopkins DA and Armour JA. Porcine intrinsic cardiac ganglia. *Anat Rec A Discov Mol Cell Evol Biol*. 2003;271:249-58.

26. Yuan BX, Ardell JL, Hopkins DA, Losier AM and Armour JA. Gross and microscopic anatomy of the canine intrinsic cardiac nervous system. *Anat Rec*. 1994;239:75-87.

27. Armour JA, Murphy DA, Yuan BX, Macdonald S and Hopkins DA. Gross and microscopic anatomy of the human intrinsic cardiac nervous system. *Anat Rec*. 1997;247:289-98.

28. Beaumont E, Salavatian S, Southerland EM, Vinet A, Jacquemet V, Armour JA and Ardell JL. Network interactions within the canine intrinsic cardiac nervous system: implications for reflex control of regional cardiac function. *J Physiol*. 2013;591:4515-33.

29. Hoard JL, Hoover DB, Mabe AM, Blakely RD, Feng N and Paolocci N. Cholinergic neurons of mouse intrinsic cardiac ganglia contain noradrenergic enzymes, norepinephrine transporters, and the neurotrophin receptors tropomyosin-related kinase A and p75. *Neuroscience*. 2008;156:129-42.

30. Hoover DB, Isaacs ER, Jacques F, Hoard JL, Page P and Armour JA. Localization of multiple neurotransmitters in surgically derived specimens of human atrial ganglia. *Neuroscience*. 2009;164:1170-9.

31. Smith FM. Extrinsic inputs to intrinsic neurons in the porcine heart in vitro. *Am J Physiol*. 1999;276:R455-67.

32. Cardinal R, Page P, Vermeulen M, Ardell JL and Armour JA. Spatially divergent cardiac responses to nicotinic stimulation of ganglionated plexus neurons in the canine heart. *Auton Neurosci*. 2009;145:55-62.

33. McGuirt AS, Schmacht DC and Ardell JL. Autonomic interactions for control of atrial rate are maintained after SA nodal parasympathectomy. *Am J Physiol*. 1997;272:H2525-33.

34. Armour JA. Activity of in situ stellate ganglion neurons of dogs recorded extracellularly. *Can J Physiol Pharmacol*. 1986;64:101-11.

35. Armour JA. Activity of in situ middle cervical ganglion neurons in dogs, using extracellular recording techniques. *Can J Physiol Pharmacol*. 1985;63:704-16.

36. Armour JA and Janes RD. Neuronal activity recorded extracellularly from in situ canine mediastinal ganglia. *Can J Physiol Pharmacol*. 1988;66:119-27.

37. Crick SJ, Wharton J, Sheppard MN, Royston D, Yacoub MH, Anderson RH and Polak JM. Innervation of the human cardiac conduction system. A quantitative immunohistochemical and histochemical study. *Circulation*. 1994;89:1697-708.

38. Vaseghi M, Ajijola OA, Mahajan A and Shivkumar K. Sympathetic Innervation, Denervation, and Cardiac Arrhythmias. In: D. P. Zipes and J. Jalife, eds. *Cardiac Electrophysiology: From Cell to Bedside.* 6 ed. Philadelphia, PA: Elsevier Saunders; 2013: 409-418.

39. Armour JA and Kember GC. Cardiac Sensory Neurons. In: J. A. Armour and J. L. Ardell, eds. *Basic and Clinical Neurocardiology* New York, NY: Oxford University Press; 2004: 79-117.

40. Agostoni E, Chinnock JE, De Daly MB and Murray JG. Functional and histological studies of the vagus nerve and its branches to the heart, lungs and abdominal viscera in the cat. *J Physiol*. 1957;135:182-205.

41. Standish A, Enquist LW and Schwaber JS. Innervation of the heart and its central medullary origin defined by viral tracing. *Science*. 1994;263:232-4.

42. Pauziene N, Alaburda P, Rysevaite-Kyguoliene K, Pauza AG, Inokaitis H, Masaityte A, Rudokaite G, Saburkina I, Plisiene J and Pauza DH. Innervation of the rabbit cardiac ventricles. *J Anat*. 2016;228:26-46.

43. Ulphani JS, Cain JH, Inderyas F, Gordon D, Gikas PV, Shade G, Mayor D, Arora R, Kadish AH and Goldberger JJ. Quantitative analysis of parasympathetic innervation of the porcine heart. *Heart Rhythm*. 2010;7:1113-9.

44. Dhein S, van Koppen CJ and Brodde OE. Muscarinic receptors in the mammalian heart. *Pharmacol Res*. 2001;44:161-82.

45. Harvey RD and Belevych AE. Muscarinic regulation of cardiac ion channels. *Br J Pharmacol*. 2003;139:1074-84.

46. Hoover DB, Ganote CE, Ferguson SM, Blakely RD and Parsons RL. Localization of cholinergic innervation in guinea pig heart by immunohistochemistry for high-affinity choline transporters. *Cardiovasc Res*. 2004;62:112-21.

47. Kalia M and Sullivan JM. Brainstem projections of sensory and motor components of the vagus nerve in the rat. *J Comp Neurol*. 1982;211:248-65.

48. Randall WC and Armour JA. Complex cardiovascular responses to vagosympathetic stimulation. *Proc Soc Exp Biol Med*. 1974;145:493-9.

49. Randall WC and Armour JA. Regional vagosympathetic control of the heart. *Am J Physiol*. 1974;227:444-52.

50. Ardell JL and Randall WC. Selective vagal innervation of sinoatrial and atrioventricular nodes in canine heart. *Am J Physiol*. 1986;251:H764-73.

51. Vaseghi M, Yamakawa K, Sinha A, So EL, Zhou W, Ajijola OA, Lux RL, Laks M, Shivkumar K and Mahajan A. Modulation of regional dispersion of repolarization and T-peak to T-end interval by the right and left stellate ganglia. *Am J Physiol Heart Circ Physiol*. 2013;305:H1020-30.

52. Yamakawa K, So EL, Rajendran PS, Hoang JD, Makkar N, Mahajan A, Shivkumar K and Vaseghi M. Electrophysiological effects of right and left vagal nerve stimulation on the ventricular myocardium. *Am J Physiol Heart Circ Physiol*. 2014;307:H722-31.

53. Hopkins DA and Ellenberger HH. Cardiorespiratory neurons in the medulla oblongata: input and output relationships. In: J. A. Armour and J. L. Ardell, eds. *Neurocardiology* New York, NY: Oxford University Press; 1994: 277-308.

54. Levy MN. Sympathetic-parasympathetic interactions in the heart. *Circ Res*. 1971;29:437-45.

55. Levy MN. Sympathetic-vagal interactions in the sinus and atrioventricular nodes. *Prog Clin Biol Res*. 1988;275:187-97.

56. Armour JA. Peripheral Autonomic Neural Interactions in Cardiac Regulation. In: J. A. Armour and J. L. Ardell, eds. *Neurocardiology* New York, NY: Oxford University Press; 1994: 219-244.

57. Levy MN. Cardiac sympathetic-parasympathetic interactions. *Fed Proc*. 1984;43:2598-602.

58. Guyenet PG. The sympathetic control of blood pressure. *Nat Rev Neurosci*. 2006;7:335-46.

59. Ondicova K and Mravec B. Multilevel interactions between the sympathetic and parasympathetic nervous systems: a minireview. *Endocr Regul*. 2010;44:69-75.

60. Urthaler F, Neely BH, Hageman GR and Smith LR. Differential sympathetic-parasympathetic interactions in sinus node and AV junction. *Am J Physiol*. 1986;250:H43-51.

61. Takahashi N and Zipes DP. Vagal modulation of adrenergic effects on canine sinus and atrioventricular nodes. *Am J Physiol*. 1983;244:H775-81.

62. Jakobs KH, Minuth M, Bauer S, Grandt R, Greiner C and Zubin P. Dual regulation of adenylate cyclase. A signal transduction mechanism of membrane receptors. *Basic Res Cardiol*. 1986;81:1-9.

63. Warner MR and Levy MN. Neuropeptide Y as a putative modulator of the vagal effects on heart rate. *Circ Res*. 1989;64:882-9.

64. Revington ML and McCloskey DI. Sympathetic-parasympathetic interactions at the heart, possibly involving neuropeptide Y, in anaesthetized dogs. *J Physiol*. 1990;428:359-70.

65. Loffelholz K and Pappano AJ. The parasympathetic neuroeffector junction of the heart. *Pharmacol Rev*. 1985;37:1-24.

66. Kostis JB, McCrone K, Moreyra AE, Gotzoyannis S, Aglitz NM, Natarajan N and Kuo PT. Premature ventricular complexes in the absence of identifiable heart disease. *Circulation*. 1981;63:1351-6.

67. Messineo FC. Ventricular ectopic activity: prevalence and risk. *Am J Cardiol*. 1989;64:53J-56J.

68. Hamon D, Blaye-Felice MS, Bradfield JS, Chaachoui N, Tung R, Elayi CS, Vaseghi M, Dhanjal TS, Boyle NG, Maury P, Shivkumar K and Lellouche N. A New Combined Parameter to Predict Premature Ventricular Complexes Induced Cardiomyopathy: Impact and Recognition of Epicardial Origin. *J Cardiovasc Electrophysiol*. 2016;27:709-17.

69. Potfay J, Kaszala K, Tan AY, Sima AP, Gorcsan J, 3rd, Ellenbogen KA and Huizar JF. Abnormal Left Ventricular Mechanics of Ventricular Ectopic Beats: Insights Into Origin and Coupling Interval in Premature Ventricular Contraction-Induced Cardiomyopathy. *Circ Arrhythm Electrophysiol*. 2015;8:1194-200.

70. Wang Y, Eltit JM, Kaszala K, Tan A, Jiang M, Zhang M, Tseng GN and Huizar JF. Cellular mechanism of premature ventricular contraction-induced cardiomyopathy. *Heart Rhythm*. 2014;11:2064-72.

71. Maslov PZ, Breskovic T, Brewer DN, Shoemaker JK and Dujic Z. Recruitment pattern of sympathetic muscle neurons during premature ventricular contractions in heart failure patients and controls. *Am J Physiol Regul Integr Comp Physiol*. 2012;303:R1157-64.

72. Welch WJ, Smith ML, Rea RF, Bauernfeind RA and Eckberg DL. Enhancement of sympathetic nerve activity by single premature ventricular beats in humans. *J Am Coll Cardiol*. 1989;13:69-75.

73. Kawamura M, Badhwar N, Vedantham V, Tseng ZH, Lee BK, Lee RJ, Marcus GM, Olgin JE, Gerstenfeld EP and Scheinman MM. Coupling interval dispersion and body mass index are independent predictors of idiopathic premature ventricular complex-induced cardiomyopathy. *J Cardiovasc Electrophysiol*. 2014;25:756-62.

74. Bradfield JS, Homsi M, Shivkumar K and Miller JM. Coupling interval variability differentiates ventricular ectopic complexes arising in the aortic sinus of valsalva and great cardiac vein from other sources: mechanistic and arrhythmic risk implications. *J Am Coll Cardiol*. 2014;63:2151-8.

75. Lee CH, Park KH, Nam JH, Lee J, Choi YJ, Kong EJ, Lee HW, Son JW, Kim U, Park JS, Kim YJ and Shin DG. Increased variability of the coupling interval of premature ventricular contractions as a predictor of cardiac mortality in patients with left ventricular dysfunction. *Circ J*. 2015;79:2360-6.

76. De Palo G, Facchetti G, Mazzolini M, Menini A, Torre V and Altafini C. Common dynamical features of sensory adaptation in photoreceptors and olfactory sensory neurons. *Sci Rep*. 2013;3:1251.

77. Grill-Spector K, Henson R and Martin A. Repetition and the brain: neural models of stimulus-specific effects. *Trends Cogn Sci*. 2006;10:14-23.

78. Tops LF, Schalij MJ and Bax JJ. The effects of right ventricular apical pacing on ventricular function and dyssynchrony implications for therapy. *J Am Coll Cardiol*. 2009;54:764-76.

79. Roque C, Trevisi N, Silberbauer J, Oloriz T, Mizuno H, Baratto F, Bisceglia C, Sora N, Marzi A, Radinovic A, Guarracini F, Vergara P, Sala S, Paglino G, Gulletta S, Mazzone P, Cireddu M, Maccabelli G and Della Bella P. Electrical storm induced by cardiac resynchronization therapy is determined by pacing on epicardial scar and can be successfully managed by catheter ablation. *Circ Arrhythm Electrophysiol*. 2014;7:1064-9.

80. Wilkoff BL, Cook JR, Epstein AE, Greene HL, Hallstrom AP, Hsia H, Kutalek SP, Sharma A and Investigators DCaVIDT. Dual-chamber pacing or ventricular backup pacing in patients with an implantable defibrillator: the Dual Chamber and VVI Implantable Defibrillator (DAVID) Trial. *JAMA*. 2002;288:3115-23.

81. Sweeney MO, Hellkamp AS, Ellenbogen KA, Greenspon AJ, Freedman RA, Lee KL, Lamas GA and Investigators MST. Adverse effect of ventricular pacing on heart failure and atrial fibrillation among patients with normal baseline QRS duration in a clinical trial of pacemaker therapy for sinus node dysfunction. *Circulation*. 2003;107:2932-7.

82. Taylor JA, Morillo CA, Eckberg DL and Ellenbogen KA. Higher sympathetic nerve activity during ventricular (VVI) than during dual-chamber (DDD) pacing. *J Am Coll Cardiol*. 1996;28:1753-8.

83. Herre JM and Thames MD. Responses of sympathetic nerves to programmed ventricular stimulation. *J Am Coll Cardiol*. 1987;9:147-53.

84. Armour JA. Myocardial ischaemia and the cardiac nervous system. *Cardiovasc Res*. 1999;41:41-54.

85. Armour JA, Linderoth B, Arora RC, DeJongste MJ, Ardell JL, Kingma JG, Jr., Hill M and Foreman RD. Long-term modulation of the intrinsic cardiac nervous system by spinal cord neurons in normal and ischaemic hearts. *Auton Neurosci*. 2002;95:71-9.

86. Randall DC, Brown DR, McGuirt AS, Thompson GW, Armour JA and Ardell JL. Interactions within the intrinsic cardiac nervous system contribute to chronotropic regulation. *Am J Physiol Regul Integr Comp Physiol*. 2003;285:R1066-75.

87. Driessen AH, Berger WR, Krul SP, van den Berg NW, Neefs J, Piersma FR, Chan Pin Yin DR, de Jong JS, van Boven WP and de Groot JR. Ganglion Plexus Ablation in Advanced Atrial Fibrillation: The AFACT Study. *J Am Coll Cardiol*. 2016;68:1155-65.

88. Osman F, Kundu S, Tuan J, Jeilan M, Stafford PJ and Ng GA. Ganglionic plexus ablation during pulmonary vein isolation--predisposing to ventricular arrhythmias? *Indian Pacing Electrophysiol J*. 2010;10:104-7.

89. He B, Lu Z, He W, Wu L, Cui B, Hu X, Yu L, Huang C and Jiang H. Effects of ganglionated plexi ablation on ventricular electrophysiological properties in normal hearts and after acute myocardial ischemia. *Int J Cardiol*. 2013;168:86-93.

90. Lo LW, Scherlag BJ, Chang HY, Lin YJ, Chen SA and Po SS. Paradoxical long-term proarrhythmic effects after ablating the "head station" ganglionated plexi of the vagal innervation to the heart. *Heart Rhythm*. 2013;10:751-7.

91. Murphy DA, Thompson GW, Ardell JL, McCraty R, Stevenson RS, Sangalang VE, Cardinal R, Wilkinson M, Craig S, Smith FM, Kingma JG and Armour JA. The heart reinnervates after transplantation. *Ann Thorac Surg*. 2000;69:1769-81.

92. Ardell JL, Butler CK, Smith FM, Hopkins DA and Armour JA. Activity of in vivo atrial and ventricular neurons in chronically decentralized canine hearts. *Am J Physiol*. 1991;260:H713-21.

93. Vaseghi M, Boyle NG, Kedia R, Patel JK, Cesario DA, Wiener I, Kobashigawa JA and Shivkumar K. Supraventricular tachycardia after orthotopic cardiac transplantation. *J Am Coll Cardiol*. 2008;51:2241-9.

94. Vaseghi M, Lellouche N, Ritter H, Fonarow GC, Patel JK, Moriguchi J, Fishbein MC, Kobashigawa JA and Shivkumar K. Mode and mechanisms of death after orthotopic heart transplantation. *Heart Rhythm*. 2009;6:503-9.

95. Vaseghi M, Gima J, Kanaan C, Ajijola OA, Marmureanu A, Mahajan A and Shivkumar K. Cardiac sympathetic denervation in patients with refractory ventricular arrhythmias or electrical storm: intermediate and long-term follow-up. *Heart Rhythm*. 2014;11:360-6.

96. Kember G, Armour JA and Zamir M. Neural control hierarchy of the heart has not evolved to deal with myocardial ischemia. *Physiol Genomics*. 2013;45:638-44.

97. Thompson GW, Horackova M and Armour JA. Sensitivity of canine intrinsic cardiac neurons to H2O2 and hydroxyl radical. *Am J Physiol*. 1998;275:H1434-40.

98. Huang MH, Horackova M, Negoescu RM, Wolf S and Armour JA. Polysensory response characteristics of dorsal root ganglion neurones that may serve sensory functions during myocardial ischaemia. *Cardiovasc Res*. 1996;32:503-15.

99. Huang HS, Pan HL, Stahl GL and Longhurst JC. Ischemia- and reperfusion-sensitive cardiac sympathetic afferents: influence of H2O2 and hydroxyl radicals. *Am J Physiol*. 1995;269:H888-901.

100. Thames MD, Kinugawa T and Dibner-Dunlap ME. Reflex sympathoexcitation by cardiac sympathetic afferents during myocardial ischemia. Role of adenosine. *Circulation*. 1993;87:1698-704.

101. Zhou S, Chen LS, Miyauchi Y, Miyauchi M, Kar S, Kangavari S, Fishbein MC, Sharifi B and Chen PS. Mechanisms of cardiac nerve sprouting after myocardial infarction in dogs. *Circ Res*. 2004;95:76-83.

102. Ajijola OA, Wisco JJ, Lambert HW, Mahajan A, Stark E, Fishbein MC and Shivkumar K. Extracardiac neural remodeling in humans with cardiomyopathy. *Circ Arrhythm Electrophysiol*. 2012;5:1010-116.

103. Ajijola OA, Yagishita D, Reddy NK, Yamakawa K, Vaseghi M, Downs AM, Hoover DB, Ardell JL and Shivkumar K. Remodeling of Stellate Ganglion Neurons following Spatially Targeted Myocardial Infarction: Neuropeptide And Morphologic Changes. *Heart Rhythm*. 2015.

104. Han S, Kobayashi K, Joung B, Piccirillo G, Maruyama M, Vinters HV, March K, Lin SF, Shen C, Fishbein MC, Chen PS and Chen LS. Electroanatomic remodeling of the left stellate ganglion after myocardial infarction. *J Am Coll Cardiol*. 2012;59:954-61.

105. Zhou S, Jung BC, Tan AY, Trang VQ, Gholmieh G, Han SW, Lin SF, Fishbein MC, Chen PS and Chen LS. Spontaneous stellate ganglion nerve activity and ventricular arrhythmia in a canine model of sudden death. *Heart Rhythm*. 2008;5:131-9.

106. Hopkins DA, Macdonald SE, Murphy DA and Armour JA. Pathology of intrinsic cardiac neurons from ischemic human hearts. *Anat Rec*. 2000;259:424-36.

107. Hardwick JC, Ryan SE, Beaumont E, Ardell JL and Southerland EM. Dynamic remodeling of the guinea pig intrinsic cardiac plexus induced by chronic myocardial infarction. *Auton Neurosci*. 2014;181:4-12.

108. Hardwick JC, Southerland EM and Ardell JL. Chronic myocardial infarction induces phenotypic and functional remodeling in the guinea pig cardiac plexus. *Am J Physiol Regul Integr Comp Physiol*. 2008;295:R1926-33.

109. Li M, Zheng C, Sato T, Kawada T, Sugimachi M and Sunagawa K. Vagal nerve stimulation markedly improves long-term survival after chronic heart failure in rats. *Circulation*. 2004;109:120-4.

110. Premchand RK, Sharma K, Mittal S, Monteiro R, Dixit S, Libbus I, DiCarlo LA, Ardell JL, Rector TS, Amurthur B, KenKnight BH and Anand IS. Autonomic regulation therapy via left or right cervical vagus nerve stimulation in patients with chronic heart failure: results of the ANTHEM-HF trial. *J Card Fail*. 2014;20:808-16.

111. Zannad F, De Ferrari GM, Tuinenburg AE, Wright D, Brugada J, Butter C, Klein H, Stolen C, Meyer S, Stein KM, Ramuzat A, Schubert B, Daum D, Neuzil P, Botman C, Castel MA, D'Onofrio A, Solomon SD, Wold N and Ruble SB. Chronic vagal stimulation for the treatment of low ejection fraction heart failure: results of the NEural Cardiac TherApy foR Heart Failure (NECTAR-HF) randomized controlled trial. *Eur Heart J*. 2015;36:425-33.

112. Premchand RK, Sharma K, Mittal S, Monteiro R, Dixit S, Libbus I, DiCarlo LA, Ardell JL, Rector TS, Amurthur B, KenKnight BH and Anand IS. Extended Follow-Up of Patients With Heart Failure Receiving Autonomic Regulation Therapy in the ANTHEM-HF Study. *J Card Fail*. 2016;22:639-42.

113. Gold MR, Van Veldhuisen DJ, Hauptman PJ, Borggrefe M, Kubo SH, Lieberman RA, Milasinovic G, Berman BJ, Djordjevic S, Neelagaru S, Schwartz PJ, Starling RC and Mann DL. Vagus Nerve Stimulation for the Treatment of Heart Failure: The INOVATE-HF Trial. *J Am Coll Cardiol*. 2016;68:149-58.

CHAPTER 2

Vagus nerve stimulation activates vagal afferent fibers that reduce cardiac efferent parasympathetic effects

The autonomic nervous system plays a central role in the initiation and maintenance of ventricular arrhythmias.[1, 2] Parasympathetic withdrawal, as manifested by decreased heart rate (HR) variability and baroreflex sensitivity, is pro-arrhythmic, while increasing parasympathetic input to the heart via vagus nerve stimulation (VNS) is thought to be cardio-protective.[3-7] Specifically, VNS has been shown to decrease infarct size,[8, 9] reduce ischemia-related ventricular arrhythmias,[9, 10] and improve survival in animal models of heart failure.[11] The electrophysiological effects of stimulation of the intact right and left vagosympathetic trunk appear to be similar in a porcine model, without significant global or regional differences.[12] Although the vagosympathetic trunk provides cardiomotor efferent fibers to the heart, more than 80% of the fibers contained within the vagus nerve are afferents, transducing information from visceral organs, including the heart, to the central nervous system.[13-15] VNS likely leads to activation of both afferent and efferent fibers, and may cause reflex autonomic activation through the contralateral trunk and via the paravertebral chain and dorsal root ganglia. However, the role of afferent fibers on efferent parasympathetic outflow during VNS remains unknown. Furthermore, whether VNS elicits primarily activation of afferent fibers in the stimulated trunk, or activation of afferent and efferent fibers in the contralateral trunk due to reflex mechanisms remains to be elucidated. This is especially important, as many of the studies that demonstrated an anti-arrhythmic benefit from VNS were performed in the decentralized state, after transection of the vagal trunk, stimulating only the efferent fibers.[16-25] Other studies have used an isolated innervated preparation, where cardiac afferent fibers no longer play an important role.[26-28] Meanwhile, the majority of the studies showing pro-arrhythmic effects were done in the intact state.[29-33] Furthermore, a large-scale human clinical trial of VNS for the management of heart failure did not reproduce the expected benefit noted in animal studies.[34] These conflicting results are likely due to a lack of understanding of the contribution of afferent fibers to efferent cardiac control during VNS. The purpose of this study was to characterize the effects of afferent

activation during VNS on modulation of cardiac electrical and mechanical indices by comparing states with the vagus nerve intact *vs.* transected.

METHODS

All procedures were performed in accordance with guidelines of University of California, Los Angeles (UCLA) Institutional Animal Care and Use Committee and the National Institutes of Health *Guide for the Care and Use of Laboratory Animals*.

Surgical preparation

Yorkshire pigs (n = 37, male or female, weighing 50 ± 3 kg) were sedated with telazol (6-8 mg/kg, intramuscular), followed by endotracheal intubation, mechanical ventilation, and anesthesia with isoflurane (1-1.5%, inhalation). Intermittent boluses of fentanyl (50-100 mcg, intravenous) were given for analgesia during surgical preparation. A surface 12-lead electrocardiogram was obtained via Prucka Cardio Lab System (GE Healthcare, Fairfield, CT, USA). Arterial blood pressure monitoring was performed via a 5-French sheath in the femoral artery, and saline and medications were infused via a 5-French sheath in the femoral vein. Lateral neck dissections were performed and the cervical vagus nerves were isolated at the cricoid level bilaterally, and the heart was exposed via a median sternotomy. Arterial blood gas levels were measured hourly. The ventilator settings were adjusted or sodium bicarbonate administered to maintain acid-base homeostasis. After completion of surgery, anesthetics were switched from isoflurane to α-chloralose (50 mg/kg intravenous bolus, followed by 20-30 mg/kg/hr, continuous intravenous infusion), followed by a stabilization period of 1 hour. Animals were euthanized by an overdose of sodium pentobarbital (200 mg/kg, intravenous), followed by potassium chloride (150 mg/kg, intravenous) to arrest the heart.

VNS

Bipolar cuff electrodes (PerenniaFlex Model 304; Cyberonics Inc., Houston, TX, USA) were placed around the cervical vagal trunks and connected to a Grass S88 stimulator (Grass Technologies, Warwick, RI, USA) via photoelectric current isolation units (PSIU6; Grass Technologies). VNS was performed with square pulses (10 Hz, 1 ms). Bradycardia threshold for each vagus nerve was defined as the current required to achieve a 10% decrease in HR. VNS was performed for 20 seconds at 1.2x threshold.

Cardiac electrophysiological recordings and analysis

Multiple unipolar epicardial electrograms were continuously recorded from a 56-electrode sock placed over the ventricles, connected to a Prucka Cardio Lab System (GE Healthcare). The activation recovery interval (ARI) from each electrode was analyzed using Scaldyn (University of Utah, Salt Lake City, UT, USA).[12, 35, 36] Briefly, activation time (AT) was defined as the interval from the beginning of the QRS to the minimum dV/d*t* of the activation wavefront, and recovery time (RT) was defined as the interval from the beginning of the QRS to the maximum dV/d*t* of the repolarization wavefront. ARI was then calculated by subtracting AT from RT. ARI has been shown to correlate well with local action potential duration.[37, 38] For purposes of this manuscript, anterior refers to the ventral aspect and posterior refers to the dorsal aspect of the animal. Mean ARIs in the following regions were quantified: left ventricle (LV) anterior, LV lateral, LV posterior, LV apex, right ventricle (RV) anterior, RV lateral, RV posterior, and RV outflow tract. The median number of electrodes in each region was 4 (range: 3-6). Polar maps were also generated from the sock electrode array to assess regional ARIs qualitatively using the program map3d (University of Utah, Salt Lake City, UT, USA; Figure 1).

The PR interval was measured from the beginning of the P wave to the start of the Q wave on the surface electrocardiogram. Either lead II or aVF was used, whichever provided the

clearest P wave. The same lead was used under all conditions in each animal.

Hemodynamic assessment

A 12-pole conductance pressure catheter (5 French) was placed in the LV via the left carotid artery and connected to a MPVS Ultra Pressure Volume Loop System (Millar Instruments, Houston, TX, USA). Appropriate catheter placement was confirmed by cardiac ultrasound (GE Healthcare, Fairfield, CT, USA) and via the pressure-volume loops recorded. Tau was calculated using the method, defined by Weiss et al. from the pressure-volume loop as a parameter describing the time course of the exponential decay in LV pressure during isovolumic relaxation.[39] The following equation was used to calculate Tau:

$$P(t) = A^{(-t/\mathrm{Tau})}.$$

where P is LV pressure, A is a constant, and t is time from $-dP/dt_{max}$.

Experimental protocol

The experimental protocol and the number of animals used in each group are shown in Figure 2.

Intact VNS

Unilateral right (RVNS) and left VNS (LVNS) were performed randomly (10 Hz, 1 ms, 1.2x threshold) with both vagus nerves intact (n = 25).

Ipsilateral vagus nerve transection (VNTx)

Subsequently, the right (n = 11) or the left vagus nerve (n = 14) was transected 2 cm above the stimulation probe. At least 20 minutes of observation was used to allow for cardiac electrical and mechanical indices to return to stable values. Next, the threshold test was repeated, and the

current required to achieve a 10% decrease in HR was re-measured. After the new threshold was obtained, ipsilateral stimulation of efferent fibers (i.e., stimulation of the distal/caudal end of the vagal trunk) was performed using the same current as the intact state.

Contralateral VNTx

RVNS was performed in the setting of left (contralateral) VNTx (n = 10), and LVNS in the setting of right (contralateral) VNTx (n = 7). After contralateral transection, at least 20 minutes of observation was allowed for stabilization of cardiac electrical and mechanical indices. Next, the threshold current required for a 10% decrease in HR was re-measured in the setting of contralateral transection. RVNS or LVNS in the setting of contralateral transection was then performed using the same current as the intact state.

Bilateral VNTx

After right or left VNTx, the remaining intact vagus nerve was transected to study the effect of bilateral transection on cardiac electrical and mechanical indices. The new threshold current for either RVNS or LVNS was re-measured after bilateral transection. Subsequently, RVNS or LVNS (i.e., stimulation of the distal/caudal end of the vagal trunk) was then performed using the same current as the intact state.

Atropine infusion

To compare cardiac electrical and mechanical effects of efferent muscarinic blockade with bilateral VNTx, atropine was administered (0.04 mg/kg bolus, intravenous) with both vagus nerves intact (n = 12). The HR, systolic blood pressure (SBP), LV contractility, and ARIs were measured at baseline and after 5 minutes of infusion. Comparison of muscarinic efferent blockade with atropine to bilateral transection was performed to provide insight as to whether

the hemodynamic and electrophysiological changes observed after transection were due to either sympathoexcitation or withdrawal of parasympathetic efferent tone.

Statistical analysis

Data are presented as mean ± the standard error of the mean. Comparison of the change in ARI with atropine to bilateral VNTx was performed using the Wilcoxon rank-sum test. Baseline values and percent changes from baseline during VNS were compared between various experimental conditions (intact, ipsilateral, contralateral, and bilateral VNTx) using separate linear mixed effects models, including random animal effects to account for repeated measurements. Comparisons between pairs of conditions were performed using model contrasts. P values < 0.05 were considered to be statistically significant. To account for multiple comparisons within each experiment, we report which differences remained significant after controlling for the false discovery rate at 5%. The Benjamini-Hochberg procedure was used to control the false discovery rate. All analyses were performed using SAS version 9.4 (SAS Institute Inc., Cary, NC, USA).

RESULTS

Effect of VNTx on cardiac electrical and mechanical indices

The hemodynamic and electrophysiological responses to ipsilateral and bilateral VNTx are shown in Table 1. Right transection increased HR, decreased SBP, and decreased Tau ($P < 0.05$), but did not affect LV contractility. Left transection also increased HR and decreased Tau ($P < 0.05$), but did not affect SBP or LV contractility. There were no differences in hemodynamic indices with bilateral compared to ipsilateral transection.

Both right and left transection shortened PR interval ($P < 0.05$). Mean global ventricular ARI was decreased by right (338 ± 15 to 298 ± 20 ms; $P < 0.01$) and left transection (361 ± 14

to 330 ± 13 ms; P < 0.01; Figures 3 and 4). The hemodynamic and electrophysiological effects, however, stabilized at ~5 minutes after transection and remained stable at 20 minutes (Table 2). Immediately after right transection, an increase in HR, SBP, and LV dP/dt_{max} and a decrease in LV dP/dt_{min} was noted that returned to baseline after 5 minutes (P < 0.05). This pattern was also seen after left transection. After bilateral transection, differences in hemodynamic and electrophysiological indices remained significant compared to the intact state, but were not different than ipsilateral transection. The mean global ventricular ARI in all animals decreased from the intact state after bilateral transection (351 ± 10 ms in the intact state to 303 ± 13 ms after bilateral VNTx; ΔARI of 47 ± 9 ms; %change ARI of 14 ± 3%; P < 0.001). AT was not affected by either right or left transection.

Effect of atropine on cardiac electrical and mechanical indices

Atropine increased HR (75 ± 3 to 91 ± 3 bpm; P < 0.05) and SBP (124 ± 5 to 130 ± 6 mmHg; P < 0.05). Atropine shortened ARI (365 ± 20 to 319 ± 15 ms; P < 0.05). Furthermore, the change in ARI with atropine (ΔARI of 46 ± 12 ms, %change ARI of 11 ± 2%) was not different than that after bilateral VNTx (ΔARI of 51 ± 10 ms, %change ARI of 15 ± 13%; P = 0.6).

Hemodynamic response to RVNS and LVNS in the setting of intact, ipsilateral, contralateral, and bilateral VNTx

Intact VNS

With both vagus nerves intact, RVNS and LVNS decreased HR, SBP, and dP/dt$_{max}$ and increased dP/dt$_{min}$ and Tau (P < 0.05; Table 3).

Ipsilateral and bilateral VNTx and VNS

In response to RVNS after ipsilateral VNTx, HR, SBP, dP/dt$_{max}$, and Tau decreased and dP/dt$_{min}$

increased ($P < 0.05$; Table 1). RVNS after bilateral transection had no additional effects.

A decrease in SBP and an increase in dP/dt_{min} was observed with LVNS after ipsilateral transection compared to the intact state ($P < 0.05$), but no changes in HR, dP/dt_{max}, and Tau were noted. After subsequent contralateral transection (i.e., bilateral VNTx), the hemodynamic effects of LVNS were further augmented, and the changes in HR, dP/dt_{max}, and Tau reached significance compared to the intact state ($P < 0.05$).

Contralateral VNTx and VNS

RVNS in the setting of contralateral VNTx did not affect HR, SBP, dP/dt_{max}, dP/dt_{min}, or Tau compared to the intact state (Table 3). Similarly, LVNS in the setting of contralateral VNTx did not alter hemodynamic or electrophysiological indices.

Impact of ipsilateral, contralateral, and bilateral VNTx on bradycardia threshold during RVNS and LVNS

Bradycardia threshold, the current required to produce a 10% reduction in HR, with RVNS was reduced after ipsilateral and bilateral VNTx compared to the intact state ($P < 0.05$; Figure 3). Similarly, a reduction in threshold was also observed with LVNS after ipsilateral and bilateral transection ($P < 0.05$; Figure 4). There were no differences in the threshold current between ipsilateral *vs.* bilateral transection for RVNS or LVNS. The RVNS threshold decreased after contralateral transection compared to the intact state ($P < 0.05$), whereas LVNS threshold was not changed by contralateral transection (Figure 5).

Effect of ipsilateral, contralateral, and bilateral VNTx on cardiac electrical indices during RVNS and LVNS

Using the same current as the intact state, RVNS after ipsilateral VNTx augmented the

percentage change in ARI (2.2 ± 0.9% to 5.8 ± 1.7%; P < 0.01; Figure 3). After subsequent contralateral transection (i.e., bilateral VNTx), RVNS did not demonstrate additional effects. LVNS after ipsilateral transection demonstrated a trend towards increasing ARI (1.1 ± 0.5% to 3.6 ± 0.7%), but these differences did not reach significance (P = 0.07; Figure 4). After subsequent contralateral transection (i.e., bilateral VNTx), LVNS caused a significant increase in ARI compared to the intact state (6.6 ± 1.6% *vs.* 1.1 ± 0.5%; P < 0.01).

In the setting of ipsilateral transection, both RVNS and LVNS prolonged PR interval compared to the intact state (P < 0.05; Table 1). After bilateral transection, the increase in PR interval with RVNS and LVNS remained significant compared to the intact state, but was not different from ipsilateral transection.

RVNS in the setting of contralateral transection did not alter ARI compared to the intact state (3.3 ± 1% *vs.* 2.8 ± 1%; P = 0.53; Figure 5). Similarly, LVNS in the setting of contralateral transection did not change ARI compared to the intact state (6 ± 2% *vs.* 4 ± 1%; P = 0.15).

AT was not affected by VNS in the intact state (24 ± 2 at baseline *vs.* 25 ±2 ms during RVNS; 22 ± 1 ms at baseline *vs.* 21 ± 1 ms during LVNS). Furthermore, ipsilateral, contralateral, and bilateral transection did not affect AT.

The impact of VNTx on regional ARI

After right VNTx, regional ARI shortened in all regions (P < 0.05; Figure 6). RVNS after ipsilateral transection had an augmented effect on ARI across all regions compared to the intact state (P < 0.05). RVNS after bilateral transection did not show significant additional prolongation beyond ipsilateral transection. Left transection also shortened ARI in all regions compared to the intact state (P < 0.05; Figure 7). However, the additional change in ARI after bilateral transection was not significant compared to ipsilateral transection. LVNS after ipsilateral transection showed a trend for greater prolongation in ARI across all regions compared to the intact state, but these

differences did not reach significance after controlling for the false discovery rate. However, after subsequent contralateral transection (i.e., bilateral VNTx), LVNS significantly augmented the effects on regional ARI compared to the intact state ($P < 0.05$).

DISCUSSION

Major findings

In this study, a comprehensive evaluation of the effects of VNS on cardiac electrical and mechanical indices before and after VNTx was undertaken to assess the role of vagal afferent fiber activation on cardiac efferent parasympathetic control. The major findings are:

(1) Activation of vagal afferent fibers with VNS reduces its efferent effects and diminishes parasympathetic drive. Therefore, the effect of VNS on hemodynamic and electrophysiological parameters was augmented after ipsilateral transection. This suggests that activation of afferent fibers in the stimulated trunk directly contributes to withdrawal of parasympathetic tone, and possibly, sympathoexcitation.

(2) The magnitude of the effects of bilateral transection was similar to infusion of atropine, suggesting that these changes were driven primarily by withdrawal of efferent parasympathetic tone, rather than sympathetic activation due nerve injury or decrease in inhibition of sympathetic fibers by afferent fibers in the vagus nerve.

(3) Unilateral transection (right or left) is sufficient to cause a significant withdrawal in parasympathetic tone in the porcine model.

Impact of VNTx on global ventricular repolarization

Despite the fact that the vagus is a complex nerve, consisting of predominantly afferent fibers,[14, 15] the detailed effects of VNTx on cardiac electrical and mechanical indices have not been elucidated. The effect of transection on HR, sinus cycle length, and AH interval had been

previously reported,[40-43] but no further delineations of the reason for these effects were undertaken. In addition, MacCanon and Horvath in 1957 performed chronic bilateral transection in a canine model and, in the animals that survived, noted an initial increase in HR and SBP that returned to baseline levels within 15-20 minutes. They further observed a sustained decrease in cardiac output over time.[42] In the porcine model, unilateral and bilateral transection caused significant hemodynamic and electrophysiological effects that were maintained at 20 minutes. Unlike our study, that shows that unilateral transection causes a significant withdrawal of parasympathetic tone, in canines with normal hearts unilateral transection did not affect HR and only after bilateral transection was tachycardia observed, suggesting significant interspecies differences.[41] Brooks and colleagues showed a decrease in repetitive extrasystole threshold, a surrogate of ventricular vulnerability to ventricular fibrillation, after either right or left transection in canines with normal hearts, but the effect on VNS or other cardiac indices after transection were not reported.[17] They did note that bilateral transection had minimal additional effects to unilateral transection on repetitive extrasystole threshold. Schwartz and colleagues assessed the effects of transection and atropine on ventricular refractory periods. Unlike our findings, this study demonstrated a modest effect of bilateral transection on refractory period (2-3 ms) after atropine infusion.[44] Possible explanations for the differences observed are due the fact that, in the study by Schwartz and colleagues, ventricular refractory periods were measured with ventricular pacing/extrastimulus testing, which is known to causes an enhanced sympathetic tone[45] that could additionally shorten refractory period, diluting the results. Furthermore, spatial heterogeneities across the RV and LV have not been previously assessed. In this study, we show that bilateral transection has significant effects on HR, PR interval, ARI, and Tau. Regional ARI effects were similar. Possible explanations for these findings are loss of inhibition of sympathetic tone by vagal afferent fibers after transection, leading to sympathoexcitation, or withdrawal of efferent parasympathetic tone. The effects of bilateral transection on ARI were

similar to atropine infusion, suggesting that the majority of the electrophysiological effects of transection are due withdrawal of efferent parasympathetic tone.

Effect of VNS during intact, and after ipsilateral, contralateral, and bilateral VNTx on cardiac electrical and mechanical indices

Vagal afferent fibers from the heart and baroreceptors travel via pseudo-unipolar neurons through the nodose ganglia (inferior vagal ganglia) and synapse in the nucleus tractus solitarus. Efferent vagal fibers originate in the nucleus ambiguus and dorsal motor nucleus,[46, 47] innervating the sinoatrial node, the atrioventricular node, and atrial and ventricular myocardium through the intrinsic cardiac nervous system.[48, 49] We had previously shown that stimulation of the intact right or left vagus nerves has similar hemodynamic and electrophysiological effects,[12] as both of these nerves provide preganglionic efferent fibers that synapse in intrinsic cardiac ganglia. As the vagal trunk consists primarily of afferent fibers, the role of these fibers, particularly during stimulation, need to be clearly assessed. Multiple studies have shown beneficial effects of VNS in preventing arrhythmias, but the large majority of these studies were performed in animal models in the decentralized state, after VNTx,[16-25, 50] or in isolated innervated hearts,[26, 27, 51] where afferent activation was not possible. Other studies that demonstrated some benefit in the intact state often had mixed results, showing a reduction of polymorphic ventricular arrhythmias, but an increase in monomorphic ventricular tachycardia.[52] Still, other studies have reported pro-arrhythmic effects or greater burden of ventricular arrhythmias during intact stimulation with or without ischemia.[29-33] Meanwhile, a large randomized prospective clinical trial, *Ne*ural *C*ardiac *T*hera*p*y Fo*r H*eart *F*ailure (NECTAR-HF) failed to demonstrate the benefits of VNS in heart failure patients that had been observed in animal models.[34] The mixed results of these studies may be due to the method of stimulation, neglecting the role of afferent fiber activation.[50] In our study, vagal afferent fibers did not play a

significant role on cardiac electrophysiological and hemodynamic parameters in the resting state, and the primary effects of transection could be explained by the removal of efferent parasympathetic tone. However, during VNS, afferent fibers were activated and played a significant role in reducing the effects of cardiac efferent parasympathetic control. Transection of the ipsilateral and bilateral vagal trunks followed by stimulation significantly augmented the electrophysiological and hemodynamic effects of VNS. Transection of the contralateral vagal trunk and removal of the contralateral vagal afferents did not have as great of an effect, as this was not the trunk that was being actively stimulated. However, the inhibitory role of even these contralateral afferents at modest stimulation levels, as demonstrated by the decrease in threshold of RVNS after left transection, suggests that the autonomic nervous system is an integrated network that senses hemodynamic changes acutely and acts to return these changes to the baseline state. Direct stimulation of afferent fibers and hemodynamic changes transduced by contralateral vagal afferent fibers can lead to activation of neurons in the nucleus tractus solitarus that subsequently could inhibit parasympathetic outflow from the dorsal motor nucleus or nucleus ambiguous and may even cause sympathoexcitation. It is also possible that activation of these fibers could lead to sympathoexcitation either via reflex activation or by direct activation of these fibers in the vagal trunk. It has been reported that vagus nerve is a complex nerve that has contains sympathetic fibers, particularly at the level of the thorax.[53] Therefore, the possibility of activating these fibers also exists with electrical stimulation. However, in this study, the role of these sympathetic fibers is likely to be negligible. If these fibers were responsible for sympathoexcitation, then upon transection, similar sympathetic effects would have been observed. Instead, an increase in parasympathetic effects was found.

Previous studies had also suggested an inhibitory role of vagal afferent fibers on reflex sympathetic outflow.[54, 55] Based on these studies, we would have expected a decrease in the magnitude of the effects of VNS after VNTx, rather than augmentation, since the inhibitory input

of vagal afferents on sympathetic efferents would be removed. The results of our study were surprising, but do show that activation of afferent fibers by electrical stimulation of the vagus nerve reduces parasympathetic efferent outflow and may cause reflex sympathoexcitation, counteracting or reducing the beneficial effects of VNS. Therefore, the role of these afferent fibers must be considered when performing VNS in the intact state.

Right *vs.* left VNTx and effects of VNS

Compared to RVNS, the effect of LVNS on ARI was more significant after bilateral VNTx compared ipsilateral transection. This may suggest that the right vagus nerve may contain greater cardiac afferent mechanoreceptor fibers. These fibers are intact in the setting of ipsilateral (left) transection, and may be activated by the reduction in SBP and dP/dt_{max} during VNS, causing reflex sympathetic activation or greater withdrawal of parasympathetic tone through this intact nerve, and subsequently inhibiting to some degree, the increase in ventricular ARI observed during LVNS. Our results support those of Hirota and Ishiko, who performed VNTx before and after bilateral cranial nerve IX stimulation to assess the effect of afferent activation using gustatory stimuli.[40] As in our study, Hirota and Ishiko also noted subtle differences in HR and blood pressure, depending on the order that the vagus nerves were transected, with less tachycardia after left compared to right transection.[40] They also showed that the tachycardia response to gustatory stimuli was reduced more after right than left transection, again suggesting that the right vagus nerve may contain more cardiac afferents fibers.[40] Chen et al. showed an increase in HR, blood pressure, LV systolic pressure, and dP/dt_{min} after both unilateral right and left transection.[56] However, baroreflex sensitivity was increased only after right transection, also suggesting a greater role for cardiac vagal afferent fibers in the right vagus nerve.

LIMITATIONS

General anesthesia can cause suppression of nerve activity. However, we were able to reliably record a cardiomotor response during VNS. To reduce the effect of inhaled anesthetics, *α*-chloralose infusion was used during the assessment of VNS on cardiac electrical and mechanical indices. For global and regional analysis, ARIs were not corrected for HR, as any HR effects, particularly with regards to assessment of parasympathetic tone are physiologically important. Furthermore, HR would not affect regional differences, as these were assessed at the same HR and percentage changes used to assess regional differences. Atrial and ventricular pacing was not performed to correct for HR, given the effect of pacing on altering autonomic tone.[45] Effects of VNS were evaluated at 1 frequency and pulse width. This frequency and pulse width was chosen to avoid aggressive stimulation. Higher frequencies that are thought to specifically and only activate afferent fibers in epilepsy studies were avoided. Additionally, narcotics, such as fentanyl, can cause central modulation of parasympathetic tone through interaction with the mu opioid and OLR-1 receptors in the nucleus ambiguus. However, the use of fentanyl was standardized across all animals and recordings were performed after initiation of *α*-chloralose during steady state. Finally, the vagus nerve contains afferent fibers from many visceral organs. Therefore, it is not clear from this study activation of which afferent fibers may have led to a reduction in cardiac parasympathetic efferent outflow or sympathoexcitation.

CONCLUSIONS

Parasympathetic efferent cardiomotor fibers in both the right and left vagus nerve are required for maintaining the resting basal parasympathetic tone. Vagal afferents are activated during VNS and decrease efferent parasympathetic electrophysiological and hemodynamic effects. The activation of both ipsilateral afferent fibers and reflex activation of the autonomic nervous system must be considered when applying VNS.

ACKNOWLEDGEMENTS

We would like to acknowledge Jonathon Hoang for his contributions to this study.

GRANTS

This study was supported by American Heart Association Grant 11FTF75500 to M.V. and by National Institutes of Health National Heart, Lung, & Blood Institute Grant R01HL084261 to K.S.

DISCLOSURES

No conflicts of interest, financial or otherwise, are declared by the authors.

AUTHOR CONTRIBUTIONS

K.Y., P.S.R, T.T., D.Y., E.L.S., and M.V. performed experiments; K.Y., T.T., D.Y., E.L.S, and M.V. analyzed data; K.Y., D.Y., A.M., K.S., and M.V. interpreted results of experiments; K.Y. and M.V. prepared figures; K.Y. and M.V. drafted manuscript; K.Y., P.S.R., A.M., K.S., and M.V. edited and revised manuscript; K.Y., P.S.R., T.T., D.Y., E.L.S., A.M., K.S., and M.V. approved final version of manuscript; K.S. and M.V. conception and design of research.

	Intact			Ipsilateral VNTx			Bilateral VNTx		
	BL	**VNS**	**%Change**	**BL**	**VNS**	**%Change**	**BL**	**VNS**	**%Change**
HR (beats/min)									
Right (*n* = 11)	82 ± 4	74 ± 4*	−10 ± 1	96 ± 5#	82 ± 5*	−15 ± 2§	101 ± 5#	87 ± 6*	−14 ± 2§
Left (*n* = 14)	74 ± 3	67 ± 3*	−10 ± 1	84 ± 2#	72 ± 3*	−15 ± 1	91 ± 4#	74 ± 3*	−18 ± 2§
SBP (mmHg)									
Right (*n* = 11)	117 ± 6	112 ± 7*	−5 ± 2	104 ± 7#	95 ± 6*	−9 ± 1§	96 ± 7#	86 ± 6*	−11 ± 1§
Left (*n* = 14)	126 ± 6	120 ± 6*	−5 ± 1	127 ± 6	115 ± 6*	−10 ± 1§	122 ± 8	102 ± 7*	−16 ± 1§
dP/dt_{max} (mmHg/s)									
Right (*n* = 10)	1,830 ± 149	1,752 ± 137*	−4 ± 1	1,666 ± 111	1,518 ± 107*	−9 ± 1§	1,560 ± 129	1,402 ± 116*	−10 ± 1§
Left (*n* = 13)	1,679 ± 111	1,628 ± 104*	−3 ± 1	1,799 ± 122	1,722 ± 116*	−4 ± 1	1,883 ± 249	1,731 ± 205*	−7 ± 2§
dP/dt_{min} (mmHg/s)									
Right (*n* = 10)	−2,859 ± 438	−2,686 ± 429*	8 ± 2	−2,540 ± 380	−2,180 ± 362*	17 ± 4§	−2,211 ± 491	−1,825 ± 456*	20 ± 3§
Left (*n* = 13)	−2,869 ± 248	−2,747 ± 253*	5 ± 2	−3,222 ± 262	−2,783 ± 259*	14 ± 3§	−3,086 ± 367	−2,558 ± 336*	17 ± 5§
Tau (ms)									
Right (*n* = 9)	41 ± 2	42 ± 3	4 ± 2	35 ± 3#	39 ± 4*	10 ± 3§	33 ± 3#	37 ± 4*	10 ± 3§
Left (*n* = 12)	39 ± 2	41 ± 2*	7 ± 2	35 ± 2#	39 ± 2*	12 ± 2	34 ± 2#	39 ± 2*	14 ± 3§
PR interval (ms)									
Right (*n* = 10)	118 ± 2	135 ± 3*	13 ± 3	109 ± 3#	133 ± 5*	23 ± 5§	102 ± 3#	128 ± 7*	26 ± 6§
Left (*n* = 9)	117 ± 5	135 ± 5*	13 ± 3	109 ± 5#	132 ± 6*	23 ± 5§	105 ± 5#	128 ± 8*	24 ± 5§

Table 1. Effect of vagus nerve stimulation (VNS) on hemodynamic indices after ipsilateral and bilateral vagus nerve transection (VNTx). BL, baseline; HR, heart rate; SBP, systolic blood pressure. * $P < 0.05$ *vs.* BL; # $P < 0.05$ *vs.* intact state; § $P < 0.05$ *vs*. %change during VNS in intact state.

	Hemodynamics				
	BL	**Post 1 min**	**Post 5 min**	**Post 10 min**	**Post 20 min**
	Right VNTx (n = 8)				
HR (beats/min)	81 ± 6	91 ± 6*	91 ± 6	92 ± 6	94 ± 6
SBP (mmHg)	108 ± 6	114 ± 7*	109 ± 8*	107 ± 8	104 ± 8
dP/dt_{max} (mmHg/s)	1,837 ± 166	1,894 ± 145*	1,883 ± 135	1,875 ± 130	1,833 ± 130
dP/dt_{min} (mmHg/s)	−2,697 ± 478	−2,931 ± 430*	−2,927 ± 460	−2,832 ± 465	−2,744 ± 448
	Left VNTx (n=13)				
HR (beats/min)	73 ± 4	81 ± 4*	83 ± 5	85 ± 5	84 ± 5
SBP (mmHg)	125 ± 6	136 ± 7*	134 ± 7	135 ± 7	133 ± 7
dP/dt_{max} (mmHg/s)	1,682 ± 130	1,768 ± 131*	1,800 ± 137	1,812 ± 136	1,806 ± 145
dP/dt_{min} (mmHg/s)	−2,933 ± 226	−3,184 ± 243*	−3,219 ± 267	−3,236 ± 251	−3,249 ± 275
	Global mean ventricular ARI (ms)				
Unilateral left VNTx (n = 14)	354 ± 14	338 ± 14*	333 ± 13	331 ± 13	331 ± 12
Unilateral right VNTx (n = 9)	339 ± 20	321 ± 19*	321 ± 19	318 ± 20	316 ± 20
Bilateral VNTx (n = 23)	322 ± 11	310 ± 12*	309 ± 11	308 ± 11	310 ± 11

Table 2. Hemodynamic and electrophysiological responses to right and left vagus nerve transection (VNTx). ARI, activation recovery interval; BL, baseline; HR, heart rate; SBP, systolic blood pressure. * $P < 0.05$ *vs.* prior condition.

	Intact			Contralateral VNTx		
	BL	**VNS**	**%Change**	**BL**	**VNS**	**%Change**
HR (beats/min)						
Right (n = 10)	79 ± 4	69 ± 3*	−11 ± 2	86 ± 4#	73 ± 2*	−15 ± 2
Left (n = 8)	82 ± 5	75 ± 5*	−9 ± 1	94 ± 6#	83 ± 5*	−11 ± 2
SBP (mmHg)						
Right (n = 10)	133 ± 8	123 ± 7*	−7 ± 1	130 ± 8#	118 ± 8*	−10 ± 1
Left (n = 8)	119 ± 7	115 ± 8*	−4 ± 1	101 ± 9#	94 ± 9*	−8 ± 2
dP/dt_{max} (mmHg/s)						
Right (n = 7)	1,673 ± 102	1,576 ± 96*	−6 ± 1	1,613 ± 99	1,475 ± 82*	−8 ± 2
Left (n = 7)	2,060 ± 191	1,904 ± 173*	−7 ± 1	1,815 ± 159	1,678 ± 161*	−8 ± 2
dP/dt_{min} (mmHg/s)						
Right (n = 7)	−2,916 ± 373	−2,705 ± 368*	8 ± 1	−3,030 ± 334	−2,704 ± 321*	11 ± 2
Left (n = 7)	−3,281 ± 509	−2,981 ± 468*	10 ± 3	−2,832 ± 534	−2,565 ± 554*	14 ± 4
Tau (ms)						
Right (n = 7)	37 ± 2	41 ± 3*	10 ± 3	35 ± 2#	38 ± 3*	6 ± 2
Left (n = 7)	39 ± 5	43 ± 5*	10 ± 3	31 ± 2#	35 ± 2*	13 ± 3
PR interval (ms)						
Right (n = 10)	115 ± 4	131 ± 5*	14 ± 2	101 ± 4#	127 ± 5*	27 ± 6
Left (n = 8)	115 ± 4	141 ± 11*	22 ± 8	105 ± 3#	132 ± 9*	25 ± 6

Table 3. Effect of vagus nerve stimulation (VNS) on hemodynamic indices after contralateral vagus nerve transection (VNTx). BL, baseline; HR, heart rate; SBP, systolic blood pressure. * $P < 0.05$ *vs.* BL; # $P < 0.05$ *vs.* intact state.

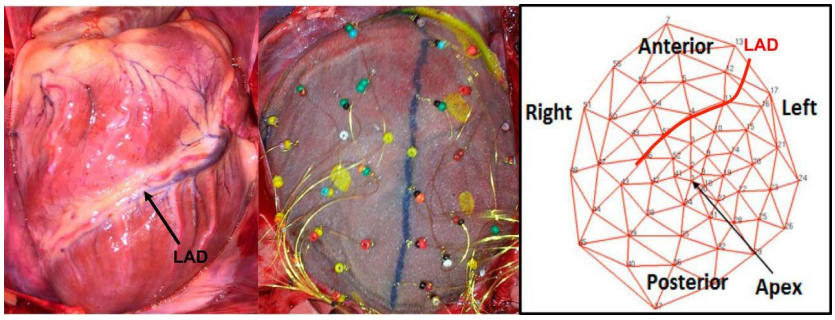

Figure 1. An example of the porcine heart, the sock electrode array on the heart, and a polar map graphic demonstrating the location of the electrodes from the sock on the polar map. The course of the left anterior descending coronary artery (LAD) is approximated on the polar map for reference.

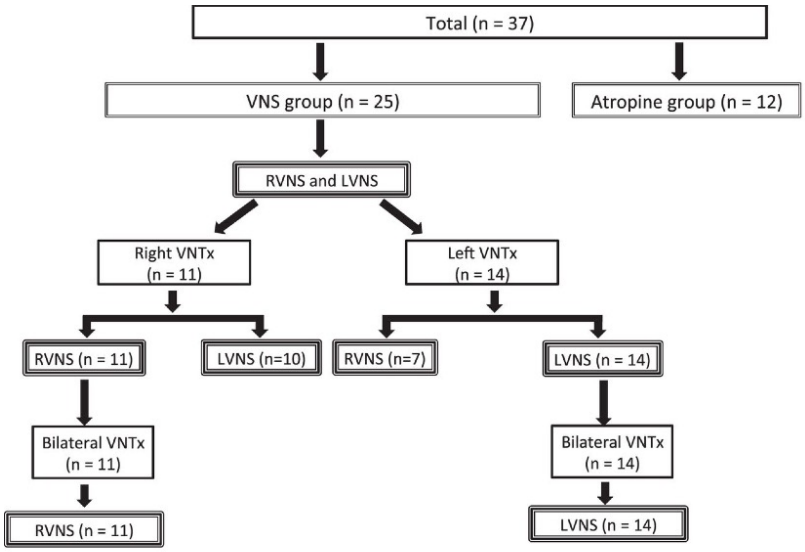

Figure 2. Flow chart of the experimental protocol. 25 of 37 animals underwent vagus nerve stimulation (VNS) followed by vagus nerve transection (VNTx), and 12 of 37 animals received only atropine infusion. Animals with ipsilateral VNTx also underwent bilateral VNTx after right (RVNS) or left VNS (LVNS).

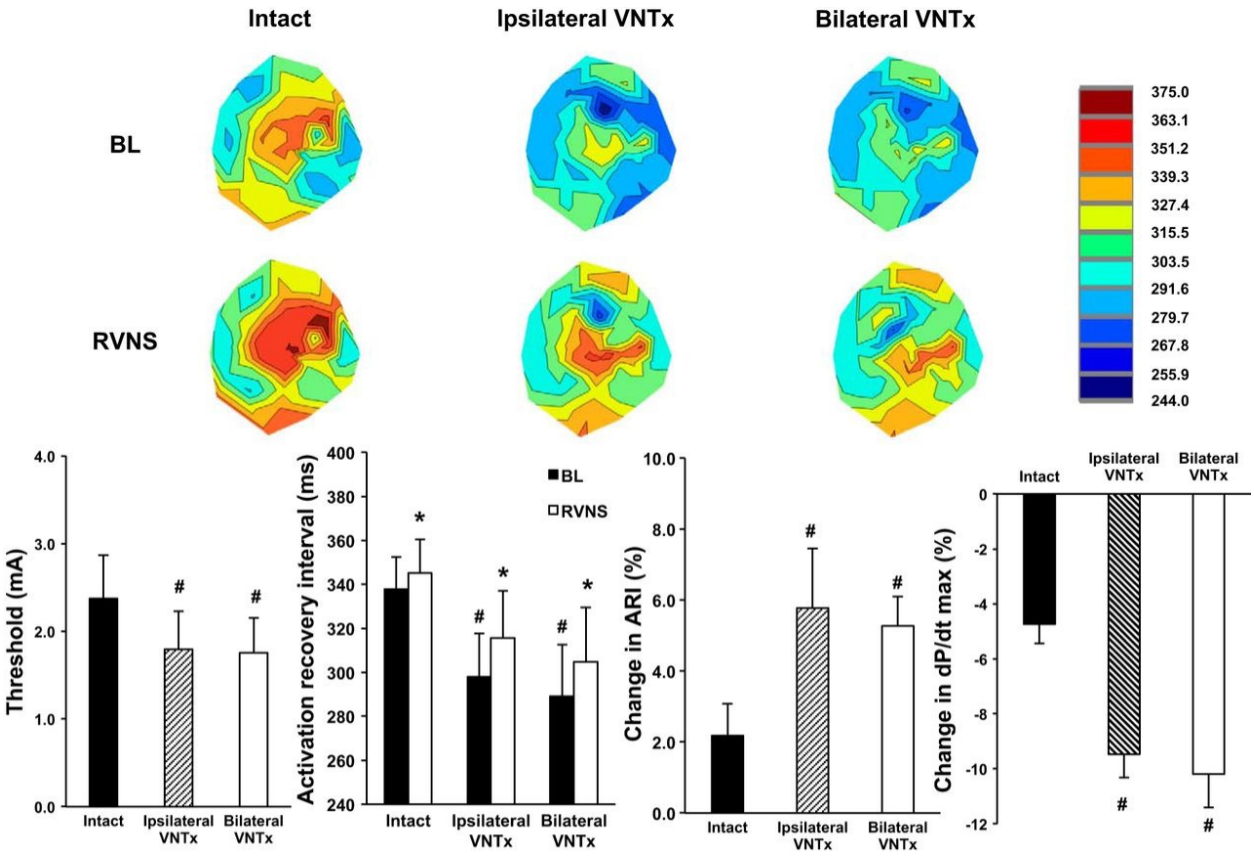

Figure 3. Effects of ipsilateral (right) and bilateral vagus nerve transection (VNTx) on cardiac electrical and mechanical indices at baseline (BL) and during right vagus nerve stimulation (RVNS). *Top*: Representative polar maps obtained from the sock electrode array of 1 animal at BL and during RVNS before and after ipsilateral and bilateral VNTx. The polar maps demonstrate that activation recovery intervals (ARIs) increased in all regions during RVNS, and during RVNS after transection, the magnitude of increase in ARI was greater. *Bottom:* Combined data from all animals that underwent RVNS before and after ipsilateral and bilateral transection. Ipsilateral and bilateral transection decreased stimulation threshold and mean global ventricular ARIs. The change in ARI and dP/dt_{max} during RVNS were augmented by ipsilateral and bilateral transection. * $P < 0.05$ *vs.* BL; # $P < 0.05$ *vs.* intact state.

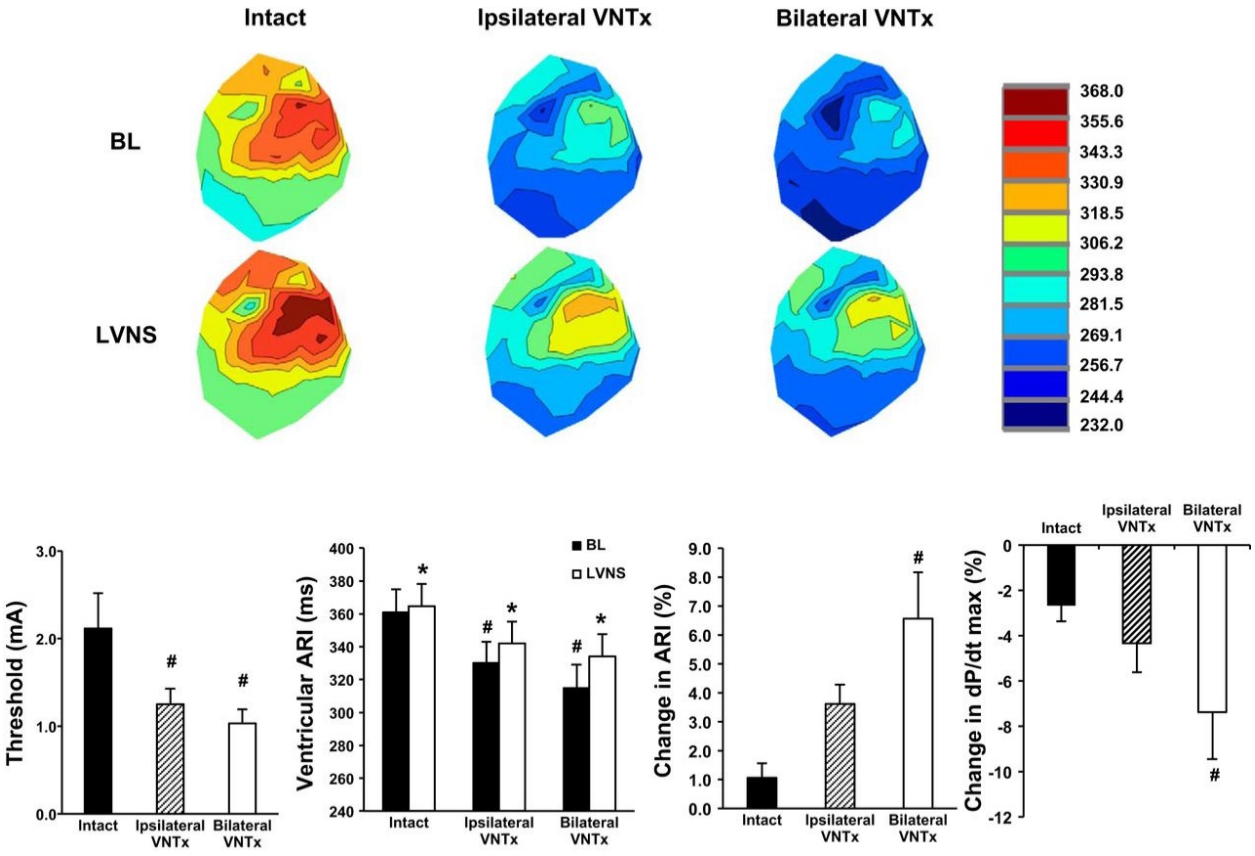

Figure 4. Effects of ipsilateral (left) and bilateral vagus nerve transection (VNTx) on cardiac electrical and mechanical indices at baseline (BL) and during left vagus nerve stimulation (LVNS). *Top*: Representative polar maps obtained from the sock electrode array of 1 animal at BL and during LVNS before and after ipsilateral and bilateral VNTx. The polar maps demonstrate that activation recovery intervals (ARIs) decreased uniformly across all regions after transection. The magnitude of increase in ARI during LVNS appeared to be greatest after bilateral transection. *Bottom:* Combined data from all animals that underwent LVNS before and after ipsilateral and bilateral transection. Ipsilateral and bilateral transection decreased stimulation threshold and mean global ventricular ARIs. The change in ARI and dP/dt_{max} during LVNS was augmented by ipsilateral transection, but this difference did not reach statistical significance until after bilateral transection. * $P < 0.05$ *vs.* BL; # $P < 0.05$ *vs.* intact state.

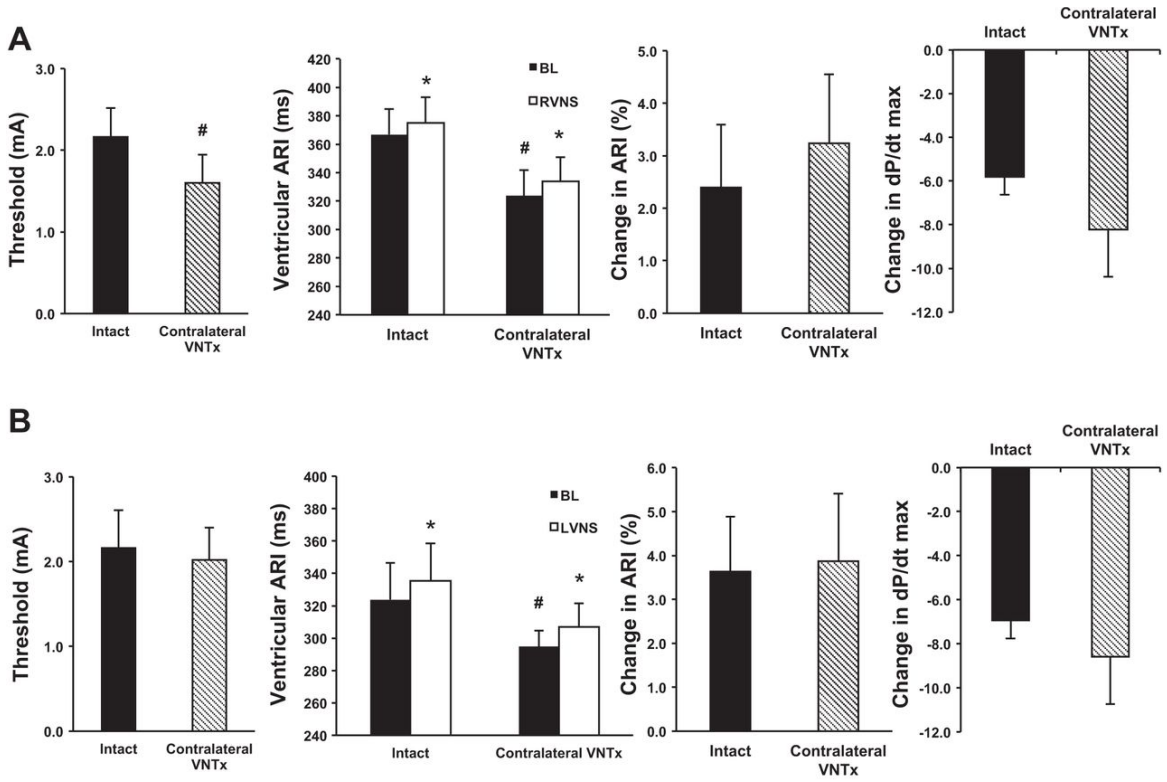

Figure 5. Effects of contralateral vagus nerve transection (VNTx) on cardiac electrical and mechanical indices during vagus nerve stimulation (VNS). (A) The current required to achieve a 10% decrease in heart rate, defined as the bradycardia threshold, was decreased during right VNS (RVNS) after contralateral VNTx. However, no significant additional changes in activation recovery interval (ARI) or dP/dt_{max} during RVNS were observed. **(B)** There were no significant changes in stimulation threshold, mean global ventricular ARI, and dP/dt_{max} during left VNS (LVNS) after contralateral transection. * $P < 0.05$ *vs.* BL. # $P < 0.05$ *vs.* intact state. BL, baseline.

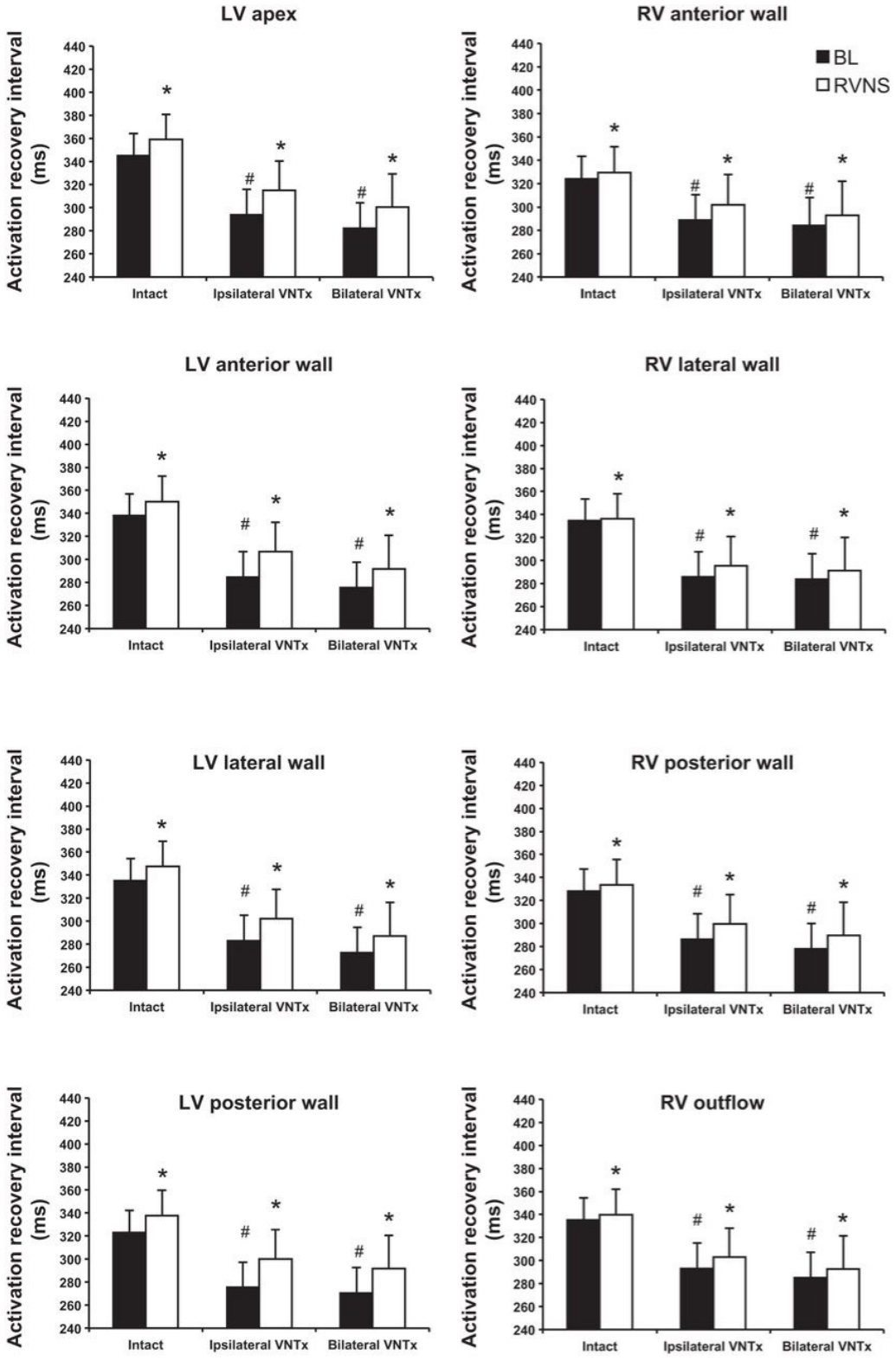

Figure 6. Regional cardiac electrical indices during right vagus nerve stimulation (RVNS) before and after ipsilateral and bilateral vagus nerve transection (VNTx). Regional

activation recovery intervals (ARIs) decreased after ipsilateral VNTx with minimal additional effects after bilateral transection. ARIs prolonged in all regions during RVNS, without significant regional differences. * $P < 0.05$ *vs.* BL; # $P < 0.05$ *vs.* intact state.

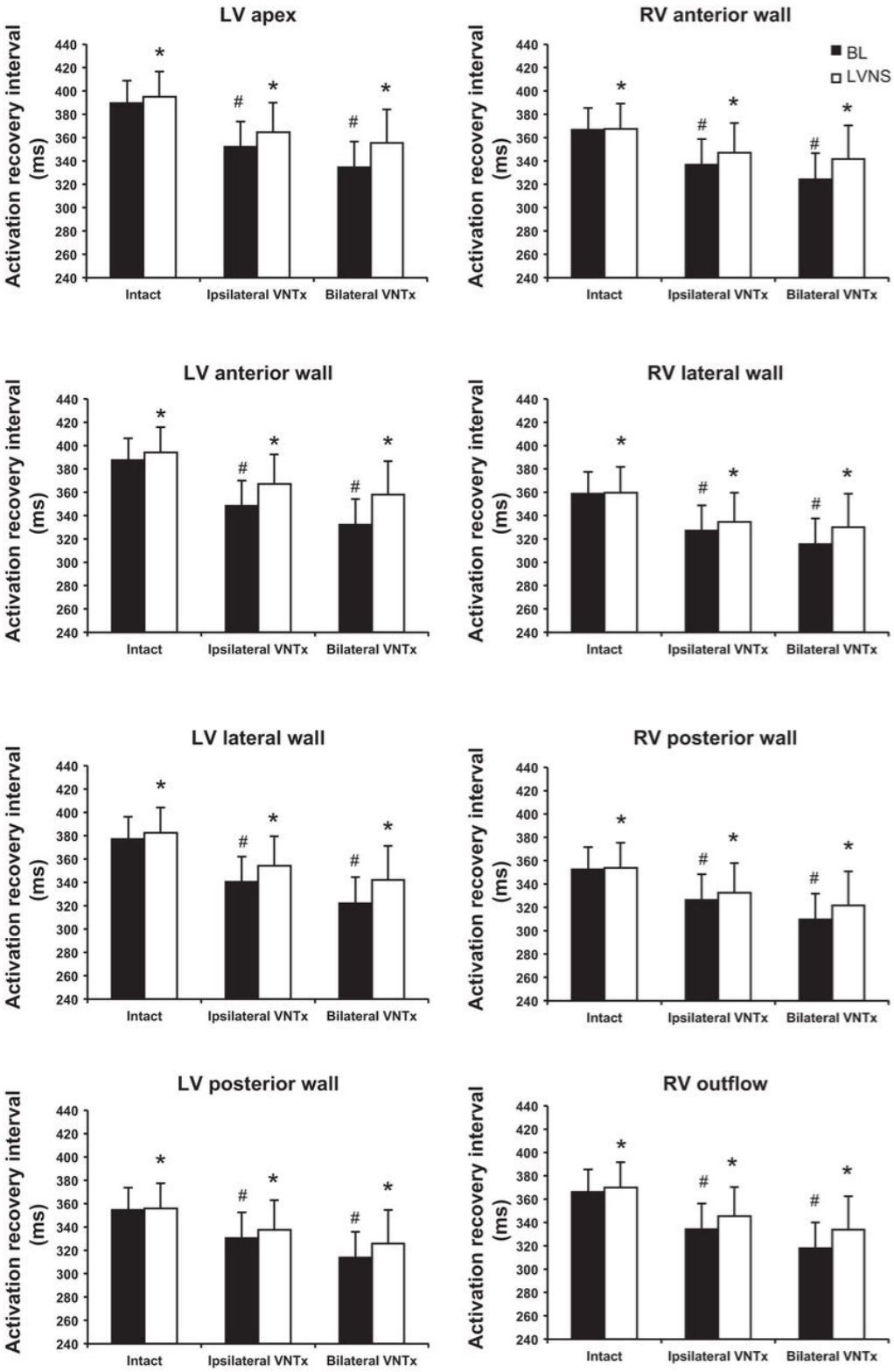

Figure 7. Regional cardiac electrical indices during left vagus nerve stimulation (LVNS) pre- and post-ipsilateral and bilateral vagus nerve transection (VNTx). Regional activation

recovery intervals (ARIs) were decreased by ipsilateral VNTx, and this difference became significant after bilateral transection. ARIs prolonged in all regions during LVNS, without significant regional differences. * $P < 0.05$ *vs.* BL; # $P < 0.05$ *vs.* intact state.

REFERENCES

1. Shen MJ and Zipes DP. Role of the autonomic nervous system in modulating cardiac arrhythmias. *Circulation research*. 2014;114:1004-21.
2. Vaseghi M and Shivkumar K. The role of the autonomic nervous system in sudden cardiac death. *Prog Cardiovasc Dis*. 2008;50:404-19.
3. Farrell TG, Paul V, Cripps TR, Malik M, Bennett ED, Ward D and Camm AJ. Baroreflex sensitivity and electrophysiological correlates in patients after acute myocardial infarction. *Circulation*. 1991;83:945-52.
4. Hull SS, Jr., Evans AR, Vanoli E, Adamson PB, Stramba-Badiale M, Albert DE, Foreman RD and Schwartz PJ. Heart rate variability before and after myocardial infarction in conscious dogs at high and low risk of sudden death. *Journal of the American College of Cardiology*. 1990;16:978-85.
5. Kleiger RE, Miller JP, Bigger JT, Jr. and Moss AJ. Decreased heart rate variability and its association with increased mortality after acute myocardial infarction. *Am J Cardiol*. 1987;59:256-62.
6. La Rovere MT, Bigger JT, Jr., Marcus FI, Mortara A and Schwartz PJ. Baroreflex sensitivity and heart-rate variability in prediction of total cardiac mortality after myocardial infarction. ATRAMI (Autonomic Tone and Reflexes After Myocardial Infarction) Investigators. *Lancet*. 1998;351:478-84.
7. Zhao M, Sun L, Liu JJ, Wang H, Miao Y and Zang WJ. Vagal nerve modulation: a promising new therapeutic approach for cardiovascular diseases. *Clin Exp Pharmacol Physiol*. 2012;39:701-5.
8. Katare RG, Ando M, Kakinuma Y, Arikawa M, Handa T, Yamasaki F and Sato T. Vagal nerve stimulation prevents reperfusion injury through inhibition of opening of mitochondrial permeability transition pore independent of the bradycardiac effect. *J Thorac Cardiovasc*

Surg. 2009;137:223-31.

9. Shinlapawittayatorn K, Chinda K, Palee S, Surinkaew S, Thunsiri K, Weerateerangkul P, Chattipakorn S, KenKnight BH and Chattipakorn N. Low-amplitude, left vagus nerve stimulation significantly attenuates ventricular dysfunction and infarct size through prevention of mitochondrial dysfunction during acute ischemia-reperfusion injury. *Heart Rhythm*. 2013;10:1700-7.
10. Schwartz PJ, Billman GE and Stone HL. Autonomic mechanisms in ventricular fibrillation induced by myocardial ischemia during exercise in dogs with healed myocardial infarction. An experimental preparation for sudden cardiac death. *Circulation*. 1984;69:790-800.
11. Sabbah HN, Ilsar I, Zaretsky A, Rastogi S, Wang M and Gupta RC. Vagus nerve stimulation in experimental heart failure. *Heart Fail Rev*. 2011;16:171-8.
12. Yamakawa K, So EL, Rajendran PS, Hoang JD, Makkar N, Mahajan A, Shivkumar K and Vaseghi M. Electrophysiological effects of right and left vagal nerve stimulation on the ventricular myocardium. *Am J Physiol Heart Circ Physiol*. 2014;307:H722-31.
13. Prechtl JC and Powley TL. The fiber composition of the abdominal vagus of the rat. *Anatomy and embryology*. 1990;181:101-15.
14. W J. Functional anatomy of the peripheral sympathetic and parasympathetic system. . In: J. W., ed. *The Integrative Action of the Autonomic Nervous System: Neurobiology of Homeostasis* Cambridge: Cambridge University Press; 2006: 13-34.
15. Hoover DB, Shepherd AV, Southerland EM, Armour JA and Ardell JL. Neurochemical diversity of afferent neurons that transduce sensory signals from dog ventricular myocardium. *Autonomic neuroscience : basic & clinical*. 2008;141:38-45.
16. Ando M, Katare RG, Kakinuma Y, Zhang D, Yamasaki F, Muramoto K and Sato T. Efferent vagal nerve stimulation protects heart against ischemia-induced arrhythmias by preserving connexin43 protein. *Circulation*. 2005;112:164-70.

17. Brooks WW, Verrier RL and Lown B. Influence of vagal tone on stellectomy-induced changes in ventricular electrical stability. *The American journal of physiology*. 1978;234:H503-7.

18. James R, Arnold J, Allen JD, Pantridge JF and Shanks RG. The effects of heart rate, myocardial ischemia and vagal stimulation on the threshold for ventricular fibrillation. *Circulation*. 1977;55:311-317.

19. Kolman BS, Verrier RL and Lown B. The effect of vagus nerve stimulation upon vulnerability of the canine ventricle: role of sympathetic-parasympathetic interactions. *Circulation*. 1975;52:578-85.

20. Matta RJ, Verrier RL and Lown B. Repetitive extrasystole as an index of vulnerability to ventricular fibrillation. *The American journal of physiology*. 1976;230:1469-73.

21. Rosenshtraukh L, Danilo P, Anyukhovsky EP, Steinberg SF, Rybin V, Brittain-Valenti K, Molina-Viamonte V and Rosen MR. Mechanisms for vagal modulation of ventricular repolarization and of coronary occlusion-induced lethal arrhythmias in cats. *Circulation research*. 1994;75:722-732.

22. Takahashi N, Ito M, Iwao T, Ohie T, Yonemochi H, Nakagawa M, Saikawa T and Sakata T. Vagal modulation of ventricular tachyarrhythmias induced by left ansae subclaviae stimulation in rabbits. *Jpn Heart J*. 1998;39:503-11.

23. Waxman MB, Sharma AD, Asta J, Cameron DA and Wald RW. The protective effect of vagus nerve stimulation on catecholamine-halothane-induced ventricular fibrillation in dogs. *Can J Physiol Pharmacol*. 1989;67:801-9.

24. Yoon MS, Han J, Tse WW and Rogers R. Effects of vagal stimulation, atropine, and propranolol on fibrillation threshold of normal and ischemic ventricles. *Am Heart J*. 1977;93:60-5.

25. Zuanetti G, De Ferrari GM, Priori SG and Schwartz PJ. Protective effect of vagal

stimulation on reperfusion arrhythmias in cats. *Circulation research*. 1987;61:429-435.

26. Brack KE, Coote JH and Ng GA. Vagus nerve stimulation protects against ventricular fibrillation independent of muscarinic receptor activation. *Cardiovascular research*. 2011;91:437-46.

27. Brack KE, Patel VH, Coote JH and Ng GA. Nitric oxide mediates the vagal protective effect on ventricular fibrillation via effects on action potential duration restitution in the rabbit heart. *J Physiol*. 2007;583:695-704.

28. Ng GA, Brack KE and Coote JH. Effects of direct sympathetic and vagus nerve stimulation on the physiology of the whole heart--a novel model of isolated Langendorff perfused rabbit heart with intact dual autonomic innervation. *Exp Physiol*. 2001;86:319-29.

29. Imataka K, Yamaoki K, Seki A, Takayama Y and Fujii J. Peculiar mitral valve and papillary muscle lesions induced by vagus manipulations in rabbits. An experimental model for nonrheumatic mitral regurgitation. *Japanese heart journal*. 1986;27:377-86.

30. Kerzner J, Wolf M, Kosowsky BD and Lown B. Ventricular Ectopic Rhythms following Vagal Stimulation in Dogs with Acute Myocardial Infarction. *Circulation*. 1973;47:44-50.

31. Scherf D, Blumenfeld S and Yildiz M. Experimental study on ventricular extrasystoles provoked by vagal stimulation. *American heart journal*. 1961;62:670-5.

32. Scherlag BJ, Kabell G, Harrison L and Lazzara R. Mechanisms of bradycardia-induced ventricular arrhythmias in myocardial ischemia and infarction. *Circulation*. 1982;65:1429-1434.

33. Takato T, Ashida T, Seko Y, Fujii J and Kawai S. Ventricular tachyarrhythmia-related basal cardiomyopathy in rabbits with vagal stimulation--a novel experimental model for inverted Takotsubo-like cardiomyopathy. *Journal of cardiology*. 2010;56:85-90.

34. Zannad F, De Ferrari GM, Tuinenburg AE, Wright D, Brugada J, Butter C, Klein H, Stolen C, Meyer S, Stein KM, Ramuzat A, Schubert B, Daum D, Neuzil P, Botman C, Castel MA,

D'Onofrio A, Solomon SD, Wold N and Ruble SB. Chronic vagal stimulation for the treatment of low ejection fraction heart failure: results of the NEural Cardiac TherApy foR Heart Failure (NECTAR-HF) randomized controlled trial. *European heart journal*. 2015;36:425-33.

35. Ajijola OA, Yagishita D, Patel KJ, Vaseghi M, Zhou W, Yamakawa K, So E, Lux RL, Mahajan A and Shivkumar K. Focal myocardial infarction induces global remodeling of cardiac sympathetic innervation: neural remodeling in a spatial context. *Am J Physiol Heart Circ Physiol*. 2013;305:H1031-40.
36. Vaseghi M, Yamakawa K, Sinha A, So EL, Zhou W, Ajijola OA, Lux RL, Laks M, Shivkumar K and Mahajan A. Modulation of regional dispersion of repolarization and T-peak to T-end interval by the right and left stellate ganglia. *Am J Physiol Heart Circ Physiol*. 2013;305:H1020-30.
37. Haws CW and Lux RL. Correlation between in vivo transmembrane action potential durations and activation-recovery intervals from electrograms. Effects of interventions that alter repolarization time. *Circulation*. 1990;81:281-8.
38. Millar CK, Kralios FA and Lux RL. Correlation between refractory periods and activation-recovery intervals from electrograms: effects of rate and adrenergic interventions. *Circulation*. 1985;72:1372-9.
39. Weiss JL, Frederiksen JW and Weisfeldt ML. Hemodynamic determinants of the time-course of fall in canine left ventricular pressure. *J Clin Invest*. 1976;58:751-60.
40. Hirota K and Ishiko N. Influences of the sympathetic and parasympathetic nerve transection on cardiovascular reflexes induced by volleys in the IXth nerve fibers of rat. *Journal of the autonomic nervous system*. 1994;46:237-49.
41. Jellinek M, Kaye MP, Kaiser GC and Cooper T. Effect of cervical vagosympathectomy on myocardial catecholamine concentration. *The American journal of physiology*.

1965;209:951-4.

42. Maccanon DM and Horvath SM. Effect of bilateral cervical vagotomy in the dog. *The American journal of physiology*. 1957;189:569-72.

43. Olgin JE, Takahashi T, Wilson E, Vereckei A, Steinberg H and Zipes DP. Effects of thoracic spinal cord stimulation on cardiac autonomic regulation of the sinus and atrioventricular nodes. *Journal of cardiovascular electrophysiology*. 2002;13:475-81.

44. Schwartz PJ, Verrier RL and Lown B. Effect of stellectomy and vagotomy on ventricular refractoriness in dogs. *Circulation research*. 1977;40:536-40.

45. Herre JM and Thames MD. Responses of sympathetic nerves to programmed ventricular stimulation. *Journal of the American College of Cardiology*. 1987;9:147-53.

46. Kalia M and Sullivan JM. Brainstem projections of sensory and motor components of the vagus nerve in the rat. *J Comp Neurol*. 1982;211:248-65.

47. Standish A, Enquist LW and Schwaber JS. Innervation of the heart and its central medullary origin defined by viral tracing. *Science*. 1994;263:232-4.

48. Armour JA. The little brain on the heart. *Cleve Clin J Med*. 2007;74 Suppl 1:S48-51.

49. Armour JA, Murphy DA, Yuan BX, Macdonald S and Hopkins DA. Gross and microscopic anatomy of the human intrinsic cardiac nervous system. *Anat Rec*. 1997;247:289-98.

50. Huang WA, Shivkumar K and Vaseghi M. Device-based autonomic modulation in arrhythmia patients: the role of vagal nerve stimulation. *Current treatment options in cardiovascular medicine*. 2015;17:379.

51. Ng GA, Brack KE, Patel VH and Coote JH. Autonomic modulation of electrical restitution, alternans and ventricular fibrillation initiation in the isolated heart. *Cardiovascular research*. 2007;73:750-60.

52. Takahashi N, Ito M, Ishida S, Fujino T, Saikawa T and Arita M. Effects of vagal stimulation on cesium-induced early afterdepolarizations and ventricular arrhythmias in rabbits.

Circulation. 1992;86:1987-1992.

53. Randall WC and Armour JA. Complex cardiovascular responses to vagosympathetic stimulation. *Proceedings of the Society for Experimental Biology and Medicine Society for Experimental Biology and Medicine*. 1974;145:493-9.

54. Schwartz PJ, Pagani M, Lombardi F, Malliani A and Brown AM. A cardiocardiac sympathovagal reflex in the cat. *Circulation research*. 1973;32:215-20.

55. Barron KW and Bishop VS. The influence of vagal afferents on the left ventricular contractile response to intracoronary administration of catecholamines in the conscious dog. *Circulation research*. 1981;49:159-69.

56. Chen LN, Zang WJ, Yu XJ, Liu J, Li DL, Kong SS, Lu J and Xu XL. Compensatory recovery of vagal control of hemodynamics after unilateral vagotomy. *Physiological research / Academia Scientiarum Bohemoslovaca*. 2008;57:119-32.

CHAPTER 3

Central-peripheral neural network interactions evoked by vagus nerve stimulation: functional consequences on control of cardiac function

Cardiac control is a manifestation of a neural hierarchy that can be considered in 3 levels.[1-3] Level 1 comprises the spinal cord and medulla as modulated by higher centers of the central nervous system.[4-7] Level 2 comprises extracardiac intrathoracic neurons contained in the stellate, middle cervical, and mediastinal ganglia.[8-10] Level 3 involves the intrinsic cardiac nervous system.[1] The peripheral levels (levels 2 and 3) form cardio-centric control loops, while the central nervous system (level 1) engages neural mechanisms for both cardiac and peripheral vasculature regulation.[3, 11] Acting together, these hierarchical populations regulate regional cardiac electrical, mechanical, and metabolic indices throughout each cardiac cycle.[1, 12, 13] Endogenous or exogenous stresses have the potential to impact multiple levels of this hierarchy.[2, 11, 14, 15] It is through the understanding of such hierarchical control and how it adapts to acute and chronic stress that rationale, mechanistic-based approaches can be devised to target the cardiac neural hierarchy in order to manage cardiovascular pathology.[2, 15, 16]

The vagus nerve is a complex neural structure, containing descending efferent parasympathetic fibers and ascending afferent fibers. Efferent parasympathetic fibers modulate several cardiac indices including chronotropy, dromotropy, inotropy, and lusitropy.[17, 18] The majority of fibers (~80%) contained within the vagus are afferent (sensory) in nature.[19, 20] Thus, the vagus is an important pathway that carries sensory information from visceral organs, including the heart, to the central nervous system. There is also structural and functional data suggesting that the cervical vagal trunk contains a small population of sympathetic fibers.[21, 22]

Any bioelectronic approach for therapeutic neuromodulation must consider both direct and reactive (reflex) responses.[16] The vagus can be stimulated in many different ways, at a number of different levels, and for multiple pathologies. As such, the anatomic characteristics of the nerves being stimulated (afferent/efferent) and the functional impact of stimulation parameters (current, frequency, pulse width, waveform, and duty cycle) must be considered.[16, 19] Ultimately, these factors influence both off-target adverse effects, and more importantly, the acute and chronic efficacy of the applied therapy. In most clinical applications for cardiovascular

pathologies, electrical vagus nerve stimulation (VNS) is imposed unilaterally to either the right or left cervical vagosympathetic trunk.[23-25]

While preclinical and clinical studies have yielded encouraging results for VNS safety and efficacy for cardiovascular therapeutics,[16, 26] there is a major information deficit in understanding how VNS impacts central and peripheral aspects of the cardiac nervous system to exert its influence on cardiac control. Therefore, the objective of this study was to investigate the functional role of VNS-evoked changes in afferent *vs.* efferent fiber activation on integrated control of cardiac function.

METHODS

Mongrel dogs (n = 26, male or female, weighing 22.2 ± 0.5 kg) were used in this study. All experiments were performed in accordance with the guidelines set forth by the National Institutes of Health *Guide for the Care and Use of Laboratory Animals* and were approved by the East Tennessee State University Institutional Animal Care and Use Committee.

Surgical preparation

Animals were sedated with propofol (3-8 mg/kg, intravenous [i.v.]), followed by endotracheal intubation and mechanical ventilation. General anesthesia was maintained with isoflurane (1-2%, inhalation). Depth of anesthesia was assessed by monitoring corneal reflexes, jaw tone, and hemodynamic indices. Left femoral venous access was obtained for maintenance fluid and drug administration. Right femoral arterial access was obtained for monitoring aortic blood pressure. A pressure transducer catheter (Mikro-Tip; Millar Instruments, Houston, TX, USA) was inserted into the left ventricle (LV) chamber via the left femoral artery. Lateral incisions of the neck were made bilaterally to expose the cervical vagosympathetic trunks. At the completion of the surgery, general anesthesia was switched to *α*-chloralose (50 mg/kg i.v. bolus followed by 8-12 mg/kg/hr continuous i.v. infusion). Acid-base status was evaluated hourly (Irma TruePoint;

ITC, Edison, NJ, USA); respiratory rate and tidal volume were adjusted and/or sodium bicarbonate was infused as necessary to maintain blood gas homeostasis. At the completion of the experiments, animals were euthanized under deep anesthesia by inducing ventricular fibrillation via direct current stimulation.

VNS

Bipolar stimulating cuff electrodes (PerenniaFlex Model 304; Cyberonics Inc., Houston, TX, USA) were placed around the right and left cervical vagosympathetic trunks with the anodes positioned cephalad to the cathode. A stimulator with a photoelectric stimulation isolation unit (S88 and PSIU6; Grass Technologies, Warwick, RI, USA) was used to deliver square pulses to the nerves. Bradycardia threshold was defined as the current required to first produce a 5% decrease in heart rate (HR) at a frequency of 10 Hz and a pulse width of 500 μs in the intact state, and tachycardia threshold as the current required to first produce a 5% increase in HR. The effects of VNS on chronotropic, LV inotropic, and LV lusitropic function were evaluated over a range of currents (0-4.0 mA) at 10 Hz frequency and 500 μs pulse width. The effects of VNS were also evaluated over a range of frequencies (2, 5, 10, 15, 20, and 30 Hz), delivered at a current 1.2x the bradycardia threshold determined in the intact state and 500 μs pulse width. VNS was performed for 14 s followed by a 66-s off-phase. This time period was sufficient for cardiac indices to return to baseline with no degradation in the responses to VNS over the entire duration of the experiment. Following stimulations in the intact state, the vagus nerve was transected cranial to the stimulating electrode, and only vagal efferent fibers were stimulated in subsequent parts of the protocol.

Hemodynamic assessment

A pressure transducer catheter (Mikro-Tip; Millar Instruments) was inserted into the LV chamber and connected to a control unit (PCU-200; Millar Instruments). A lead II electrocardiogram was

recorded via subdermal needle electrodes and amplified by a pre-amplifier (P511; Grass Technologies). Hemodynamic data were collected with a data acquisition system (Power1401; Cambridge Electronic Design, Cambridge, UK) and analyzed off-line with Spike2 (Cambridge Electronic Design). Derived indices included HR, aortic blood pressure, LV end-systolic pressure, maximum rate of change in LV pressure (LV dP/dt_{max}), and minimum rate of change in LV pressure (LV dP/d$t_{min)}$. Off-line analysis was used to determine the average response for each of the indices at baseline and during VNS.

Experimental protocol

Animals were divided into 3 experimental groups (n = 26). In Group 1 (n = 10), the right and left vagus nerves were individually stimulated in the under the following 3 conditions: (1) intact state; (2) following right vagus nerve transection (VNTx); and then (3) following left transection (i.e., bilateral VNTx). In Group 2 (n = 10), the right and left vagus were individually stimulated under the following 3 conditions: (1) intact state; (2) following left transection; and then (3) following right transection (i.e., bilateral VNTx). In Group 3 (n = 6), the right and left vagus nerves were stimulated individually under the following 4 conditions: (1) intact state; (2) intact state + timolol, a non-selective beta-blocker (1 mg/kg i.v. bolus with 0.5 mg/kg i.v. bolus every 90 min as needed); (3) bilateral transection + timolol; and then (4) bilateral transection + timolol + atropine, a muscarinic blocker (1 mg/kg i.v. bolus).

Statistics

Data are presented as mean ± standard error of the mean. A repeated measures mixed analysis of variance model was used for comparisons of mean current and frequency curves generated under the different conditions. Repeated measures analysis of variance model with Tukey multiple comparison was used for analysis of threshold. P values < 0.05 were considered

to be statistically significant. Statistical analyses were performed with JMP Pro v11.2 (SAS Institute Inc., Cary, NC, USA).

RESULTS

VNS impacted multiple cardiac electrical and mechanical indices. Figure 1 shows a representative example of the response to right VNS (RVNS) at an intensity sufficient to evoke acute changes in cardiovascular function. Note that VNS caused a decrease in HR, blood pressure, left ventricular pressure, and LV dP/dt_{max} and an increase in LV dP/d$t_{min.}$ At VNS offset, all these indices rapidly recovered to baseline with a potential to transiently overshoot, especially at higher current and frequency levels.

Central-peripheral neural network interactions with VNS: effects on current intensity

Figure 2 shows percent changes in chronotropy, LV inotropy, and LV lusitropy in response to RVNS across different currents at the same frequency (10 Hz) and pulse width (500 μs) (1) in the intact state, (2) following ipsilateral (left panels) or contralateral VNTx (right panels), and then (3) following bilateral transection. Figure 3 shows the corresponding HR levels in each of the 3 conditions. In the intact state, RVNS evoked a tachycardia at lower currents (starting at ~0.25-0.50 mA) and a bradycardia at higher currents (Figures 2A and B, 3). This augmentation in HR at lower currents was eliminated following ipsilateral, but not contralateral, transection ($P < 0.004$ ipsilateral transection *vs.* intact state). RVNS following either ipsilateral or contralateral transection resulted in a larger reduction in HR and LV dP/dt_{max} and increase in LV dP/dt_{min} compared to the intact state. RVNS following bilateral transection resulted in a greater change in these indices beyond unilateral transection ($P < 0.0001$). This result is evident when evaluating either the relative (Figure 2) or absolute levels (Figure 3) of evoked responses to RVNS.

Figure 4 shows the percent changes in chronotropy, LV inotropy, and LV lusitropy in response to left VNS (LVNS) across a range of current intensities (1) in the intact state, (2) following ipsilateral (left panels) or contralateral transection (right panels), and then (3) following bilateral transection. The augmentation in HR at lower currents (starting at ~0.5 mA) was eliminated following ipsilateral, but not contralateral, transection ($P < 0.002$ ipsilateral transection *vs.* intact state). In the intact state, LVNS resulted in negligible changes in LV dP/dt_{max} and dP/dt_{min}, even at currents as high as 4.0 mA (Figure 4C-F). However, following ipsilateral, but not contralateral, transection, LVNS resulted in a larger reduction in HR and LV dP/dt_{max} and increase in LV dP/dt_{min} compared to the intact state ($P < 0.004$). LVNS following bilateral transection further enhanced these effects when compared to unilateral transection ($P < 0.0001$).

Central-peripheral neural network interactions with VNS: effects on threshold

Bradycardia threshold was defined as the current required to first produce a 5% decrease in HR with VNS at 10 Hz frequency and 500 μs pulse width. In Group 1, in which the right vagus was transected first, threshold for the RVNS in the intact state was 2.91 ± 0.18 mA and for LVNS was 3.47 ± 0.20 mA (Figure 5A). Following right VNTx, the thresholds decreased compared to the intact state (1.69 ± 0.17 mA, $P < 0.001$ for RVNS; 3.04 ± 0.27 mA, $P < 0.04$ for LVNS). Thresholds decreased further following bilateral transection (1.29 ± 0.16 mA for RVNS; 1.74 ± 0.19 mA for LVNS; $P < 0.001$ *vs.* intact state, $P < 0.002$ *vs.* right VNTx). Figure 5B displays the percent change in bradycardia threshold for RVNS and LVNS following right and bilateral transection compared to the intact state. A similar pattern was observed in the Group 2, in which the left vagus was transected first. Threshold for the RVNS in the intact state was 3.03 ± 0.24 mA and for LVNS was 2.99 ± 0.15 mA (Figure 5C). The thresholds decreased following left transection (2.56 ± 0.25 mA, $P < 0.001$ for RVNS; 1.81 ± 0.22 mA, $P < 0.001$ for LVNS). The thresholds decreased further following bilateral transection (1.64 ± 0.21 mA for RVNS; 1.32 ±

0.22 mA for LVNS; $P < 0.001$ *vs.* intact, $P < 0.002$ *vs.* left VNTx). Figure 5D displays the percent change in bradycardia threshold for RVNS and LVNS following left and bilateral transection compared to the intact state. Taken together, the bradycardia threshold following bilateral transection was ~50% lower than that established in the intact state for either RVNS or LVNS.

Tachycardia threshold was defined as the current required to first produce a 5% increase in HR during VNS. Across all animals in the intact state, the tachycardia threshold was 0.62 ± 0.04 mA for RVNS and 0.65 ± 0.06 for LVNS. The potential for VNS to augment HR at the lower ranges of current was maintained following contralateral transection (Figures 2B, 3B, and 4B), but eliminated by ipsilateral transection (Figures 2A, 3A, and 4A). VNS-evoked changes in chronotropic function occurred against a significant background of parasympathetic central drive, as evidenced by elevations in baseline HR following bilateral transection *vs.* the intact state (~110 *vs.* 60 beats/min; Table 1 and Figure 3).

Central-peripheral neural network interactions with VNS: effects of frequency

After determining thresholds in the intact state, the effects of VNS on chronotropy, LV inotropy, and LV lusitropy were evaluated over a range of frequencies (2-30 Hz) at the same current (1.2x bradycardia threshold determined in the intact state) and pulse width (500 μs). Figure 6 shows the percent changes in chronotropy, LV inotropy, and LV lusitropy in response to RVNS across a range of frequencies (1) in the intact state, (2) following ipsilateral (left panels) or contralateral VNTx (right panels), and then (3) following bilateral transection. In all conditions, increasing frequency resulted in a larger decrease in HR and LV dP/dt_{max} and increase in LV dP/dt_{min}. RVNS following ipsilateral transection resulted in a greater change in all indices compared to the intact state ($P < 0.0001$); however, only LV dP/dt_{min} was affected with RVNS after contralateral transection ($P < 0.0001$). RVNS following bilateral transection resulted in an additional change in all indices beyond unilateral transection ($P < 0.0001$).

Figure 7 shows the percent changes in chronotropy, LV inotropy, and LV lusitropy in response to LVNS across a range of frequencies (1) in the intact state, (2) following ipsilateral (left panels) or contralateral VNTx (right panels), and then (3) following bilateral transection. In all conditions, increasing frequency resulted in a larger reduction in HR and LV dP/dt_{max} and increase in LV dP/d$t_{min.}$ LVNS following either ipsilateral or contralateral transection resulted in a greater change in all indices compared to the intact state ($P < 0.0001$), with the exception of LV dP/dt_{max} following ipsilateral transection. LVNS following bilateral transection further enhanced these effects when compared to unilateral transection ($P < 0.0001$).

Central-peripheral neural network interactions with VNS: effects of autonomic blockade

Changes in cardiac function mediated by the autonomic nervous system are manifest, in part, by changes in parasympathetic and/or sympathetic outflows. While unilateral VNTx and timolol exerted minimal effects on hemodynamic indices, bilateral transection was associated with an ~55% increase in HR (Tables 1 and 2). Figures 8 and 9 summarize VNS-evoked effects on chronotropy (Figures 8A and 9A), left ventricular end-systolic pressure (Figures 8B and 9B), LV inotropy, and LV lusitropy (Figures 8C and D, 9C and D) (1) in the intact state, (2) intact state + beta-blockade with timolol, (3) following bilateral transection + timolol, and finally (4) bilateral transection + timolol + muscarinic blockade with atropine. While timolol by itself exerted no effects on hemodynamic indices in response to RVNS (Figure 8), it did alter HR, LV dP/dt_{max}, and LV dP/dt_{min} in response to LVNS (Figure 9). Subsequent bilateral transection substantially enhanced VNS-induced changes in hemodynamic indices, which were abolished by atropine.

DISCUSSION

The aim of the present study was to determine the role of VNS-evoked afferent *vs.* efferent fiber activation on integrated control of regional cardiac indices. The major findings of this study are as follows:

(1) VNS-evoked changes in cardiac function, delivered to an intact vagus nerve, reflect the dynamic interplay between direct activation of descending efferent fibers against afferent-induced changes in central drive.
(2) The functional threshold for activation of vagal afferent fibers is lower than that for activation of efferent fibers.
(3) Activation of vagal afferents is primarily reflected as withdrawal of central parasympathetic drive.
(4) The potential exists for low-level sympathoexcitation as a result of bioelectric activation of vagal afferents.

Structure/function of the cervical vagosympathetic trunk: relationship to the neural hierarchy for cardiac control

The cervical vagosympathetic trunk is a mixed nerve containing both afferent and efferent fibers.[19, 27] Figure 10 schematically depicts the relationship of these projections within the overall framework of the cardiac neural hierarchy. The vagus contains ~80% afferent fibers, including both myelinated and unmyelinated axons.[19, 20] Cardiac-related vagal afferent neurons have cell bodies in the nodose ganglia that project sensory information onto secondary neurons located in the nucleus tractus solitarii of the medulla.[27-29] These secondary neurons project primarily to neurons in the nucleus ambiguus for control of efferent parasympathetic preganglionic neurons and, via brainstem reticulospinal projections, to the spinal cord intermediolateral cell column for control of efferent sympathetic preganglionic neurons.[4, 11, 28, 30] Sympathetic afferents, arising from the dorsal root ganglia, likewise input to the nucleus tractus solitarii via spinoreticular projections to contribute to reflex control of cardiac function.[4, 11, 31]

Cardiac-related efferent projections contained within the cervical vagosympathetic trunk are predominantly parasympathetic preganglionic fibers.[17, 22] Parasympathetic preganglionic neurons have cell bodies in the nucleus ambiguus and projections that innervate intrinsic

cardiac ganglia located within atrial and ventricular myocardial tissue, directly synapsing on parasympathetic postganglionic neurons (Figure 10). They also modulate the activity of local circuit neurons contained within intrinsic cardiac ganglia.[1, 12] Local circuit neurons represent the predominant subpopulation (~80%) contained within intrinsic cardiac nervous system (ICNS) and are responsible for local reflex control of cardiac function.[1, 12, 32] The direct parasympathetic projection pathway (i.e., pre- to postganglionic neurons) represents ~15% of intrinsic cardiac neurons.[12, 33, 34] The remaining 5% are afferent.[12, 32] There is also anatomical and functional evidence to indicate that the vagosympathetic trunk contains a small number of sympathetic efferent fibers.[21, 22] These sympathetic fibers are thought to originate from neurons in the superior and middle cervical ganglia.[18, 21, 30] Sympathetic fibers to the heart can either directly project to cardiac myocyte end-effectors or modulate cardiac function via interactions mediated within the ICNS.[12, 35-37]

VNS induced changes in regional cardiac function: hierarchical interactions

Any bioelectronic approach for neuromodulation needs to be considered in the context of the cardiac nervous system as a whole, as there are both direct and reactive (reflex) responses that are evoked.[16] Thus, to understand the central and peripheral neural network interactions within the cardiac neuronal hierarchy evoked by VNS, we studied the effects of VNS in the intact state, following sequential transection, and in the presence of autonomic blockade.

Chronotropic control: In the intact state, tachycardias evoked at low stimulus intensities (~0.6 mA) transitioned to bradycardias at higher intensities (~3.0 mA). VNS-induced tachycardias were maintained after contralateral transection, but eliminated by ipsilateral transection. Pre-treatment with a beta-blocker did not affect VNS-evoked positive chronotropic effects. The positive chronotropic responses were also manifest at stimulus intensities below that required to evoke bradycardias following bilateral transection. Moreover, VNS-evoked changes in HR in the intact state were elicited against a significant background of

parasympathetic central drive, as evidenced by elevations in baseline HR following bilateral transection *vs*. the intact state (~110 *vs.* 60 beats/min; Table 1 and Figure 3). Taken together, these data support the hypothesis that vagal afferent fibers are activated at lower currents and that stimulation of these fibers leads to withdrawal of central parasympathetic drive.

In the present study, we also demonstrate that the VNS bradycardia threshold, the current required to first produce a 5% decrease in HR, reflects the interdependent interactions between central and peripheral aspects of the cardiac nervous system. This threshold progressively decreased following sequential transection, regardless of whether the right or left vagus was transected first. Compared to the intact state, the bradycardia threshold was reduced by approximately 50% when the peripheral ends of the cervical vagosympathetic trunks were stimulated in the decentralized state.

Efferent outflow from the ICNS to cardiac tissues reflect the dynamic interactions between central drive and local afferent feedback as modulated by LCNs. LCNs subserve intra- and inter-ganglionic communication, thereby acting as coordinators of regional cardiac function.[1, 12, 32] When intrinsic cardiac ganglion function is evaluated *in vitro*, the principal synapse between pre- to postganglionic parasympathetic fibers is primarily obligatory in nature.[38-40] Thus, the evoked response to VNS when delivered in the bilateral decentralized state *in vivo* most closely approximates that *in vitro* condition. The differences in VNS-evoked responses between bilateral transection, unilateral transection, and the intact state reflect the hierarchical organization of the interdependent reflex control circuits whose ultimate function is to stabilize and optimize cardiac electrical, mechanical, and metabolic function.[12]

There are multiple hypotheses to explain observed decreases in threshold. The first reflects the role of vagal afferent fibers in reflexly modulating parasympathetic efferent outflow to the heart. Our data indicate that activated vagal afferents initiate centrally-mediated reflexes that inhibit parasympathetic efferent outflow to the heart. As such, the level of activity on a given parasympathetic postganglionic neuron within an intrinsic cardiac ganglion would reflect not only

diminished endogenous central drive, but also inputs arising from direct electrical activation of parasympathetic efferent fibers. Since both vagi project to neurons throughout the ICNS,[1, 41] this would have the net effect of shifting the VNS chronotropic response surface/curve to the right. A second hypothesis is that bioelectrical stimulation of the cervical vagosympathetic trunk activates fibers projecting to the LCNs in the ICNS that, in turn, inhibit the direct pre- to postganglionic parasympathetic neuron pathways.[42] We have previously demonstrated that similar inputs to the ICNS can initiate directionally opposite responses from adjacent intrinsic cardiac neurons that reflect this potential.[12] In the context of the current study, this proposed descending direct inhibitory mechanism is unlikely to be functionally important since it should also occur following unilateral VNTx and, as such, response surfaces would not have shifted, as was observed in this study. A third hypothesis involves induced alterations in sympathetic-parasympathetic interactions both within the ICNS and at the end-effectors.[36, 37] Such a mechanism would, at best, represent a minor component, as reflected in the minimal changes observed with VNS in the presence of beta-blockade. However, the fall in LV pressure and systemic blood pressure following bilateral transection may reflect a tonic sympathetic component mediated by fibers contained within the cervical vagosympathetic trunks, or alterations in integrated reflex control resulting from the loss of afferent inputs. A fourth possibility is that transection alters the neural interactions/balance for control of the sinoatrial nodal complex.[36] In this regard, a similar mechanism could also occur within other intrinsic cardiac LCN populations regulating atrial and/or ventricular contractile function.[43, 44] Future experiments will be required to explore these hypotheses.

Inotropic and lusitropic control: Integrated parasympathetic control of atrial, atrioventricular, and ventricular function is mediated via parasympathetic preganglionic inputs to the distributed network of interdependent intrinsic cardiac ganglionated plexi.[1, 43, 45] While earlier work suggested that vagal restraint on inotropic function is manifest against an enhanced sympathetic background (e.g., accentuated antagonism),[46, 47] later work has demonstrated that

activation of the ICNS, either endogenously or exogenously, impacts cardiac contraction and relaxation directly.[43, 44, 48] As is evident from the VNS intensity plots depicted herein (Figures 2-4), with intact vagi the magnitude of the evoked inotropic and lusitropic responses are moderate (~5% of baseline). Subsequent to transection, responses evoked in ventricular contractility were shifted to the left to substantially greater levels. This shift is likewise evident when a fixed output current was applied (Figures 6 and 7), where even at the lowest frequency (2 Hz), the minimal change in contractility evoked in the intact state transitioned to ~15-25% decreases following bilateral transection. These data demonstrate that in the intact state the neuronal hierarchy for cardiac control has a substantial buffering capacity that acts reflexly to maintain cardiac stability in the face of endogenous and exogenous stresses, including those induced by VNS itself.

Differential effects of VNS on autonomic efferent outflows

Parasympathetic and sympathetic divisions of the autonomic nervous system cannot be considered in isolation as they function as interdependent components of the cardiac neuronal hierarchy.[1, 2, 49] As such, changes in autonomic efferent outflow in response to VNS therapy reflect: (1) direct activation of autonomic efferent fibers; (2) central reflex-induced changes in efferent activity in response to bioelectrical activation of vagal afferent fibers; and (3) reflex induced changes in autonomic function as cardiovascular afferents transduce altered mechanical stress in both cardiac and extracardiac (e.g., arterial baroreceptors) sites that accompany VNS-induced effects on cardiac function.[11, 50, 51] Data presented in Figures 8 and 9 demonstrate that sympathetic efferent fibers within the vagosympathetic trunk have a minor contribution to the evoked response to VNS, as delineated by the minimal changes in VNS-induced effects on cardiac indices post-timolol infusion. In contrast, atropine blocked induced changes in chronotropic, LV inotropic, and LV lusitropic function, even against the enhanced sensitivity imposed by bilateral transection.

VNS and the neural fulcrum

When considering stimulation parameters necessary for VNS therapy one must be cognizant of not only the anatomic/functional characteristics of the fibers being stimulated (afferent/efferent), but also the effects of direct *vs.* reactive (reflex) changes that result from the entire cardiac neuronal hierarchy attempting to maintain stability of cardiac function.[16] Since the hierarchy normally acts as a negative feedback system, perturbing the system in one direction evokes a corresponding reflex response in the opposite direction. The greater the perturbation, the greater the reflex response and instability of the entire system.

As such, we propose that the optimum therapeutic parameters for VNS therapy are at the point at which afferent and efferent fibers are activated in a balanced manner. That is, when afferent-driven decreases in central parasympathetic drive are counteracted by direct activation of the cardiac parasympathetic efferent projections to the heart, with the net result being a null HR response.[42, 52] We define this point as the neural fulcrum. VNS performed near the neural fulcrum operates within the normal constraints of the cardiac neuronal hierarchy, without evoking the reactive changes that occur when high currents and/or frequencies are utilized.[42]

Clinical perspectives

Autonomic imbalance plays an important role in the genesis of cardiac arrhythmias and progression of heart failure.[2, 14, 53, 54] Sympathetic activation and parasympathetic withdrawal is not only pro-arrhythmic,[2] but also accelerates progression of heart failure.[11, 15, 55, 56] Furthermore, heart failure patients with poor vagal tone are known to have a worse prognosis.[57] In animal models of chronic heart failure, VNS has been shown to decrease resting HR, improve LV function, and decrease mortality, presumably by preventing adverse cardiac remodeling.[58] Given the promising results from preclinical studies, VNS is currently being evaluated in multiple clinical trials for reduced ejection fraction heart failure. These include the *In*crease *o*f *Va*gal *T*on*e* in *H*eart *F*ailure (INOVATE-HF), *N*e*u*ral *C*ardiac *T*herapy fo*r H*eart *F*ailure (NECTAR-HF),

and *A*utonomic *N*eural Regulation *Th*erapy to *E*nhance *M*yocardial Function in *H*eart *F*ailure (ANTHEM-HF).[23-25] Initials results of these trials have been positive for INOVATE-HF and ANTHEM-HF, with neutral effects for NECTAR-HF after the first 6 months of follow-up. One of the key differences between these trials is the choice of stimulation parameters (current, frequency, pulse width and duty cycle) and, in the case of INOVATE-HF, a proposed methodology to induce transient vagal afferent block with VNS. Based on our data, for proposed application of afferent blockade, one should consider potential deleterious effects on the effective gain of VNS therapy.[25] Nevertheless, it is obvious from these ongoing trials that VNS is safe and feasible in the setting of reduced ejection fraction heart failure. Data from randomized, controlled studies are required to elucidate the impact of VNS on morbidity and mortality in patients with chronic heart failure syndrome.

In view of the data presented herein, future studies should consider what is subthreshold VNS. Multiple studies have recently evaluated the effects of low-level VNS for treatment of atrial arrhythmias and heart failure.[59, 60] It is obvious from our data that central and peripheral elements of the hierarchy for cardiac control become engaged by output current levels well below those required to cause a decrease in chronotropy. Thus, these data lead us to propose that (1) the chronic effects of VNS therapy rest primarily on the indirect pathways that target intrinsic cardiac LCNs, and (2) the optimal VNS stimulus parameters are coincident with the neural fulcrum.[42] Future studies on the efficacy of VNS therapy for heart failure should focus on optimization of stimulation parameters, patient selection, and therapeutic transition where indicated in the standard of care. As such, future preclinical and clinical studies should be designed to employ the entire cardiac nervous system to achieve long-term therapeutic benefits while minimizing off-target effects of VNS.

GRANTS

This work was supported by National Institutes of Health (NIH) National Heart, Lung and Blood Institute Grant R01HL071830 (J.L.A.) and Cyberonics Inc. (J.L.A.). P.S.R. was supported by NIH National Institute of General Medical Sciences Grant 2T32GM065823 and American Heart Association Grant 15PRE22230011.

DISCLOSURES

J.L.A. and J.A.A. serve as scientific advisors to Cyberonics, Inc. B.H.K. is an employee of Cyberonics. P.S.R. and H.A.N. report no conflicts of interest.

AUTHOR CONTRIBUTIONS

J.L.A. developed the concept and designed the research; J.L.A. and H.A.N. performed the experiments; J.L.A., P.S.R., and H.A.N. analyzed the data; J.L.A., P.S.R., H.A.N., B.H.K., and J.A.A. interpreted the results of the experiments; J.L.A. and P.S.R. prepared the figures; J.L.A., P.S.R., and J.A.A. drafted the manuscript; J.L.A., P.S.R., B.H.K., and J.A.A. edited and revised the manuscript; J.L.A., P.S.R., B.H.K., and J.A.A. approved the final version of the manuscript.

State	LV d*P*/dt$_{max}$ (mmHg/s)	LV d*P*/d*t*$_{min}$ (mmHg/s)	LVSP (mmHg)	Aortic BP (mmHg)	HR (beats/min)
Intact	2,011 ± 130	−2,402 ± 175	152.5 ± 6.3	127.4 ± 4.0	59.3 ± 3.6
Right vagus cut	1,819 ± 123	−2,334 ± 196	138.4 ± 8.2	119.8 ± 6.2	69.8 ± 4.0
Both vagi cut	1,914 ± 164	−2,234 ± 201	121.5 ± 9.4*#	111.5 ± 8.9*	112.8 ± 7.7*#
Intact	1,956 ± 153	−2,451 ± 176	149.5 ± 6.8	127.5 ± 6.3	62.0 ± 2.7
Left vagus cut	1,751 ± 140	−2,340 ± 163	150.0 ± 9.2	131.3 ± 7.6	69.2 ± 6.5
Both vagi cut	1,751 ± 152*	−2,180 ± 222	128.7 ± 12.3*#	119.9 ± 13.2	106.0 ± 5.4*#

Table 1. Hemodynamics effects of sequential vagus nerve transection. * $P \leq 0.05$ *vs.* intact state; # $P \leq 0.05$ unilateral vs. bilateral vagus transection. BP, blood pressure; HR, heart rate; LV, left ventricle; LVSP, left ventricular end-systolic pressure.

State	LV dP/dt$_{max}$ (mmHg/s)	LV dP/dt$_{min}$ (mmHg/s)	LVSP (mmHg)	Aortic BP (mmHg)	HR (beats/min)
Intact	2,045 ± 165	−2,700 ± 189	154.6 ± 13.0	131.7 ± 6.7	74.8 ± 4.6
Timolol	1,791 ± 52	−2,302 ± 117	143.4 ± 9.2	124.6 ± 3.6	67.7 ± 3.5
Timolol + vagi cut	2,060 ± 108	−2,375 ± 101	165.2 ± 16.5	143.9 ± 13.8	111.7 ± 6.0*#
Timolol + vagi cut + atropine	1,911 ± 110	−2,348 ± 109	142.9 ± 8.1	129.7 ± 7.2	114.2 ± 7.8*#

Table 2. Effects of beta-blockade, bilateral vagus nerve transection, and muscarinic blockade on hemodynamic indices. * $P \leq 0.05$ *vs.* intact state; # $P \leq 0.05$ *vs.* timolol. BP, blood pressure; HR, heart rate; LV, left ventricle; LVSP, left ventricular end-systolic pressure.

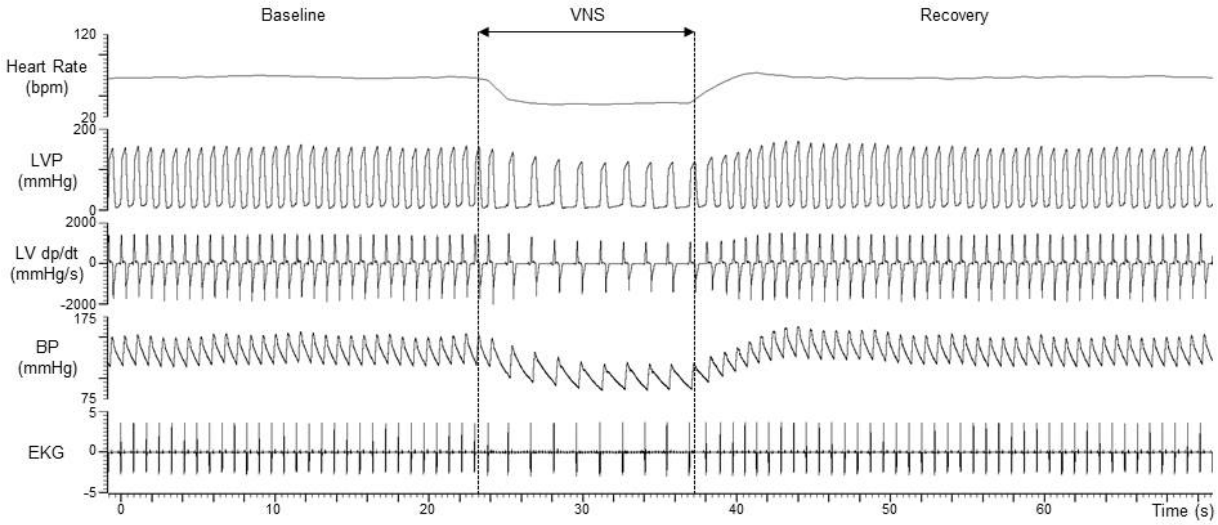

Figure 1. Representative hemodynamic response to right cervical vagus nerve stimulation (VNS) with both vagi intact. VNS was delivered at 10 Hz frequency, 500 μs pulse width, and 2.50 mA current for 14 s. BP, blood pressure; EKG, electrocardiogram; LVP, left ventricular pressure.

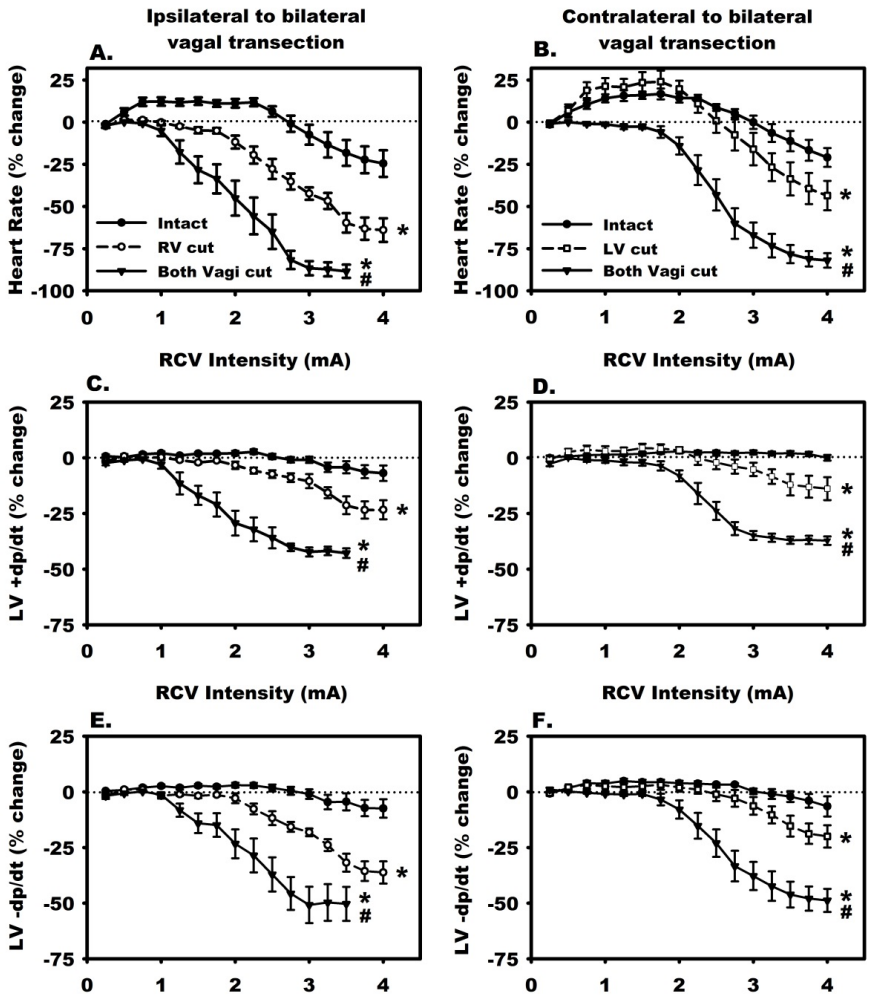

Figure 2. Evoked changes in cardiac hemodynamics in response to right cervical vagus nerve stimulation (RCV) at a range of currents (1) in the intact state, (2) following ipsilateral (left panels) or contralateral vagus transection (right panels), and then (3) following bilateral transection. RCV was delivered at 10 Hz frequency and 500 μs pulse width for 14 s. Responses reflect percent change from baseline during RCV as a function of stimulus intensity. Note that the augmenting effects of RCV were eliminated when the ipsilateral vagus was transected. * $P < 0.004$ *vs.* intact state; # $P < 0.0001$ unilateral *vs.* bilateral transection. LV, left ventricle.

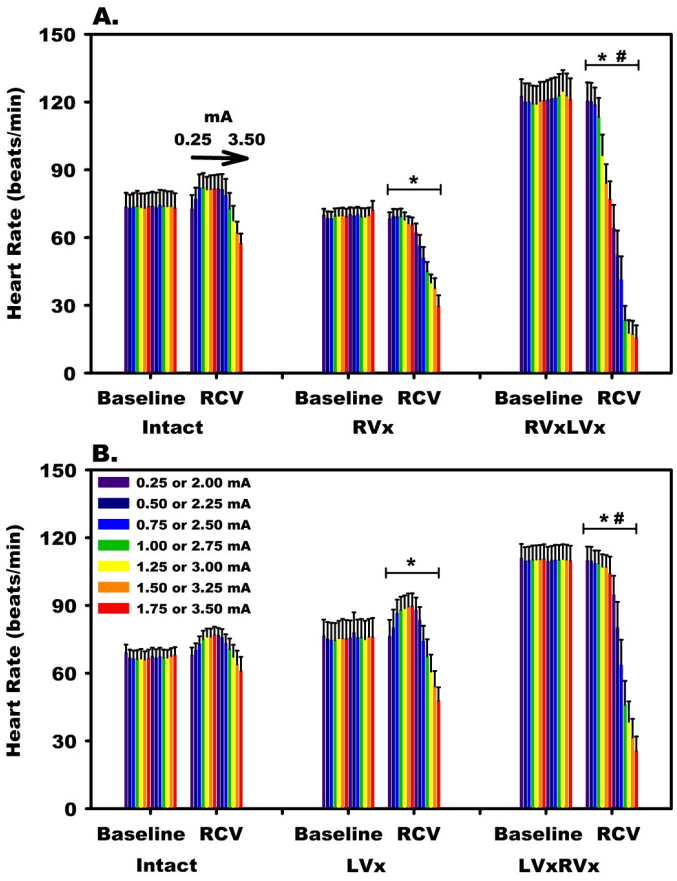

Figure 3. Evoked changes in heart rate in response to right cervical vagus nerve stimulation (RCV) at a range of currents (1) in the intact state, (2) following ipsilateral (panel A) or contralateral vagus transection (panel B), and then (3) following bilateral transection. RCV was delivered at 10 Hz frequency and 500 μs pulse width for 14 s. Note that all positive chronotropic responses to RCV were eliminated when the ipsilateral vagus was transected, and negative chronotropic responses progressively increased following unilateral and bilateral transection. * P < 0.001 *vs*. intact state; # P < 0.005 unilateral *vs.* bilateral vagus transection. LVx, left vagus transection; RVx, right vagus transection; RVxLVx/LVxRVx, bilateral transection.

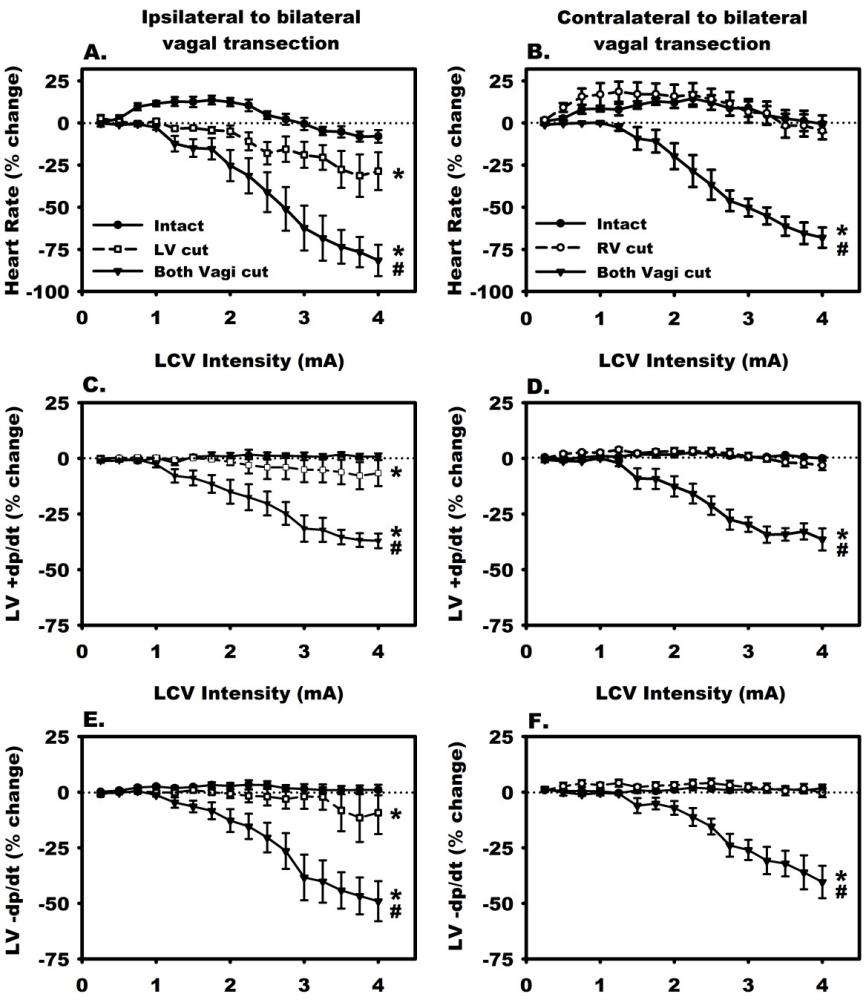

Figure 4. Evoked changes in cardiac hemodynamics in response to left cervical vagus nerve stimulation (LCV) at a range of currents (1) in the intact state, (2) following ipsilateral (left panels) or contralateral vagus nerve transection (right panels), and then (3) following bilateral transection. LCV was delivered at 10 Hz frequency and 500 μs pulse width for 14 s. Responses reflect percent change from baseline during LCV as a function of stimulus intensity. Note that the augmenting effects of LCV were eliminated when the ipsilateral vagus was transected. * $P < 0.002$ *vs.* intact state; # $P < 0.0001$ unilateral *vs.* bilateral transection. LV, left ventricle.

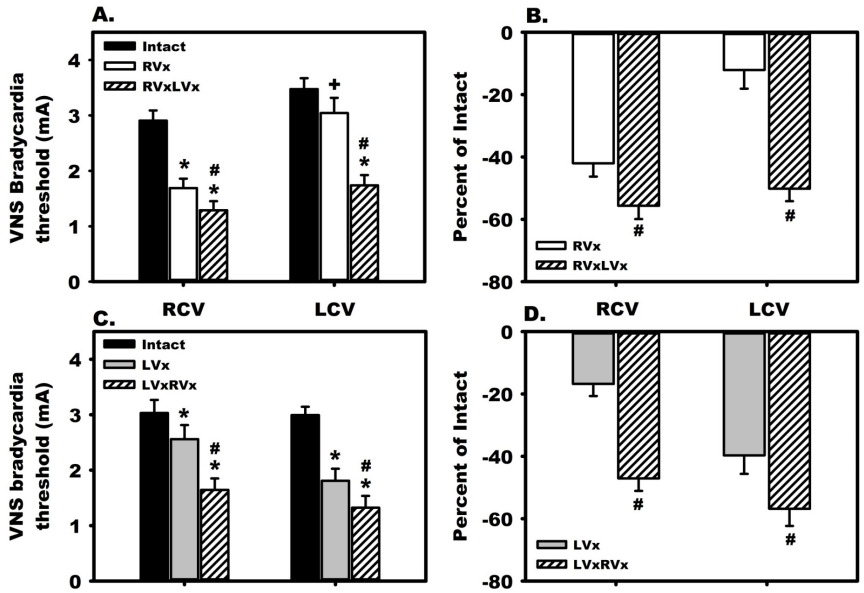

Figure 5. Vagus nerve stimulation (VNS) bradycardia threshold was reduced with sequential vagus nerve transection. Threshold was defined as the current required to evoke a 5% decrease in heart rate. **(A, C)** The threshold current (1) in the intact state, (2) following ipsilateral or contralateral vagus transection, and then (3) following bilateral transection. **(B, D)** The percent change in threshold from the intact state. * $P < 0.001$ *vs.* intact state; + $P < 0.04$ *vs.* intact state; # $P < 0.002$ unilateral *vs.* bilateral transection. LVx, left vagus transection; RVx, right vagus transection; RVxLVx/LVxRVx, bilateral transection.

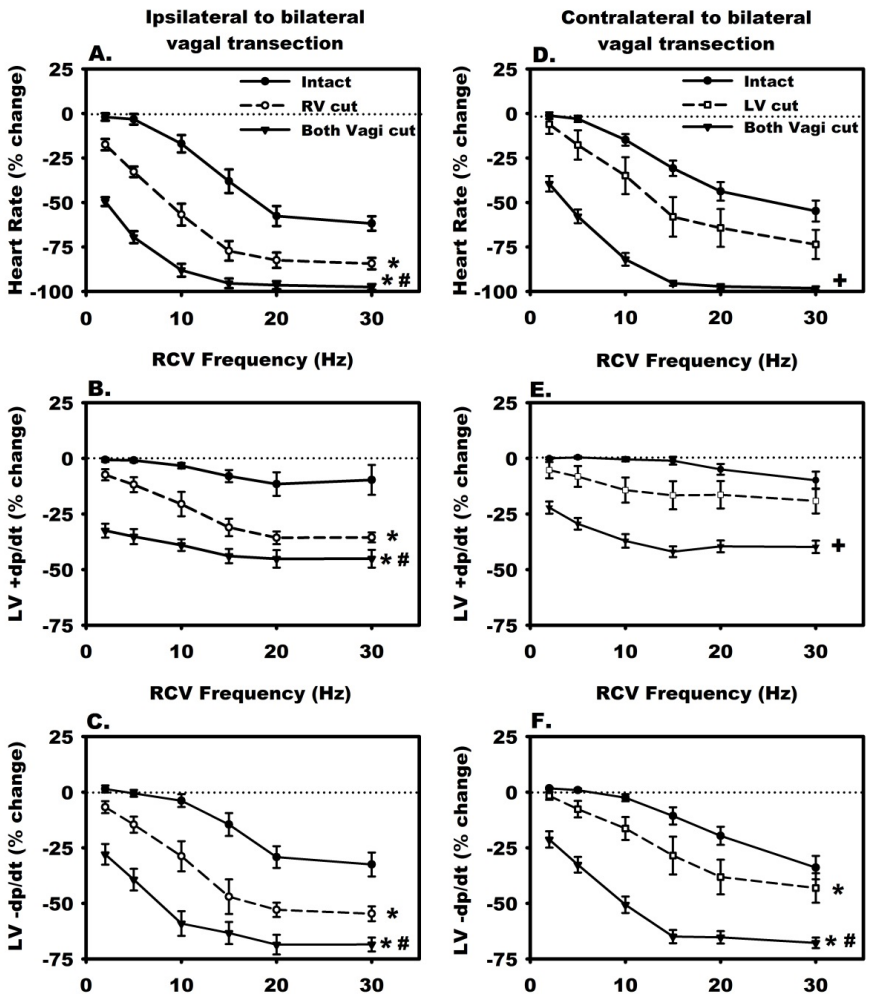

Figure 6. Evoked changes in cardiac hemodynamics in response to right cervical vagus nerve stimulation (RCV) at a range of different frequencies (1) in the intact state, (2) following ipsilateral (left panels) or contralateral vagus transection (right panels), and then (3) following bilateral transection. RCV was delivered at 1.2x the bradycardia threshold current determined in the intact state and 500 μs pulse width for 14 s. Responses reflect percent change from baseline during RCV as a function of frequency. * $P < 0.001$ *vs.* intact state; # $P < 0.0001$ unilateral *vs.* bilateral transection; + $P < 0.0001$ intact state *vs.* bilateral transection.

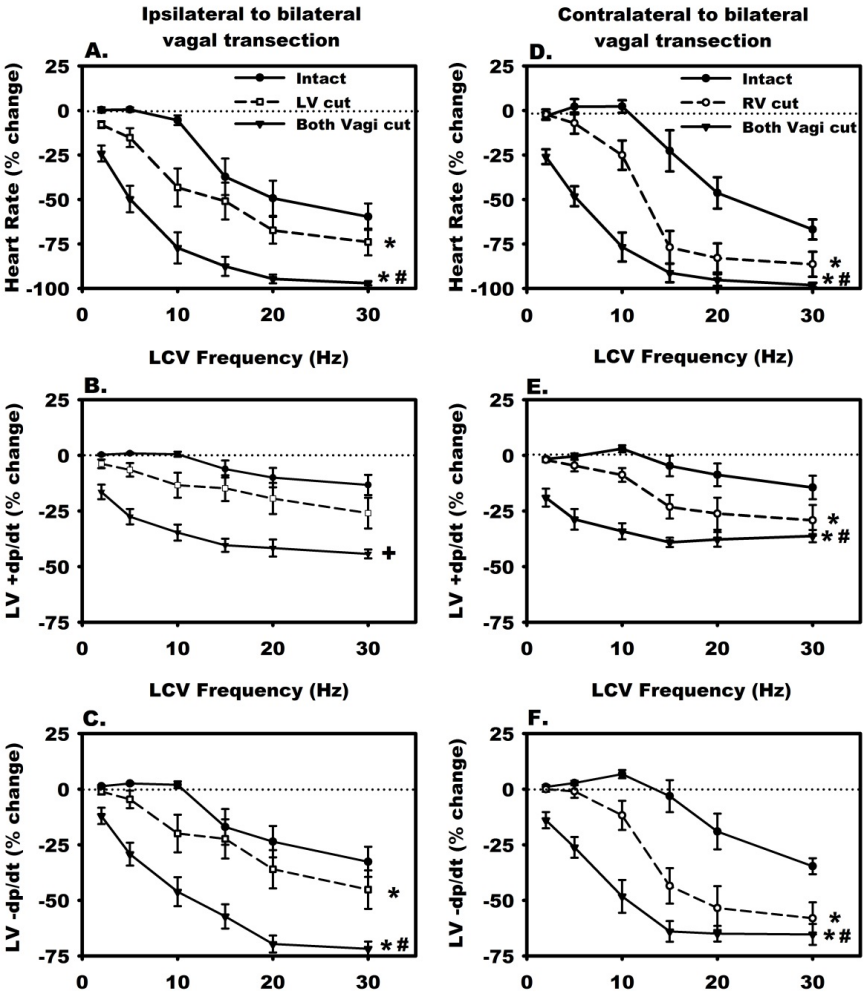

Figure 7. Evoked changes in cardiac hemodynamics in response to left cervical vagus nerve stimulation (LCV) at a range of different frequencies (1) in the intact state, (2) following ipsilateral (left panels) or contralateral vagus transection (right panels), and then (3) following bilateral transection. LCV was delivered at 1.2x the bradycardia threshold current determined in the intact state and 500 μs pulse width for 14 s. Responses reflect percent change from baseline during LCV as a function of frequency. * $P < 0.001$ *vs.* intact state; # $P < 0.0001$ unilateral *vs.* bilateral transection; + $P < 0.0001$ intact state *vs.* bilateral transection.

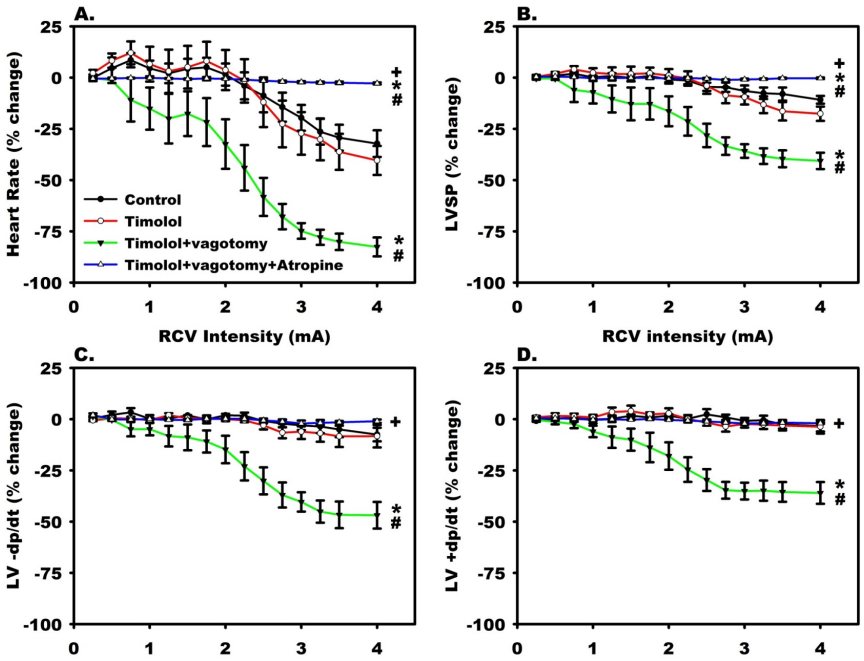

Figure 8. Evoked changes in cardiac hemodynamics in response to right cervical vagus nerve stimulation (RCV) (1) in the intact state, (2) in the intact state and non-selective beta blockade with timolol, (3) following bilateral vagus nerve transection and timolol, and then (4) following bilateral transection with timolol and muscarinic blockade with atropine. Responses reflect percent change from baseline during RCV as a function of stimulus intensity. * $P < 0.02$ vs. intact state; # $P < 0.001$ *vs*. timolol; + $P < 0.0001$ *vs.* bilateral transection and timolol. LV, left ventricle; LVSP, left ventricular end-systolic pressure.

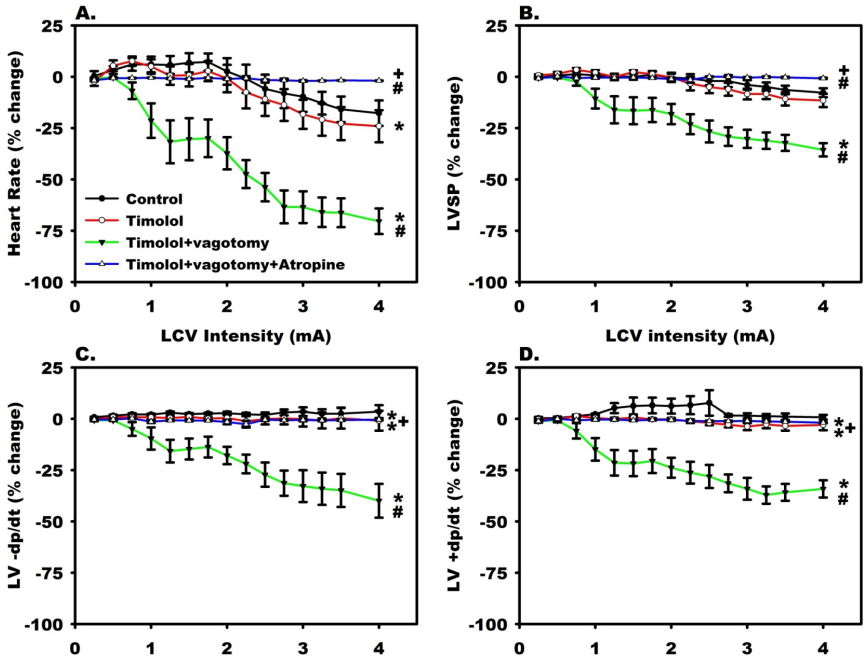

Figure 9. Evoked changes in cardiac hemodynamics in response to left cervical vagus nerve stimulation (LCV) (1) in the intact state, (2) in the intact state and non-selective beta blockade with timolol, (3) following bilateral vagus nerve transection and timolol, and then (4) following bilateral transection with timolol and muscarinic blockade with atropine. Responses reflect percent change from baseline during LCV as a function of stimulus intensity. * $P < 0.03$ vs. intact state; # $P < 0.003$ *vs*. timolol; + $P < 0.0001$ *vs.* bilateral transection and timolol. LV, left ventricle; LVSP, left ventricular end-systolic pressure.

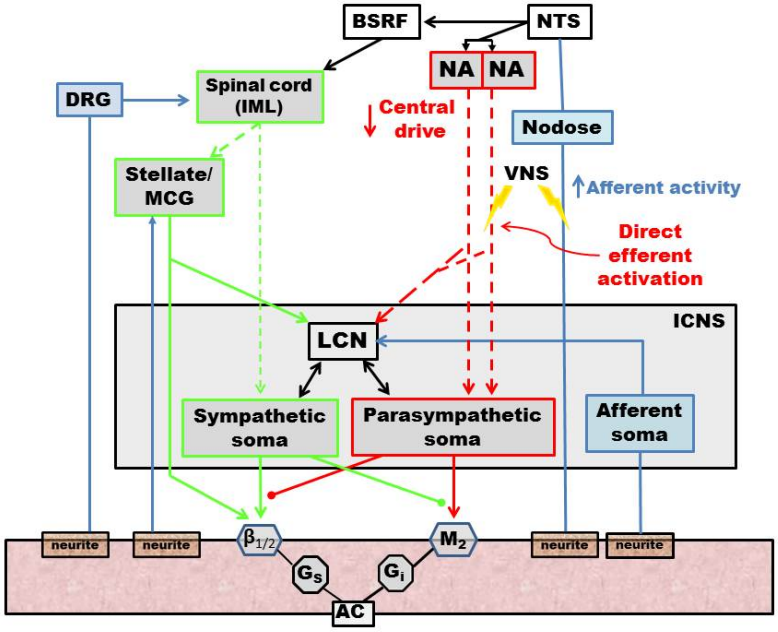

Figure 10. Schematic summarizing proposed interactions within cardiac neural hierarchy engaged by cervical vagus nerve stimulation (VNS). Dotted lines indicate preganglionic projections. AC, adenylate cyclase; β, beta adrenergic receptor; BSRF, brainstem reticular formation; DRG, dorsal root ganglia; G_i, inhibitory G-protein-coupled receptor; G_s, stimulatory G-protein-coupled receptor; IML, intermediolateral cell column; LCN, local circuit neuron; M_2, muscarinic receptor; MCG, middle cervical ganglia; NA, nucleus ambiguus; NTS, nucleus tractus solitaries.

REFERENCES

1. Armour JA. Potential clinical relevance of the 'little brain' on the mammalian heart. *Exp Physiol*. 2008;93:165-76.
2. Fukuda K, Kanazawa H, Aizawa Y, Ardell JL and Shivkumar K. Cardiac innervation and sudden cardiac death. *Circ Res*. 2015;116:2005-19.
3. Kember G, Armour JA and Zamir M. Neural control of heart rate: the role of neuronal networking. *Journal of theoretical biology*. 2011;277:41-7.
4. Andresen MC, Kunze DL and Mendelowitz D. Central Nervous System Regulation of the Heart. In: J. A. Armour and J. L. Ardell, eds. *Basic and Clincial Neurocardiology* New York: Oxford University Press; 2004: 187-219.
5. Coote JH. Myths and realities of the cardiac vagus. *The Journal of physiology*. 2013;591:4073-85.
6. Harper RM, Kumar R, Ogren JA and Macey PM. Sleep-disordered breathing: effects on brain structure and function. *Respiratory physiology & neurobiology*. 2013;188:383-91.
7. McAllen RM, Salo LM, Paton JF and Pickering AE. Processing of central and reflex vagal drives by rat cardiac ganglion neurones: an intracellular analysis. *The Journal of physiology*. 2011;589:5801-18.
8. Ardell JL, Cardinal R, Vermeulen M and Armour JA. Dorsal spinal cord stimulation obtunds the capacity of intrathoracic extracardiac neurons to transduce myocardial ischemia. *American journal of physiology Regulatory, integrative and comparative physiology*. 2009;297:R470-7.
9. Armour JA. Activity of in situ stellate ganglion neurons of dogs recorded extracellularly. *Canadian journal of physiology and pharmacology*. 1986;64:101-11.
10. Armour JA. Neuronal activity recorded extracellularly in chronically decentralized in situ canine middle cervical ganglia. *Canadian journal of physiology and pharmacology*. 1986;64:1038-46.

11. Zucker IH, Patel KP and Schultz HD. Neurohumoral stimulation. *Heart failure clinics*. 2012;8:87-99.
12. Beaumont E, Salavatian S, Southerland EM, Vinet A, Jacquemet V, Armour JA and Ardell JL. Network interactions within the canine intrinsic cardiac nervous system: implications for reflex control of regional cardiac function. *The Journal of physiology*. 2013;591:4515-33.
13. Armour JA. Cardiac neuronal hierarchy in health and disease. *American journal of physiology Regulatory, integrative and comparative physiology*. 2004;287:R262-71.
14. Kember G, Armour JA and Zamir M. Neural control hierarchy of the heart has not evolved to deal with myocardial ischemia. *Physiological genomics*. 2013;45:638-44.
15. Florea VG and Cohn JN. The autonomic nervous system and heart failure. *Circulation research*. 2014;114:1815-26.
16. Buckley U, Shivkumar K and Ardell JL. Autonomic Regulation Therapy in Heart Failure. *Curr Heart Fail Rep*. 2015.
17. Randall WC, Ardell JL and Becker DM. Differential responses accompanying sequential stimulation and ablation of vagal branches to dog heart. *The American journal of physiology*. 1985;249:H133-40.
18. Randall WC and Armour JA. Regional vagosympathetic control of the heart. *The American journal of physiology*. 1974;227:444-52.
19. Bonaz B, Picq C, Sinniger V, Mayol JF and Clarencon D. Vagus nerve stimulation: from epilepsy to the cholinergic anti-inflammatory pathway. *Neurogastroenterology and motility : the official journal of the European Gastrointestinal Motility Society*. 2013;25:208-21.
20. Prechtl JC and Powley TL. The fiber composition of the abdominal vagus of the rat. *Anatomy and embryology*. 1990;181:101-15.
21. Onkka P, Maskoun W, Rhee KS, Hellyer J, Patel J, Tan J, Chen LS, Vinters HV, Fishbein MC and Chen PS. Sympathetic nerve fibers and ganglia in canine cervical vagus nerves:

localization and quantitation. *Heart rhythm : the official journal of the Heart Rhythm Society*. 2013;10:585-91.

22. Randall WC and Armour JA. Complex cardiovascular responses to vagosympathetic stimulation. *Proceedings of the Society for Experimental Biology and Medicine Society for Experimental Biology and Medicine*. 1974;145:493-9.
23. Premchand RK, Sharma K, Mittal S, Monteiro R, Dixit S, Libbus I, DiCarlo LA, Ardell JL, Rector TS, Amurthur B, KenKnight BH and Anand IS. Autonomic Regulation Therapy via Left or Right Cervical Vagus Nerve Stimulation in Patients with Chronic Heart Failure: Results of the ANTHEM-HF Trial. *Journal of cardiac failure*. 2014;20:808-816.
24. De Ferrari GM, Tuinenburg AE, Ruble S, Brugada J, Klein H, Butter C, Wright DJ, Schubert B, Solomon S, Meyer S, Stein K, Ramuzat A and Zannad F. Rationale and study design of the NEuroCardiac TherApy foR Heart Failure Study: NECTAR-HF. *European journal of heart failure*. 2014;16:692-9.
25. De Ferrari GM, Crijns HJ, Borggrefe M, Milasinovic G, Smid J, Zabel M, Gavazzi A, Sanzo A, Dennert R, Kuschyk J, Raspopovic S, Klein H, Swedberg K, Schwartz PJ and CardioFit Multicenter Trial I. Chronic vagus nerve stimulation: a new and promising therapeutic approach for chronic heart failure. *European heart journal*. 2011;32:847-55.
26. Shen MJ and Zipes DP. Interventional and Device-Based Autonomic Modulation in Heart Failure. *Heart failure clinics*. 2015;11:337-348.
27. Hoover DB, Shepherd AV, Southerland EM, Armour JA and Ardell JL. Neurochemical diversity of afferent neurons that transduce sensory signals from dog ventricular myocardium. *Autonomic neuroscience : basic & clinical*. 2008;141:38-45.
28. Gray AL, Johnson TA, Lauenstein JM, Newton SS, Ardell JL and Massari VJ. Parasympathetic control of the heart. III. Neuropeptide Y-immunoreactive nerve terminals synapse on three populations of negative chronotropic vagal preganglionic neurons. *Journal of applied physiology*. 2004;96:2279-87.

29. Standish A, Enquist LW and Schwaber JS. Innervation of the heart and its central medullary origin defined by viral tracing. *Science*. 1994;263:232-4.
30. Hopkins DA and Armour JA. Localization of sympathetic postganglionic and parasympathetic preganglionic neurons which innervate different regions of the dog heart. *The Journal of comparative neurology*. 1984;229:186-98.
31. Foreman RD and Linderoth B. Neural mechanisms of spinal cord stimulation. *International review of neurobiology*. 2012;107:87-119.
32. Ardell JL, Butler CK, Smith FM, Hopkins DA and Armour JA. Activity of in vivo atrial and ventricular neurons in chronically decentralized canine hearts. *The American journal of physiology*. 1991;260:H713-21.
33. Armour JA and Hopkins DA. Activity of in vivo canine ventricular neurons. *The American journal of physiology*. 1990;258:H326-36.
34. Gagliardi M, Randall WC, Bieger D, Wurster RD, Hopkins DA and Armour JA. Activity of in vivo canine cardiac plexus neurons. *The American journal of physiology*. 1988;255:H789-800.
35. Vaseghi M, Zhou W, Shi J, Ajijola OA, Hadaya J, Shivkumar K and Mahajan A. Sympathetic innervation of the anterior left ventricular wall by the right and left stellate ganglia. *Heart rhythm : the official journal of the Heart Rhythm Society*. 2012;9:1303-9.
36. McGuirt AS, Schmacht DC and Ardell JL. Autonomic interactions for control of atrial rate are maintained after SA nodal parasympathectomy. *The American journal of physiology*. 1997;272:H2525-33.
37. Randall DC, Brown DR, McGuirt AS, Thompson GW, Armour JA and Ardell JL. Interactions within the intrinsic cardiac nervous system contribute to chronotropic regulation. *American journal of physiology Regulatory, integrative and comparative physiology*. 2003;285:R1066-75.

38. Hardwick JC, Southerland EM and Ardell JL. Chronic myocardial infarction induces phenotypic and functional remodeling in the guinea pig cardiac plexus. *American journal of physiology Regulatory, integrative and comparative physiology*. 2008;295:R1926-33.

39. Hardwick JC, Baran CN, Southerland EM and Ardell JL. Remodeling of the guinea pig intrinsic cardiac plexus with chronic pressure overload. *American journal of physiology Regulatory, integrative and comparative physiology*. 2009;297:R859-66.

40. Hardwick JC, Ryan SE, Beaumont E, Ardell JL and Southerland EM. Dynamic remodeling of the guinea pig intrinsic cardiac plexus induced by chronic myocardial infarction. *Autonomic neuroscience : basic & clinical*. 2014;181:4-12.

41. Ardell JL and Randall WC. Selective vagal innervation of sinoatrial and atrioventricular nodes in canine heart. *The American journal of physiology*. 1986;251:H764-73.

42. Kember G, Ardell JL, Armour JA and Zamir M. Vagal nerve stimulation therapy: what is being stimulated? *PloS one*. 2014;9:e114498.

43. Cardinal R, Page P, Vermeulen M, Ardell JL and Armour JA. Spatially divergent cardiac responses to nicotinic stimulation of ganglionated plexus neurons in the canine heart. *Autonomic neuroscience : basic & clinical*. 2009;145:55-62.

44. Yuan BX, Ardell JL, Hopkins DA and Armour JA. Differential cardiac responses induced by nicotine sensitive canine atrial and ventricular neurones. *Cardiovascular research*. 1993;27:760-9.

45. Yuan BX, Ardell JL, Hopkins DA, Losier AM and Armour JA. Gross and microscopic anatomy of the canine intrinsic cardiac nervous system. *The Anatomical record*. 1994;239:75-87.

46. Levy MN. Sympathetic-parasympathetic interactions in the heart. *Circulation research*. 1971;29:437-45.

47. Levy MN, Ng M, Martin P, Zieske H and Rogoff T. Sympathetic and parasympathetic interactions upon the left ventricle of the dog. *Circulation research*. 1966;19:5-10.

48. Randall DC, Brown DR, Li SG, Olmstead ME, Kilgore JM, Sprinkle AG, Randall WC and Ardell JL. Ablation of posterior atrial ganglionated plexus potentiates sympathetic tachycardia to behavioral stress. *The American journal of physiology*. 1998;275:R779-87.

49. Zucker IH and Gilmore JP. *Reflex Control of the Circulation*. Boca Raton: CRC Press; 1991.

50. Lohmeier TE and Iliescu R. The baroreflex as a long-term controller of arterial pressure. *Physiology*. 2015;30:148-58.

51. Armour JA and Kember G. Cardiac sensory neurons. In: J. A. Armour and J. L. Ardell, eds. *Basic and Clinical Neurocardiology* New York: Oxford University Press; 2004: 79-117.

52. Ardell JA, Beaumont E, Nier H, Southerland EM, Griffin S, KenKnight BH and Armour JA. Vagal Nerve Stimulation Elicits Heart Rate Responses that are Dependent on Relative Activation of both Central and Peripheral Limbs of the Autonomic Nervous System: Defining the Neural Fulcrum. *Heart rhythm : the official journal of the Heart Rhythm Society*. 2014.

53. Vaseghi M and Shivkumar K. The role of the autonomic nervous system in sudden cardiac death. *Progress in cardiovascular diseases*. 2008;50:404-19.

54. Shen MJ and Zipes DP. Role of the autonomic nervous system in modulating cardiac arrhythmias. *Circulation research*. 2014;114:1004-21.

55. Huang J, Qian J, Yao W, Wang N, Zhang Z, Cao C, Song B and Zhang Z. Vagus nerve stimulation reverses ventricular electrophysiological changes induced by hypersympathetic nerve activity. *Experimental physiology*. 2015;100:239-48.

56. Zhou S, Jung BC, Tan AY, Trang VQ, Gholmieh G, Han SW, Lin SF, Fishbein MC, Chen PS and Chen LS. Spontaneous stellate ganglion nerve activity and ventricular arrhythmia in a canine model of sudden death. *Heart rhythm : the official journal of the Heart Rhythm Society*. 2008;5:131-9.

57. Olshansky B, Sabbah HN, Hauptman PJ and Colucci WS. Parasympathetic nervous system and heart failure: pathophysiology and potential implications for therapy. *Circulation*. 2008;118:863-71.

58. Li M, Zheng C, Sato T, Kawada T, Sugimachi M and Sunagawa K. Vagal nerve stimulation markedly improves long-term survival after chronic heart failure in rats. *Circulation*. 2004;109:120-4.

59. Stavrakis S, Humphrey MB, Scherlag BJ, Hu Y, Jackman WM, Nakagawa H, Lockwood D, Lazzara R and Po SS. Low-level transcutaneous electrical vagus nerve stimulation suppresses atrial fibrillation. *Journal of the American College of Cardiology*. 2015;65:867-75.

60. Shen MJ, Shinohara T, Park HW, Frick K, Ice DS, Choi EK, Han S, Maruyama M, Sharma R, Shen C, Fishbein MC, Chen LS, Lopshire JC, Zipes DP, Lin SF and Chen PS. Continuous low-level vagus nerve stimulation reduces stellate ganglion nerve activity and paroxysmal atrial tachyarrhythmias in ambulatory canines. *Circulation*. 2011;123:2204-12.

CHAPTER 4

Premature ventricular contraction coupling interval variability destabilizes cardiac neuronal and electrophysiological control: insights from simultaneous cardioneural mapping

Premature ventricular contractions (PVCs) are common in clinical practice. In structurally normal hearts, despite being referred to as benign, PVCs may lead to cardiomyopathy[1] or even to sudden cardiac death.[2, 3] Recent clinical studies have identified factors that predict worse outcomes in PVC patients. Particularly, patients with PVCs showing high coupling interval (CI) variability are at a greater risk for cardiac events such as left ventricular (LV) dysfunction[4] and sudden cardiac death.[5, 6]

Precise mechanisms underlying the adverse effects of PVCs remain unknown, but are likely multifactorial including mechanical dyssynchrony,[7, 8] abnormalities in calcium handling and oxygen consumption,[9] and autonomic imbalance.[10] Of these mechanisms, the role of the autonomic nervous system (ANS) is not well understood. The ANS regulates all aspects of cardiac function.[11] Afferent sensory neurons provide beat-to-beat information regarding the cardiac milieu. Processing and integration of this information at different levels of the ANS, including the intrinsic cardiac nervous system (ICNS), provides an elegant mechanism to ensure fine-tuned regulation of efferent neural signals to the heart.[11] The ICNS, a distributed network of ganglia and interconnecting nerve fibers on the epicardial surface, represents the first level of the ANS directly impacted by cardiac injury.[12-14] Even in normal states, disruptions of ICNS function are arrhythmogenic.[15] Moreover, neural remodeling within the ICNS after cardiac injury has been correlated with arrhythmias.[11, 14]

Because both PVCs with variable CI and the ICNS have been linked to cardiomyopathy and life-threatening arrhythmias, we hypothesized that variability in PVC CI could induce destabilizing changes in the ICNS. Therefore, the purpose of this study was to evaluate in an *in vivo* porcine model the impact of PVC CI on: (1) intrinsic cardiac neuronal activity and (2) cardiac electrical and mechanical parameters using a novel cardioneural mapping approach that uses direct neuronal recordings from a beating heart.

METHODS

Animals

This study was approved by the University of California, Los Angeles Chancellor's Animal Research Committee and conforms to the National Institute of Health's *Guide for the Care and Use of Laboratory Animals*. Eight Yorkshire pigs (5 male and 3 female, weighing 57.1 $\pm$ 2.5 kg) were used.

Surgical preparation

Animals were sedated with telazol (6 mg/kg, intramuscular), intubated and mechanically ventilated. General anesthesia was maintained with isoflurane (1-2%, inhalation). Femoral vein was cannulated for fluid maintenance and drug administration. A median sternotomy was performed to expose the heart and isolate both stellate ganglia. Lateral neck dissections were performed to isolate both cervical vagal trunks. Following completion of the surgical preparation, general anesthesia was changed to *α*-chloralose (50 mg/kg bolus followed by 35 mg/kg/hr continuous intravenous infusion). Body temperature was continuously monitored and maintained via circulating water heating pads. Acid-based status was evaluated hourly; respiratory rate and tidal volume were adjusted and bicarbonate was infused as necessary to maintain blood gas homeostasis. At the completion of the experiment, animals were euthanized using sodium pentobarbital (200 mg/kg, intravenous) and potassium chloride (150 mg/kg, intravenous) to arrest the heart.

Experimental protocol

Once the animals stabilized after surgical preparation, cardiac neuronal activity was identified, and the following protocol was performed. Hemodynamic indices, cardiac electrophysiological data, and neuronal activity were recorded at baseline and during 5 minutes of PVCs and

premature atrial contractions (PACs). PVCs and PACs were delivered every 10-sensed sinus beats (SBs) during 5-minute sequences of short (effective refractory period +10 ms), long (80% of sinus rhythm cycle length), and variable CIs (random CIs generated between the short and long values). The order of sequences was chosen at random and activity was allowed to return to baseline (minimum of 10-minute recovery interval) before proceeding to the subsequent intervention. Importantly, each intervention was compared with its own baseline. In addition, neurons were functionally classified as afferent, efferent or convergent using the protocol outlined later.

Hemodynamic assessment

LV cardiac mechanical indices (LV end-systolic pressure, maximum rate of LV pressure change [dP/dt_{max}], and minimum rate of LV pressure change [dP/dt_{min}]) were continuously obtained by using a pressure transducer catheter (Mikro-Tip; Millar Instruments, Houston, TX, USA) that was ultrasound guided into the LV via the left carotid artery and connected to a control unit (PCU-200; Millar Instruments). Systemic arterial pressure was obtained by using a pressure transducer attached to a cannula in the femoral artery. In addition, a 12-lead surface electocardiogram (ECG) was obtained using a cardiac electrophysiology recording system (Prucka CardioLab; GE Healthcare, Fairfield, CT, USA). A minimum of 3 beats were averaged for these indices at baseline and during each intervention, including each of the PVC types, for hemodynamic analyses.

Heart rate variability

Five-minute intervals of ECG recording at baseline and following each of the PVC types were analyzed for heart rate variability using the Acknowledge (Biopac Systems, Goleta, CA, USA) software. Normalized low frequency band was used to estimate sympathetic tone, normalized

high frequency band for parasympathetic tone, and the ratio as an index of sympathovagal balance.[16]

Cardiac electrophysiological mapping

Activation recovery intervals (ARIs) are a well-correlated surrogate for action potential duration.[17] Epicardial ARIs were derived from unipolar electrograms recorded from a custom 56-electrode sock placed over the ventricles (Prucka CardioLab; GE Healthcare; Figure 1A). ARIs were calculated using a customized software ScalDyn (University of Utah, Salt Lake City, UT, USA), as previously described.[18, 19] Activation time was defined as the time interval from the beginning of the QRS complex to the most negative derivative of the activation wave front, and repolarization time as the time interval from the beginning of the QRS complex to the most positive derivative of the repolarization wave front. ARI was calculated as the difference between the activation and repolarization times. Global dispersion of repolarization (DOR) was calculated as the variance across all electrodes. ARIs and DOR were analyzed for the PVC and PAC beat delivered in the last minute, as well as the SBs following them (postextrasystolic sinus beat [PES-SB]) that were compared with baseline SBs (average of 5 SBs before introduction of each extrasystolic subtype). To compare fixed with variable CI (short *vs.* short and long *vs.* long), at least 1 extrasystolic beat with a CI equal to the short and long CI subtypes was induced in the last minute of variable CI sequences. Thus, electrophysiological impact of fixed *vs.* variable CI type was not influenced by the immediate extrasystolic CI.

Intrinsic cardiac neuronal recording

A linear microelectrode array (Microprobes, Gaithersburg, MD, USA) was embedded in the ventral interventricular ganglionated plexus (VIV GP), located at the origin of the left anterior descending coronary artery below the left atrial appendage,[20] to record *in vivo* extracellular

activity of cardiac neurons, as previously described (Figure 1A and C).[13, 14] The array consisted of 16 platinum–iridium electrodes (25 μm diameter electrodes with an exposed tip of 2 mm; impedance 0.3–0.5 MΩ at 1 kHz). The array was attached to a flexible cable, making it semi-floating. The electrode wires, as well as ground and reference electrodes, were connected to a microelectrode amplifier with a headstage pre-amplifier (Model 3600; A-M Systems Inc., Carlsborg, WA, USA). For each channel, filters were set to 300 Hz to 3 kHz with a gain of 1000. Cardiac neuronal waveform, hemodynamic data, and ECG were input to a data acquisition system (Power1401; Cambridge Electronic Design, Cambridge, UK). Data analysis including artifact removal and spike sorting to identify single units was performed offline using the Spike2 (Cambridge Electronic Design) software.[13, 14] It is noteworthy that each of the 16 electrodes on the array could record the extracellular action potentials of several single units (neurons), with each neuron being identified by its unique waveform using principle component analysis. The waveform of a given neuron remained constant throughout the experiment.

Functional characterization of intrinsic cardiac neurons

Cardiac neurons were functionally classified as afferent, efferent, or convergent based on their responses to cardiovascular stimuli as previously described (Figure 1F and G).[13, 14] Afferent neurons were defined as those that only received mechanosensory inputs and/or transduced changes in preload or afterload. To determine whether neurons received mechanosensory inputs, epicardial mechanical stimulus was applied for 10 seconds at the following 6 sites: (1) right ventricular (RV) outflow tract (RVOT), (2) RV mid-anterior wall, (3) RV apex, (4) LV mid-anterior wall, (5) LV lateral wall, and (6) LV apex. To determine whether neurons transduced changes in preload and afterload, transient (30 s) complete occlusions of the inferior vena cava and descending thoracic aorta were performed using balloon catheters (Atlas, 20 mm diameter;

Bard Peripheral Vascular, Inc., AZ, USA) inserted through the femoral vein and femoral artery, respectively.

Efferent neurons were defined as those that only received sympathetic and/or parasympathetic efferent inputs. For efferent stimulation, bipolar needle electrodes were inserted into the stellate ganglia and bipolar spiral cuff electrodes were wrapped around the cervical vagal trunks (PerenniaFlex Model 304; Cyberonics Inc., Houston, TX, USA) and connected to a stimulator with an isolation unit (Grass S88 and PSIU6; Natus Medical Inc., Pleasanton, CA, USA). For each stellate ganglion, threshold was defined as the current necessary to evoke a 10% increase in heart rate or blood pressure (4 Hz frequency, 4 ms pulse width). For each vagal trunk, threshold was defined as the current necessary to evoke a 10% decrease in heart rate or blood pressure (10 Hz frequency, 1 ms pulse width). Bilateral stellate ganglia and vagus nerve stimulation were then performed for 1 minute at threshold current and a frequency of 1 Hz. Low frequencies were used for stimulation to assess direct inputs to the ICNS independent of changes in hemodynamic indices (Table S1). Neurons responding to both afferent and efferent stimuli were defined as convergent.[13, 14]

For epicardial mechanical stimuli and autonomic efferent nerve stimulations, cardiac neuronal activity was compared 1 minute before the stimuli (baseline) *vs.* during the stimuli. For vascular occlusions, PVCs, PACs, and pacing, neuronal activity was compared at baseline *vs.* during the stimuli, as well as at baseline *vs.* 1 minute after the stimuli (recovery). After each stimulus, we waited for neuronal activity and hemodynamics to return to baseline levels before proceeding. A significant increase or decrease ($P < 0.05$) in neuronal firing frequency was considered as a change in neuronal activity to a given intervention (Figure 1F and G).[13, 14]

Cardiac phase analysis

Cardiac phase analysis was performed to determine if neurons displayed cardiac cycle-related periodicity, as previously described.[13, 14] Based on an activity histogram, neurons that generated at least 10 action potentials at baseline were classified as being related to a specific phase of the cardiac cycle if more than 30% of their activity occurred during the given phase.

Conditional probability analysis

Conditional probability analysis to assess ICNS network function was performed as previously described.[13, 14] The conditional probability (probability: response to Y | response to X) was estimated as the number of neurons that responded to both stimulus X and Y, divided by the number of neurons that responded to stimulus X.

PVC and PAC delivery

A cardiac stimulator (EPS320; MicroPace, Canterbury, AU) was used to induce PVCs and PACs from the RVOT and right atrium, respectively, using a quadripolar pacing catheter (St. Jude, St. Paul, MN, USA). Atrial and ventricular pacing thresholds were measured, and PACs and PVCs were induced using the same current (1.2x RVOT threshold; 2 ms pulse width). In addition to PACs and PVCs, straight pacing was also performed at the same sites for 30 seconds, just overdriving the sinus rhythm cycle length (-20 ms). This was performed as a control to differentiate the effects of PVC from electrical stimuli and activation from the same site.

Statistics

Data are presented as mean ± standard error of the mean. The significance level of changes in firing rate of each cardiac neuron between baseline *vs.* stimulus interval was assessed using a

statistical test developed for cortical neurons based on the Skellam distribution.[21] This test has been previously validated for the study of cardiac neurons.[13, 14] A χ^2 test was used to compare the neuronal response between the different stimuli. A Wilcoxon rank-sum test or paired *t* test was used as appropriate to compare hemodynamic, ARI, and heart rate variability between baseline and each intervention. Pearson correlation was used to assess the strength of the relationship between local CI and repolarization time changes. P values < 0.05 were considered to be statistically significant.

RESULTS

Functional characterization of intrinsic cardiac neurons

The *in vivo* activity of cardiac neurons from the VIV GP was obtained at baseline and in response to cardiovascular stimuli including PVCs and PACs. In 8 animals, the activity of 92 neurons (average: 11.5 ± 2.6) was recorded. The basal firing frequency of the neurons was 0.11 ± 0.02 Hz. Overall, based on their response to the cardiovascular stimuli, 44.6% of neurons were classified as afferent, 5.4% as efferent, and 23.9% as convergent (26.1% did not respond). A majority of neurons (92.8%) displayed activity clustered during a specific phase of the cardiac cycle, with 49.4% during systole, 25.3% during diastole, and the remaining 18.1% during both phases.

PVC as a stimulus for intrinsic cardiac neurons

The cardiac neuronal response to PVCs of any CI was compared with afferent and efferent cardiovascular stimuli, as well as cardiac pacing. With regards to afferent stimuli, a greater percentage of neurons were impacted by PVCs (66.3%) than by activation of mechanosensitive afferent inputs (39.1%), decrease in preload by inferior vena cava occlusion (32.6%), or increase in afterload by aortic occlusion (26.9%; P < 0.001; Figure 2A). Similarly, in regards to

efferent stimuli, the neuronal response to PVCs was greater than the response to either bilateral stellate ganglia (7.6%) or vagus nerve stimulation (28.3%; $P < 0.0001$; Figure 2B). It is noteworthy that the vast majority of neurons that responded to afferent or efferent cardiovascular stimuli also responded to PVCs. In addition, PVCs induced a greater response from neurons when compared with straight RVOT (19.0%) and right atrial pacing (13.6%; $P < 0.0001$; Figure 2C). Of all the neurons that responded to PVCs, 19.7% only responded to RVOT pacing and 14.8% did not respond to any other cardiovascular stimuli including pacing. Therefore, neither hemodynamic changes (Table S1) nor electrical stimulation or dyssynchrony particularly explain PVCs' impact on cardiac neurons.

Impact of PVC CI on intrinsic cardiac neurons

The response of cardiac neurons to PVCs of short, long, and variable CIs was compared. Overall, 29.3% of neurons responded to short CI PVCs, 39.1% to long CI PVCs, and 43.5% to variable CI PVCs ($P < 0.05$ for short *vs.* variable CI; Figure 3A). The CI did not have a differential effect on afferent or efferent neurons. Twenty-seven percent of afferent neurons responded to short CI PVCs, 43.9% responded to long CI PVCs and 34.1% to variable CI PVCs (Figure 3C). Forty percent of efferent neurons responded to short CI PVCs, 40.0% responded to long CI PVCs and 60.0% to variable CI PVCs (Figure 3D). Interestingly, the CI did have a differential effect on convergent neurons. More convergent neurons responded to variable CI PVCs (72.7%) than either short (40.9%) or long CI PVCs (40.9%; $P < 0.05$ for variable CI PVCs *vs.* short and long CI PVCs; Figure 3E). Further, of the convergent neurons that responded to only 1 PVC CI, a vast majority (75%) responded to variable CI (Figure 3B). High neuronal responses (≈30%) were seen with PACs as well. For PACs, however, all 3 CI protocols evoked similar effects on ICNS function, whether considered as a whole or subsetted into afferent, efferent, or convergent populations (Figure 3A).

Impact of PVC CI on ICNS processing of efferent inputs

We analyzed the subset of cardiac neurons that received sympathetic and/or parasympathetic inputs (efferent and convergent neurons) to determine whether the PVC CI had an impact on sympathovagal balance at the level of the ICNS. Of the neurons receiving sympathetic input, a greater percentage responded to variable CI PVCs (100.0%) than either short (42.9%) or long CI PVCs (57.1%; $P < 0.05$ for variable CI PVCs *vs.* short and long CI PVCs; Figure 3F). A similar trend was observed for neurons receiving parasympathetic input. Sixty-nine percent of neurons responded to variable CI, 42.3% to short CI, and 38.5% to long CI PVCs ($P < 0.05$ for variable CI PVCs *vs.* short and long CI PVCs; Figure 3G). We also performed a spectral analysis of the heart rate variability, which showed that variable CI PVCs elicited the greatest increase in sympathovagal balance (low frequency/high frequency) compared with baseline ($P < 0.05$; Figure 3H).

Impact of CI on electromechanical characteristics of PVCs and PACs

We analyzed ARI, DOR and hemodynamics during PVCs and PACs to determine whether CI had an impact on cardiac electrical and mechanical indices. There was no significant difference in CI between PVCs and PACs regarding short (524 ± 39 and 549 ± 37 ms, respectively) or long CI (749±56 and 765±56 ms, respectively).

Mean global ARIs of short CI PVCs (341.9 ± 22.2 ms) and PACs (347.5 ± 23.7 ms) were shorter than long CI PVCs (377.6 ± 21.2 ms) and PACs (389.2 ± 19.4 ms; $P < 0.05$ for short CI PVCs and PACs *vs.* long CI PVCs and PACs). There was no significant difference between PVCs and PACs with short CI and a small borderline difference between PVCs and PACs with long CI ($P = 0.05$). Thus, the mean global ARI seemed to be more closely related to the CI than the origin of the extrasystolic beat (Figure 4A).

The DOR (repolarization time variance), however, was greater in PVC beats (871 ± 148 and 942 ± 130 ms^2 for short and long CI, respectively) compared with PAC beats (550 ± 49 and 498 ± 69 ms^2 for short and long CI, respectively; $P < 0.05$ for PVC *vs.* PAC). The CI did not significantly affect DOR in PVC or PAC beats, and thus, changes in DOR are likely explained by the activation sequence (Figure 4B).

Similarly, mean activation time and activation time dispersion, estimating duration and variability in ventricular activation, differed significantly between PVC and PAC beats of short and long CI ($P < 0.05$), whereas CI had a minimal effect on activation time of the same extrasystolic origin. Consistent with this, the extrasystolic QRS width did not differ between short and long CI PVCs (143 ± 4 and 141 ± 4 ms) or PACs (83 ± 3 and 80 ± 3 ms). There was no significant difference in any of these parameters between fixed and variable PVCs having the same CI (e.g., fixed short *vs.* variable short).

Regarding hemodynamic indices (LV end systolic pressure, LV dP/dt_{max} and dP/dt_{min}; Table 1) of extrasystolic beats, short CI PVCs had significantly lower values as compared with long CI PVCs ($P < 0.05$ for all), while only the LV dP/dt_{max} differed between long and short CI PACs ($P < 0.05$). Therefore, both the CI and the extrasystolic origin seemed to affect hemodynamic indices, with CI being the predominant factor.

Impact of extrasystolic CI on the PES-SB indices

To assess the impact of extrasystolic beats on cardiac electrical stability, ARI and DOR were analyzed for the 5 SB after extrasystolic beats (PVC and PAC) of each CI type and were compared with baseline SB before their introduction. Maximal changes in ARI were always seen on the PES-SB, returning progressively to baseline over the subsequent SBs. Maximal increase in DOR could be seen from the PES-SB to the following 4 SBs because recovery toward baseline ARI values was sometime heterogeneous across different heart regions. However,

overall, the mean maximal increase in DOR was also seen on the PES-SB, and all comparisons were performed on this specific beat (Figure 4C and D). Overall, PVCs induced a greater increase in the PES-SB DOR than PACs ($P < 0.05$). A short CI also had a greater impact than long CI ES beat ($P < 0.05$), and finally, there was a trend for an increase in DOR with variable CI as compared with fixed CI ($P = 0.10$, paired for the exact same CI), which was driven by differences induced by PVCs ($P = 0.06$), but not PACs ($P = 0.80$). Finally, when impact of each extrasystolic subtype on PES-SB DOR was compared with its own baseline SB DOR, only the variable short CI PVCs, cumulating all aforementioned characteristics, reached statistical significance ($P < 0.05$).

Regarding the impact of extrasystolic beats on the PES-SB hemodynamics (Table 1), a PES potentiation was observed with an inverse relationship to the CI. The most affected index was LV dP/dt_{max}, which was significantly greater after a short than a long CI PVC ($P < 0.001$) or PAC ($P < 0.05$). Of note, the PES pause was greater after a short than a long CI PVC (1208 ± 97 *vs.* 992 ± 81 ms; $P < 0.05$). As a result of these compensatory effects between extrasystolic beats and PES-SB, no global heart rate or hemodynamic changes were seen during the 5 minutes of PVCs or PACs at any CI when compared with that in baseline (Table S1).

Local CI impact on extrasystolic and PES-SB dispersion

We further investigated whether some electrophysiological characteristics of PVCs and PACs could explain why at similar CIs (short) PACs and PVCs (and PES-SB) display similar mean global ARI, while they have a dramatically different effect on DOR. The activation sequence when a PVC depolarizes the heart is radically different than the SB activation sequence. Indeed, regions activated late during sinus rhythm but early during RVOT PVCs (e.g., RVOT) have a shorter CI than regions activated early during sinus rhythm but late during PVCs (e.g., apex; Figure 5). Regional differences ($\leq$ 127 ms) in local CI were observed between different

electrodes with RVOT PVCs. We found that electrodes with shorter local CI during PVCs displayed greater shortening in the local PVC repolarization time than electrodes with a longer local CI ($r = 0.83 \pm 0.07$, $P < 0.001$). Interestingly, this local CI impact partially remained on the subsequent beat (PES-SB) with a greater shortening in repolarization in regions previously affected with a shorter local PVC CI ($r = 0.32 \pm 0.05$, $P < 0.05$). On the contrary, because this local CI effect does not exist with PACs, they produce homogeneous changes in repolarization across the heart.

DISCUSSION

Main findings

This is the first study assessing the impact of PVCs, induced at different CIs, on cardiac neuronal and electrical stability with concurrent *in vivo* cardioneural mapping. Our main findings are the following:

- PVCs (even a modest burden of 10%) are a powerful stressor, altering the activity of critical cardiac neuronal populations.
- The association of an abnormal timing (CI) and activation sequence characterizing PVCs triggered these changes, with the CI being the predominant factor.
- Variable CI PVCs compared with those with fixed short or long CIs had a significantly greater impact on cardiac neurons, more specifically on convergent neurons, which are responsible for reflex processing at the level of the heart.
- Variable CI PVCs also differentially affected a greater percentage of neurons receiving sympathetic and parasympathetic input than the fixed CI PVCs. These sympathetic/parasympathetic interactions, mediated within the ICNS, may contribute to the increase in low frequency/high frequency ratio after variable CI PVCs.

- Mirroring IC neuronal changes, the greatest cardiac electrical instability in the PES-SB (i.e., increase in dispersion) was seen after variable (short) CI PVCs. Factors increasing PES-SB dispersion were PVCs as opposed to PACs (heterogeneity in local CI across the heart), a shorter CI, and a variable CI.

PVCs as a unique and powerful stressor: mechanistic implications

RVOT PVCs affected a large proportion (66.3%) of neurons contained within the VIV GP. These neurons are primarily associated with control of ventricular function.[14] Most neurons that responded to afferent and efferent cardiovascular stimuli also responded to PVCs, suggesting that PVCs preferentially engage convergent neurons (Figure 2). Similar to a previous study, 26% of neurons did not respond to afferent and efferent cardiovascular stressors used for classification of cardiac neurons.[14] Interestingly, however, almost half of these neurons (46%) responded to PVCs, which indicates that PVCs pose a strong and unique stress to ICNS neurons. We also analyzed the concomitant responses of this specific subset of neurons to PACs and straight pacing from the RVOT. These data indicated that the mechanism involved in triggering the changes in neuronal activity was predominately related to timing (i.e., neurons were also activated by PACs) and only a small percentage of neurons also responded to the same abnormal myocardial activation sequence (i.e., RVOT pacing). The remaining neurons responded to either a combination of timing with activation abnormalities or involved another mechanism (i.e., concomitant activation by both PACs and RVOT pacing or neither).

Interestingly, ventricular dyssynchrony, which involves a combination of abnormal timing and activation sequence, can be measured using strain indices[8] and is likely to be a trigger that impacts neuronal activity. Hamdan et al. have shown that biventricular pacing was associated with lower muscle sympathetic nerve activity than right ventricular pacing alone.[22] Similarly, muscle sympathetic nerve activity and coronary sinus catecholamine levels are correlated with

the burden of PVCs (induced by pacing) in patients, highlighting a sympathetic neuro-humoral impact potentially involving the heart.[23] These changes on muscle sympathetic nerve activity were subsequently confirmed in heart failure patients during spontaneous PVCs, providing further support for the validity of our experimental model involving pacing-induced PVCs.[10]

A recent study provided important insight on PVC-induced dyssynchrony, showing that the timing (i.e., CI) had the greatest impact, consistent with our data.[8] Importantly, they reported that longer CI resulted in more pronounced LV dyssynchrony. It is interesting to note that long CI PVCs tended to affect more neurons and particularly, more afferent neurons than short CI PVCs in our study. However, our electrical data showed that PVC activation time dispersion and DOR did not differ between short and long CI, and our hemodynamic data showed that short CI had a greater impact on both PVC beat and PES-SB compared with long CI. Therefore, adverse effect of PVCs is not solely hemodynamically mediated (Tables 1 and S1). Rather, a greater preload (with longer CI PVCs), although inducing a better overall hemodynamic profile, may exaggerate mechanical stretch on the myocardial wall, thereby increasing activity in sensory neurites that are locally present.[12, 24]

Finally, perturbations in atrioventricular relationship are known to increase muscle sympathetic nerve activity,[25] especially during closely coupled atrial and ventricular systole.[26] We observed similar features (close systolic coupling) during long CI PVCs, which could have had an additional impact on ICNS neurons.

Impact of variable coupling PVCs on ICNS network function

Our data demonstrates that variable CI PVCs had a significantly greater impact on cardiac neurons, especially on convergent neurons, the local reflex processors. We compared the functional connectivity of neurons that responded to variable CI PVCs *vs.* those that did not. Interestingly, we observed that functional network connectivity was greater with neurons that

responded to variable CI PVCs (Figure 6). Variable CI PVCs seem to have a more complex impact on cardiac neurons than just the addition of short and long CI PVCs. Indeed, we have shown that most (75%) convergent neurons affected by 1 CI PVC type were only activated by variable CI PVCs (Figure 3B). Similarly, variable CI PVCs differentially affected a greater percentage of neurons receiving sympathetic/parasympathetic inputs (Figure 3F and G). Finally, there was no difference in the percentage of afferent neurons affected (Figure 3C). Therefore, unpredictability in CI appeared to be a specific trigger that a subpopulation of convergent neurons can detect, further causing sympathovagal imbalance. This cardio-cardiac reflex, likely also involving higher centers in the neuraxis (Figure 7), may subsequently impact cardiomyocyte function and lead to electrical instability.

Enhanced response of neurons to a variable compared with constant stimulus has been reported in sensory neurons in visual, auditory, and olfactory system, a concept known as neural adaption.[27, 28] Similarly, in the cardiovascular system, it has been previously shown that sympathetic nerve activity measured by muscle sympathetic nerve activity was greater when the heart was paced irregularly, and these findings were independent of hemodynamic changes.[29] We speculate that variability of PVC CI compared with fixed CI may prevent neural adaptation and play an important role in reflex activation of the ANS.

Impact of PVCs on cardiac electrical stability: PES-SB DOR

Increase in the SB DOR has been described as arrhythmogenic, being a requirement for electrical reentry and lethal ventricular arrhythmias.[30, 31] Furthermore, DOR has been strongly correlated with the Tpeak-Tend interval, which is a predictor of sudden cardiac death risk in most cardiomyopathies, as well as in more heterogeneous populations.[32] Similarly, other ECG parameters estimating the spatial or temporal[33-35] DOR have been shown to improve sudden cardiac death prediction.

More specifically, a short-long sequence has been described as a major trigger for ventricular arrhythmias.[36] Therefore, part of the arrhythmogenesis may be explained by the PES-SB DOR[37] (after the short CI PVC) and another by the CI of the subsequent PVC. PES-SB dispersion was globally higher after following PVC (*vs.* same CI PAC) because of their non-uniform local CI across the heart. A malignant short-long-short sequence following a PAC (as first short) has never been reported. Heart regions that depolarize late during sinus rhythm and early during PVCs (shorter local CI) are more impacted (shorter repolarization) than regions having a longer local CI (Figure 5). Interestingly, PVCs arising from late activated regions in sinus rhythm (e.g., aortic cusps, epicardial) are associated with worse outcomes.[4, 5, 7] Finally, variable CI PVCs increased PES-SB dispersion as compared with fixed CI PVCs, despite comparisons after similar CI. Therefore, impact of variable CI on neuronal stability was the last potential mechanistic component of the increase in PES-SB dispersion that we could identify in the present study. Indeed, sympathetic stimulation has been shown to increase DOR experimentally in porcine models,[19, 38] as well as in humans,[18] and lead to lethal ventricular arrhythmias.[11] By carrying all deleterious characteristics, only variable short CI PVC induced a statistically significant increase in the PES-SB dispersion as compared with baseline. The level of dispersion necessary to initiate ventricular arrhythmias remains unknown, and given the rare incidence of such event, additional stress-mediated autonomic involvement is likely necessary to provide sufficient functional arrhythmogenic substrate.[18, 39, 40] Interestingly, in addition to inducing a greater PES-SB DOR (i.e., vulnerability), a greater CI variability would also increase the likelihood for a subsequent PVC to trigger an arrhythmia if a specific CI is required. Finally, intracellular calcium handling likely involved in acute changes in DOR may translate into heterogeneous ion channel remodeling, resulting in marked heterogeneity in action potential configurations and durations, as reported in a chronic canine model of PVC-induced cardiomyopathy,[9] which may lead to a more sustained arrhythmogenic substrate.

Neuromodulation represents an attractive approach that has been shown to specifically inhibit deleterious activity within the ICNS[15, 41] or intrathoracic extracardiac ganglia,[42] thereby mitigating the substrate and preventing arrhythmias. Further, it has antifibrotic properties,[43] and myocardial fibrosis has been characterized in a model of PVC-induced cardiomyopathy[44] and could compromise recovery, even after successful PVC suppression.

LIMITATIONS

General anesthetics may suppress evoked responses in the ANS. However, after surgical preparation, we switched to *α*-chloralose, which has minimal effects on ANS reflexes. Neuronal recording was selectively performed in the VIV GP (1 of 11 GPs in porcine heart).[20] However, GP have been described to have spatially divergent receptive fields, capable of transducing information from widespread cardiac regions, and VIV GP is primarily associated with control of ventricular function.[24] It is also noteworthy that there is a high degree of communication at all levels of the ANS and changes in low frequency/high frequency after PVCs, believed to reflect global sympathovagal balance and its effect on cardiac dynamics,[45] seemed to mirror the local impact on VIV GP neurons.

This unique set of data assessing acute changes would benefit from confirmation in a chronic PVC model, in the setting of heart disease, and prompt further assessment of functional and anatomopathological remodeling at different levels of the neuraxis. Additionally, whether the differential effect of the CI seen on cardiac electrical stability and neuronal behavior is dependent on a specific burden[46] or a PVC location remain unknown. Indeed, we studied PVCs from only 1 location (RVOT), which is the most commonly encountered clinically, and investigating different locations in this set of animals was not feasible. A 10% burden induced acutely was enough to have a significant impact, which has been previously described as the lowest burden inducing a reversible cardiomyopathy,[47] particularly with an epicardial origin.[7]

Although our data suggested that part of destabilizing cardiac repolarization changes were mediated through PVC-induced changes in IC neural activity, our study was not sufficiently powered to establish a direct temporal link between these 2 components.

Surrogate markers of arrhythmogenesis have been used in this study rather than inducibility testing, which would have compromised our model of PVC delivery subsequent to sensed SB. Moreover, cardioversion shocks required to resuscitate animals from a ventricular arrhythmia would have disrupted and/or dislodged our neuronal recording interface. An extensive literature has correlated these surrogates with sudden cardiac death.[30-35]

CLINICAL IMPLICATIONS

Currently, the clinical approach for PVC patients consists of ruling out a structural arrhythmogenic substrate and thereby, classifying the PVC as benign. However, cardiac events are known to occur with benign PVCs,[2, 3, 5] and we have yet to decipher the mechanism behind this small, but very real risk. This study provides important mechanistic insights into mechanoelectric feedback (mediated through cardiac neurons) that have the potential to contribute to a new avenue of investigation and allow more precise risk stratification in the future. If further translational and clinical data supports these findings, temporal and spatial ECG tools focusing on PES-SB repolarization and PVC CI variability should be used and further developed to improve risk stratification in PVC patients and potentially prompt more aggressive prophylactic management. Finally, understanding neural signatures associated with PVC-induced cardiomyopathy/arrhythmogenesis will pave the way for novel therapies targeting the ANS to prevent cardiac disease.

SOURCES OF FUNDING

This work was supported by National Institutes of Health (NIH) National Heart, Lung, and Blood Institute (NHLBI) Grant 4R01HL084261-09 to K.S., NIH Stimulating Peripheral Activity to Relieve Conditions (SPARC) Grant 1OT2OD023848-01 to K.S, and NIH SPARC Grant 5U18EB021799-02 to J.L.A. D.H. was supported by a Federation Francaise de Cardiology Grant. P.S.R. was supported by NIH NHLBI Grant 5F31HL127974-02.

DISCLOSURES

None.

ES	LV ESP (mmHg)	LV dP/dt_{max} (mmHg/s)	LV dP/dt_{min} (mmHg/s)
PVC short coupling	53 ± 13*	488 ± 82*	-520 ± 179*
PVC long coupling	81 ± 11	1012 ± 139	-919 ± 180
PAC short coupling	66 ± 16	722 ± 180*	-834 ± 271
PAC long coupling	83 ± 12	1072 ± 139	-1042 ± 162
PES-SB			
PVC short coupling	88 ± 12	1524 ± 179†	-1040 ± 166
PVC long coupling	84 ± 11	1213 ± 150	-1058 ± 161
PAC short coupling	84 ± 14	1308 ± 203*	-929 ± 220
PAC long coupling	85 ± 13	1207 ± 181	-991 ± 181

Table 1. Hemodynamics of extrasystolic and post-extrasystolic sinus beat. (A) Left ventricular (LV) end-systolic pressure (LV ESP), maximum rate of LV pressure change (LV dP/dt_{max}) and minimum rate of LV pressure change (LV dP/dt_{min}) for ventricular and atrial extrasystolic (ES) beats of different coupling intervals. **(B)** Hemodynamic parameters of post-extrasystolic sinus beat (PES-SB) following ventricular and atrial ES beats of different coupling intervals. * $P < 0.05$ for short *vs.* long coupling. † $P < 0.001$ for short *vs.* long coupling. PAC, premature atrial contraction; PVC, premature ventricular contraction.

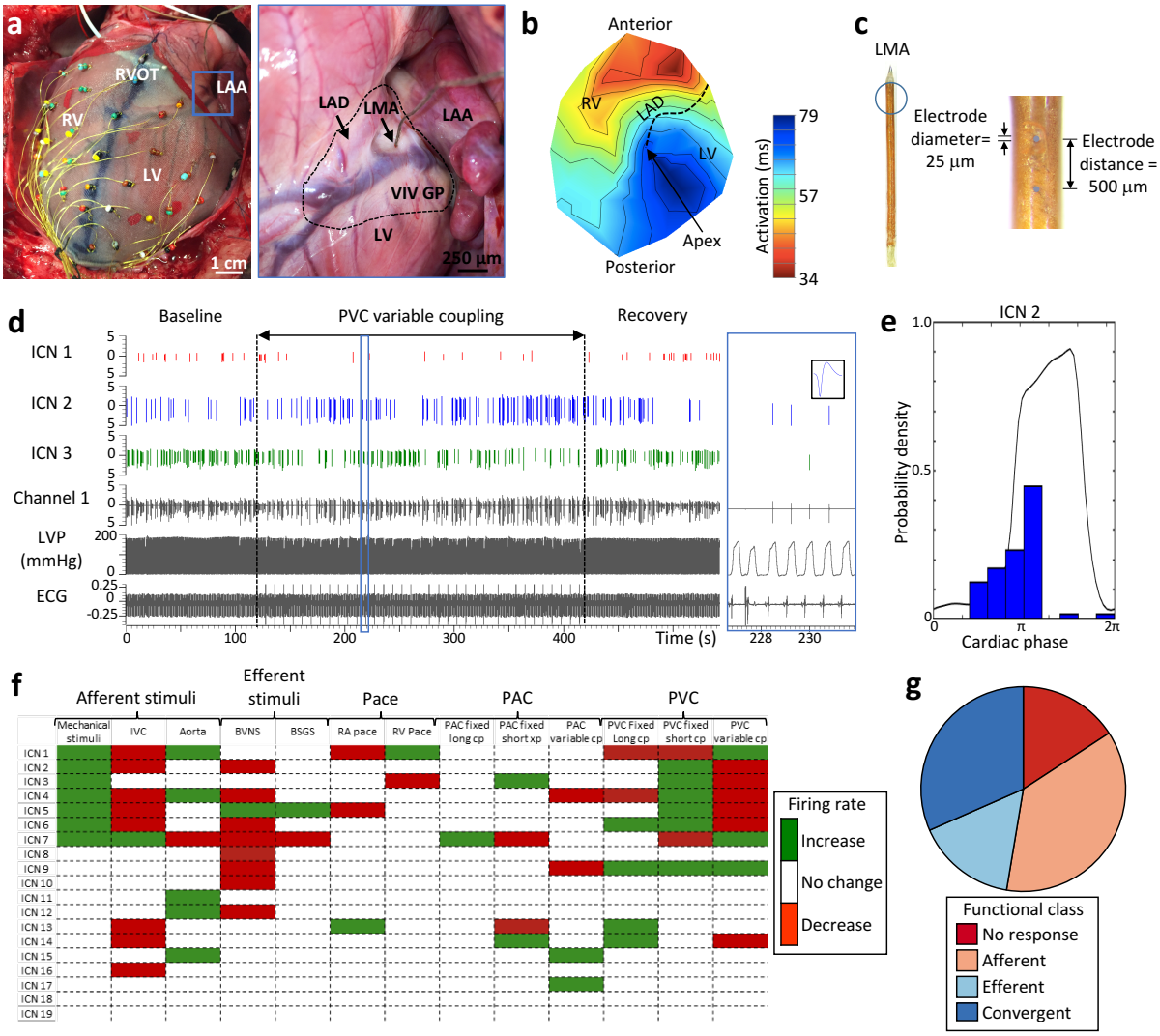

Figure 1. Cardiac electrophysiological mapping and neuronal recording: methods. **(A)** Porcine heart with 56-electrode sock array around ventricular epicardium to record unipolar cardiac electrograms and a linear microelectrode array (LMA) in the ventral interventricular ganglionated plexus (VIV GP) to record intrinsic cardiac neuronal activity. Premature ventricular contractions (PVCs) were induced via right ventricular outflow tract (RVOT) pacing. Blue box in left is a higher magnification of VIV GP (blacked dashed line in right) with embedded LMA. **(B)** Representative polar activation map of PVC induced from the RVOT. Black dotted line indicates location of left anterior descending coronary artery (LAD). **(C)** Sixteen-channel LMA used to record neuronal activity. **(D)** Representative trace showing the activity of 3 intrinsic cardiac

neurons (ICN 1, 2 and 3) from a single electrode (channel 1) of the LMA as well as left ventricular pressure (LVP) and electrocardiogram (ECG). Black vertical dotted lines indicate the time period in which variable coupling interval PVCs were delivered. Blue box is a higher magnification of the trace, with an inset showing the waveform of ICN 2. **(E)** Basal activity of one of the neurons from D (ICN 2) in relation to the cardiac cycle. Note that the activity of this neuron is predominately clustered during isovolumetric contraction. **(F)** Summary of evoked changes in neuronal activity in response to PVCs as well as other cardiovascular stimuli from a single animal. Horizontal rows represent the response of an individual neuron to a given stimulus (vertical columns). Green and red indicate significant increase or decreases in activity ($P < 0.05$), respectively. **(G)** Functional classification of neurons depicted in panel F. Neurons were classified as afferent, efferent, or convergent based on their responses to the cardiovascular stimuli. Afferent neurons were defined as those that responded only to epicardial mechanical stimuli of the right (RV) or left ventricle (LV); transient occlusion of the inferior vena cava (IVC); and/or transient occlusion of the descending thoracic aorta. Efferent neurons were defined as those that responded only to electrical stimulation of the bilateral vagus nerves (BVNS) and/or stellate ganglia (BSGS). Neurons that responded to activation of both afferent and efferent inputs were defined as convergent. PAC, premature atrial contraction; RA, right atrium.

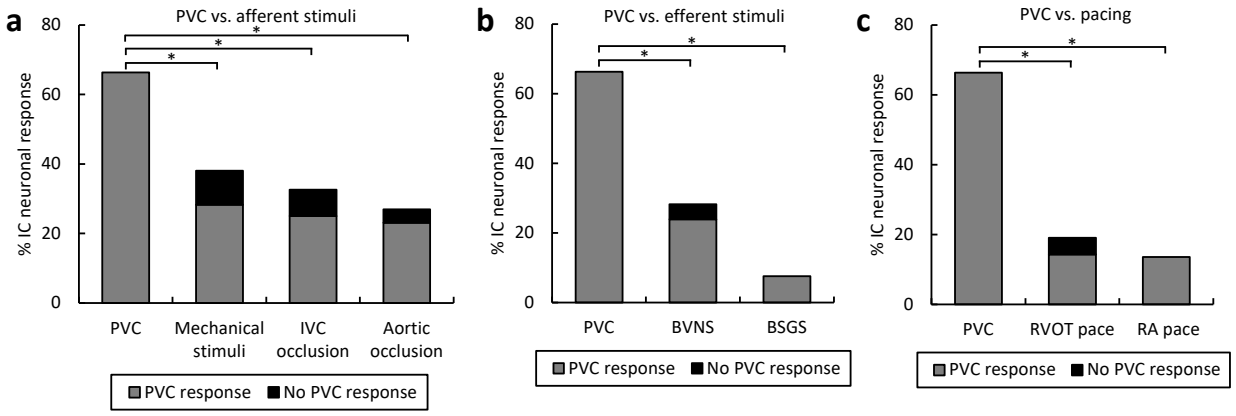

Figure 2. Premature ventricular contractions (PVCs) are a powerful and unique cardiovascular stimulus. (A) Percentage of intrinsic cardiac (IC) neurons responding to PVCs *vs.* afferent cardiovascular stimuli. **(B)** Percentage of neurons responding to PVCs *vs.* efferent cardiovascular stimuli. **(C)** Percentage of neurons responding to PVCs *vs.* pacing. Note that the vast majority of neurons that responded to afferent and efferent cardiovascular stimuli, as well as pacing, also responded to PVCs. * $P < 0.001$. BSGS, bilateral stellate ganglia stimulation; BVNS, bilateral vagus nerve stimulation; IVC, inferior vena cava; RA, right atrium; RVOT, right ventricular outflow tract.

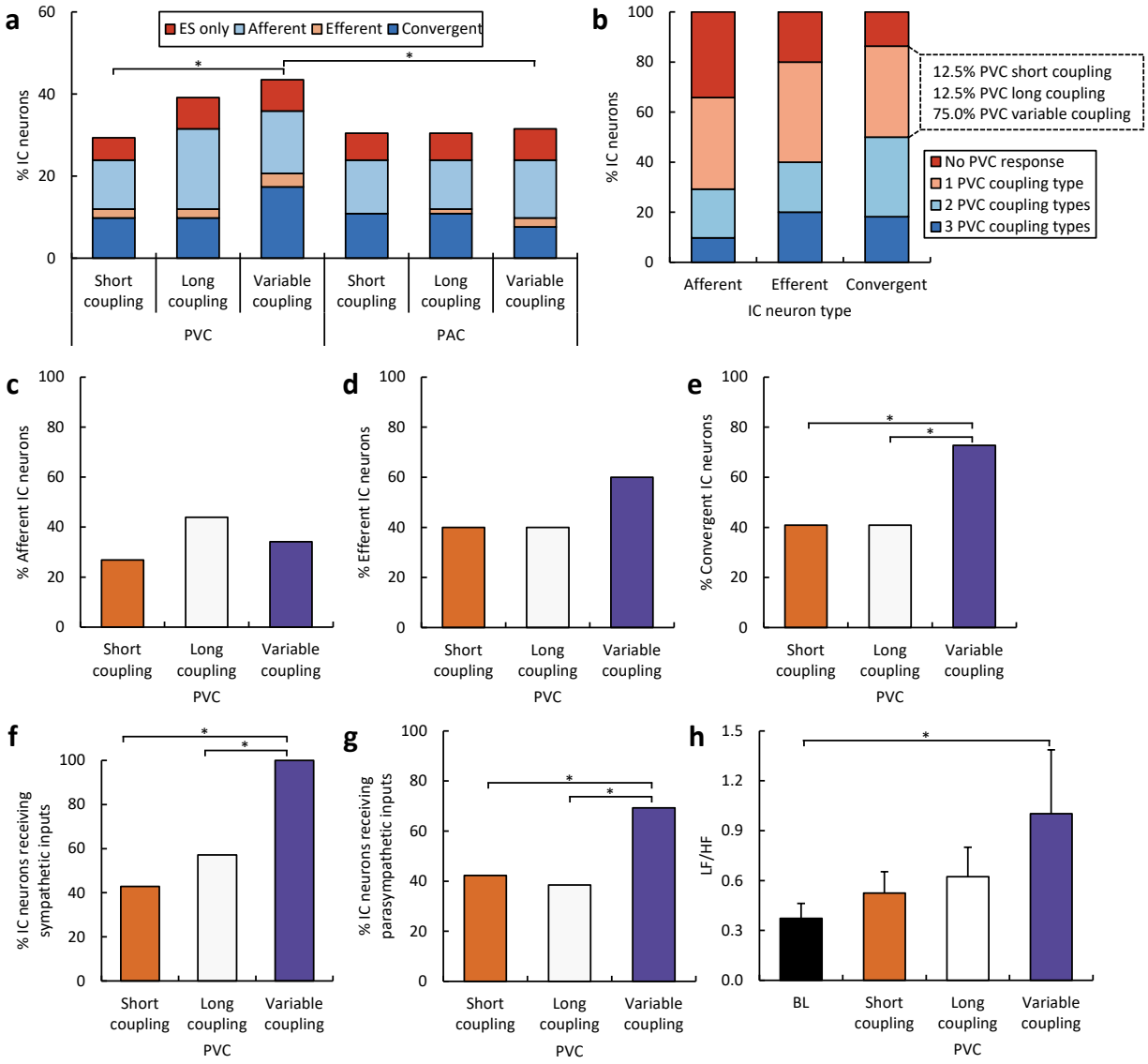

Figure 3. Impact of premature ventricular contraction coupling interval on intrinsic cardiac neurons. (A) Functional classification of intrinsic cardiac (IC) neurons responding to PVCs and premature atrial contractions (PAC) of different coupling intervals. Note that a subset of neurons responded only to the extrasystole (ES), and none of the other afferent and efferent cardiovascular stimuli. **(B)** Percentage afferent, efferent, and convergent neurons that responded to multiple PVC types. Note that of convergent neurons that responded to only 1 PVC, the vast majority responded to variable coupling interval PVCs. **(C)** Percentage of afferent neurons responding to PVCs of different coupling intervals. **(D)** Percentage of efferent neurons

responding to PVCs of different coupling intervals. **(E)** Percentage of convergent neurons responding to PVCs of different coupling intervals. **(F)** Percentage of neurons receiving sympathetic inputs from the stellate ganglia responding to PVCs of different coupling intervals. **(G)** Percentage of neurons receiving parasympathetic inputs from the vagus nerve responding to PVCs of different coupling intervals. **(H)** Low frequency (LF)/high frequency (HF) ratio following PVCs of different coupling intervals *vs.* baseline (BL). * $P < 0.05$.

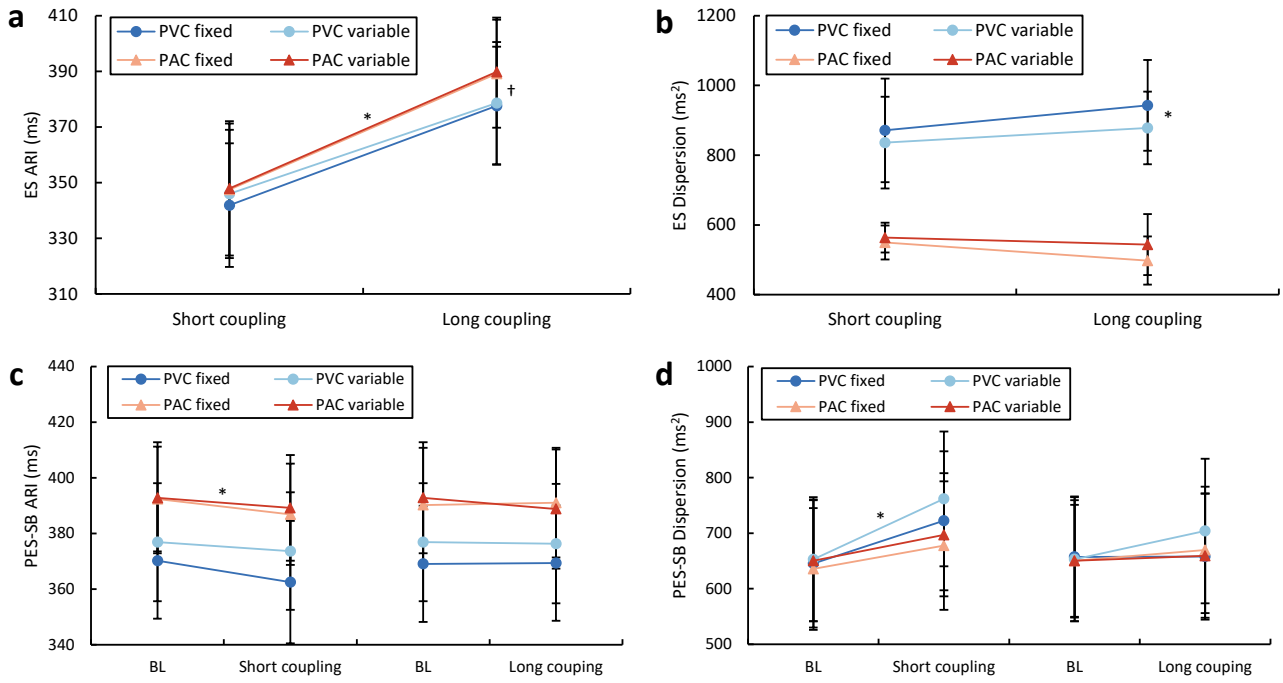

Figure 4. Impact of premature ventricular contractions (PVCs) coupling interval on cardiac electrophysiology. (A) Activation recovery intervals (ARIs) of ventricular and atrial extrasystolic (ES) beats of different coupling intervals. * P < 0.05 for short *vs.* long coupling PVCs and premature atrial contractions (PACs). † P < 0.05 for long coupling PVCs *vs.* PACs. **(B)** Dispersion of repolarization of ventricular and atrial ES beats of different coupling intervals. * P < 0.05 for short and long coupling PVCs *vs.* PACs. **(C)** ARIs of postextrasystolic sinus beat (PES-SB) after PVCs and PACs of different coupling intervals *vs.* baseline (BL) sinus beat. * P < 0.05 for fixed short coupling PACs *vs.* BL. **(D)** Dispersion of ARI for PES-SB after PVCs and PACs of different coupling intervals *vs.* BL sinus beat. * P < 0.05 for variable short coupling PVC *vs.* BL.

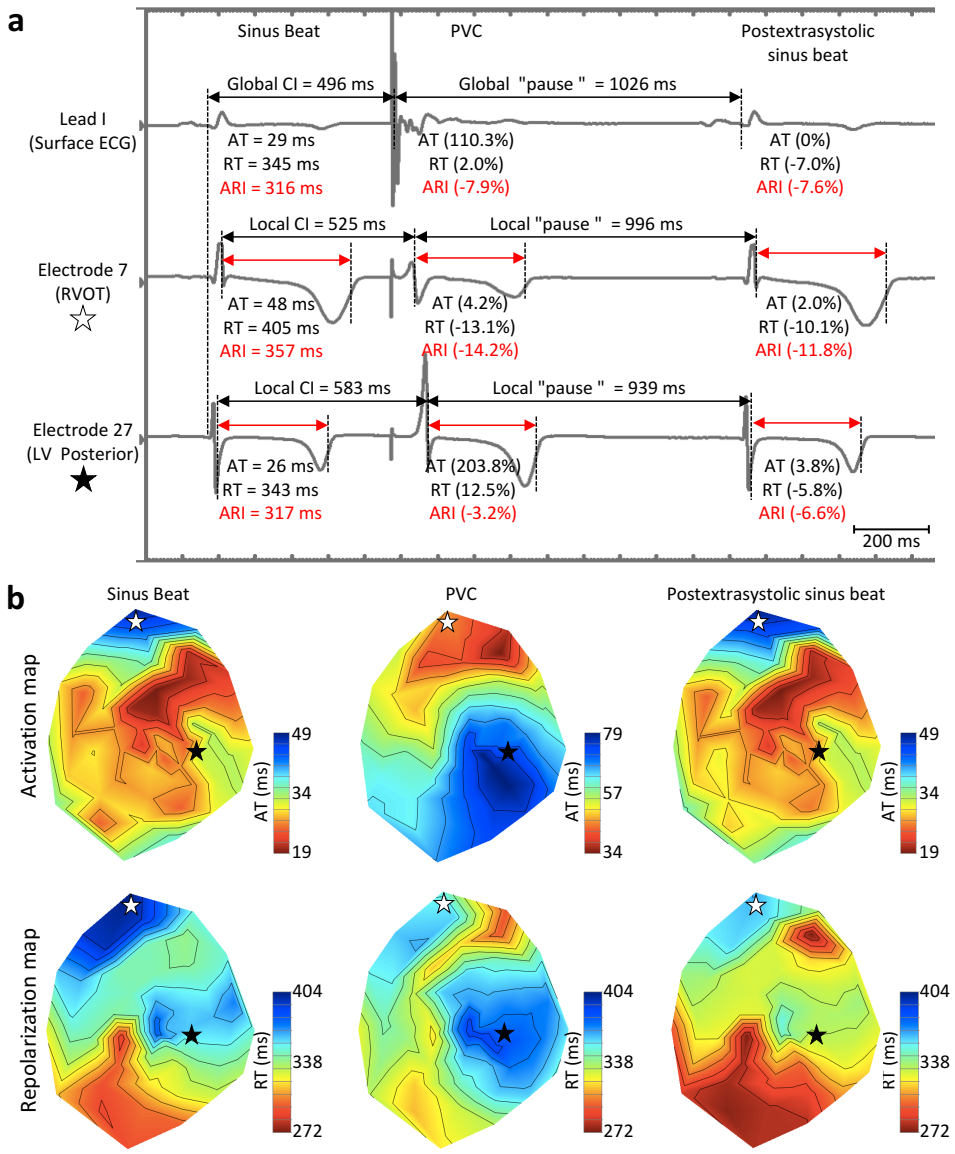

Figure 5. Premature ventricular contraction (PVC) local coupling interval (CI) impact on repolarization. (A) Representative trace showing a sinus beat followed by a PVC induced at a coupling of 496 ms and the subsequent postextrasystolic sinus beat on (1) surface ECG lead I, (2) a unipolar sock electrode recorded from the right ventricular outflow tract (RVOT), and (3) from the left ventricular (LV) posterior-apical wall. Overall, mean activation time (AT), repolarization time (RT), and activation recovery interval (ARI) across the heart and values recorded from RVOT and LV posterior electrodes are displayed under each respective trace.

(B) Polar map showing myocardial activation during the sinus beat and the subsequent PVC and postextrasystolic beats. White and black stars indicate location of RVOT and LV posterior-apical wall electrodes, respectively. Note that the RVOT electrode, which had a shorter local CI than the LV posterior-apical one, was characterized by a greater shortening in RT that remained on the postextrasystolic-sinus beat while activation pattern was back to normal. Such PVC-induced arrhythmogenic substrate may increase the likelihood for subsequent critically timed PVCs to trigger re-entry-mediated ventricular arrhythmias.

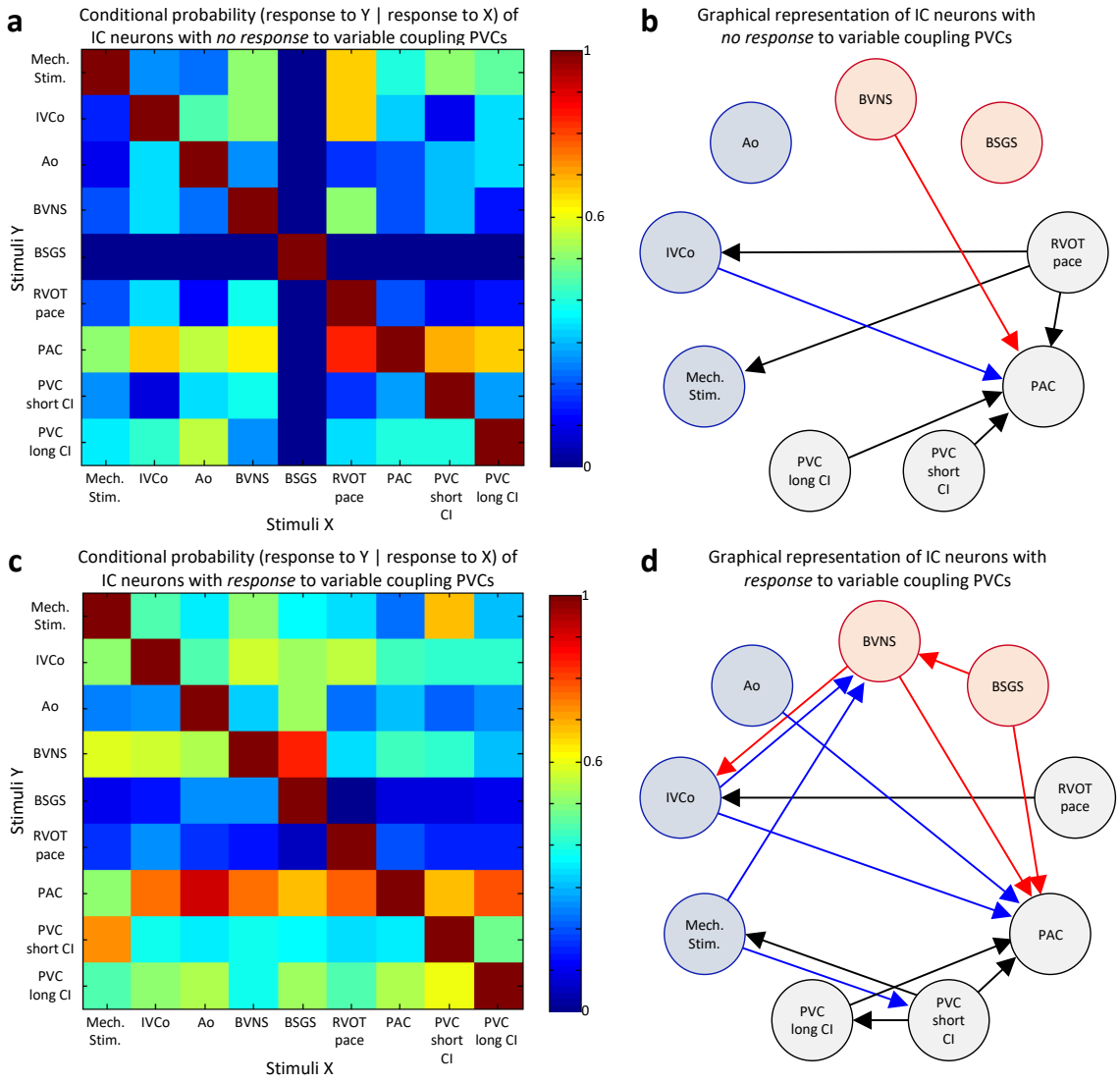

Figure 6. Impact of variable coupling interval premature ventricular contractions (PVCs) on intrinsic cardiac (IC) nervous system network function. (A, C) Conditional probability that an intrinsic cardiac neuron that responded to one stimulus (X, x-axis) also responded to another stimulus (Y, y-axis). **(A)** Conditional probability for neurons that had no response to variable coupling interval PVCs. **(C)** Conditional probability for neurons that had a response to variable coupling interval PVCs. Color scale indicates level of probability of each occurrence. **(B, D)** Graphical representation of interdependent interactions between stimuli in neurons based on their response to variable coupling interval PVCs (B, no response; D, response). Only links

with probabilities $\geq$ 0.6 are displayed. Afferent and efferent stimuli are represented by blue and red, respectively. Pacing, premature atrial contractions (PACs), and PVC are represented in black. Ao, aortic occlusion; BSGS, bilateral stellate ganglia stimulation; BVNS, bilateral vagus nerve stimulation; CI, coupling interval; IVCo, inferior vena cava occlusion; Mech., mechanical; RVOT, right ventricular outflow tract; stim., stimuli.

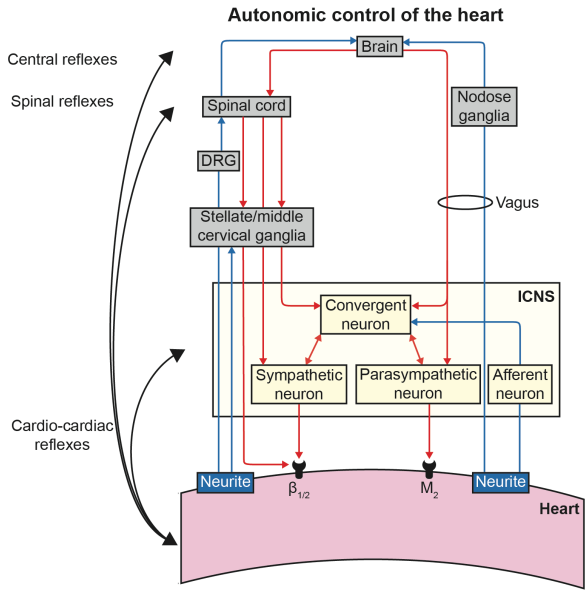

Figure 7. Autonomic control of the heart. DRG, dorsal root ganglia; ICNS, intrinsic cardiac nervous system.

	Heart Rate (bpm)		LV ESP (mmHg)	
	Baseline	**Intervention**	**Baseline**	**Intervention**
PVC short coupling	68 ± 5	70 ± 5	97 ± 13	91 ± 13
PVC long coupling	69 ± 6	70 ± 6	91 ± 10	89 ± 12
PVC variable coupling	67 ± 5	70 ± 5	90 ± 14	87 ± 14
PAC short coupling	65 ± 4	66 ± 4	87 ± 13	85 ± 13
PAC long coupling	64 ± 4	66 ± 3	84 ± 14	84 ± 14
PAC variable coupling	64 ± 4	66 ± 4	77 ± 15	79 ± 16
IVC occlusion	73 ± 6	72 ± 5	89 ± 13	55 ± 9*
Aortic occlusion	70 ± 6	67 ± 7	84 ± 8	135 ± 14*
BVNS	67 ± 5	65 ± 5	89 ± 15	85 ± 13
BSGS	71 ± 6	72 ± 6	96 ± 11	103 ± 12
	LV dP/dt_{max} (mmHg/s)		**LV dP/dt_{min} (mmHg/s)**	
PVC short coupling	1265 ± 172	1207 ± 158	-1246 ± 209	-1137 ± 207
PVC long coupling	1216 ± 142	1189 ± 151	-1057 ± 142	-1056 ± 176
PVC variable coupling	1226 ± 157	1195 ± 146	-1157 ± 189	-1110 ± 205
PAC short coupling	1156 ± 155	1174 ± 168	-1005 ± 208	-965 ± 191
PAC long coupling	1162 ± 189	1138 ± 192	-970 ± 210	-962 ± 223
PAC variable coupling	1107 ± 198	1122 ± 195	-875 ± 200	-927 ± 232
IVC occlusion	1238 ± 169	805 ± 107*	-1069 ± 201	-539 ± 101*
Aortic occlusion	1154 ± 105	1055 ± 111	-998 ± 143	-1454 ± 325
BVNS	1206 ± 194	1175 ± 187	-1030 ± 242	-902 ± 207
BSGS	1143 ± 167	1237 ± 140	-1204 ± 175	-1193 ± 152

Supplemental Table 1. Hemodynamics of interventions. * $P < 0.05$ for intervention *vs.* baseline. BSGS, bilateral stellate ganglia stimulation; BVNS, bilateral vagus nerve stimulation; IVC, inferior vena cava; LV ESP, left ventricular end-systolic pressure; PAC, premature atrial contraction; PVC, premature ventricular contraction.

REFERENCES

1. Yarlagadda RK, Iwai S, Stein KM, Markowitz SM, Shah BK, Cheung JW, Tan V, Lerman BB and Mittal S. Reversal of cardiomyopathy in patients with repetitive monomorphic ventricular ectopy originating from the right ventricular outflow tract. *Circulation*. 2005;112:1092-7.
2. Leenhardt A, Glaser E, Burguera M, Nurnberg M, Maison-Blanche P and Coumel P. Short-coupled variant of torsade de pointes. A new electrocardiographic entity in the spectrum of idiopathic ventricular tachyarrhythmias. *Circulation*. 1994;89:206-15.
3. Viskin S, Rosso R, Rogowski O and Belhassen B. The "short-coupled" variant of right ventricular outflow ventricular tachycardia: a not-so-benign form of benign ventricular tachycardia? *J Cardiovasc Electrophysiol*. 2005;16:912-6.
4. Kawamura M, Badhwar N, Vedantham V, Tseng ZH, Lee BK, Lee RJ, Marcus GM, Olgin JE, Gerstenfeld EP and Scheinman MM. Coupling interval dispersion and body mass index are independent predictors of idiopathic premature ventricular complex-induced cardiomyopathy. *J Cardiovasc Electrophysiol*. 2014;25:756-62.
5. Bradfield JS, Homsi M, Shivkumar K and Miller JM. Coupling interval variability differentiates ventricular ectopic complexes arising in the aortic sinus of valsalva and great cardiac vein from other sources: mechanistic and arrhythmic risk implications. *J Am Coll Cardiol*. 2014;63:2151-8.
6. Lee CH, Park KH, Nam JH, Lee J, Choi YJ, Kong EJ, Lee HW, Son JW, Kim U, Park JS, Kim YJ and Shin DG. Increased variability of the coupling interval of premature ventricular contractions as a predictor of cardiac mortality in patients with left ventricular dysfunction. *Circ J*. 2015;79:2360-6.
7. Hamon D, Sadron M, Bradfield JS, Chaachoui N, Tung R, Elayi C, Vaseghi M, Dhanjal TS, Boyle NG, Maury P, Shivkumar K and Lellouche N. A New Combined Parameter to Predict

Premature Ventricular Complexes Induced Cardiomyopathy: Impact and Recognition of Epicardial Origin. *J Cardiovasc Electrophysiol*. 2016; 27;709-717.

8. Potfay J, Kaszala K, Tan AY, Sima AP, Gorcsan J, 3rd, Ellenbogen KA and Huizar JF. Abnormal Left Ventricular Mechanics of Ventricular Ectopic Beats: Insights Into Origin and Coupling Interval in Premature Ventricular Contraction-Induced Cardiomyopathy. *Circ Arrhythm Electrophysiol*. 2015;8:1194-200.
9. Wang Y, Eltit JM, Kaszala K, Tan A, Jiang M, Zhang M, Tseng GN and Huizar JF. Cellular mechanism of premature ventricular contraction-induced cardiomyopathy. *Heart Rhythm*. 2014;11:2064-72.
10. Maslov PZ, Breskovic T, Brewer DN, Shoemaker JK and Dujic Z. Recruitment pattern of sympathetic muscle neurons during premature ventricular contractions in heart failure patients and controls. *Am J Physiol Regul Integr Comp Physiol*. 2012;303:R1157-64.
11. Fukuda K, Kanazawa H, Aizawa Y, Ardell JL and Shivkumar K. Cardiac innervation and sudden cardiac death. *Circ Res*. 2015;116:2005-19.
12. Armour JA. Potential clinical relevance of the 'little brain' on the mammalian heart. *Exp Physiol*. 2008;93:165-76.
13. Beaumont E, Salavatian S, Southerland EM, Vinet A, Jacquemet V, Armour JA and Ardell JL. Network interactions within the canine intrinsic cardiac nervous system: implications for reflex control of regional cardiac function. *J Physiol*. 2013;591:4515-33.
14. Rajendran PS, Nakamura K, Ajijola OA, Vaseghi M, Armour JA, Ardell JL and Shivkumar K. Myocardial infarction induces structural and functional remodelling of the intrinsic cardiac nervous system. *J Physiol*. 2016;594:321-41.
15. Gibbons DD, Southerland EM, Hoover DB, Beaumont E, Armour JA and Ardell JL. Neuromodulation targets intrinsic cardiac neurons to attenuate neuronally mediated atrial arrhythmias. *Am J Physiol Regul Integr Comp Physiol*. 2012;302:R357-64.

16. Heart rate variability: standards of measurement, physiological interpretation and clinical use. Task Force of the European Society of Cardiology and the North American Society of Pacing and Electrophysiology. *Circulation*. 1996;93:1043-65.
17. Haws CW and Lux RL. Correlation between in vivo transmembrane action potential durations and activation-recovery intervals from electrograms. Effects of interventions that alter repolarization time. *Circulation*. 1990;81:281-8.
18. Vaseghi M, Lux RL, Mahajan A and Shivkumar K. Sympathetic stimulation increases dispersion of repolarization in humans with myocardial infarction. *Am J Physiol Heart Circ Physiol*. 2012;302:H1838-46.
19. Vaseghi M, Zhou W, Shi J, Ajijola OA, Hadaya J, Shivkumar K and Mahajan A. Sympathetic innervation of the anterior left ventricular wall by the right and left stellate ganglia. *Heart Rhythm*. 2012;9:1303-9.
20. Arora RC, Waldmann M, Hopkins DA and Armour JA. Porcine intrinsic cardiac ganglia. *Anat Rec A Discov Mol Cell Evol Biol*. 2003;271:249-58.
21. Shin HC, Aggarwal V, Acharya S, Schieber MH and Thakor NV. Neural decoding of finger movements using Skellam-based maximum-likelihood decoding. *IEEE Trans Biomed Eng*. 2010;57:754-60.
22. Hamdan MH, Zagrodzky JD, Joglar JA, Sheehan CJ, Ramaswamy K, Erdner JF, Page RL and Smith ML. Biventricular pacing decreases sympathetic activity compared with right ventricular pacing in patients with depressed ejection fraction. *Circulation*. 2000;102:1027-32.
23. Smith ML, Hamdan MH, Wasmund SL, Kneip CF, Joglar JA and Page RL. High-frequency ventricular ectopy can increase sympathetic neural activity in humans. *Heart Rhythm*. 2010;7:497-503.

24. Cardinal R, Page P, Vermeulen M, Ardell JL and Armour JA. Spatially divergent cardiac responses to nicotinic stimulation of ganglionated plexus neurons in the canine heart. *Auton Neurosci*. 2009;145:55-62.

25. Taylor JA, Morillo CA, Eckberg DL and Ellenbogen KA. Higher sympathetic nerve activity during ventricular (VVI) than during dual-chamber (DDD) pacing. *J Am Coll Cardiol*. 1996;28:1753-8.

26. Hamdan MH, Zagrodzky JD, Page RL, Wasmund SL, Sheehan CJ, Adamson MM, Joglar JA and Smith ML. Effect of P-wave timing during supraventricular tachycardia on the hemodynamic and sympathetic neural response. *Circulation*. 2001;103:96-101.

27. De Palo G, Facchetti G, Mazzolini M, Menini A, Torre V and Altafini C. Common dynamical features of sensory adaptation in photoreceptors and olfactory sensory neurons. *Sci Rep*. 2013;3:1251.

28. Grill-Spector K, Henson R and Martin A. Repetition and the brain: neural models of stimulus-specific effects. *Trends Cogn Sci*. 2006;10:14-23.

29. Segerson NM, Sharma N, Smith ML, Wasmund SL, Kowal RC, Abedin M, Macgregor JF, Pai RK, Freedman RA, Klein RC, Wall TS, Stoddard G and Hamdan MH. The effects of rate and irregularity on sympathetic nerve activity in human subjects. *Heart Rhythm*. 2007;4:20-6.

30. Kuo CS, Munakata K, Reddy CP and Surawicz B. Characteristics and possible mechanism of ventricular arrhythmia dependent on the dispersion of action potential durations. *Circulation*. 1983;67:1356-67.

31. Vassallo JA, Cassidy DM, Kindwall KE, Marchlinski FE and Josephson ME. Nonuniform recovery of excitability in the left ventricle. *Circulation*. 1988;78:1365-72.

32. Panikkath R, Reinier K, Uy-Evanado A, Teodorescu C, Hattenhauer J, Mariani R, Gunson K, Jui J and Chugh SS. Prolonged Tpeak-to-tend interval on the resting ECG is associated with increased risk of sudden cardiac death. *Circ Arrhythm Electrophysiol*. 2011;4:441-7.

33. Ichikawa T, Sobue Y, Kasai A, Kiyono K, Hayano J, Yamamoto M, Okuda K, Watanabe E and Ozaki Y. Beat-to-beat T-wave amplitude variability in the risk stratification of right ventricular outflow tract-premature ventricular complex patients. *Europace*. 2016;18:138-45.

34. Swerdlow C, Chow T, Das M, Gillis AM, Zhou X, Abeyratne A and Ghanem RN. Intracardiac electrogram T-wave alternans/variability increases before spontaneous ventricular tachyarrhythmias in implantable cardioverter-defibrillator patients: a prospective, multi-center study. *Circulation*. 2011;123:1052-60.

35. Verrier RL, Klingenheben T, Malik M, El-Sherif N, Exner DV, Hohnloser SH, Ikeda T, Martinez JP, Narayan SM, Nieminen T and Rosenbaum DS. Microvolt T-wave alternans physiological basis, methods of measurement, and clinical utility--consensus guideline by International Society for Holter and Noninvasive Electrocardiology. *J Am Coll Cardiol*. 2011;58:1309-24.

36. Gomes JA, Alexopoulos D, Winters SL, Deshmukh P, Fuster V and Suh K. The role of silent ischemia, the arrhythmic substrate and the short-long sequence in the genesis of sudden cardiac death. *J Am Coll Cardiol*. 1989;14:1618-25.

37. Viskin S, Heller K, Barron HV, Kitzis I, Hamdan M, Olgin JE, Wong MJ, Grant SE and Lesh MD. Postextrasystolic U wave augmentation, a new marker of increased arrhythmic risk in patients without the long QT syndrome. *J Am Coll Cardiol*. 1996;28:1746-52.

38. Yagishita D, Chui RW, Yamakawa K, Rajendran PS, Ajijola OA, Nakamura K, So EL, Mahajan A, Shivkumar K and Vaseghi M. Sympathetic nerve stimulation, not circulating norepinephrine, modulates T-peak to T-end interval by increasing global dispersion of repolarization. *Circ Arrhythm Electrophysiol*. 2015;8:174-85.

39. Han J and Moe GK. Nonuniform Recovery of Excitability in Ventricular Muscle. *Circ Res*. 1964;14:44-60.

40. Vaseghi M and Shivkumar K. The role of the autonomic nervous system in sudden cardiac death. *Prog Cardiovasc Dis*. 2008;50:404-19.

41. Yu L, Scherlag BJ, Li S, Sheng X, Lu Z, Nakagawa H, Zhang Y, Jackman WM, Lazzara R, Jiang H and Po SS. Low-level vagosympathetic nerve stimulation inhibits atrial fibrillation inducibility: direct evidence by neural recordings from intrinsic cardiac ganglia. *J Cardiovasc Electrophysiol*. 2010;22:455-63.

42. Shen MJ, Shinohara T, Park HW, Frick K, Ice DS, Choi EK, Han S, Maruyama M, Sharma R, Shen C, Fishbein MC, Chen LS, Lopshire JC, Zipes DP, Lin SF and Chen PS. Continuous low-level vagus nerve stimulation reduces stellate ganglion nerve activity and paroxysmal atrial tachyarrhythmias in ambulatory canines. *Circulation*. 2011;123:2204-12.

43. Wang Z, Yu L, Wang S, Huang B, Liao K, Saren G, Tan T and Jiang H. Chronic intermittent low-level transcutaneous electrical stimulation of auricular branch of vagus nerve improves left ventricular remodeling in conscious dogs with healed myocardial infarction. *Circ Heart Fail*. 2014;7:1014-21.

44. Tanaka Y, Rahmutula D, Duggirala S, Nazer B, Fang Q, Olgin J, Sievers R and Gerstenfeld EP. Diffuse fibrosis leads to a decrease in unipolar voltage: Validation in a swine model of premature ventricular contraction-induced cardiomyopathy. *Heart Rhythm*. 2016;13:547-54.

45. Piccirillo G, Ogawa M, Song J, Chong VJ, Joung B, Han S, Magri D, Chen LS, Lin SF and Chen PS. Power spectral analysis of heart rate variability and autonomic nervous system activity measured directly in healthy dogs and dogs with tachycardia-induced heart failure. *Heart Rhythm*. 2009;6:546-52.

46. Tan AY, Hu YL, Potfay J, Kaszala K, Howren M, Sima AP, Shultz M, Koneru JN, Ellenbogen KA and Huizar JF. Impact of ventricular ectopic burden in a premature ventricular contraction-induced cardiomyopathy animal model. *Heart Rhythm*. 2016;13:755-61.

47. Baman TS, Lange DC, Ilg KJ, Gupta SK, Liu TY, Alguire C, Armstrong W, Good E, Chugh A, Jongnarangsin K, Pelosi F, Jr., Crawford T, Ebinger M, Oral H, Morady F and Bogun F. Relationship between burden of premature ventricular complexes and left ventricular function. *Heart Rhythm*. 2010;7:865-9.

CHAPTER 5

Myocardial infarction induces structural and functional remodeling of the intrinsic cardiac nervous system

Sudden cardiac death due to ventricular arrhythmias is one of the leading causes of mortality in the world, resulting in an estimated 4-5 million deaths each year.[1, 2] Dysregulation of the autonomic nervous system (ANS) following myocardial infarction (MI) plays a crucial role in the genesis of arrhythmias and progression of heart failure.[3-5] The cardiac neuraxis is responsible for the dynamic regulation of cardiac electrical and mechanical function,[6, 7] and involves neural networks located from the level of the heart[8] to that of the insular cortex.[9, 10]

At the organ level, the intrinsic cardiac nervous system (ICNS) comprises a distributed network of ganglia and interconnecting nerves.[8] The ICNS, in concert with higher neuraxial centers (intrathoracic extracardiac ganglia, spinal cord, brain stem, and cortex), regulates cardiac excitability and contractile function on a beat-to-beat basis.[6, 7, 11] The ICNS contains all the neuronal elements necessary for intracardiac reflex control independent of higher centers,[12] namely sensory neurons, cholinergic and adrenergic efferent postganglionic neurons, as well as interposed local circuit neurons (LCNs).[8, 11] The largest subpopulation, LCNs, account for the intra- and interganglionic communication that occurs among neurons within the ICNS and is responsible for local information processing.[8, 11]

Cardiac diseases, such as MI, adversely impact the myocardium and its associated neural components.[13-16] Neural signals conveying cardiac injury are transduced by afferents to multiple levels of the cardiac neuraxis.[17] Remodeling within the cardiac neuraxis and its processing of that sensory signal post-MI[18] contribute to neurohumoral activation[19] and the potential for sudden cardiac death.[5] Intrinsic cardiac (IC) neurons from humans with ischemic heart disease contain inclusions and vacuoles, and display degenerative changes in their dendrites and axons.[20] *In vitro* intracellular studies of IC neurons derived from chronic MI animals show enhanced excitability, altered synaptic efficacy, and adaptive changes in neurochemical phenotypes and neuromodulation.[21] However, there is limited knowledge on the

functional consequences of such changes on neural signaling *in vivo*, in the context of a healed infarct.

The objectives of this study were to (1) examine morphological and phenotypic remodeling within the ICNS, and (2) directly evaluate remodeling of ICNS processing of afferent and efferent (parasympathetic and sympathetic) inputs, and their integration by LCNs following MI. In the present study, we show that MI leads to morphological and neurochemical changes within certain IC ganglia. This structural remodeling is paralleled by functional alterations in the processing of afferent and efferent neural signals by the ICNS and a decrease in overall functional network connectivity, or the ability of neurons to respond to independent pairs of stimuli. The heterogeneity in afferent neural signals, along with the remodeling of convergent neurons, could play an important role in the genesis of arrhythmias and progression to heart failure. Characterization of this adverse neural signature in ischemic heart disease has the potential of serving as a marker of disease progression, and can potentially be used for monitoring and evaluating therapies targeting the ANS.

METHODS

Ethical approval

Yorkshire pigs with normal hearts (n = 16; 8 male and 8 female; 49 ± 3 kg) and Yorkshire pigs with healed anteroapical MI (n = 16; 6 male and 10 female; 46 ± 2 kg) were used in this study. All animal experiments were performed in accordance with the National Institute of Health *Guide for the Care and Use of Laboratory Animals* and approved by the UCLA Chancellor's Animal Research Committee.

Creation of MI

MI was induced as previously described.[22] Briefly, animals were sedated with telazol (8 mg/kg, intramusclar), intubated and ventilated. General anesthesia consisted of isoflurane (1-2%, inhalation). A 12-lead electrocardiogram and arterial pressure were monitored. Left femoral arterial access was obtained, and a guidewire (0.035-inch Amplatz Super Stiff Guidewire with J-Tip; Boston Scientific, Marlborough, MA, USA) was placed into the left main coronary artery under fluoroscopy. A 3 mm angioplasty balloon catheter (FoxCross PTA Catheter; Abbot Vascular, Temecula, CA, USA) was then advanced over the guidewire and inflated at approximately the third diagonal coronary artery that arose from the left anterior descending coronary artery. Thirty seconds after balloon inflation, a 5 ml suspension of saline containing 1 ml polystyrene microspheres (Polybead, 90 μm diameter; Polysciences Inc., Warrington, PA, USA) was injected distally into the artery through the central lumen of the catheter. Occlusion of the artery was visualized by contrast angiography, and acute MI was confirmed by the presence of ST-segment elevations in the limb and precordial leads.

Experimental protocol post-MI

Healed MI animals were studied 42 ± 2 days post-MI. MI and age-matched control animals were sedated with telazol (8 mg/kg, intramuscular), intubated and ventilated. General anesthesia was maintained with isoflurane (1-2%, inhalation). Depth of anesthesia was monitored by hemodynamic indices, jaw tone, and pedal withdrawal reflex; anesthesia was adjusted as necessary. Right femoral venous access was obtained for maintenance fluid administration, and right femoral arterial access for monitoring arterial pressure. A median sternotomy was performed to expose the heart, as well as the stellate ganglia, inferior vena cava (IVC), and descending thoracic aorta. A lateral incision of the neck was performed to expose the cervical vagi and carotid arteries. Snare occluders were placed around the vessels (IVC, aorta, and

carotid arteries), and stimulating electrodes placed around (vagi) or into (stellate ganglia) autonomic efferent neural structures. Following the completion of surgery, general anesthesia was changed to α-chloralose (50 mg/kg intravenous bolus with 10 mg/kg/hr continuous intravenous infusion). Body temperature was monitored and maintained via heating pads. Acid-base status was evaluated hourly; respiratory rate and tidal volume were adjusted and bicarbonate was infused as necessary to maintain blood gas homeostasis. At the completion of the experiments, animals were euthanized by an overdose of sodium pentobarbital (100 mg/kg, intravenous) followed by potassium chloride (150 mg/kg, intravenous) to arrest the heart.

Recording IC neuronal activity

A linear microelectrode array (MicroProbes, Gaithersburg, MD, USA) was used to record the *in vivo* activity generated by neurons in the ventral interventricular ganglionated plexus (VIV GP) (Figure 1A). The linear microelectrode array consisted of 16 platinum-iridium electrodes (25 μm diameter electrodes with an exposed tip of 2 mm; impedance 0.3-0.5 MΩ at 1 kHz) (Figure 1B). The electrode was embedded in the VIV GP, which lies near the origin of the left anterior descending coronary artery from the left main coronary artery (Figure 1A).[23] The linear microelectrode array was attached to a flexible cable, thereby allowing it to be semi-floating. The electrode wires, as well as earth and reference electrodes, were connected to a 16-channel microelectrode amplifier with a headstage pre-amplifier (Model 3600; A-M Systems Inc.; Carlsborg, WA, USA). For each channel, filters were set to 300 Hz to 3 kHz with a gain of 5000. An electrode was sewn to the right atrial myocardium to provide a reference right atrial electrogram. Neuronal waveform, electrocardiogram, right atrial electrogram, and hemodynamic data were input to a data acquisition system (Power1401; Cambridge Electronic Design, Cambridge, UK). Data were analyzed offline using the software Spike2 (Cambridge Electronic Design), as previously described.[11]

Left ventricular (LV) hemodynamic assessment

A pressure catheter (Mikro-Tip; Millar Instruments, Houston, TX, USA) was placed into the LV chamber via the left femoral artery and connected to a control unit (PCU-2000; Millar Instruments). LV systolic function was evaluated by end-systolic pressure and maximum rate of pressure change (dP/dt_{max}). LV diastolic function was evaluated by end-diastolic pressure and minimum rate of chamber pressure change.

Afferent neural input assessment

To determine the capacity of IC neurons to transduce mechanosensory afferent inputs, epicardial mechanical stimuli (gentle touch) were applied for 10 seconds at the following 4 sites: (1) right ventricular (RV) outflow tract, (2) RV apex, (3) LV mid-anterior wall, and (4) LV apex. Transient (30 s) occlusions of the IVC and aorta were then performed using a snare occluder to determine the capacity of neurons to transduce acute changes in preload and afterload, respectively.

Efferent neural input assessment

To determine which IC neurons receive parasympathetic and sympathetic efferent inputs, bipolar spiral cuff electrodes (PerenniaFlex Model 304; Cyberonics Inc., Houston, TX, USA) were placed around the cervical vagi and bipolar needle electrodes inserted into the stellate ganglia bilaterally. A stimulator with a photoelectric isolation unit (S88 and PSIU6; Grass Technologies, Warwick, RI, USA) was used to modulate efferent inputs to IC neurons. For each vagus nerve, threshold was defined as the current necessary to evoke a 10% decrease in heart rate or blood pressure (20 Hz frequency, 1 ms pulse width). For each stellate ganglia, threshold was defined as the current necessary to evoke a 10% increase in heart rate or blood pressure (4 Hz frequency, 4 ms pulse width). Each vagus nerve and stellate ganglion was then stimulated

individually for 1 minute at threshold current and a frequency of 1 Hz. This was done to assess direct inputs to the ICNS independent of any changes in cardiac function. Transient (1 min) occlusion of the bilateral carotid arteries (caudal to carotid sinus) was then performed using a snare occluder to determine the capacity of the carotid baroreflex to modulate efferent inputs to IC neurons.

Epicardial pacing

To determine the capacity of IC neurons to respond to cardiac electrical stimulation, a bipolar pacing electrode (St. Jude, St. Paul, MN, USA) was placed at various epicardial sites and pacing (6 mA current; 2 ms pulse width) was performed at 10% above baseline heart rate for 10 captured beats. The following 4 sites were paced: (1) right atrial appendage, (2) RV outflow tract, (3) RV apex, and (4) LV apex.

Ventricular tachyarrhythmia (VT) inducibility

In a separate set of control (n = 8) and healed anteroapical MI animals (n = 8), VT inducibility was evaluated by programmed ventricular stimulation (EPS320; Micropace, New South Wales, Australia) at 2 different cycle lengths (600 ms and 400 ms) with up to 3 extra stimuli (200 ms minimum) from 2 different sites (RV apex and LV anterior wall epicardium).

Tissue processing

Following completion of IC neuronal recording, animals were sacrificed and hearts immediately excised. The fat pads containing the VIV GP, dorsal interventricular ganglionated plexus, right marginal artery ganglionated plexus, and right atrial ganglionated plexus were removed, rinsed in cold (4°C) saline, and transferred to cold 10% phosphate-buffered formalin (Fisher Scientific, Pittsburgh, PA, USA) for 4 days. Afterwards, the tissue was transferred to 70% ethanol (Sigma-

Aldrich, St Louis, MO, USA) and paraffin embedded within 3 days. Sections of 4 μm thickness were cut from the paraffin blocks.

Histologic staining

IC neuronal size was determined from hematoxylin and eosin stained sections (Fisher Scientific, Pittsburgh, PA, USA) using computerized morphometric analysis (Aperio ImageScope; Leica Biosystems, Buffalo Grove, IL, USA).

Immunohistochemical stains

IC neuronal cholinergic phenotype by choline acetyltransferase immunoreactivity (1:200 dilution; cat. no. AB144-P; Millipore Billerica, MA, USA); neuronal adrenergic phenotype was quantified by tyrosine hydroxylase immunoreactivity (1:2000 dilution; cat. no. ab112; Abcam Cambridge, MA, USA); and vasoactive intestinal peptide (VIP) immunoreactivity (cat. no. 20077; ImmunoStar, Hudson, WI, USA). Secondary detection was performed with Dako EnVision+ System– HRP Labeled Polymer Anti-Rabbit (cat. no. K4003; Dako North America Inc., Carpinetria, CA, USA) for tyrosine hydroxylase and VIP at 1:500, and polyclonal rabbit anti-goat immunoglobulins/biotinylated (E0466, Dako) for choline acetyltransferase. Secondary immunoreactivity was detected by diaminobenzidine (Life Technologies, Green Island, NY, USA) as per manufacturer's recommended protocol for all stains. The slides were then scanned digitally and analyses performed on the electronic images. All neurons present in the slides were quantified using computerized image analysis (Aperio ImageScope) at 20-40X magnifications. Staining and quantification of the groups were performed in a blinded fashion.

Data analysis: signal processing of multi-unit IC neuronal activity

Artifact removal and IC neuronal identification were performed using off-line analysis, as previously described (Figure 1C).[11] Briefly, recorded neuronal activity was contaminated by endogenous electrical artifact arising from the activity of the adjacent atrial and ventricular myocardium, as well as by exogenous electrical artifact arising from stimulation of autonomic efferent nerves. Simultaneously occurring activity displaying similar waveforms in more than 3 adjacent channels of the linear microelectrode array was also considered to be artifact. After identification, artifacts were removed from all channels by blanking, or setting the amplitudes of the time interval containing them to 0. This process resulted in a maximum loss of 3% of the total signal. Following artifact removal, individual units were sorted using principal component analysis of waveform shapes.[11]

Data analysis: monitoring the activity of individual IC neurons

For epicardial mechanical stimuli and autonomic efferent nerve stimulations, IC neuronal activity was compared 1 min before the stimuli (baseline) *vs.* during the stimuli. For vascular occlusions and pacing, neuronal activity was compared at baseline *vs.* during the stimuli, as well as at baseline *vs.* 1 min after the stimuli (recovery). After each stimulus, we waited at least 5 min for neuronal activity and hemodynamics to return to baseline levels before proceeding. IC neurons were functionally classified as afferent, efferent or convergent based on their response characteristics to the cardiovascular stimuli (Figure 2B and C). Afferent neurons were defined as those that responded solely to epicardial mechanical stimuli and/or occlusion of the IVC or aorta. Efferent neurons were defined as those that responded solely to stimulation of autonomic efferent nerves (vagus nerve or stellate ganglia) and/or occlusion of the bilateral carotid arteries. Neurons that responded to activation of both afferent and efferent inputs were defined as convergent.[11]

Data analysis: conditional probability

Conditional probability analysis was used to determine whether an IC neuron that responded to 1 stimulus also responded to another stimulus, as previously described.[11] The potential for a functional relationship between stimulus X and Y was quantified within neurons identified in each animal as a conditional probability that a neuron that responded to stimulus Y also responded to stimulus X. The conditional probability (probability: response to Y | response to X) was estimated as the number of neurons that responded to both stimulus X and Y, divided by the number of neurons that responded to stimulus X.

Statistics

The significance level of changes in the firing rate of each IC neuron between baseline *vs.* stimulus and recovery interval was assessed using a statistical test developed for cortical neurons based on the Skellam distribution.[24] This test has been previously validated for the study of IC neurons.[11] A $_X^2$ test was used to compare the neuronal response, and VT inducibility in MI *vs.* control animals. A Wilcoxon's signed-rank test or Mann-Whitney *U* test was used to compare neuronal firing frequencies, resting hemodynamic indices, as well as morphological and phenotypic changes in neurons in MI *vs.* control animals. Data are represented as mean ± standard error of the mean. P values $\leq$ 0.05 were considered to be statistically significant. Statistical analyses were performed using SigmaPlot 12.0 (Systat Software Inc., San Jose, CA, USA).

RESULTS

Healed anteroapical MI animals were in a chronic compensated state and not in overt heart failure, as evidenced by similar resting hemodynamic indices such as LV end-diastolic pressure (3 ± 1 *vs.* 4 ± 1 mmHg; P = 0.59) and LV dP/dt_{max} (1436 ± 112 *vs.* 1426 ± 151 mmHg/s; P =

1.00) in MI *vs.* control animals, respectively. Figure 3J and K illustrates a typical pattern of scar formation induced by the microembolization technique. Since ventricular fibrillation is a terminal event, VT inducibility in this model was evaluated in a separate set of animals. While none of the control animals (n = 8) were inducible, 75% of the MI animals (n = 8) developed ventricular tachycardia and/or fibrillation ($P < 0.01$).

MI induces differential IC neuronal enlargement and phenotypic changes

Histologic and immunohistochemical analyses were performed on VIV GP neurons for size, adrenergic-cholinergic phenotype, and VIP phenotype to evaluate for potential morphological and neurochemical changes induced by MI. VIP is a modulator of cardiac function and a putative afferent marker.[25-28]

VIV GP neurons from MI animals were significantly larger than those from controls (946 ± 23 *vs.* 755 ± 22 μm^2, respectively; $P < 0.01$; Figure 3A-C). A histogram of neuronal size distribution from MI and control animals is shown in Figure 3B. Neuronal enlargement was observed in the VIV GP, dorsal interventricular ganglionated plexus, and right marginal artery ganglionated plexus, which exert preferential influence over the ventricles, but was not observed in the right atrial ganglionated plexus, which exerts preferential influence over the atria (Figure 4A-C).

There was a significant decrease in the percentage of IC neurons expressing choline acetyltransferase in MI animals compared to controls (87 ± 2% *vs.* 91 ± 2%, respectively; $P = 0.04$; Figure 3D and E). In contrast, there was no significant difference in tyrosine hydroxylase expression in MI relative to control animals (3 ± 1% *vs.* 2 ± 1%, respectively; $P = 0.15$; Figure 3F and G). VIP expression was significantly increased in MI *vs.* control animals (66 ± 2% *vs.* 37 ± 3%, respectively; $P < 0.01$; Figure 3H and I). VIP expression was also significantly increased in all the other ganglionated plexi (GPs) studied (Figure 4D and E).

Functional characterization of IC neurons post-MI

The *in vivo* activity of neurons from the VIV GP was recorded in control and MI animals using a microelectrode array to evaluate functional changes in neuronal response characteristics induced by MI (Figures 1 and 2). In 8 control animals, the activity generated by 118 IC neurons from the VIV GP was studied (average: 15 ± 3 neurons per animal; Figure 5A, left panel). In 8 MI animals, the activity generated by 102 neurons was studied (average: 10 ± 2 neurons per animal; Figure 5A, right panel). The spontaneous firing rates of neurons were derived from pooling data from baseline intervals. The average spontaneous firing rate of the neurons from control animals was 0.31 Hz (range: 0 to 4.42 Hz), while the average of those from MI animals was 0.21 Hz (range: 0 to 1.59 Hz). The distribution was overall similar in both states, with more than 90% of neurons firing below 1 Hz.

Based on their response characteristics to the cardiovascular stimuli, IC neurons were functionally classified as afferent, efferent, or convergent (Figures 2B and C, and 5B). In control and MI animals, convergent neurons represented the largest subpopulation (47% *vs.* 48%, respectively), followed by fewer afferent (27% *vs.* 18%, respectively) and efferent (13% *vs.* 15%, respectively) neurons (Figure 5B). In control animals 13% of neurons and in MI animals 20% did not respond to any of the stimuli. There was no significant difference in the overall classifications in either state ($P = 0.26$).

The activity of IC neurons was compared to the cardiac cycle to determine if they exhibited cardiac cycle-related periodicity (Figures 1D and 5C). Based on an activity histogram, neurons that generated at least 100 action potentials at baseline were classified as being related to a specific phase of the cardiac cycle if more than 30% of their activity occurred during the given phase. Forty-six neurons (39%) in control animals and 30 neurons (29%) in MI animals that satisfied this criterion were analyzed for cardiac cycle-related periodicity (Figure 5C). In control animals, 52% of neurons displayed diastolic-related activity, 28% displayed

systolic-related activity, 17% displayed dual diastolic- and systolic-related activity, and 2% displayed stochastic behavior. In contrast, in MI animals, 43% of neurons displayed diastolic-related activity, 50% displayed systolic-related activity, 3% displayed dual diastolic- and systolic-related activity, and 3% displayed stochastic behavior.

Afferent remodeling of IC neurons post-MI

MI differentially affected the capacity of IC neurons to transduce mechanosensitive afferent inputs arising from the infarct *vs.* border and remote zones of the heart, as assessed by applying mechanical stimuli to myocardial tissue overlying these regions (Figure 6A and B). The neuronal response to activation of mechanosensitive inputs arising from border and remote zones (RV outflow tract, RV apex, and LV mid-anterior wall) in MI animals was similar to that in controls (34% in MI *vs.* 24% in control; P = 0.12). In contrast, significantly fewer neurons responded to activation of mechanosensitive inputs arising from the infarct (LV apex) following MI (7% in MI *vs.* 19% in control; P = 0.03).

The capacity of IC neurons to transduce changes in cardiac loading conditions was also impacted following MI (Figure 6C). In MI animals, the neuronal response to a decrease in preload, induced by transient IVC occlusion, was significantly diminished (41% in MI *vs.* 54% in control; P = 0.05). There was no significant difference in the neuronal response to an increase in afterload induced by transient partial occlusion of the descending aorta (47% in MI *vs.* 35% in control; P = 0.13). MI likewise did not significantly alter the overall capacity of neurons to transduce multimodal afferent neural signals (Figure 6D; a similar percentage of neurons in both states received 1, 2, or greater than 3 afferent inputs [P = 0.84]). These afferent inputs included epicardial mechanical stimuli and transient occlusion of the IVC and aorta.

Efferent remodeling of IC neurons post-MI

MI did not affect the capacity of IC neurons to individually transduce parasympathetic and sympathetic efferent inputs, as assessed by low frequency stimulation of the cervical vagi and stellate ganglia, respectively (Figure 6E). Stimulation of these autonomic efferent nerves was carried out at low frequencies to evaluate direct efferent inputs to the ICNS, rather than an indirect response resulting from changes in cardiac function. There was no significant difference in the percentage of neurons receiving inputs from either the left or right cervical vagus nerve in MI animals compared to controls (35% *vs.* 27%, respectively; P = 0.23). A similar pattern was observed with regards to the percentage of neurons receiving inputs from either the left or right stellate ganglion (41% in MI *vs.* 31% in control; P = 0.12). Interestingly, there was a significant increase in the percentage of neurons that received efferent inputs from both the sympathetic and parasympathetic divisions of the ANS in MI animals relative to controls (21% *vs.* 10%, respectively; P = 0.03). Of these neurons that received both parasympathetic and sympathetic inputs, 90% also responded to stimulation of 1 or more afferent inputs in both control (10 of 11 neurons) and MI (19 of 21 neurons) animals. As such, these neurons were classified as convergent.

To assess the effects of MI on baroreflex modulation of efferent inputs to IC neurons, the bilateral carotid arteries were occluded caudal to carotid sinus (Figure 6F). There was no significant difference in the percentage of neurons responding to carotid artery occlusion in either state (34% in MI *vs.* 32% in control; P = 0.77).

MI induces changes in IC neuronal response to pacing

MI differentially impacted the response of IC neurons to epicardial pacing (Figures 7A and 8A). Whereas the neuronal response to right atrial appendage pacing (with ventricular capture) was not altered (31% in MI *vs.* 36% in control; P = 0.46), the response to ventricular pacing was

reduced (44% in MI *vs.* 63% in control; $P < 0.01$). Neurons that responded to pacing were classified functionally as afferent, efferent, or convergent (Figures 7B and C, and 8B). The neuronal response evoked from pacing at the RV outflow tract (remote zone) and LV apex (infarct) was most dramatically affected post-MI ($P = 0.05$). This alteration was primarily reflected as an upregulation of pacing-responsive convergent neurons and a corresponding downregulation in pacing-responsive afferent neurons. It is also noteworthy that in all sites evaluated in control animals and most sites in MI animals pacing engaged a unique subpopulation of neurons, which only responded to pacing and none of the other afferent or efferent stimuli (Figure 8B, red bars).

State dependence of IC neurons: impact on evoked response

Basal activity impacts IC neuronal response to subsequent cardiovascular stimuli, including pacing (Figure 9). In both control and MI animals, neurons with low basal activity tended to be activated by pacing ($P < 0.01$). Conversely, neurons with high basal activity tended to be suppressed by pacing ($P < 0.01$). These results indicate the state-dependent nature of such neurons.

Interdependence of IC neuronal response to stimuli post-MI

The relationship between the IC neuronal responses to afferent and efferent stimuli, as well as pacing, was determined in both control and MI animals. The conditional probability of whether a neuron that responded to 1 stimulus also responded to another stimulus is represented in a matrix format (Figure 10A and C). These data are also depicted graphically as a network, with only links with conditional probabilities ≥ 0.6 displayed (Figure 10B and D). These relationships reflect the concordant behavior among VIV GP neuronal populations induced by pairs of independent stimuli. MI reduces the overall functional network connectivity within the ICNS.

DISCUSSION

The present study characterized structural and *in vivo* functional remodeling of neuronal elements within the ICNS following MI, and represents the first 'cardiac electroneurogram' of the chronic infarcted heart. Network function of the ICNS was assessed in the VIV GP, a plexus primarily associated with control of ventricular function.[29] There are several major findings from this study.

(1) IC ganglia undergo morphological and phenotypic remodeling post-MI. The site of injury determines which ganglia remodel.

(2) Afferent neural signals from the infarcted region to IC neurons are attenuated, while those from border and remote regions are preserved following MI, giving rise to a 'neural sensory border zone', or heterogeneity in afferent information from injured vs. adjacent non-injured myocardial tissue (Figure 11). Alteration in afferent neural signals is also manifested by a reduced capacity of IC neurons to transduce changes in preload.

(3) Autonomic efferent inputs to the ICNS are maintained post-MI (Figure 11).

(4) Convergent IC LCNs, those receiving both afferent and efferent inputs, have enhanced transduction capacity following MI (Figure 11).

(5) Functional network connectivity within the ICNS is reduced post-MI.

(6) MI reduces the response and alters the characteristics of IC neurons to ventricular pacing.

The only difference between control and MI animals was the presence of an infarct scar. Therefore, the structural and functional changes we noted are likely attributed to the MI. We studied the remodeling of the ICNS 6 weeks after the creation of the MI. This represents a stable phase for autonomic adaptations and is beyond the acute phase remodeling, characterized by myocyte death and neural degeneration.[21] Based on hemodynamic indices such as LV end-diastolic pressure and contractility, the animals were in a chronic compensated

state and had not transitioned into overt heart failure. We recorded neuronal activity from the VIV GP because it is primarily involved in control of ventricular function[29] and its neuronal somata are located upstream from the infarct zone.[23] Thus, the neural remodeling we observed is not due to direct ischemic injury to the neurons.

We evaluated VT inducibility and demonstrated that MI animals in this model have a significantly higher inducibility. Since ventricular fibrillation is a terminal event, inducibility was evaluated in a separate set of animals. Specifically, the cardioversion shocks required to resuscitate the animals would have disrupted and/or dislodged our neuronal recording interface and precluded our detailed characterization of the ICNS. Moreover, the shocks by themselves have the potential to alter subsequent neural activity. We have also previously demonstrated that heterogeneous pharmacological or electric activation of the ICNS is arrhythmogenic,[11, 30] and that blunting of the neural response reduces the potential for arrhythmias.[31-33] Taken together, we can now hypothesize that the altered neural signature we observed following MI could be relevant to ventricular arrhythmogenesis.

Differential morphological and neurochemical remodeling of neurons within the ICNS

MI induced morphological changes in neurons within the VIV GP. IC neuronal enlargement was observed in the GPs that exert preferential influence over the ventricles, and not the GP that exerts preferential influence over the atria.[29] Neurons have been reported to hypertrophy in response injury[34-36] and chronic signaling.[37] However, since the GPs that we studied were located upstream from the infarct, the latter mechanism is likely the case here. The differential enlargement in neuronal size suggests that there is heterogeneity in afferent and efferent neural signals following MI, with neurons directly involved in control of the infarcted regions most impacted. Further, the site of injury determines which ganglia remodel. This heterogeneity, observed both in our structural and functional data, potentially has an important role in

arrhythmogenesis.[38] These structural changes are similar to those that have been reported in intrathoracic extracardiac ganglia in both humans and animals models of ischemic cardiomyopathy.[15, 37, 39, 40]

MI induced a decrease in the cholinergic phenotype within the VIV GP. The decrease in cholinergic neurons may correlate with the centrally mediated parasympathetic withdrawal seen post-MI.[41, 42] While we did not evaluate for adrenergic-cholinergic transdifferentiation, there is strong evidence indicating that this occurs within other ganglia of the cardiac neuraxis in disease states.[5, 43] There was also increased expression of VIP in all of the GPs following MI (Figure 4D and E). VIP is known to act as a coronary vasodilator and have inotropic and chronotropic effects.[25-27] The increased expression of VIP within the ICNS following MI may represent a compensatory mechanism to maintain cardiac function by vasodilation to improve coronary blood flow, as well as enhanced inotropy and chronotropy. VIP has also been implicated in nociception.[28] The increase in VIP-positive neurons may also be a result of enhanced afferent signaling post-MI.

Neural sensory inputs from infarct border zones

While alterations in efferent neural signals post-MI has been extensively documented, little attention has been given to afferent neural signals originating from the injured and adjacent non-injured myocardial tissue. Anatomical and functional studies have identified unipolar neurons in IC ganglia with sensory neurites located in atrial and ventricular tissues.[8] These afferent neurons transduce the local mechanical and chemical milieu of the heart.[8] Afferent neurons contained within each GP have spatially divergent receptive fields,[29, 44] allowing for transduction of sensory information from widespread cardiac regions. We show that VIV GP neurons, located adjacent the origin of the left anterior descending coronary artery from the left main coronary artery,[23] transduce sensory inputs arising from diverse cardiac regions overlying the RV and LV.

Following MI, myocardial necrosis occurs in the infarct zone secondary to ischemia. Further, a lack of energy substrates and a buildup of molecules such as reactive oxygen species trigger a cascade of intracellular signaling processes that result in remodeling of myocytes in the infarct border zone.[45] Concurrent with myocyte remodeling, there are adaptive and maladaptive changes that occur at multiple levels of the cardiac neuraxis including the ICNS.[17] In the acute state, there is excessive and aberrant activation of IC neurons transducing afferent signals from the injured myocardial tissue.[17, 46] Our data demonstrate that in the chronic state, afferent signals from the infarct to the ICNS are reduced but not completely abolished, while those from border and remote regions are preserved. This heterogeneity in afferent neural signals gives rise to boundary conditions and a 'neural sensory border zone' analogous to the myocardial border zone induced by scar formation. The importance of sensory boundary conditions has already been shown in other neural circuits, such as the visual system where there is an enhanced ability for retinal ganglion cells to detect non-uniform light fields.[47] We hypothesize that the MI-induced asymmetry in afferent inputs to the ICNS may underlie reflex activation of the ANS, including sympathoexcitation. In this regard, application of resiniferatoxin, a potent agonist of transient receptor potential vanilloid 1, post-MI decreases cardiac afferent nociceptive signaling, reduces sympathoexcitation, and is associated with preserved cardiac function.[18] These data point to the fundamental importance of afferent neural signals in the progression of cardiac disease and their role as a therapeutic target to manage the disease process.

Convergent LCNs: information processing within the ICNS

In the present study, we show that a subpopulation of IC neurons, termed convergent LCNs, receive both afferent and efferent inputs. Convergent LCNs, together with afferent and efferent neurons, form the basic constituents of the IC neural circuitry.[8, 11] Within this circuit, convergent

LCNs integrate and process information, and the presence of a large subpopulation of these neurons even in the MI state demonstrate that the capacity for local information processing is maintained. While there was no difference in the overall functional classification of neurons post-MI (afferent, efferent, and convergent), the integrated neural network response to cardiovascular stimuli adapted and/or remodeled. This was evident in the neuronal response to changes in preload and to regional pacing, as well as the altered functional neural network connectivity as assessed by the conditional probability analysis. Although most neurons that responded to pacing were also found to transduce dynamic cardiovascular changes, there was a unique subset that solely responded to pacing. The altered ICNS response to pacing at not only the infarct but also remote zones of the heart indicates that pacing may place additional stress on the ICNS on top of that imposed by the MI. In the clinical setting, ventricular pacing has been shown to have detrimental effects on cardiac function, causing dyssynchrony of the ventricles.[48] Pacing in the presence of an infarct scar has also been reported to cause electrical storm.[49] Further, it can accelerate the progression of heart failure and increase mortality.[50, 51] A potential mechanism underlying these adverse events relates to activation of the neuroendocrine system.[52] It is intriguing to hypothesize that modulation of ICNS activity, in conjunction with MI-induced remodeling of afferent neural signals, could be a fundamental link between pacing and neuroendocrine system activation.

Efferent neural control

The ICNS was classically viewed as a simple relay station for parasympathetic preganglionic efferent projections to the heart.[53] Contrary to this view and in support of data obtained in a canine model,[11] we show that a large percentage of porcine IC neurons received inputs from the sympathetic or parasympathetic nervous system, as well as complex cardiovascular afferent inputs. The fact that a subset of IC neurons received a confluence of efferent inputs (inputs from

both a stellate ganglion and vagus nerve) implies that a significant degree of sympathetic-parasympathetic interactions occur within the ICNS.[54, 55]

Alterations in efferent neural signals following MI occur at multiple levels of the cardiac neuraxis.[13-15, 17, 21, 39, 40, 56, 57] At the organ level, sympathetic denervation of the infarcted myocardium and hyperinnervation of the border zones has been observed.[13, 14] Morphological and neurochemical changes have also been noted in neurons contained within sympathetic ganglia such as the stellate.[15, 39] The increases in sympathetic influences are accompanied by a withdrawal in centrally mediated parasympathetic influences.[41, 42] Despite these alterations in sympathovagal balance, our data demonstrate sympathetic and parasympathetic inputs to the ICNS are maintained post-MI. In fact, the percentage of IC neurons receiving convergent efferent inputs doubled following MI. The vast majority of these IC neurons, in turn, were convergent local circuit in nature as evidenced by the fact that 90% of them were impacted by afferent stimuli. This adaptation may be an attempt to maintain peripheral neural network stability in face of the destabilizing effects imposed by sympathovagal imbalance and the disparate afferent inputs arising from the infarct *vs.* border and remote regions of the heart.

LIMITATIONS

General anesthetics can suppress the activity of the nervous system. To reduce the effects of inhaled anesthetics, we switched to *α*-chloralose infusion immediately after completing the surgical preparation. We used gentle touch as a mechanical stimulus to determine the sensory fields of afferent neurons contained within the VIV GP. While there are methods to record and label neurons, we were recording neurons from a beating heart, which necessitated the use of a floating microelectrode array. Therefore, we focused on characterizing the *in vivo* function of the neurons with *post hoc* evaluation for structural changes. We studied the functional neural remodeling that occurred in only 1 of the 7 GPs in the porcine heart;[23] however, this GP is

primarily associated with control of ventricular function[29] and was likely most impacted by the infarction, as supported by our histological data. We evaluated structural and functional changes in the ICNS at a fixed point in time following MI. There are dynamic changes that occur in the cardiac neuraxis during the evolution of cardiac disease,[5, 21] and therefore, the neural signature may show different features as disease progresses. Finally, while we demonstrated that MI animals in this model have enhanced arrhythmogenesis, we did not obtain neuronal recordings in the same animals that underwent VT inducibility and attempt to characterize the ICNS neural signature during ventricular tachycardia and/or fibrillation. The cardioversion shocks required to resuscitate the animals would have disrupted and/or dislodged our neuronal recording interface and precluded detailed characterization of the ICNS.

ADDITIONAL INFORMATION

Competing interests

None.

Author contributions

P.S.R., J.L.A., and K.S. designed all experiments; P.S.R. performed all neuronal recording experiments and related analyses; K.N. and O.A.A. performed all immunohistochemical experiments and related analyses; P.S.R. and M.V. performed all VT inducibility studies; all authors contributed to writing the paper. All authors have approved the final version of the manuscript and agree to be accountable for all aspects of the work. All persons designated as authors qualify for authorship, and all those who qualify for authorship are listed.

Funding

This work was supported by National Institutes of Health (NIH) National Heart, Lung, and Blood Institute (NHLBI) Grant R01HL084261 to K.S. and R01HL071830 to J.L.A. P.S.R. was supported by NIH National Institute of General Medical Sciences Grant 2T32GM065823, American Heart Association Grant 15PRE22230011, and NIH NHLBI Grant F31HL127974. O.A.A. was supported by NIH NHLBI Grant K08HL125730. M.V. was supported by American Heart Association Grant 11FTF7550004.

TRANSLATIONAL PERSPECTIVE

The present study provides direct evidence that the functional neural signature of the ICNS is altered in MI in a clinically relevant large animal model, and highlights the utility of neuronal recordings in elucidating the neural adaptation and/or maladaptation to cardiac disease. The heterogeneity of afferent neural signals is likely fundamental to reflex activation of the ANS, thereby impacting the potential for arrhythmias[5, 38] and progression to heart failure.[19] Modulation of afferent neural signals from the diseased myocardium to the ICNS, intrathoracic extracardiac ganglia, and higher centers of the cardiac neuraxis should be investigated as a novel therapeutic approach to mitigating ischemic heart disease. These findings also raise the possibility that ‘cardiac electroneurography’ could serve as a modality for studying cardiac physiology and pathophysiology by providing a potential way to monitor disease progression and the effects of interventions.

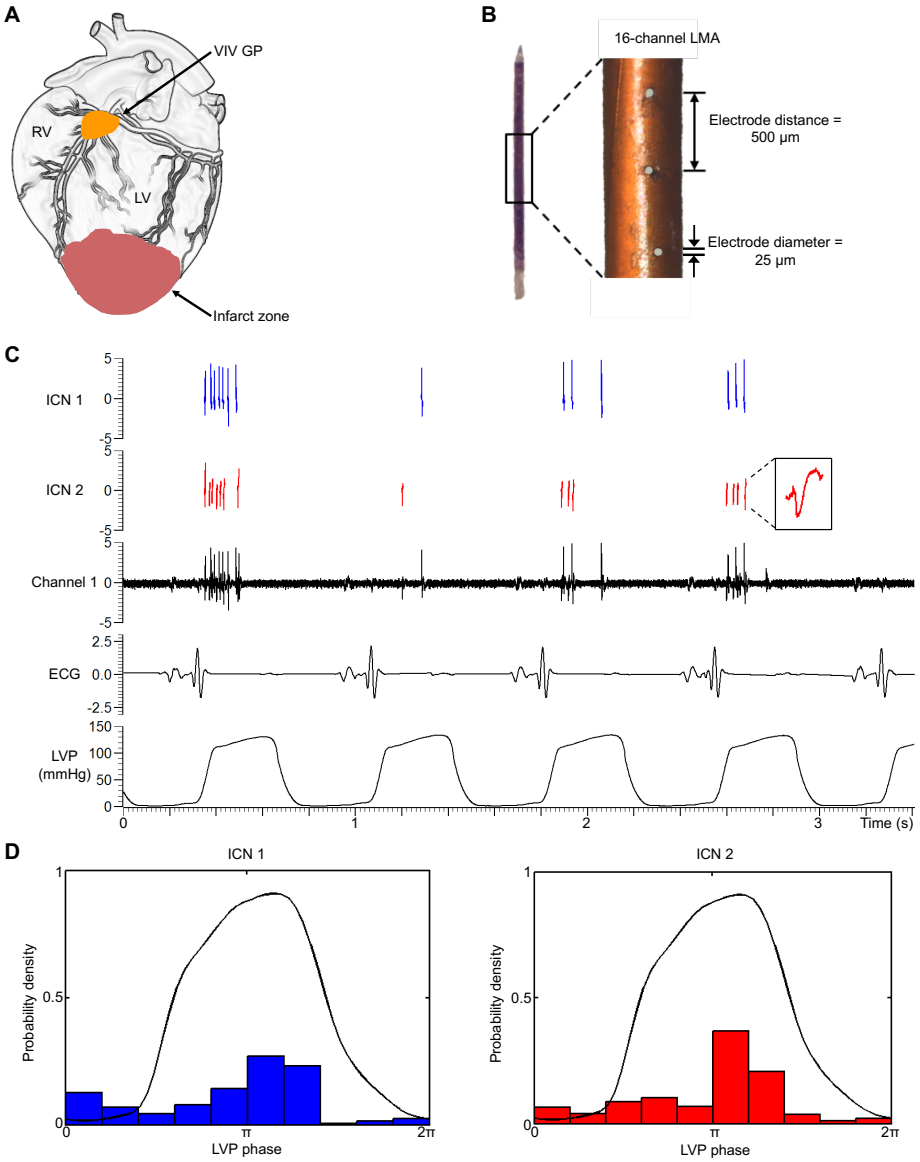

Figure 1. Methods: intrinsic cardiac neuronal recording. (A) Schematic showing location of ventral interventricular ganglionated plexus (VIV GP), from which neuronal activity was recorded. **(B)** 16-channel linear microelectrode array (LMA) used to record *in vivo* activity of multiple individual neurons contained within the VIV GP. **(C)** Representative trace showing the activity of 2 intrinsic cardiac neurons (ICNs) (ICN 1 and ICN 2) identified from a single electrode (channel 1) of the LMA. ICN 2 inset is an expanded version of identified neuron. **(D)** Basal activity of the neurons from panel C in relation to the cardiac cycle. Note that the activity of both

neurons is clustered predominantly during systole. ECG, electrocardiogram; LV, left ventricle, LVP, left ventricular pressure; RV, right ventricle.

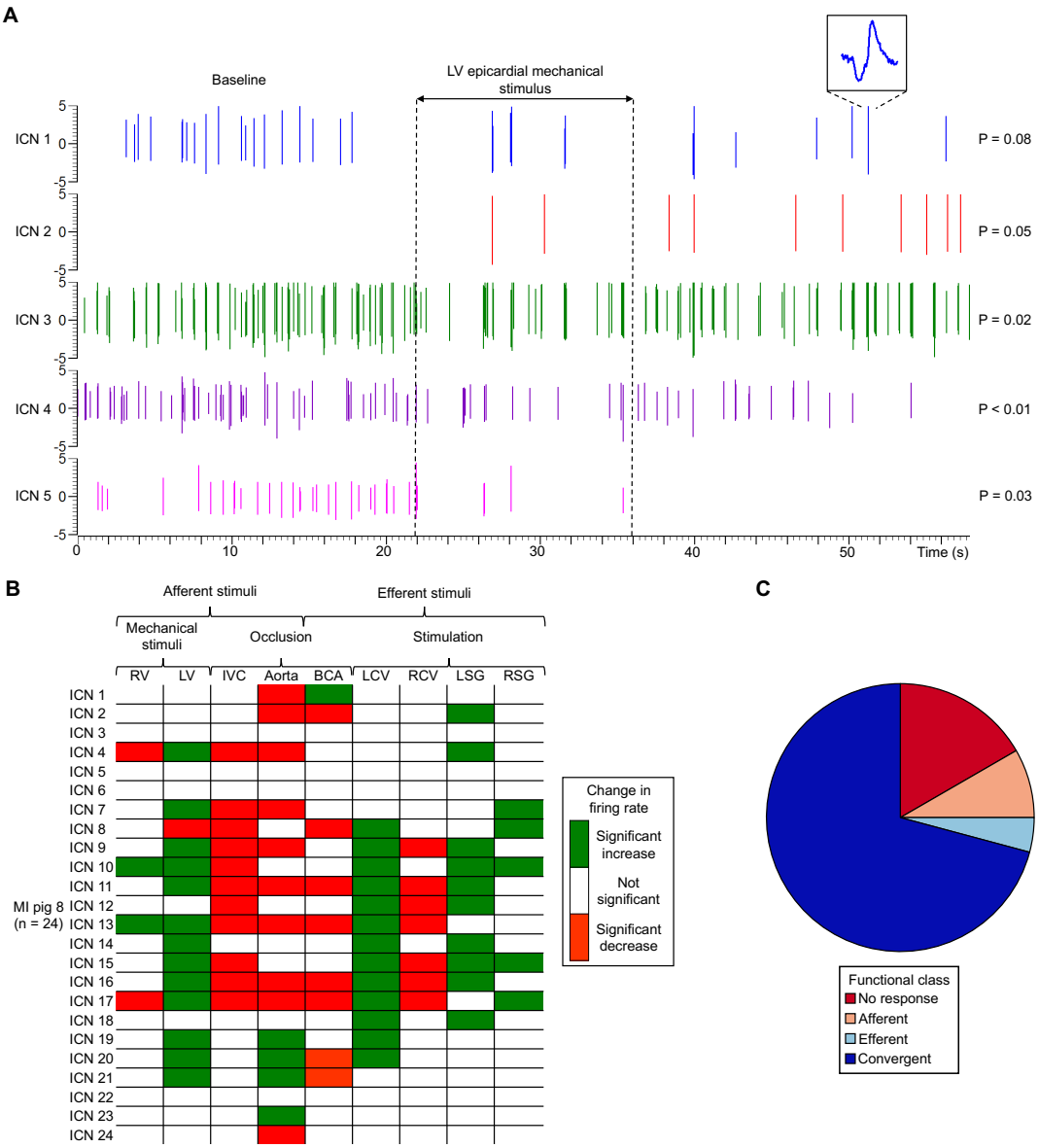

Figure 2. Analytics and functional classification of intrinsic cardiac neurons (ICNs). (A) Spiking activity recorded from 5 ICNs in a control heart. Vertical dotted lines indicate the onset and offset of left ventricular (LV) epicardial mechanical stimulus. ICN 1 inset is an expanded version of identified neuron. Note that subpopulations of neurons showed an increase (ICN 2), a decrease (ICN 3, 4, and 5), or no change in activity (ICN 1) from baseline. The significance levels of induced changes in activity are shown to the right of each trace. P values were derived based on the analysis described in the Methods. **(B)** Summary of evoked changes in neuronal

activity in response to cardiovascular stimuli in a myocardial infarction (MI) animal. Horizontal rows represent the response of an individual neuron to a given stimulus (vertical columns). Green indicates significant increases in activity ($P < 0.05$); red indicates significant decreases ($P < 0.05$). **(C)** Functional classification of neurons depicted in panel B. Neurons were classified as afferent, efferent, or convergent based on their responses to the cardiovascular stimuli. Afferent neurons were defined as those that responded solely to: epicardial mechanical stimuli of the right ventricle (RV) or LV; transient occlusion of the inferior vena cava (IVC); and/or transient occlusion of the descending thoracic aorta. Efferent neurons were defined as those that responded solely to: electrical stimulation of the left (LCV) or right cervical vagus nerve (RCV); electrical stimulation of the left (LSG) or right stellate ganglion (RSG); and/or transient occlusion of the bilateral carotid arteries (BCA). Neurons that responded to activation of both afferent and efferent inputs were defined as convergent.

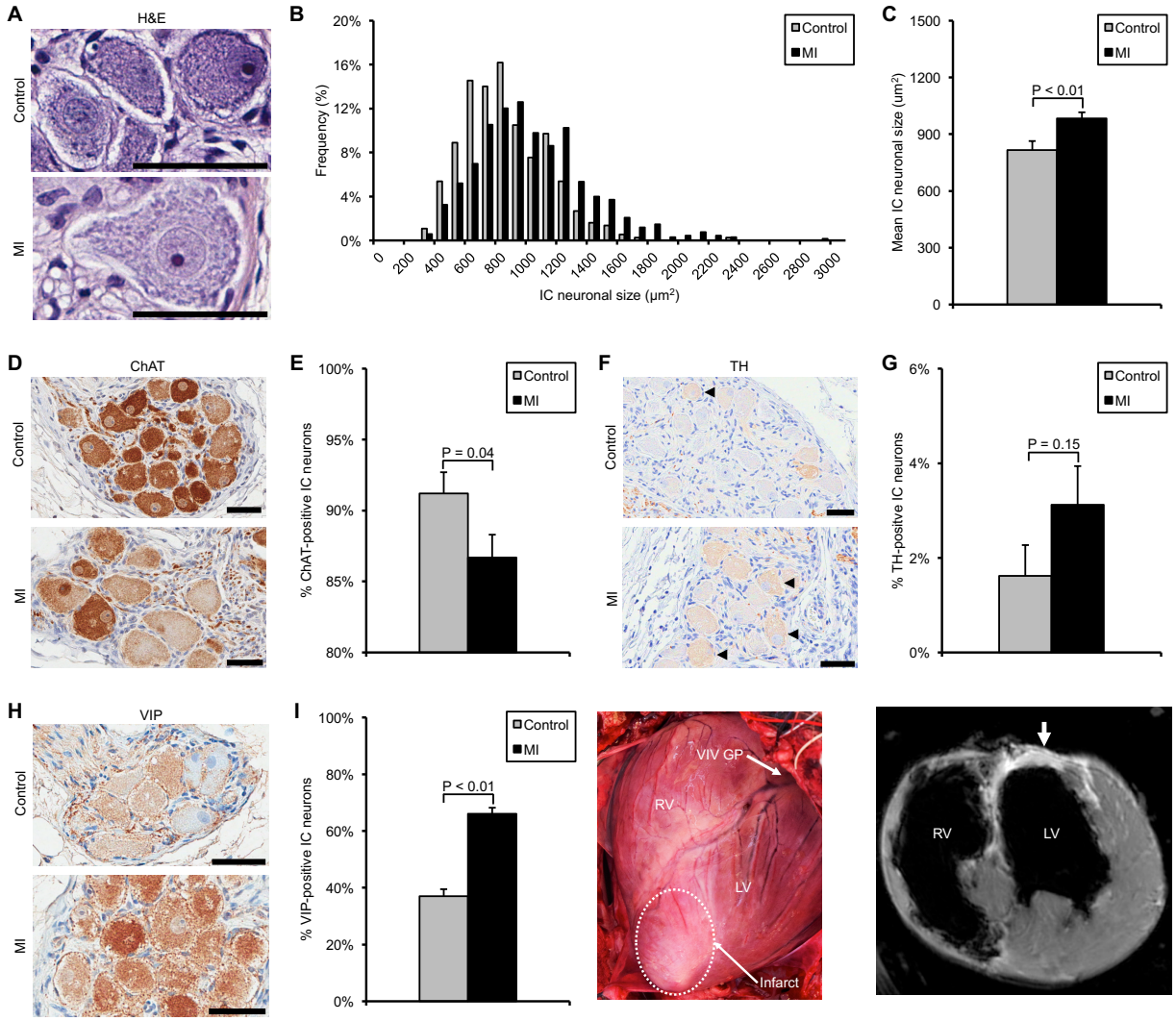

Figure 3. Myocardial infarction (MI) induces morphological and phenotypic remodeling of intrinsic cardiac (IC) neurons. (A) Photomicrographs showing hematoxylin and eosin (H&E) stained neurons from the ventral interventricular ganglionated plexus (VIV GP) in control *vs.* MI animals. **(B)** Histogram of IC neuronal size distribution in control *vs.* MI animals. **(C)** Mean neuronal size in control *vs.* MI animals. **(D)** Photomicrographs showing VIV GP stained with choline acetyltransferase (ChAT) in control *vs.* MI animals. ChAT catalyzes the synthesis of acetylcholine and was used to identify putative cholinergic neurons. **(E)** Percentage of ChAT-positive neurons in control *vs.* MI animals. **(F)** Photomicrographs showing VIV GP stained with tyrosine hydroxylase (TH) in control *vs.* MI animals. TH catalyzes the rate-limiting step in the

synthesis of norepinephrine and was used to identify putative adrenergic neurons (black arrowheads). **(G)** Percentage of TH-positive neurons in control *vs.* MI animals. **(H)** Photomicrographs showing VIV GP stained with vasoactive intestinal peptide (VIP) in control *vs.* MI animals. VIP is a modulator of cardiac function and a marker of putative afferent neurons. **(I)** Percentage of VIP-positive neurons in control and MI animals. **(J)** Image of a porcine heart with a healed anteroapical MI. The location of the VIV GP in relation to the infarct scar (white dashed scar) is shown. **(K)** Corresponding short-axis cardiac magnetic resonance image of the heart. White arrow indicates areas of delayed hyperenhancement resulting from scar tissue. Data in C, E, G, and I are presented as mean ± standard error of the mean. Mann-Whitney *U* test was used in C, E, G, and I to determine significance between groups. Scale bars in A, D, F, and H represent 50 μm. RV, right ventricle.

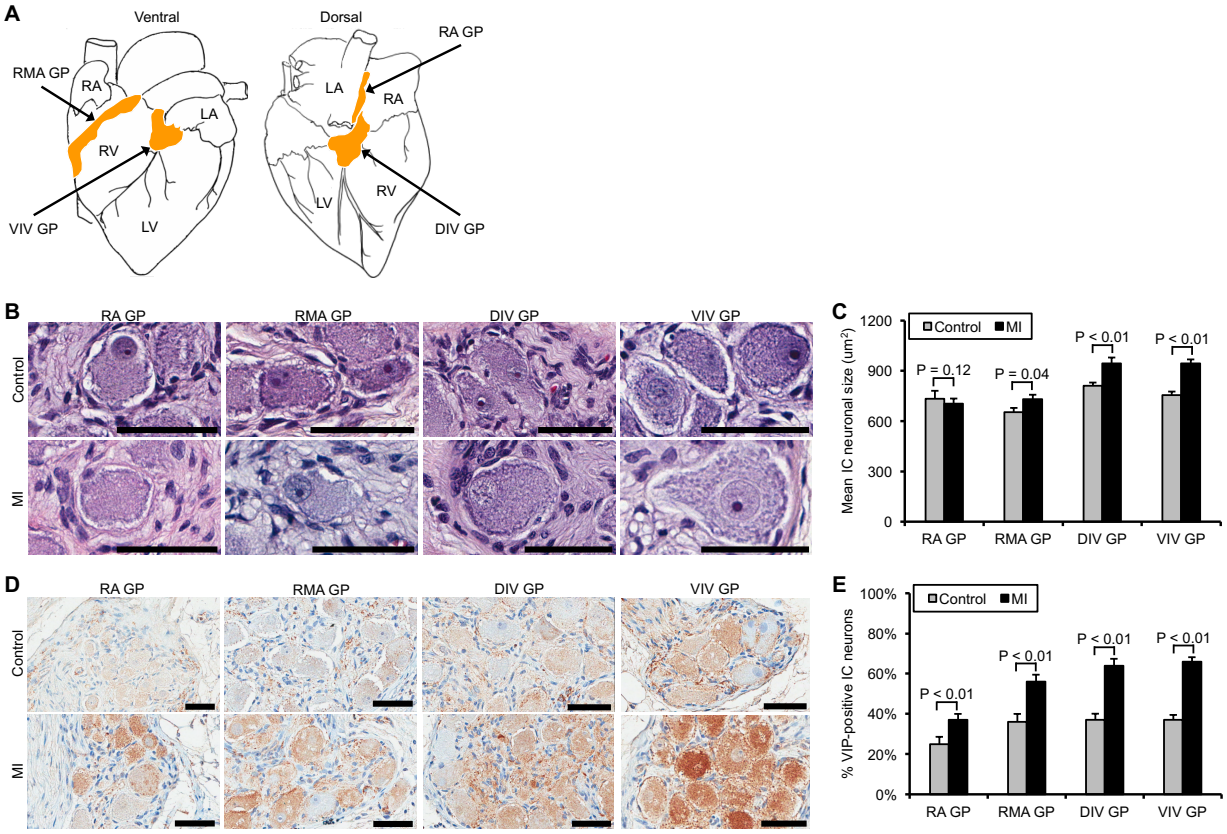

Figure 4. Myocardial infarction (MI) induces differential morphological and neurochemical remodeling of intrinsic cardiac (IC) neurons. **(A)** Schematic showing location of right atrial ganglionated plexus (RA GP), right marginal artery ganglionated plexus (RMA GP), dorsal interventricular ganglionated plexus (DIV GP), and ventral interventricular ganglionated plexus (VIV GP). The RA GP and RMA GP exert preferential influence over the right atrium (RA) and right ventricle (RV), respectively, whereas the DIV GP and VIV GP exert preferential influence over the left ventricle (LV). **(B)** Photomicrographs showing hematoxylin and eosin stained neurons from the ganglionated plexi studied in control *vs.* MI animals. **(C)** Mean IC neuronal size in the ganglionated plexi in control *vs.* MI animals. **(D)** Photomicrographs showing the ganglionated plexi stained with VIP in control *vs.* MI animals. **(E)** Percentage of VIP-positive neurons in the ganglionated plexi in control *vs.* MI animals. Data in C and E are

presented as mean ± standard error of the mean. Mann-Whitney *U* test was used in C and E to determine significance between groups. Scale bars in B and D represent 50 μm. LA, left atrium.

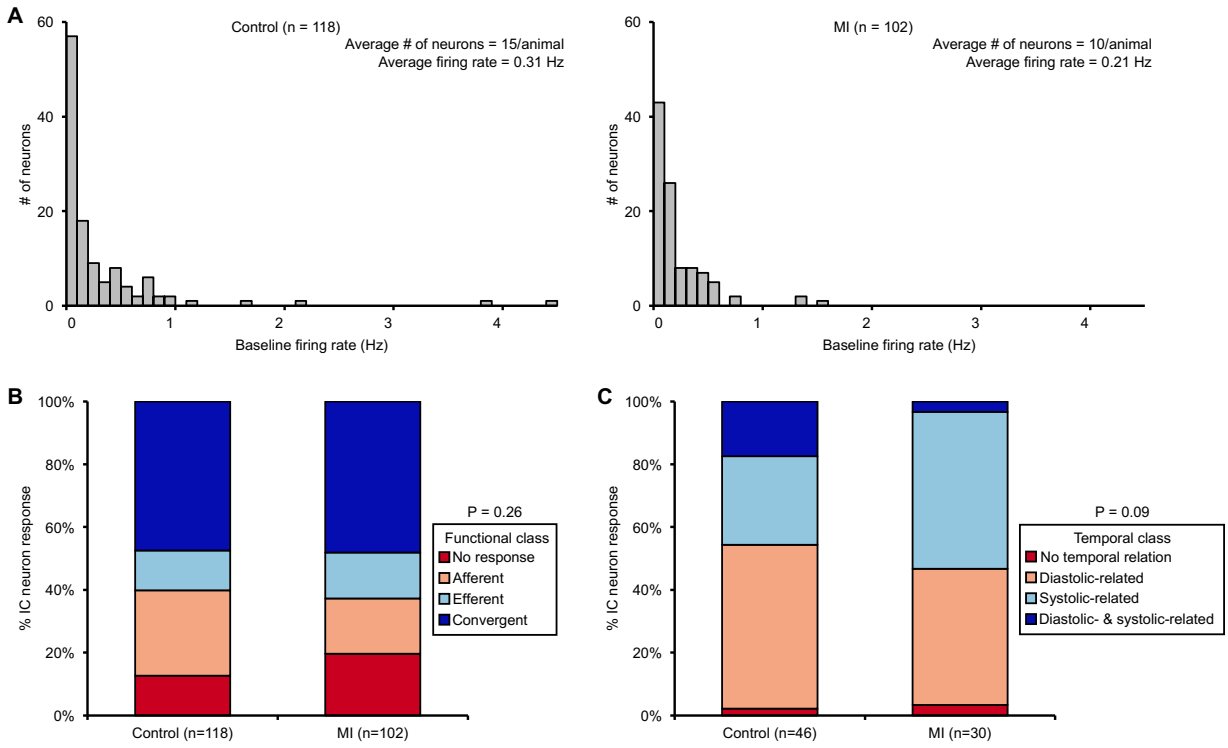

Figure 5. Myocardial infarction (MI) induces no overall change in functional or temporal characteristics of intrinsic cardiac (IC) neurons. (A) Histogram of baseline firing rates of IC neurons identified in control *vs.* MI hearts. **(B)** Functional classification of neurons in control *vs.* MI hearts. **(C)** Cardiac cycle–related periodicity of neurons in control *vs.* MI hearts. Note that subpopulations of neurons displayed diastolic-related activity, systolic-related activity, diastolic- and systolic-related activity, or stochastic behavior. MI did not significantly alter the functional or temporal characteristics of the neurons. A χ^2 test was used in B and C to determine significance between groups.

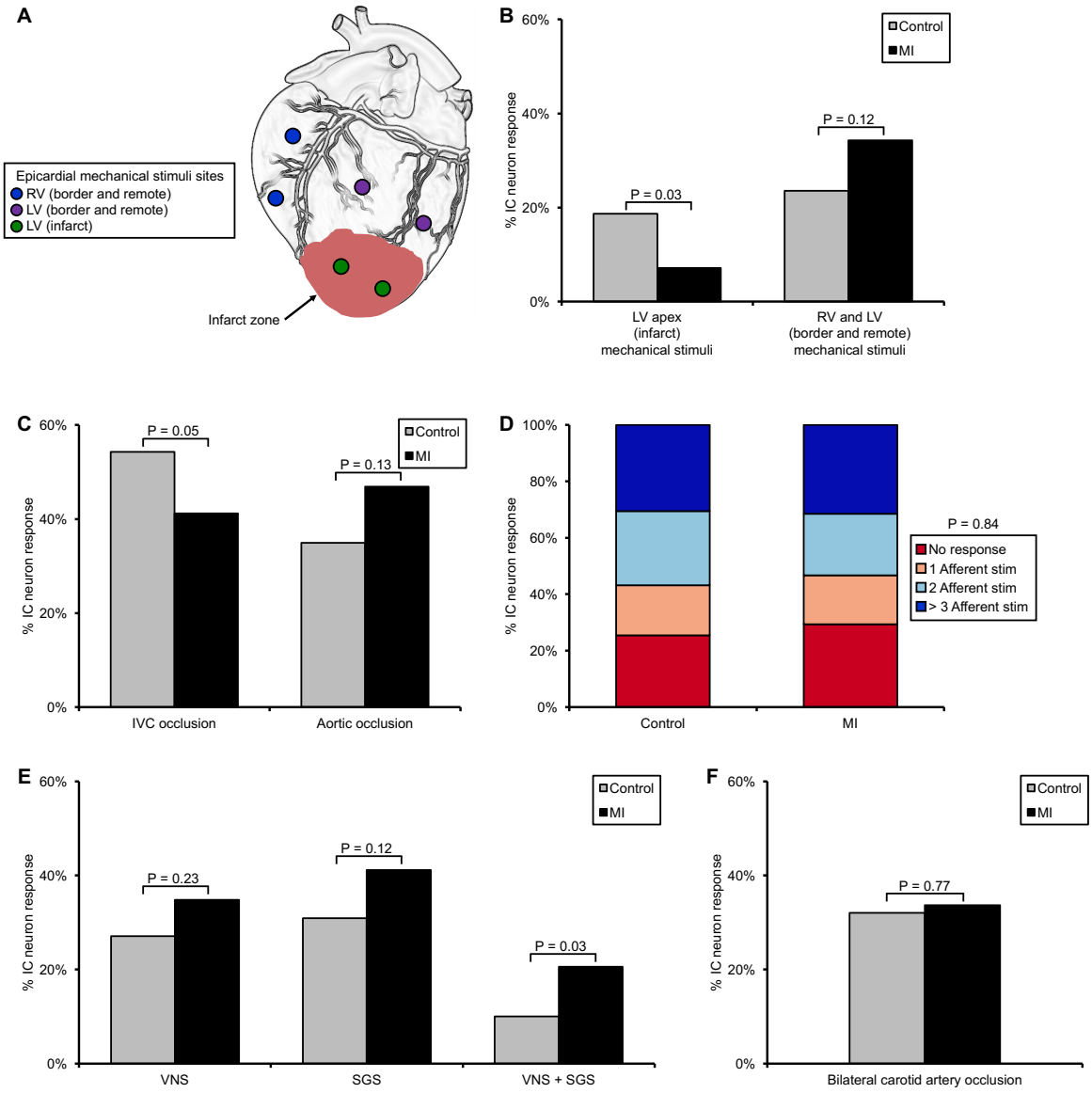

Figure 6. Myocardial infarction (MI) induces afferent and efferent remodeling of intrinsic cardiac (IC) neurons. **(A)** Sites of epicardial mechanical stimuli that were used to assess the capacity of IC neurons to transduce mechanosensitive afferent inputs arising from the right (RV) or left ventricle (LV). **(B)** Percentage of neurons receiving mechanosensitive inputs arising from the LV apex (infarct) *vs.* RV and LV (border and remote zones) in control *vs.* MI hearts. **(C)** Percentage of neurons responding to transient inferior vena cava (IVC) or aortic occlusion in control *vs.* MI hearts. IVC and aortic occlusions were used to assess the capacity of neurons to transduce changes in preload and afterload, respectively. **(D)** Percentage of neurons

transducing multiple afferent inputs in control *vs.* MI hearts. **(E)** Percentage of neurons receiving efferent inputs from parasympathetic and/or sympathetic nervous system, as assessed by cervical vagus nerve stimulation (VNS) and stellate ganglia stimulation (SGS), respectively, in control *vs.* MI hearts. **(F)** Percentage of neurons responding to transient bilateral carotid artery occlusion in control *vs.* MI hearts. Carotid artery occlusion was used to assess the capacity of the baroreflex to modulate efferent inputs to neurons. A $_X^2$ test was used in B, C, D, E, and F to determine significance between groups.

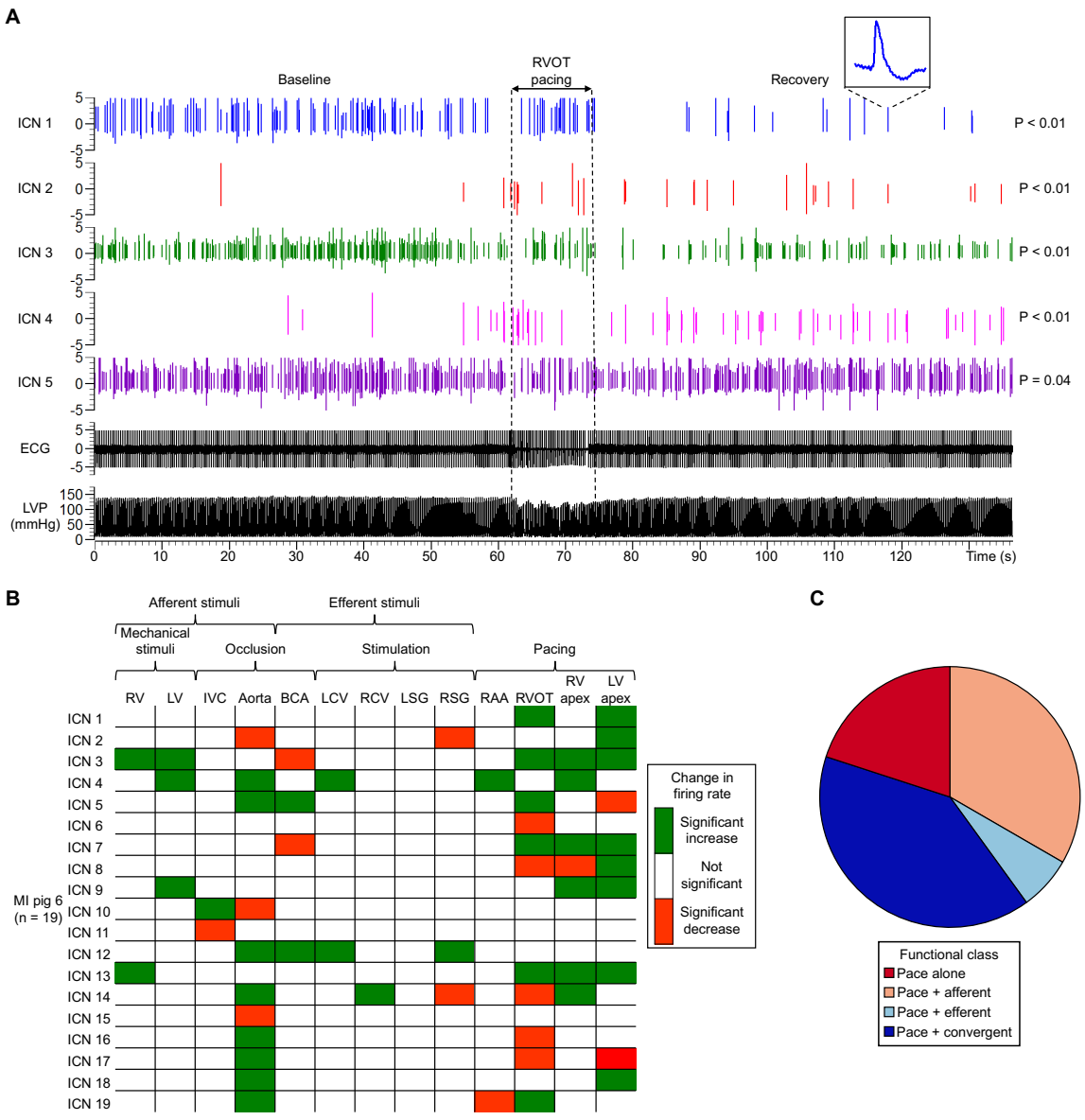

Figure 7. Analytics and functional classification of intrinsic cardiac neurons (ICNs) responsive to pacing. **(A)** Spiking activity recorded from 5 ICNs in a control animal. Vertical dotted lines indicate the onset and offset of epicardial pacing at the right ventricular outflow tract (RVOT). ICN 1 inset is an expanded version of identified neuron. Note that subpopulations of neurons showed an increase, a decrease, or no change in activity from baseline. The significance levels of induced changes in activity for each neuron are shown to the right of the trace. P values were derived based on the analysis described in the Methods. **(B)** Summary of

evoked changes in neuronal activity in response to regional epicardial pacing in a myocardial infarct (MI) animal, along with responses to other cardiovascular stimuli. Green indicates significant increases in activity ($P<0.05$); red indicates significant decreases ($P<0.05$). **(C)** Functional classification of pace-responsive neurons depicted in panel B using protocol outlined in Figure 2. BCA, bilateral carotid artery; ECG, electrocardiogram; IVC, inferior vena cava; LCV, left cervical vagus; LSG, left stellate ganglion; LV, left ventricle; LVP, left ventricular pressure; RAA, right atrial appendage; RCV, right cervical vagus; RSG, right stellate ganglion; RV, right ventricle.

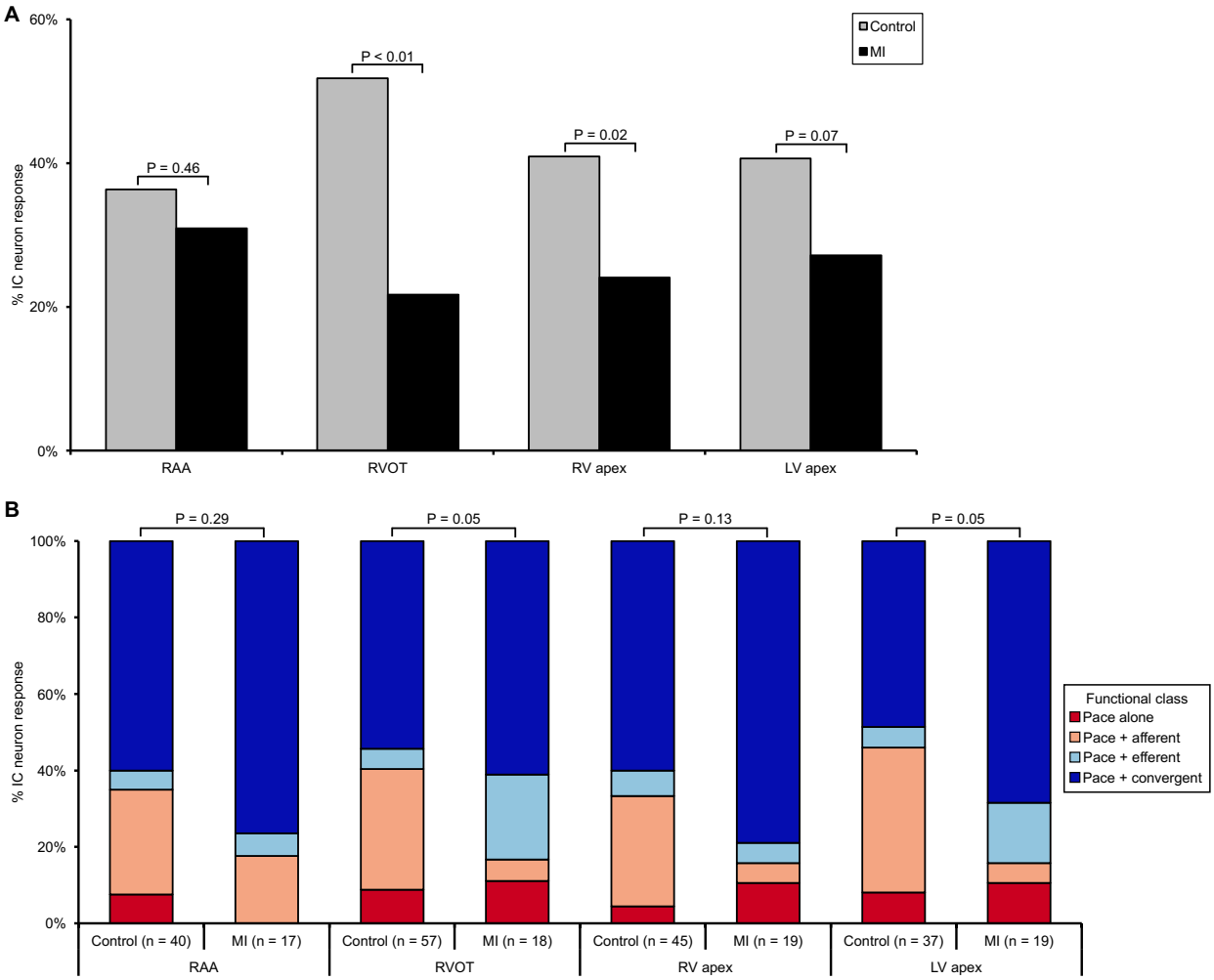

Figure 8. Myocardial infarction (MI) alters response and characteristics of intrinsic cardiac (IC) neurons to pacing. **(A)** Percentage of IC neurons responding to epicardial pacing at the right atrial appendage (RAA), right ventricular outflow tract (RVOT), right ventricular (RV) apex, or left ventricular (LV) apex in control *vs.* MI hearts. MI induced a differential decrease in the neuronal response to ventricular *vs.* atrial pacing. **(B)** Functional classification of pace-responsive neurons in control *vs.* MI animals. MI altered the response characteristics to pacing at both infarct (LV apex) and remote zones (RVOT). A χ^2 test was used to determine significance between groups.

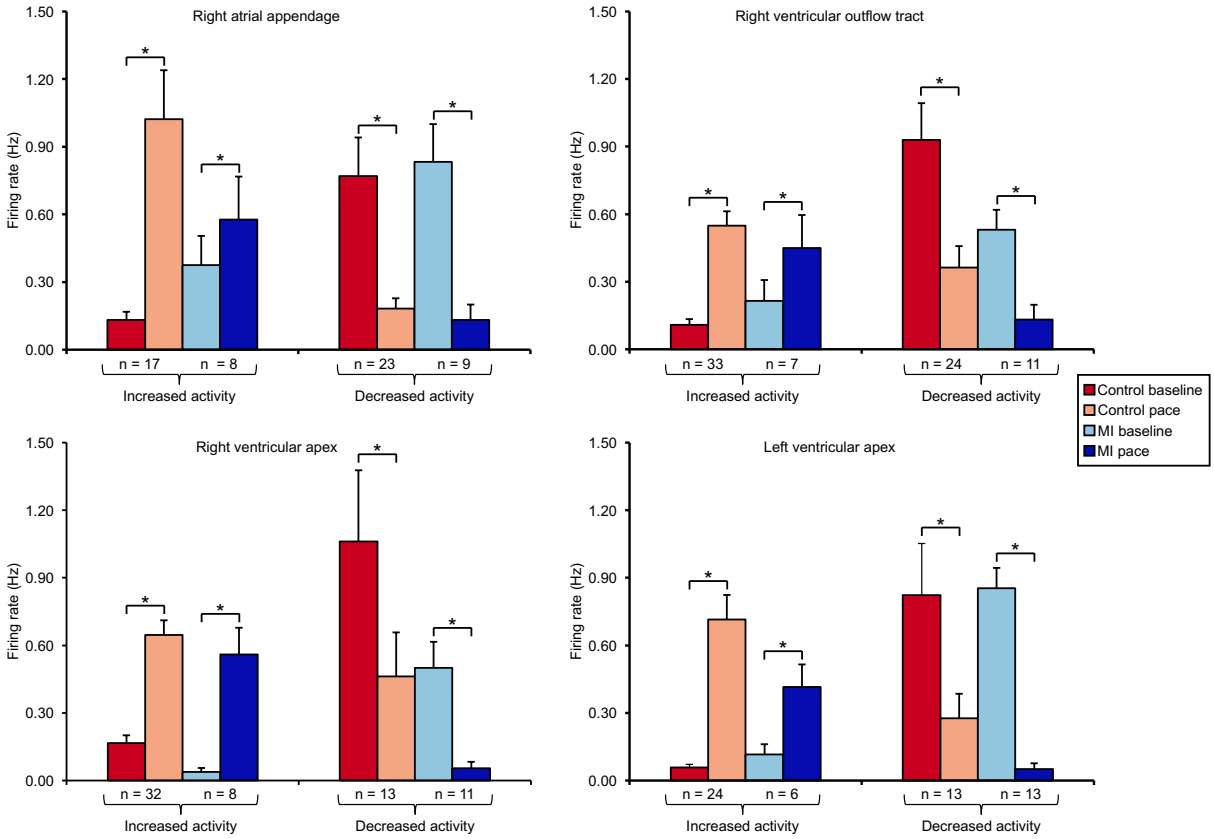

Figure 9. State dependence of intrinsic cardiac neurons. Intrinsic cardiac neuronal activity at baseline and in response to epicardial pacing at the right atrial appendage, right ventricular outflow tract, right ventricular apex, or left ventricular apex in control *vs.* myocardial infarct (MI) animals. Neurons are subdivided based on evoked increases *vs.* decreases in activity in response to pacing. Neurons that had a low basal activity were activated by pacing, while those with a high basal activity were suppressed, suggesting a state-dependent nature. Data are presented as mean ± standard error of the mean. Wilcoxon's signed-rank test was used to determine significance between groups. * $P < 0.01$.

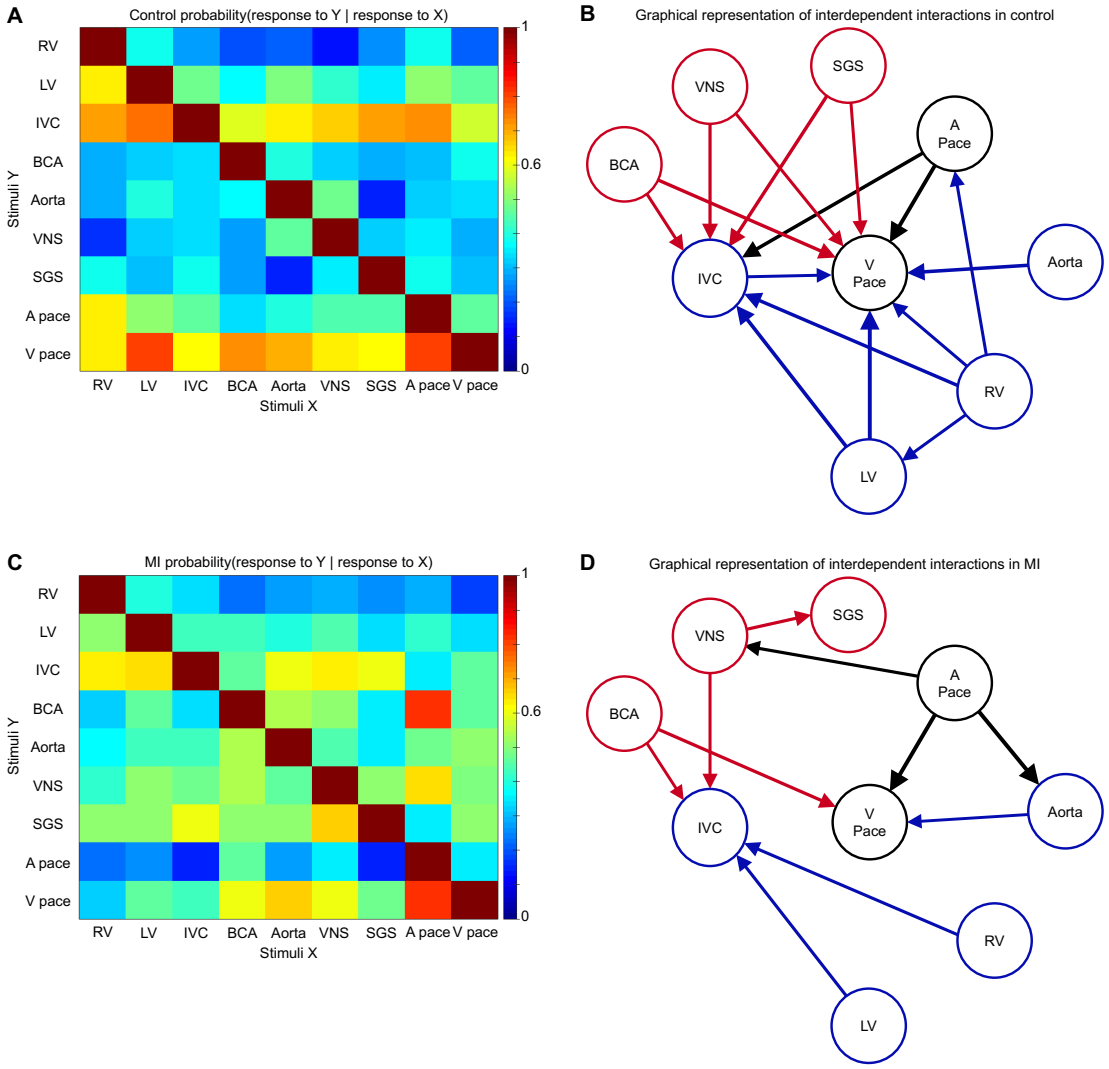

Figure 10. Myocardial infarction (MI) reduces functional network connectivity within the intrinsic cardiac nervous system. **(A)** Conditional probability that an intrinsic cardiac neuron that responded to 1 stimulus (X, x-axis) also responded to another stimulus (Y, y-axis) in control animals. **(B)** Graphical representation of interdependent interactions between stimuli in control animals. **(C)** Conditional probability that a neuron that responded to 1 stimulus (X, x-axis) also responded to another stimulus (Y, y-axis) in MI animals. **(D)** Graphical representation of interdependent interactions between stimuli in MI animals. Color scale in A and C indicates level of probability of each occurrence. Arrow thickness in B and D is proportional to the strength of conditional probability. Only links with probabilities $\geq$ 0.6 are displayed. Afferent and efferent

stimuli are represented by blue and red, respectively. Atrial (A pace) and ventricular pacing (V pace) are represented by black. Aorta, aortic occlusion; BCA, bilateral carotid artery occlusion; IVC, inferior vena cava occlusion; LV, left ventricular epicardial stimuli; RV, right ventricular epicardial stimuli; SGS, stellate ganglia stimulation; VNS, vagus nerve stimulation.

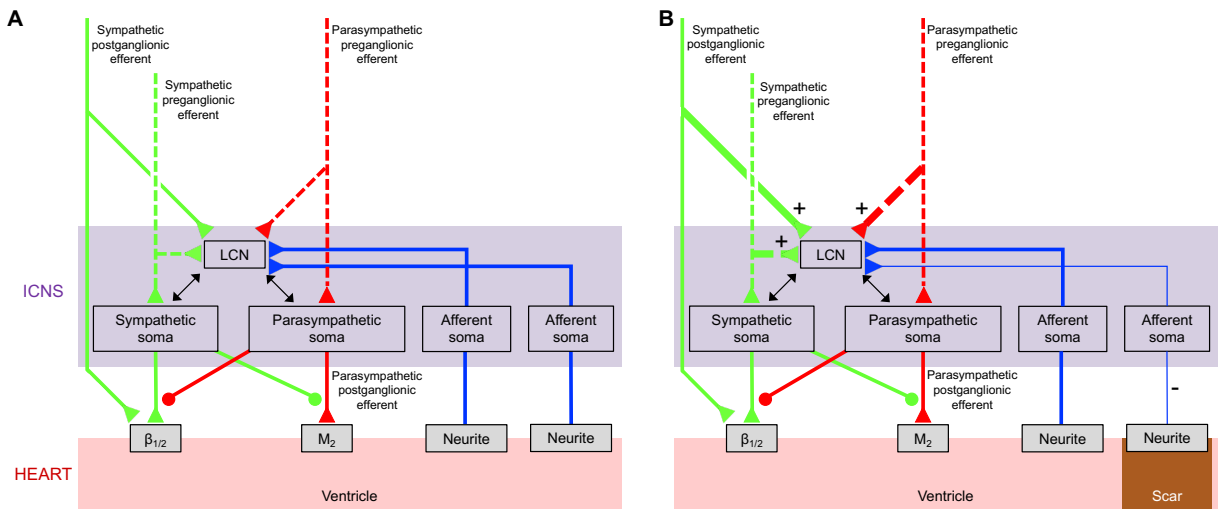

Figure 11. Functional remodeling of the intrinsic cardiac nervous system (ICNS) post-myocardial infarction. **(A)** Schematic showing neural connections between the ICNS and the heart, as well as inputs from higher centers of the cardiac neuraxis, in health. **(B)** Schematic showing the alterations in neural connections between ICNS and heart that occur following myocardial infarction. There is an increase in sympathetic and parasympathetic inputs to convergent local circuit neurons (LCNs), while there is a decrease in afferent inputs from the infarct compared to border and remote regions of the heart. Green and red dashed *vs.* solid lines represent pre- and postganglionic fibers, respectively.

REFERENCES

1. Chugh SS, Reinier K, Teodorescu C, Evanado A, Kehr E, Al Samara M, Mariani R, Gunson K and Jui J. Epidemiology of sudden cardiac death: clinical and research implications. *Progress in cardiovascular diseases*. 2008;51:213-28.
2. Zipes DP and Wellens HJ. Sudden cardiac death. *Circulation*. 1998;98:2334-51.
3. Vaseghi M and Shivkumar K. The role of the autonomic nervous system in sudden cardiac death. *Progress in cardiovascular diseases*. 2008;50:404-19.
4. Shen MJ and Zipes DP. Role of the autonomic nervous system in modulating cardiac arrhythmias. *Circulation research*. 2014;114:1004-1021.
5. Fukuda K, Kanazawa H, Aizawa Y, Ardell JL and Shivkumar K. Cardiac innervation and sudden cardiac death. *Circ Res*. 2015;116:2005-19.
6. Armour JA. Cardiac neuronal hierarchy in health and disease. *American journal of physiology Regulatory, integrative and comparative physiology*. 2004;287:R262-71.
7. Ardell J. Intrathoracic neuronal regulation of cardiac function. In: J. Armour and J. Ardell, eds. *Basic and Clinical Neurocardiology* New York: Oxford University Press; 2004: 187–219.
8. Armour JA. Potential clinical relevance of the 'little brain' on the mammalian heart. *Exp Physiol*. 2008;93:165-76.
9. Oppenheimer S and Hopkins D. Suprabulbar neuronal regulation of the heart. In: J. Armour and J. Ardell, eds. *Neurocardiology* New York: Oxford University Press; 1994: 309-342.
10. Gray MA, Taggart P, Sutton PM, Groves D, Holdright DR, Bradbury D, Brull D and Critchley HD. A cortical potential reflecting cardiac function. *Proc Natl Acad Sci USA*. 2007;104:6818-23.

11. Beaumont E, Salavatian S, Southerland EM, Vinet A, Jacquemet V, Armour JA and Ardell JL. Network interactions within the canine intrinsic cardiac nervous system: implications for reflex control of regional cardiac function. *J Physiol*. 2013;591:4515-33.
12. Murphy DA, Thompson GW, Ardell JL, McCraty R, Stevenson RS, Sangalang VE, Cardinal R, Wilkinson M, Craig S, Smith FM, Kingma JG and Armour JA. The heart reinnervates after transplantation. *Ann Thorac Surg*. 2000;69:1769-81.
13. Vracko R, Thorning D and Frederickson RG. Nerve fibers in human myocardial scars. *Hum Pathol*. 1991;22:138-46.
14. Cao JM, Fishbein MC, Han JB, Lai WW, Lai AC, Wu TJ, Czer L, Wolf PL, Denton TA, Shintaku IP, Chen PS and Chen LS. Relationship between regional cardiac hyperinnervation and ventricular arrhythmia. *Circulation*. 2000;101:1960-9.
15. Ajijola OA, Yagishita D, Reddy NK, Yamakawa K, Vaseghi M, Downs AM, Hoover DB, Ardell JL and Shivkumar K. Remodeling of stellate ganglion neurons after spatially targeted myocardial infarction: Neuropeptide and morphologic changes. *Heart Rhythm*. 2015;12:1027-35.
16. Kember G, Armour JA and Zamir M. Neural control hierarchy of the heart has not evolved to deal with myocardial ischemia. *Physiol Genomics*. 2013;45:638-44.
17. Armour JA. Myocardial ischaemia and the cardiac nervous system. *Cardiovascular Research*. 1999;41:41-54.
18. Wang HJ, Wang W, Cornish KG, Rozanski GJ and Zucker IH. Cardiac sympathetic afferent denervation attenuates cardiac remodeling and improves cardiovascular dysfunction in rats with heart failure. *Hypertension*. 2014;64:745-55.
19. Zucker IH, Patel KP and Schultz HD. Neurohumoral stimulation. *Heart Fail Clin*. 2012;8:87-99.

20. Hopkins DA, Macdonald SE, Murphy DA and Armour JA. Pathology of intrinsic cardiac neurons from ischemic human hearts. *Anat Rec*. 2000;259:424-36.

21. Hardwick JC, Ryan SE, Beaumont E, Ardell JL and Southerland EM. Dynamic remodeling of the guinea pig intrinsic cardiac plexus induced by chronic myocardial infarction. *Autonomic Neuroscience*. 2014;181:4-12.

22. Nakahara S, Vaseghi M, Ramirez RJ, Fonseca CG, Lai CK, Finn JP, Mahajan A, Boyle NG and Shivkumar K. Characterization of myocardial scars: electrophysiological imaging correlates in a porcine infarct model. *Heart Rhythm*. 2011;8:1060-7.

23. Arora RC, Waldmann M, Hopkins DA and Armour JA. Porcine intrinsic cardiac ganglia. *Anat Rec A Discov Mol Cell Evol Biol*. 2003;271:249-58.

24. Shin HC, Aggarwal V, Acharya S, Schieber MH and Thakor NV. Neural decoding of finger movements using Skellam-based maximum-likelihood decoding. *IEEE Trans Biomed Eng*. 2010;57:754-60.

25. Frase LL, Gaffney FA, Lane LD, Buckey JC, Said SI, Blomqvist CG and Krejs GJ. Cardiovascular effects of vasoactive intestinal peptide in healthy subjects. *Am J Cardiol*. 1987;60:1356-61.

26. Brum JM, Bove AA, Sufan Q, Reilly W and Go VL. Action and localization of vasoactive intestinal peptide in the coronary circulation: evidence for nonadrenergic, noncholinergic coronary regulation. *J Am Coll Cardiol*. 1986;7:406-13.

27. Weihe E and Reinecke M. Peptidergic innervation of the mammalian sinus nodes: vasoactive intestinal polypeptide, neurotensin, substance P. *Neurosci Lett*. 1981;26:283-8.

28. Rytel L, Palus K and Całka J. Co-expression of PACAP with VIP, SP and CGRP in the Porcine Nodose Ganglion Sensory Neurons. *Anat Histol Embryol*. 2015;44:86-91.

29. Cardinal R, Pagé P, Vermeulen M, Ardell JL and Armour JA. Spatially divergent cardiac responses to nicotinic stimulation of ganglionated plexus neurons in the canine heart. *Auton Neurosci*. 2009;145:55-62.

30. Armour JA, Richer LP, Pagé P, Vinet A, Kus T, Vermeulen M, Nadeau R and Cardinal R. Origin and pharmacological response of atrial tachyarrhythmias induced by activation of mediastinal nerves in canines. *Auton Neurosci*. 2005;118:68-78.

31. Gibbons DD, Southerland EM, Hoover DB, Beaumont E, Armour JA and Ardell JL. Neuromodulation targets intrinsic cardiac neurons to attenuate neuronally mediated atrial arrhythmias. *Am J Physiol Regul Integr Comp Physiol*. 2012;302:R357-64.

32. Ardell JL, Cardinal R, Beaumont E, Vermeulen M, Smith FM and Andrew Armour J. Chronic spinal cord stimulation modifies intrinsic cardiac synaptic efficacy in the suppression of atrial fibrillation. *Auton Neurosci*. 2014;186:38-44.

33. Richer LP, Vinet A, Kus T, Cardinal R, Ardell JL and Armour JA. Alpha-adrenoceptor blockade modifies neurally induced atrial arrhythmias. *Am J Physiol Regul Integr Comp Physiol*. 2008;295:R1175-80.

34. Barr ML and Hamilton JD. A quantitative study of certain morphological changes in spinal motor neurons during axon reaction. *J Comp Neurol*. 1948;89:93-121.

35. Geuna S, Borrione P, Poncino A and Giacobini-Robecchi MG. Morphological and morphometrical changes in dorsal root ganglion neurons innervating the regenerated lizard tail. *Int J Dev Neurosci*. 1998;16:85-95.

36. Hendrickson A and Dineen JT. Hypertrophy of neurons in dorsal lateral geniculate nucleus following striate cortex lesions in infant monkeys. *Neurosci Lett*. 1982;30:217-22.

37. Zhou S, Chen LS, Miyauchi Y, Miyauchi M, Kar S, Kangavari S, Fishbein MC, Sharifi B and Chen PS. Mechanisms of cardiac nerve sprouting after myocardial infarction in dogs. *Circ Res*. 2004;95:76-83.

38. Chen PS, Chen LS, Fishbein MC, Lin SF and Nattel S. Role of the autonomic nervous system in atrial fibrillation: pathophysiology and therapy. *Circ Res*. 2014;114:1500-15.

39. Ajijola OA, Wisco JJ, Lambert HW, Mahajan A, Stark E, Fishbein MC and Shivkumar K. Extracardiac neural remodeling in humans with cardiomyopathy. *Circ Arrhythm Electrophysiol*. 2012;5:1010-116.

40. Han S, Kobayashi K, Joung B, Piccirillo G, Maruyama M, Vinters HV, March K, Lin SF, Shen C, Fishbein MC, Chen PS and Chen LS. Electroanatomic remodeling of the left stellate ganglion after myocardial infarction. *J Am Coll Cardiol*. 2012;59:954-61.

41. Vanoli E, De Ferrari GM, Stramba-Badiale M, Hull SS, Foreman RD and Schwartz PJ. Vagal stimulation and prevention of sudden death in conscious dogs with a healed myocardial infarction. *Circ Res*. 1991;68:1471-81.

42. Billman GE. Heart rate response to onset of exercise: evidence for enhanced cardiac sympathetic activity in animals susceptible to ventricular fibrillation. *Am J Physiol Heart Circ Physiol*. 2006;291:H429-35.

43. Kanazawa H, Ieda M, Kimura K, Arai T, Kawaguchi-Manabe H, Matsuhashi T, Endo J, Sano M, Kawakami T, Kimura T, Monkawa T, Hayashi M, Iwanami A, Okano H, Okada Y, Ishibashi-Ueda H, Ogawa S and Fukuda K. Heart failure causes cholinergic transdifferentiation of cardiac sympathetic nerves via gp130-signaling cytokines in rodents. *J Clin Invest*. 2010;120:408-21.

44. Waldmann M, Thompson GW, Kember GC, Ardell JL and Armour JA. Stochastic behavior of atrial and ventricular intrinsic cardiac neurons. *J Appl Physiol*. 2006;101:413-9.

45. Sutton MG and Sharpe N. Left ventricular remodeling after myocardial infarction: pathophysiology and therapy. *Circulation*. 2000;101:2981-8.

46. Huang MH, Ardell JL, Hanna BD, Wolf SG and Armour JA. Effects of transient coronary artery occlusion on canine intrinsic cardiac neuronal activity. *Integr Physiol Behav Sci*. 1993;28:5-21.

47. Tessier-Lavigne M. Visual Processing by the Retina. In: E. R. Kandel, J. H. Schwartz and T. M. Jessell, eds. *Principles of Neural Science.* 4th ed. New York, NY: McGraw-Hill; 2000: 507-522.

48. Tops LF, Schalij MJ and Bax JJ. The effects of right ventricular apical pacing on ventricular function and dyssynchrony implications for therapy. *J Am Coll Cardiol*. 2009;54:764-76.

49. Roque C, Trevisi N, Silberbauer J, Oloriz T, Mizuno H, Baratto F, Bisceglia C, Sora N, Marzi A, Radinovic A, Guarracini F, Vergara P, Sala S, Paglino G, Gulletta S, Mazzone P, Cireddu M, Maccabelli G and Della Bella P. Electrical storm induced by cardiac resynchronization therapy is determined by pacing on epicardial scar and can be successfully managed by catheter ablation. *Circ Arrhythm Electrophysiol*. 2014;7:1064-9.

50. Wilkoff BL, Cook JR, Epstein AE, Greene HL, Hallstrom AP, Hsia H, Kutalek SP, Sharma A and Investigators DCaVIDT. Dual-chamber pacing or ventricular backup pacing in patients with an implantable defibrillator: the Dual Chamber and VVI Implantable Defibrillator (DAVID) Trial. *JAMA*. 2002;288:3115-23.

51. Sweeney MO, Hellkamp AS, Ellenbogen KA, Greenspon AJ, Freedman RA, Lee KL, Lamas GA and Investigators MST. Adverse effect of ventricular pacing on heart failure and atrial fibrillation among patients with normal baseline QRS duration in a clinical trial of pacemaker therapy for sinus node dysfunction. *Circulation*. 2003;107:2932-7.

52. Zhang YY, Wu DY, Fu NK, Lu FM and Xu J. Neuroendocrine and haemodynamic changes in single-lead atrial pacing and dual-chamber pacing modes. *J Int Med Res*. 2013;41:1057-66.

53. Langley JN. The autonomic nervous system Part 1. 1921:2 leaves, 80 p.

54. McGuirt AS, Schmacht DC and Ardell JL. Autonomic interactions for control of atrial rate are maintained after SA nodal parasympathectomy. *Am J Physiol*. 1997;272:H2525-33.

55. Randall DC, Brown DR, McGuirt AS, Thompson GW, Armour JA and Ardell JL. Interactions within the intrinsic cardiac nervous system contribute to chronotropic regulation. *Am J Physiol Regul Integr Comp Physiol*. 2003;285:R1066-75.

56. Zhou S, Jung BC, Tan AY, Trang VQ, Gholmieh G, Han SW, Lin SF, Fishbein MC, Chen PS and Chen LS. Spontaneous stellate ganglion nerve activity and ventricular arrhythmia in a canine model of sudden death. *Heart Rhythm*. 2008;5:131-9.

57. Ajijola OA, Yagishita D, Patel KJ, Vaseghi M, Zhou W, Yamakawa K, So E, Lux RL, Mahajan A and Shivkumar K. Focal myocardial infarction induces global remodeling of cardiac sympathetic innervation: neural remodeling in a spatial context. *Am J Physiol Heart Circ Physiol*. 2013;305:H1031-40.

CHAPTER 6

Conclusions/Interpretations/Future Directions

CONCLUSIONS

Cardiovascular diseases such as hypertension, arrhythmias, and heart failure are the leading causes of morbidity and mortality in the United States and worldwide.[1-4] Autonomic dysfunction plays an important role in the pathophysiology of these diseases[5-7] and, therefore, represents an emerging target for treatment and prevention of disease progression. Neuromodulatory approaches for cardiovascular diseases have already shown great promise;[8, 9] however, fundamental gaps exist in our understanding of the structure and function of autonomic nerves that regulate the heart. The autonomic nervous system (ANS) allows for integrative control of the viscera to ensure the survival of the organism.[10] Regarding the heart, the ANS regulates cardiac electrical and mechanical function to maintain normal rhythm and sustain the circulation of blood.[5-7] The cardiac ANS is composed of a series of interacting feedback loops from the level of the heart[11] to that of the brain.[5-7, 12-14] At the organ level, the intrinsic cardiac nervous system (ICNS) is the final common pathway for integration of neural inputs to the heart.[11] The focus of this dissertation is to (1) understand how the vagus, a mixed peripheral nerve, mediates interactions between central and peripheral aspects of the ANS for cardiac control, and (2) characterize the remodeling of the ICNS as it adapts to acute stress and chronic cardiac pathology. The major findings are as follows:

(1) Activation of cervical vagal afferent fibers reduces efferent parasympathetic outflow (Chapters 2 and 3).
(2) The evoked cardiovascular response to cervical vagus nerve stimulation (VNS) represents a dynamic interplay between direction activation of vagal afferent and efferent fibers and reflex responses of the cardiac ANS (Chapter 2 and 3).
(3) Premature ventricular contractions (PVCs) are a strong and destabilizing stress on the ICNS (Chapter 4).

(4) PVCs with variable coupling intervals affect local circuit neurons (LCNs) within the ICNS and alter cardiac repolarization, more than those with fixed coupling interval, leading to neural and electrical instability of the heart. (Chapter 4)

(5) Intrinsic cardiac neurons undergo differential morphological and phenotypic remodeling after myocardial infarction (MI) in a pattern that reflects the site of injury (Chapter 5).

(6) Afferent signals from the infarct scar to the ICNS are attenuated, while those from scar border and remote zones are preserved post-MI, giving rise to a neural sensory border zone (Chapter 5).

(7) The convergence of efferent inputs onto LCNs within the ICNS is enhanced after MI (Chapter 5).

(8) Functional network connectivity within the ICNS is reduced post-MI (Chapter 5).

Taken together, these findings provide insights into the role of cardiac afferents in normal physiology and mechanisms by which injury to the heart initiates afferent-mediated reflex activation and remodeling of the ANS.

INTERPRETATIONS

The vagus nerve as a therapeutic target for cardiac disease

The vagus nerve is a major pathway for bidirectional communication between the brain and the periphery. At the level of the neck, vagus is composed of ~15% efferent and 85% afferent fibers.[15] Efferent fibers of the vagus project to thoracic and abdominal organs to control motor functions such as rate and contractility of the heart[16, 17] and motility and secretion in the gut.[15, 18] Vagal afferents consist of A, B, and C fibers and transduce a variety of sensory modalities, including the chemical milieu, metabolites, stretch, temperature, and pain.[19] Given the diverse tissues innervated and range of functions modulated by the vagus, VNS has emerged as a novel therapeutic option for a number of conditions, including epilepsy,[20] depression,[21] cardiac arrhythmias,[22] heart failure,[9, 23-25] obesity,[26] and inflammatory diseases.[27] However, for this same

reason, maximizing efficacy for a given disease while minimizing off-target effects of VNS is a challenge.

Since sympathetic activation and parasympathetic withdrawal are pro-arrhythmic[5, 28] and accelerate the progression of heart failure,[29, 30] cervical VNS is being evaluated as a treatment for both these diseases.[9, 22-25] There have been 3 clinical trials of VNS for heart failure: *In*crease *o*f *Va*gal *T*on*e* in *H*eart *F*ailure (INOVATE-HF), *Ne*ural *C*ardiac *T*her*a*py fo*r H*eart *F*ailure (NECTAR-HF), and *A*utonomic *N*eural Regulation *Th*erapy to *E*nhance *M*yocardial Function in *H*eart *F*ailure (ANTHEM-HF).[9, 23-25] Despite promising preclinical data,[31] the results of these trials have been neutral to slightly positive at best.[9, 23-25] A difficultly in extrapolating findings from preclinical studies of VNS in small and even large animals to humans is the interspecies differences in the anatomy of the vagus, including the number, type, and size of fibers and thickness of the epineurium (connective tissue around nerves), all of which impact the ability to recruit fibers and evoke a response.[32] The shortcomings of the VNS clinical trials are likely due to technical limitations and conceptual misunderstandings regarding the nature of the cardiac ANS. One of the key differences between these trials was the choice of stimulation parameters (current, frequency, pulse width, waveform, and duty cycle). In the NECTAR-HF trial, for example, VNS was applied at a current of ~1.4 mA and frequency of 20Hz[23] and in the INOVATE-HF trial at a current ~3.9 mA and a fixed duration after the R wave of the QRS.[25, 33] Both trials failed to meet their primary and secondary endpoints of reducing heart failure deaths and improving left ventricular function, respectively. On the other hand, the ANTHEM-HF trial, which operated between 1.5 to 3 mA and at 10 Hz, showed a significant increase in left ventricular function. In our studies, we have demonstrated that at low currents and frequencies VNS evokes an afferent-mediated withdrawal of central efferent parasympathetic outflow, while at higher currents and frequencies it induces the reduction in heart rate and contractility typically associated with VNS. Further, we hypothesize that optimal VNS parameters for cardiac applications are around the neural fulcrum, the point at which balanced activation of afferent

and efferent vagal fibers produces a null heart rate response. VNS applied at the neural fulcrum would have the advantage of not evoking reactive responses from the cardiac ANS that mitigate its beneficial effects.

One important consideration when applying VNS, particularly at the cervical level, which is the convergence point for efferents to and afferents from the viscera, is the off-target and long-term effects. For instance, Patel and colleagues demonstrated that they could preferentially activate efferent and block afferent fibers to produce a systemic anti-inflammatory response by using kilohertz frequency electrical stimulation of the cervical vagus.[34] While this represents an exciting technological advancement, *what are consequences of disrupting visceral afferent inputs to the brain that convey important information regarding the state of the body?* An alternative approach may be to apply VNS at different locations or closer to the target organ. Recent studies of tragal stimulation, which activates the auricular branch of the vagus, have shown encouraging results for suppressing the incidence of atrial fibrillation[35, 36] and preventing cardiac remodeling after MI.[37, 38] Although more difficult to access than the cervical vagus, cardiopulmonary branches may be a better target for cardiac applications.[39] In addition, the evolution of electrode technologies[40] and novel stimulation paradigms may enable modulation of select fibers.[41] As VNS moves forward clinically, it will be critical to determine how best to achieve organ and tissue specificity, and this will rely on studies that dissect the complexity of the vagus.

Neural sensory border zone

Following MI, there is not only formation of a scar but also alterations in regulation of the heart by multiple levels of the ANS.[13] The peri-infarct region or border zone is structurally[42] and electrophysiologically complex.[43] It is characterized by islands of viable myocardium surrounded by fibrotic tissue[44] and provides an anatomical substrate for re-entrant ventricular tachyarrhythmias. Re-entrant ventricular tachyarrhythmias can occur when the depolarization

wavefront propagates around an anatomical or functional obstacle and re-excites the site of origin, or when there is a large dispersion of repolarization between two areas.[45] While the infarct creates an anatomical substrate, the ANS is a major factor in the formation of a functional substrate. At the level of the myocardium, denervation of the infarct and sympathetic hyperinnervation of the border zone has been reported.[46, 47] Ajijola *et al.* demonstrated that stellate ganglia stimulation increases heterogeneity in activation in the peri-infarct region and can alter propagation through putative ventricular tachyarrhythmias circuits in infarcted hearts.[48] Numerous studies have also shown that enhanced sympathetic activity proceeds the onset of ventricular tachyarrhythmias post-MI.[28, 49] Since afferent-mediated sympathoexcitation plays an important role in ventricular arrhythmogenesis, understanding the mechanisms that lead to such reflex autonomic activation are paramount.

Afferent neurons in intrinsic cardiac, nodose, and dorsal root ganglia respond to chemosensory, mechanosensory, and nocioceptive stimuli, with many neurons being multimodal.[50] In the sequelae after MI, a lack of energy substrates and oxidative stress leads to the production and accumulation of chemicals (e.g., reactive oxygen species,[51] adenosine,[52] bradykinin[53, 54]) that activate afferent neurons. Acutely, afferent-mediated sympathoexcitation increases contractility of the heart to maintain cardiac output; however, chronically, it leads to adverse cardiac and neural remodeling,[13] as evidenced by the fact the beta-blocker therapy post-MI increases ventricular function, reverses ventricular remodeling, reduces arrhythmias, and improves survival.[55-57] Despite changes in the chemical milieu, afferent-mediated sympathoexcitation still exists in the setting of a heal infarct but the mechanisms are not well understood.

In this regard, we have put forth a concept called the neural sensory border zone that may contribute to reflex autonomic activation in not only acute but also chronic states following MI. Cardiac mechanoreceptors are distributed throughout the atria and ventricles and detect stretch of the myocardial wall and coronary vessels.[58-62] Activity of these neurons also display a

tight relationship with different phases of the cardiac cycle.[63] After MI, we hypothesize that the presence of contractile myocardium in the border zone adjacent to non-contractile fibrotic tissue in the infarct, in addition to alterations in the local chemical milieu, leads to aberrant and excessive activation of mechanosensitive afferent neurons and resultant sympathoexcitation. In support of this hypothesis, we have demonstrated that mechanoreceptor inputs from the infarct to the ICNS are attenuated post-MI, while those from border and remote zones of the heart are preserved. The importance of sensory boundary conditions has already been shown in other neural networks, such as the visual system where retinal ganglion cells are better able to detect non-uniform light fields.[64]

Given their role in reflex sympathoexcitation, targeting afferents may represent a novel approach to treat cardiac disease. Wang and colleagues showed that selective deletion of transient receptor potential vanilloid receptor 1-expressing afferents on the heart, which are important for mechanical sensitivity,[65] by epicardial application of resiniferatoxin, an ultrapotent analogue of capsaicin, prevents exaggerated sympathetic activity and protects against cardiac remodeling following MI.[66] In patients with MI, surgical removal of non-contractile areas and revascularization of the heart improved cardiac function and increase the sense of well-being in patients.[67] Taken together, these findings are consistent with our idea of a sensory border zone.

LCNs and neural network interactions

The basic constituents of the ICNS circuitry are afferent, efferent, and local circuit neurons, with LCNs representing the predominant subpopulation.[11] The convergence of inputs and the interconnections between ganglia distributed throughout the heart allow LCNs to serve as local information processors and coordinate regional cardiac function.[11, 63, 68] Thus, LCNs are critical for the integrated control of the heart. We have characterized, for the first time, the impact that an acute stress in the form of PVCs and chronic stress as manifest by MI on the ICNS. In both cases, we have observed alterations in the function of LCNs and the overall neural network.

Specifically, the neural signature of the ICNS after chronic MI is defined by increased heterogeneity in afferent information and enhanced convergence of inputs onto LCNs. Further, the dynamic responses that the ICNS displays to physiological stressors in the healthy state is blunted. We hypothesize that these changes may underlie, at least in part, the electrical instability and mechanical dyssynchrony seen in PVC-induced cardiomyopathy, MI, and other cardiac diseases.[5-7] While this dissertation provides insight into remodeling of the ICNS as it adapts to cardiac pathology, many important questions remain. *How do neural signatures evolve from acute to chronic states? Are their specific signatures that indicate worse prognoses? Do neuromodulatory approaches (e.g., VNS, bilateral cervicothoracic sympathetic decentralization) restore these signatures closer to healthy states?* Future studies utilizing chronic implanted electrodes in atrial and ventricular intrinsic cardiac ganglia and in higher levels of the ANS will be critical to answer these questions and develop novel therapies targeting the ANS for cardiac disease.

FUTURE DIRECTIONS

A major unmet need in the field of neurocardiology is a lack of comprehensive maps of neural circuits that regulate cardiac function. Numerous studies have used electrical stimulation to activate autonomic ganglia and nerves and examine their effects on cardiac electrical and mechanical indices. Although these studies have provided important insights into autonomic control of cardiac function, they have oversimplified the complexity of these neural structures, which are composed of heterogeneous neuronal populations and mixed fibers. Until recently, characterization of the anatomical structure and function of cardiac neural circuits has been hampered primarily by a lack of tools that target the peripheral nervous system. To address this problem, we have employed a multi-technique approach, which includes tissue clearing, viral-based labeling and tracing, optogenetics, and physiological recordings, to map the circuity of the cardiac ANS, starting with the ICNS.

Tissue clearing to assess cardiac innervation

Methods for evaluating the microscopic structure of tissues have traditionally relied on sectioning into thin slices. However, these approaches make it difficult to appreciate the inherent 3-dimensional nature of tissues in the body. The primary challenge to imaging deep into thick slices or intact tissues is the diffraction of light by the dense lipid membrane surrounding cells.[69] To address this issue, a variety of novel methods (e.g., Sca*l*e,[70, 71] CLARITY,[72-74] *c*lear *u*nobstructed *b*rain *i*maging *c*ocktails and *c*omputational analysis [CUBIC],[75] uDISCO[76]) have been developed to render thick slices and even intact, whole organs optically transparent to facilitate deep imaging while preserving 3-dimensional molecular and cellular structure. We have used one such approach, the *pa*ssive *C*LARITY *t*echnique (PACT), to clear and study the neural innervation of mouse hearts. Briefly, PACT involves embedding fixed tissues in a hydrogel solution, crosslinking the proteins with the hydrogel, and then using a detergent to remove the lipid membranes.[73, 74] Cleared hearts are compatible with endogenous fluorescence and immunohistochemistry, both of which enable cell type-specific labeling. Through this approach, we have visualized the ICNS and the dense network of fibers on the heart in its spatial context (Figure 1). Antibody-based approaches, as seen in Figure 1, allow for morphological and phenotypic characterization of neurons but do not provide the resolution required for neural circuit tracing. Thus, we have also used viral-based approaches in conjunction with tissue clearing.

Viral-based approaches for structural mapping of cardiac circuits

Adeno-associated viruses (AAVs) are a prominent tool for viral-mediated circuit mapping because they not only exhibit low immunogenicity and toxicity but also permit long-term gene expression in a variety of cell types.[77] AAVs have recently been engineered for enhanced gene transfer throughout peripheral tissues. We have used a novel AAV capsid variant, PHP.S, identified through an AAV cell type-specific *in vivo* selection method.[78] PHP.S transduces the

heart with a greater efficiency than the current gold standard, AAV9. PHP.S can be used to deliver genes for fluorescent proteins or light-activated channels to target cells populations in the cardiac ANS, enabling tagging and functional manipulation. When combined with high-resolution imaging through cleared tissue, AAV-based labeling can facilitate anatomical mapping of the cardiac neural circuits. We have developed an AAV-based multicolor labeling system to mark specific subsets of peripheral motor and sensory neurons (Figures 2). To label cholinergic neurons within the ICNS, for example, we deliver a mixture of 3 Cre-dependent AAVs carrying reporter genes for either a red, green, or blue fluorescent protein to choline acetyltransferase-Cre mice via systemic injection. Viral delivery results in stochastic transduction of cholinergic neurons, and when cells are transduced by multiple vectors, a wide range of colors can be visualized (Figure 3). This method allows us to identify individual neurons by a unique color barcode and follow their projections through cleared tissues for high-resolution neuronal tract-tracing. Even with multicolor labeling, single cell analysis is challenging when the labeling density is high. Therefore, we have also developed a 2-component vector system for cell type-specific, sparse labeling (Figure 3, middle panels). Using this approach, we have begun to trace neurons from the ICNS to regions they innervate.

Optogenetics for functional mapping of cardiac circuits

Optogenetics has initially been used to study neural circuits in the brain,[79] but advances in the field of viral engineering have now enabled the use of this tool to understand peripheral neural circuits involved in functional control of organs such as the heart.[80-83] Optogenetics involves expressing opsins, light-activated ion channels, in desired cell populations and allows for precise temporal and spatial control of cellular activity.[84] In combination with Cre transgenics, optogenetics can be used to probe the function of defined cell populations,[80, 85, 86] in contrast to traditional electrical stimulation, which is less selective. Cell-type specificity is critical due to the complexity of the peripheral nervous system and the fact that many peripheral ganglia and

nerves contain heterogeneous neuronal populations and mixed fibers, respectively.[80] In our experiments, PHP.S is used to deliver the Channelrhodopsin-2 gene to defined cell types within the ICNS. In *ex vivo* Langendorff and *in vivo* experiments, light is used to modulate the activity of specific subsets of neurons while concurrently recording cardiac electrical and mechanical indices. We have preliminarily shown that optical stimulation of cholinergic neurons within the inferior PV ganglion of the mouse heart modulates sinoatrial and atrioventricular nodal function, suggesting 2 putative cardiac neural circuits identified through this approach (Figure 4).

Overall, multi-technique approaches such as the one described herein are needed to dissect neural regulation of organ function. Comprehensive structural and functional mapping of cardiac neural circuits in health and disease will pave the way for the development of neuroscience-based therapies for cardiovascular disease. The future promises to be an exciting time for peripheral neuroscience. Embrace the complexity!

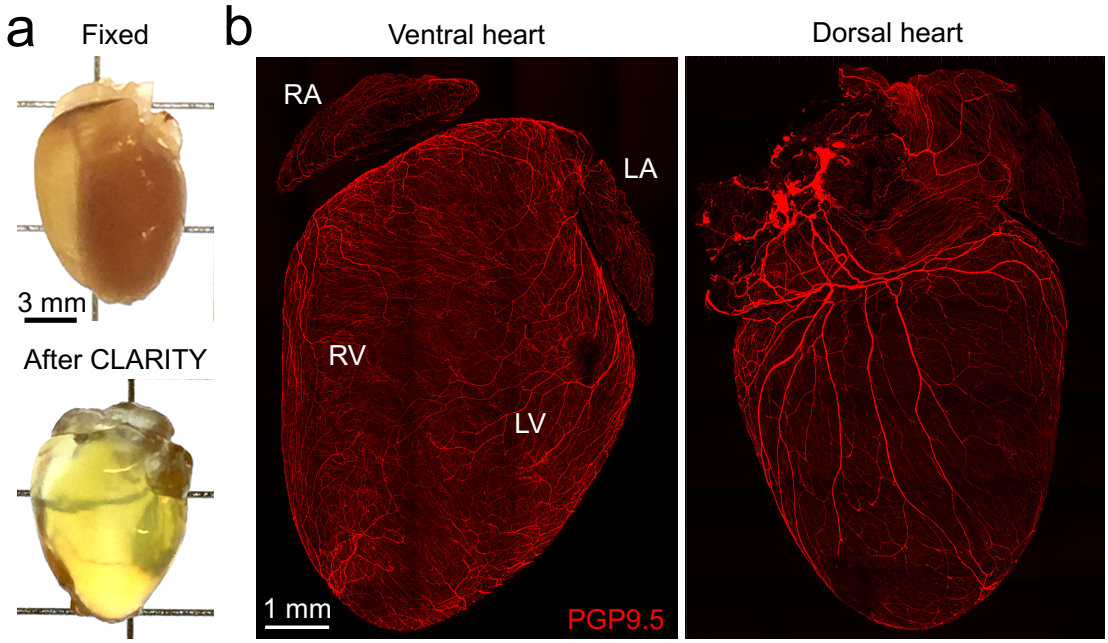

Figure 1. Tissue clearing to assess cardiac innervation. (A) Mouse heart before and after the passive CLARITY technique. **(B)** Ventral and dorsal surface of cleared heart stained with pan-neuronal marker protein gene product 9.5 (PGP9.5). Intrinsic cardiac ganglia can be appreciated on the dorsal surface around the pulmonary veins. LA, left atrium; LV, left ventricle; RA, right atrium; RV, right ventricle.

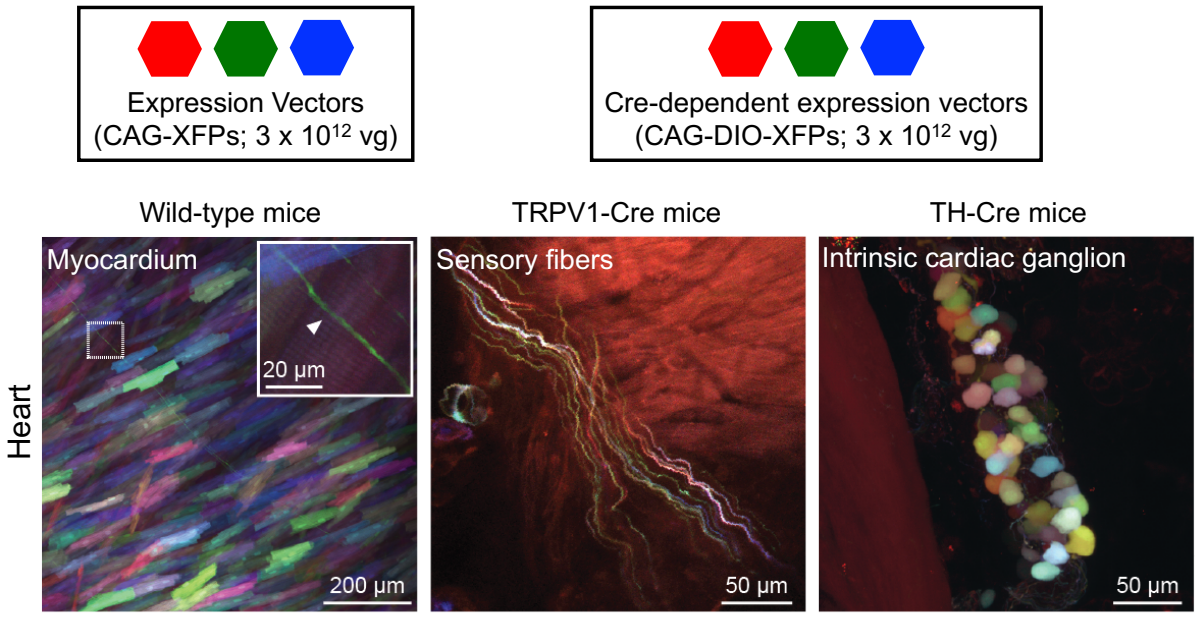

Figure 2. Viral-based multicolor labeling of the heart. A mixture of adeno-associated viruses carrying reporter genes for red, green, or blue fluorescent proteins are systemically injected into wild-type or Cre transgenic mice. Stochastic transduction results in multicolor labeling. Diverse cell types can be labeled in the heart with a wide range of colors, including myocytes (from injection in wild-type mouse; left panel), transient receptor potential vanilloid 1 (TRPV1)-positive sensory fibers (from injection in TRPV1-Cre mouse; middle panel), and tyrosine hydroxylase (TH)-positive motor neurons (from injection in TH-Cre mouse; right panel).

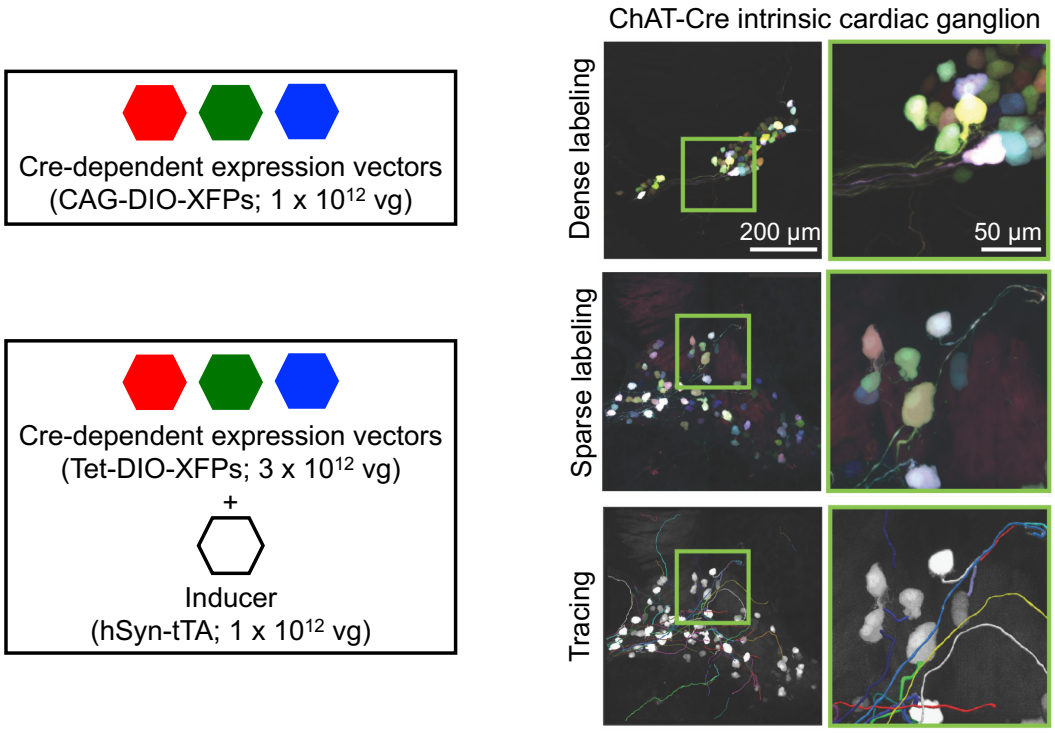

Figure 3. Viral-based multicolor labeling and tracing of cardiac neurons. Images show intrinsic cardiac ganglia from choline acetyltransferase (ChAT)-Cre mice injected with adeno-associated viruses for dense (top panels) or sparse labeling (middle panels). Bottom panels show semi-automatic tracing of sparsely labeled neurites from middle panels. Detailed tracing of projections across multiple samples will be used to build a composite atlas of average circuit connectivity. Scale bars in top panels apply to all images.

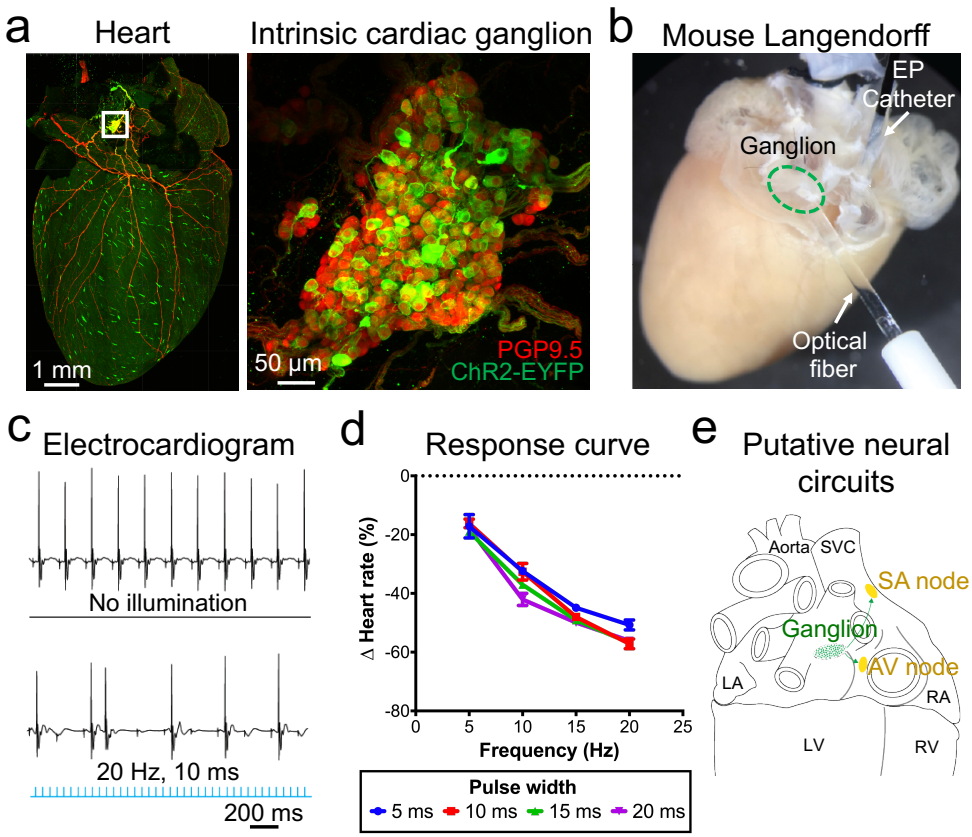

Figure 4. Optogenetic modulation of cholinergic neurons on the heart. (A) Choline acetyltransferase-Cre mice were systemically injected with an adeno-associated virus carrying the Channelrhodopsin 2-enhanced yellow fluorescent protein (ChR2-EYFP) gene. Strong expression was observed in cholinergic neurons and fibers on the heart. **(B)** Cholinergic neurons were optically stimulated in an *ex vivo* Langendorff preparation while concurrently recording cardiac electrophysiologic (EP) parameters. **(C)** Representative electrocardiograms during optical stimulation at 20 Hz frequency and 10 ms pulse width *vs.* no stimulation. Note that stimulation evoked both bradycardia and block of the atrioventricular node. **(D)** Heart rate response from 1 animal to optical stimulation at different frequencies and pulse widths. **(E)** Putative cardiac neural circuits identified through this approach. LA, left atrium; LV, left ventricle; PGP9.5, protein gene product 9.5; RA, right atrium; RV, right ventricle; SVC, superior vena cava.

REFERENCES

1. Kearney PM, Whelton M, Reynolds K, Muntner P, Whelton PK and He J. Global burden of hypertension: analysis of worldwide data. *Lancet*. 2005;365:217-23.
2. Zipes DP. Epidemiology and mechanisms of sudden cardiac death. *Can J Cardiol*. 2005;21 Suppl A:37A-40A.
3. Chugh SS, Reinier K, Teodorescu C, Evanado A, Kehr E, Al Samara M, Mariani R, Gunson K and Jui J. Epidemiology of sudden cardiac death: clinical and research implications. *Prog Cardiovasc Dis*. 2008;51:213-28.
4. Roger VL. Epidemiology of heart failure. *Circ Res*. 2013;113:646-59.
5. Fukuda K, Kanazawa H, Aizawa Y, Ardell JL and Shivkumar K. Cardiac innervation and sudden cardiac death. *Circ Res*. 2015;116:2005-19.
6. Ardell JL, Andresen MC, Armour JA, Billman GE, Chen PS, Foreman RD, Herring N, O'Leary DS, Sabbah HN, Schultz HD, Sunagawa K and Zucker IH. Translational neurocardiology: preclinical models and cardioneural integrative aspects. *J Physiol*. 2016;594:3877-909.
7. Shivkumar K, Ajijola OA, Anand I, Armour JA, Chen PS, Esler M, De Ferrari GM, Fishbein MC, Goldberger JJ, Harper RM, Joyner MJ, Khalsa SS, Kumar R, Lane R, Mahajan A, Po S, Schwartz PJ, Somers VK, Valderrabano M, Vaseghi M and Zipes DP. Clinical neurocardiology defining the value of neuroscience-based cardiovascular therapeutics. *J Physiol*. 2016;594:3911-54.
8. Vaseghi M, Gima J, Kanaan C, Ajijola OA, Marmureanu A, Mahajan A and Shivkumar K. Cardiac sympathetic denervation in patients with refractory ventricular arrhythmias or electrical storm: intermediate and long-term follow-up. *Heart Rhythm*. 2014;11:360-6.
9. Premchand RK, Sharma K, Mittal S, Monteiro R, Dixit S, Libbus I, DiCarlo LA, Ardell JL, Rector TS, Amurthur B, KenKnight BH and Anand IS. Autonomic regulation therapy via left

or right cervical vagus nerve stimulation in patients with chronic heart failure: results of the ANTHEM-HF trial. *J Card Fail*. 2014;20:808-16.

10. Jänig W. *The integrative action of the autonomic nervous system : neurobiology of homeostasis*. Cambridge, UK ; New York: Cambridge University Press; 2006.
11. Armour JA. Potential clinical relevance of the 'little brain' on the mammalian heart. *Exp Physiol*. 2008;93:165-76.
12. Andresen MC, Kunze DL and Mendelowitz D. Central Nervous System Regulation of the Heart. In: J. A. Armour and J. L. Ardell, eds. *Basic and Clinical Neurocardiology* New York, NY: Oxford University Press; 2004: 187-219.
13. Armour JA. Cardiac neuronal hierarchy in health and disease. *Am J Physiol Regul Integr Comp Physiol*. 2004;287:R262-71.
14. Gray MA, Taggart P, Sutton PM, Groves D, Holdright DR, Bradbury D, Brull D and Critchley HD. A cortical potential reflecting cardiac function. *Proc Natl Acad Sci U S A*. 2007;104:6818-23.
15. Agostoni E, Chinnock JE, De Daly MB and Murray JG. Functional and histological studies of the vagus nerve and its branches to the heart, lungs and abdominal viscera in the cat. *J Physiol*. 1957;135:182-205.
16. Ardell JL and Randall WC. Selective vagal innervation of sinoatrial and atrioventricular nodes in canine heart. *Am J Physiol*. 1986;251:H764-73.
17. Yamakawa K, So EL, Rajendran PS, Hoang JD, Makkar N, Mahajan A, Shivkumar K and Vaseghi M. Electrophysiological effects of right and left vagal nerve stimulation on the ventricular myocardium. *Am J Physiol Heart Circ Physiol*. 2014;307:H722-31.
18. Browning KN and Travagli RA. Central nervous system control of gastrointestinal motility and secretion and modulation of gastrointestinal functions. *Compr Physiol*. 2014;4:1339-68.

19. Woodbury DM and Woodbury JW. Effects of vagal stimulation on experimentally induced seizures in rats. *Epilepsia*. 1990;31 Suppl 2:S7-19.

20. Handforth A, DeGiorgio CM, Schachter SC, Uthman BM, Naritoku DK, Tecoma ES, Henry TR, Collins SD, Vaughn BV, Gilmartin RC, Labar DR, Morris GL, 3rd, Salinsky MC, Osorio I, Ristanovic RK, Labiner DM, Jones JC, Murphy JV, Ney GC and Wheless JW. Vagus nerve stimulation therapy for partial-onset seizures: a randomized active-control trial. *Neurology*. 1998;51:48-55.

21. Rush AJ, Marangell LB, Sackeim HA, George MS, Brannan SK, Davis SM, Howland R, Kling MA, Rittberg BR, Burke WJ, Rapaport MH, Zajecka J, Nierenberg AA, Husain MM, Ginsberg D and Cooke RG. Vagus nerve stimulation for treatment-resistant depression: a randomized, controlled acute phase trial. *Biol Psychiatry*. 2005;58:347-54.

22. Huang WA, Shivkumar K and Vaseghi M. Device-based autonomic modulation in arrhythmia patients: the role of vagal nerve stimulation. *Curr Treat Options Cardiovasc Med*. 2015;17:379.

23. Zannad F, De Ferrari GM, Tuinenburg AE, Wright D, Brugada J, Butter C, Klein H, Stolen C, Meyer S, Stein KM, Ramuzat A, Schubert B, Daum D, Neuzil P, Botman C, Castel MA, D'Onofrio A, Solomon SD, Wold N and Ruble SB. Chronic vagal stimulation for the treatment of low ejection fraction heart failure: results of the NEural Cardiac TherApy foR Heart Failure (NECTAR-HF) randomized controlled trial. *Eur Heart J*. 2015;36:425-33.

24. Premchand RK, Sharma K, Mittal S, Monteiro R, Dixit S, Libbus I, DiCarlo LA, Ardell JL, Rector TS, Amurthur B, KenKnight BH and Anand IS. Extended Follow-Up of Patients With Heart Failure Receiving Autonomic Regulation Therapy in the ANTHEM-HF Study. *J Card Fail*. 2016;22:639-42.

25. Gold MR, Van Veldhuisen DJ, Hauptman PJ, Borggrefe M, Kubo SH, Lieberman RA, Milasinovic G, Berman BJ, Djordjevic S, Neelagaru S, Schwartz PJ, Starling RC and Mann

DL. Vagus Nerve Stimulation for the Treatment of Heart Failure: The INOVATE-HF Trial. *J Am Coll Cardiol*. 2016;68:149-58.

26. Berthoud HR. The vagus nerve, food intake and obesity. *Regul Pept*. 2008;149:15-25.
27. Pavlov VA and Tracey KJ. The vagus nerve and the inflammatory reflex--linking immunity and metabolism. *Nat Rev Endocrinol*. 2012;8:743-54.
28. Zhou S, Jung BC, Tan AY, Trang VQ, Gholmieh G, Han SW, Lin SF, Fishbein MC, Chen PS and Chen LS. Spontaneous stellate ganglion nerve activity and ventricular arrhythmia in a canine model of sudden death. *Heart Rhythm*. 2008;5:131-9.
29. Florea VG and Cohn JN. The autonomic nervous system and heart failure. *Circ Res*. 2014;114:1815-26.
30. Zucker IH, Patel KP and Schultz HD. Neurohumoral stimulation. *Heart Fail Clin*. 2012;8:87-99.
31. Li M, Zheng C, Sato T, Kawada T, Sugimachi M and Sunagawa K. Vagal nerve stimulation markedly improves long-term survival after chronic heart failure in rats. *Circulation*. 2004;109:120-4.
32. Yoo PB, Lubock NB, Hincapie JG, Ruble SB, Hamann JJ and Grill WM. High-resolution measurement of electrically-evoked vagus nerve activity in the anesthetized dog. *J Neural Eng*. 2013;10:026003.
33. Hauptman PJ, Schwartz PJ, Gold MR, Borggrefe M, Van Veldhuisen DJ, Starling RC and Mann DL. Rationale and study design of the increase of vagal tone in heart failure study: INOVATE-HF. *Am Heart J*. 2012;163:954-962 e1.
34. Patel YA, Saxena T, Bellamkonda RV and Butera RJ. Kilohertz frequency nerve block enhances anti-inflammatory effects of vagus nerve stimulation. *Sci Rep*. 2017;7:39810.
35. Stavrakis S, Humphrey MB, Scherlag BJ, Hu Y, Jackman WM, Nakagawa H, Lockwood D, Lazzara R and Po SS. Low-level transcutaneous electrical vagus nerve stimulation suppresses atrial fibrillation. *J Am Coll Cardiol*. 2015;65:867-75.

36. Yu L, Scherlag BJ, Li S, Fan Y, Dyer J, Male S, Varma V, Sha Y, Stavrakis S and Po SS. Low-level transcutaneous electrical stimulation of the auricular branch of the vagus nerve: a noninvasive approach to treat the initial phase of atrial fibrillation. *Heart Rhythm*. 2013;10:428-35.

37. Wang Z, Yu L, Wang S, Huang B, Liao K, Saren G, Tan T and Jiang H. Chronic intermittent low-level transcutaneous electrical stimulation of auricular branch of vagus nerve improves left ventricular remodeling in conscious dogs with healed myocardial infarction. *Circ Heart Fail*. 2014;7:1014-21.

38. Ajijola OA and Hamon D. Non-Invasive Neuromodulation Via Tragal Stimulation: Time to Lend an Ear? *JACC Clin Electrophysiol*. 2016;2:340-342.

39. Janes RD, Brandys JC, Hopkins DA, Johnstone DE, Murphy DA and Armour JA. Anatomy of human extrinsic cardiac nerves and ganglia. *Am J Cardiol*. 1986;57:299-309.

40. Burns J, Yee-Hsee H, Mueller A, Chevallier J, Sriram TS, Lewis SJ, Chew D, Achyuta A and Fiering J. High density penetrating electrode arrays for autonomic nerves. *Conf Proc IEEE Eng Med Biol Soc*. 2016;2016:2802-2805.

41. Peclin P and Rozman J. Alternative paradigm of selective vagus nerve stimulation tested on an isolated porcine vagus nerve. *The Scientific World Journal*. 2014;2014:310283.

42. Sun Y and Weber KT. Infarct scar: a dynamic tissue. *Cardiovasc Res*. 2000;46:250-6.

43. Nakahara S, Vaseghi M, Ramirez RJ, Fonseca CG, Lai CK, Finn JP, Mahajan A, Boyle NG and Shivkumar K. Characterization of myocardial scars: electrophysiological imaging correlates in a porcine infarct model. *Heart Rhythm*. 2011;8:1060-7.

44. Fenoglio JJ, Jr., Pham TD, Harken AH, Horowitz LN, Josephson ME and Wit AL. Recurrent sustained ventricular tachycardia: structure and ultrastructure of subendocardial regions in which tachycardia originates. *Circulation*. 1983;68:518-33.

45. Antzelevitch C and Burashnikov A. Overview of Basic Mechanisms of Cardiac Arrhythmia. *Card Electrophysiol Clin*. 2011;3:23-45.

46. Cao JM, Fishbein MC, Han JB, Lai WW, Lai AC, Wu TJ, Czer L, Wolf PL, Denton TA, Shintaku IP, Chen PS and Chen LS. Relationship between regional cardiac hyperinnervation and ventricular arrhythmia. *Circulation*. 2000;101:1960-9.

47. Vracko R, Thorning D and Frederickson RG. Nerve fibers in human myocardial scars. *Hum Pathol*. 1991;22:138-46.

48. Ajijola OA, Lux RL, Khahera A, Kwon O, Aliotta E, Ennis DB, Fishbein MC, Ardell JL and Shivkumar K. Sympathetic modulation of electrical activation in normal and infarcted myocardium: implications for arrhythmogenesis. *Am J Physiol Heart Circ Physiol*. 2017;312:H608-H621.

49. Ogawa M, Zhou S, Tan AY, Song J, Gholmieh G, Fishbein MC, Luo H, Siegel RJ, Karagueuzian HS, Chen LS, Lin SF and Chen PS. Left stellate ganglion and vagal nerve activity and cardiac arrhythmias in ambulatory dogs with pacing-induced congestive heart failure. *J Am Coll Cardiol*. 2007;50:335-43.

50. Armour JA and Kember GC. Cardiac Sensory Neurons. In: J. A. Armour and J. L. Ardell, eds. *Basic and Clinical Neurocardiology* New York, NY: Oxford University Press; 2004: 79-117.

51. Whyte KA, Hogg RC, Dyavanapalli J, Harper AA and Adams DJ. Reactive oxygen species modulate neuronal excitability in rat intrinsic cardiac ganglia. *Auton Neurosci*. 2009;150:45-52.

52. Huang MH, Sylven C, Pelleg A, Smith FM and Armour JA. Modulation of in situ canine intrinsic cardiac neuronal activity by locally applied adenosine, ATP, or analogues. *Am J Physiol*. 1993;265:R914-22.

53. Baker DG, Coleridge HM, Coleridge JC and Nerdrum T. Search for a cardiac nociceptor: stimulation by bradykinin of sympathetic afferent nerve endings in the heart of the cat. *J Physiol*. 1980;306:519-36.

54. Thames MD, Kinugawa T and Dibner-Dunlap ME. Reflex sympathoexcitation by cardiac sympathetic afferents during myocardial ischemia. Role of adenosine. *Circulation*. 1993;87:1698-704.

55. Effect of metoprolol CR/XL in chronic heart failure: Metoprolol CR/XL Randomised Intervention Trial in Congestive Heart Failure (MERIT-HF). *Lancet*. 1999;353:2001-7.

56. Dargie HJ. Effect of carvedilol on outcome after myocardial infarction in patients with left-ventricular dysfunction: the CAPRICORN randomised trial. *Lancet*. 2001;357:1385-90.

57. Syrkin AL, Poltavskaia MG, Shumilova KM, Ivanov GG, Churganova L, Sheianov MV and Gavril'eva SA. [Effect of metoprolol CR/XL on remodeling of the heart and cardiac rhythm disturbances after myocardial infarction in patients with chronic heart failure]. *Kardiologiia*. 2003;43:48-53.

58. Fox IJ, Gerasch DA and Leonard JJ. Left ventricular mechanoreceptors: a haemodynamic study. *J Physiol*. 1977;273:405-25.

59. Purtock RV, Zuperku EJ, Peters SR, Coon RL and Kampine JP. Response of left ventricular mechanoreceptors to changes in pressure and muscle length. *Proc Soc Exp Biol Med*. 1977;154:500-4.

60. Wright C, Drinkhill MJ and Hainsworth R. Reflex effects of independent stimulation of coronary and left ventricular mechanoreceptors in anaesthetised dogs. *J Physiol*. 2000;528 Pt 2:349-58.

61. Thoren P. Left ventricular receptors activated by severe asphyxia and by coronary artery occlusion. *Acta Physiol Scand*. 1972;85:455-63.

62. Thoren PN. Characteristics of left ventricular receptors with nonmedullated vagal afferents in cats. *Circ Res*. 1977;40:415-21.

63. Beaumont E, Salavatian S, Southerland EM, Vinet A, Jacquemet V, Armour JA and Ardell JL. Network interactions within the canine intrinsic cardiac nervous system: implications for reflex control of regional cardiac function. *The Journal of physiology*. 2013;591:4515-33.

64. Tessier-Lavigne M. Visual Processing by the Retina. In: E. R. Kandel, J. H. Schwartz and T. M. Jessell, eds. *Principles of Neural Science.* 4th ed. New York, NY: McGraw-Hill; 2000: 507-522.

65. Walder RY, Radhakrishnan R, Loo L, Rasmussen LA, Mohapatra DP, Wilson SP and Sluka KA. TRPV1 is important for mechanical and heat sensitivity in uninjured animals and development of heat hypersensitivity after muscle inflammation. *Pain*. 2012;153:1664-72.

66. Wang HJ, Wang W, Cornish KG, Rozanski GJ and Zucker IH. Cardiac sympathetic afferent denervation attenuates cardiac remodeling and improves cardiovascular dysfunction in rats with heart failure. *Hypertension*. 2014;64:745-55.

67. Kitamura S, Echevarria M, Kay JH, Krohn BG, Redington JV, Mendez A, Zubiate P and Dunne EF. Left ventricular performance before and after removal of the noncontractile area of the left ventricle and revascularization of the myocardium. *Circulation*. 1972;45:1005-17.

68. Cardinal R, Page P, Vermeulen M, Ardell JL and Armour JA. Spatially divergent cardiac responses to nicotinic stimulation of ganglionated plexus neurons in the canine heart. *Auton Neurosci*. 2009;145:55-62.

69. Richardson DS and Lichtman JW. Clarifying Tissue Clearing. *Cell*. 2015;162:246-57.

70. Hama H, Kurokawa H, Kawano H, Ando R, Shimogori T, Noda H, Fukami K, Sakaue-Sawano A and Miyawaki A. Scale: a chemical approach for fluorescence imaging and reconstruction of transparent mouse brain. *Nat Neurosci*. 2011;14:1481-8.

71. Hama H, Hioki H, Namiki K, Hoshida T, Kurokawa H, Ishidate F, Kaneko T, Akagi T, Saito T, Saido T and Miyawaki A. ScaleS: an optical clearing palette for biological imaging. *Nat Neurosci*. 2015;18:1518-29.

72. Chung K, Wallace J, Kim SY, Kalyanasundaram S, Andalman AS, Davidson TJ, Mirzabekov JJ, Zalocusky KA, Mattis J, Denisin AK, Pak S, Bernstein H, Ramakrishnan C,

Grosenick L, Gradinaru V and Deisseroth K. Structural and molecular interrogation of intact biological systems. *Nature*. 2013;497:332-7.

73. Yang B, Treweek JB, Kulkarni RP, Deverman BE, Chen CK, Lubeck E, Shah S, Cai L and Gradinaru V. Single-cell phenotyping within transparent intact tissue through whole-body clearing. *Cell*. 2014;158:945-58.
74. Treweek JB, Chan KY, Flytzanis NC, Yang B, Deverman BE, Greenbaum A, Lignell A, Xiao C, Cai L, Ladinsky MS, Bjorkman PJ, Fowlkes CC and Gradinaru V. Whole-body tissue stabilization and selective extractions via tissue-hydrogel hybrids for high-resolution intact circuit mapping and phenotyping. *Nat Protoc*. 2015;10:1860-96.
75. Susaki EA, Tainaka K, Perrin D, Kishino F, Tawara T, Watanabe TM, Yokoyama C, Onoe H, Eguchi M, Yamaguchi S, Abe T, Kiyonari H, Shimizu Y, Miyawaki A, Yokota H and Ueda HR. Whole-brain imaging with single-cell resolution using chemical cocktails and computational analysis. *Cell*. 2014;157:726-39.
76. Pan C, Cai R, Quacquarelli FP, Ghasemigharagoz A, Lourbopoulos A, Matryba P, Plesnila N, Dichgans M, Hellal F and Erturk A. Shrinkage-mediated imaging of entire organs and organisms using uDISCO. *Nat Methods*. 2016;13:859-67.
77. Betley JN and Sternson SM. Adeno-associated viral vectors for mapping, monitoring, and manipulating neural circuits. *Hum Gene Ther*. 2011;22:669-77.
78. Deverman BE, Pravdo PL, Simpson BP, Kumar SR, Chan KY, Banerjee A, Wu WL, Yang B, Huber N, Pasca SP and Gradinaru V. Cre-dependent selection yields AAV variants for widespread gene transfer to the adult brain. *Nat Biotechnol*. 2016;34:204-9.
79. Zhang F, Gradinaru V, Adamantidis AR, Durand R, Airan RD, de Lecea L and Deisseroth K. Optogenetic interrogation of neural circuits: technology for probing mammalian brain structures. *Nature protocols*. 2010;5:439-56.

80. Montgomery KL, Iyer SM, Christensen AJ, Deisseroth K and Delp SL. Beyond the brain: Optogenetic control in the spinal cord and peripheral nervous system. *Sci Transl Med*. 2016;8:337rv5.
81. Bruegmann T, Malan D, Hesse M, Beiert T, Fuegemann CJ, Fleischmann BK and Sasse P. Optogenetic control of heart muscle in vitro and in vivo. *Nat Methods*. 2010;7:897-900.
82. Nussinovitch U and Gepstein L. Optogenetics for in vivo cardiac pacing and resynchronization therapies. *Nat Biotechnol*. 2015;33:750-4.
83. Wengrowski AM, Wang X, Tapa S, Posnack NG, Mendelowitz D and Kay MW. Optogenetic release of norepinephrine from cardiac sympathetic neurons alters mechanical and electrical function. *Cardiovascular research*. 2015;105:143-50.
84. Deisseroth K. Optogenetics. *Nat Methods*. 2011;8:26-9.
85. Chang RB, Strochlic DE, Williams EK, Umans BD and Liberles SD. Vagal Sensory Neuron Subtypes that Differentially Control Breathing. *Cell*. 2015;161:622-33.
86. Williams EK, Chang RB, Strochlic DE, Umans BD, Lowell BB and Liberles SD. Sensory Neurons that Detect Stretch and Nutrients in the Digestive System. *Cell*. 2016.